Understanding the immune microenvironment of precancerous lesions of pancreatic cancer

Sophie Hughes

Balliol College, University of Oxford

Thesis submitted for the degree of Doctor of Philosophy in Oncology

Michaelmas 2022









Supervisor

Professor Eric O'Neill (University of Oxford)



The work presented in this thesis was performed at the Department of Oncology, Old Road Campus Research Building (ORCRB), University of Oxford. This study was funded by Medical Research Council funded Prize Studentship. Additional funding was provided by PRECISION-Panc, Cancer Research UK and the Kadani Foundation.

Declaration

I confirm that the work presented in this thesis is my own, unless indicated, and has not been submitted in whole or in part for consideration for any other degree or qualification in this, or any other university. Whenever I have presented collaborated work, I confirm that this has been credited in the thesis.

Understanding the immune microenvironment of precancerous lesions of pancreatic cancer

Sophie Hughes

Balliol College, University of Oxford

Thesis submitted for the degree of Doctor of Philosophy in Oncology

Abstract

The prognosis for patients with pancreatic ductal adenocarcinoma (PDAC) is alarming, with a 10-year survival in only 1% of patients, due to late diagnosis, its propensity to metastasise and lack of therapeutic efficacy under current chemotherapeutic regimes. Poor response rates to immunotherapy, and a lack of knowledge surrounding the immunological repertoire of early disease, require further investigation. This study sought to investigate the immune microenvironment of pancreatic intraepithelial neoplasia (PanIN) lesions present in the KC murine model (*Kras$^{G12D/+}$;Pdx-1-Cre*) and how it may contribute to PDAC progression.

To do so, a multi-colour flow cytometry panel was developed to characterise major immune populations in the systemic blood and pancreatic or tumour locale. Initial validation of the established PDAC immune microenvironment was characterised on KPC (*LSL-Kras$^{G12D/+}$;LSL-Trp53$^{R172H/+}$;Pdx-1-Cre*) and syngeneic orthotopic models. Low-grade PanIN lesions were associated with granulocyte infiltration, indicating immunological monitoring. NK and CD8+ T-cells are capable of PanIN-2 infiltration but splenic-PMN-MDSC, isolated from KC mice bearing high-grade lesions, could generate a suppressive microenvironment. The transition between PanIN-2 and PanIN-3 indicates loss of immunological control. More importantly, this study indicates a suppressive microenvironment is established prior to carcinoma formation. Loss of peripheral B-cells, an influx of splenic-B-cells and loss of systemic IL-27 was associated with low-grade but

not high-grade lesions. The complexities of B-cells and loss of IL-27, either hindering or promoting early PanIN lesion development, will require further investigation. Overall, this study has contributed towards greater understanding of the dynamic immunological landscape during sequential PanIN progression.

Acknowledgements

First, I would like to extend a huge thanks my supervisor, Professor Eric O'Neill. The encouragement, support and guidance you have given me has been a tremendous help over the past four years. More importantly, your enthusiasm for science has made working in your lab an unforgettable experience and helped me to become the scientist I am today. Thank you. Furthermore, I am very grateful to the Medical Research Council for funding my DPhil and providing fantastic opportunities to develop as a scientist beyond the bench. Without their support, this work would not have been possible.

I would like to extend my thanks to our collaborators in the THL Lab and the Blagden Lab, particularly Leticia Campo Urriza, Kendra Perez Smith and Masooma Rajput for their help with the immunofluorescent staining and the exciting results that followed. I would like to give a huge thanks to Dr Helen Ferry for her wisdom and guidance in flow cytometry, it has been integral to this DPhil and helped me develop as a scientist in this field.

I am very grateful to the members of the O'Neill Lab, past and present. I feel very privileged to have worked with you all over the years and greatly miss our morning coffee breaks together. Thank you to Simone for your help generating the orthotopic PDAC model and Keaton for providing great advice. I am incredibly thankful to Asmita, Luana and Maria for your friendships. Watching you all become the incredible scientists you are today has been a privilege and inspiration. To Frances, I greatly appreciate all you have done for me, both in and out of the lab. Your kindness is unmatched. I would like to give a huge thanks to Dan for all your words of wisdom and many Netflix recommendations. I am very thankful we were able to start our DPhils together. And finally, to Tess and Simei. I cannot tell you how much I appreciate everything you have done for me in the last stretch of my DPhil. Although I wish our time together in the lab had been longer, I feel very privileged to have learnt so much from you both. You are both fantastic scientists and wonderful people.

To the amazing friends I've met in Oxford: Bridie, Caroline, Aleena, Linda van Bijsterveldt, Paul, Rachel, Lia, Vicky, Linda Phan and Anna. I am very thankful for all the laughter and support throughout our DPhils together and I am so proud of everything you have all achieved. I would especially like to thank Letitia and Moa; your friendships mean the world to me. I cannot wait to continue to celebrate every achievement, big or small, together. I am forever grateful to my life-long friends, Alice, Sophie, Phoebe and Hester, for all the unforgettable memories and many more to come.

I am eternally thankful to my family for their love and support. Thanks so much to Tim and Claire for your kind words of support and encouragement. To my grandparents, this journey would not have been possible without you both. I am continuously inspired by you both and am incredibly proud to be your granddaughter. To my sister Keri, your kindness and wisdom continues to amaze me and serves as an inspiration each day. You are the best sister I could have asked for. To my wonderful parents, you have been my biggest support, provided endless love and encouragement. I would not be where I am today without you both and cannot begin to express how thankful I am to be your daughter.

And finally, to Andrew. Your never-ending love, support and motivation has helped me each and every day of my DPhil and beyond. The laughter and happiness you have given us has encouraged me even on the hardest of days. I could not have done this without you.

Table of Contents

Abstract ..... **III**

Acknowledgements ..... **V**

List of Figures ..... **XII**

List of Tables ..... **XV**

List of Abbreviations ..... **XVII**

1. Introduction **1**

1.1 Pancreatic cancer *1*

1.1.1 Biology of the pancreas 1

1.1.2 Types of pancreatic cancer 2

1.2 Epidemiology and etiology of pancreatic cancer *6*

1.3 PDAC diagnosis *7*

1.4 PDAC treatment *8*

1.5 Molecular biology of PDAC *11*

1.5.1 *KRAS* mutations 11

1.5.2 Other genetic mutations in PDAC 12

1.6 Pancreatic precursor lesions *13*

1.6.1 PanIN incidence and molecular association 16

1.7 Precursor lesions in other cancers *18*

1.8 Murine models to study PDAC *21*

1.9 Cancer immunology *23*

1.10 PDAC immune microenvironment *26*

1.10.1 Stromal barrier 26

1.10.2 Tumour-associated macrophages 27

1.10.3 Myeloid Derived Suppressor Cells 27

1.10.4 T-regulatory cells 28

1.10.5 CD8 T-cells 29
1.10.6 B-cells 29
1.10.7 Other immune subsets 30
1.10.8 Immunotherapeutic perturbations 31

1.11 Immune microenvironment of PanIN lesions 33

1.12 Aims of this study 35

2. Materials and Methods 36

2.1 Materials 36

2.1.1 Mouse strains 36
2.1.2 General laboratory reagents 37
2.1.3 Buffers and solutions 38
2.1.4 qPCR primers 39
2.1.5 Antibodies 40
2.1.6 Cell lines and cell culture reagents 43

2.2 Cell culture 44

2.2.1 Primary cell culture 45
2.2.2 Organoid culture 46
2.2.3 Bone-marrow derived myeloid suppressor cells 47
2.2.4 KC myeloid derived suppressor cells 47
2.2.5 *Ex vivo* CFSE assay 48

2.3 Western blotting 49

2.3.1 Protein extraction 49
2.3.2 SDS-polyacrylamide gel electrophoresis (SDS-PAGE) 50
2.3.3 Immunoblotting 50

2.4 RNA isolation and quantitative polymerase chain reaction (qPCR) 51

2.5 Genotyping 52

2.6 Establishment of an orthotopic model 52

2.6.1 MRI scanning 53
2.6.2 *In vivo* drug and radiation treatments 54

2.7 Collection of murine blood and tissue 54

2.7.1 Plasma isolation 55

2.8 Formalin fixation and paraffin embedding (FFPE) *55*

2.9 Histological analysis *56*

2.9.1 Haematoxylin and eosin staining (H&E) 56

2.9.2 Immunohistochemical staining (IHC) 57

2.10 Multiplex immunofluorescence *57*

2.11 17-colour spectral flow cytometry *58*

2.11.1 Tissue dissociation 59

2.11.2 Antibody titration 59

2.11.3 Fluorescence minus one (FMO) 61

2.11.4 17-colour spectral flow cytometry assay 62

2.12 CFSE flow cytometry *62*

2.13 Multiplex cytokine array *63*

2.14 ELISA *64*

2.14.1 Plasma samples 64

2.14.2 Organoid supernatant 65

2.15 Statistical analysis *65*

3. Panel design and optimisation for high-dimensional immune-phenotyping of PDAC mouse models using spectral flow cytometry 67

3.1 Introduction *67*

3.2 Aims *69*

3.3 Results *70*

3.3.1 Panel design for spectral flow cytometry 70

3.3.2 Antibody titration 76

3.3.3 Fluorescence minus one control 78

3.3.4 Determining whether tissue dissociations buffers cleave immune antigen 79

3.3.5 Immune-phenotyping peripheral blood and tumour infiltrate in an orthotopic PDAC model 81

3.4 Discussion *85*

4. High-dimensional immune-phenotyping of established PDAC mouse models and dynamic perturbation of the immune microenvironment using combination immunotherapy and radiotherapy 90

4.1 Introduction 90

4.2 Aims 93

4.3 Results 93

4.3.1 Characterisation of the immune microenvironment in established PDAC models at late-stage disease. 93

4.3.2 Combination of fractionated low-dose radiation and immunotherapy reduces tumour volume in a PDAC orthotopic model. 100

4.3.3 Immune response in orthotopic tumour following combination fractionated low-dose radiation and immunotherapy. 104

4.3.4 Spatial resolution reveals a non-activated NK cell signature associated with CD8 T-cell infiltration and reduction in tumour volume following combination treatment. 107

4.4 Discussion 111

4.4.1 Immune microenvironment surrounding advanced models of PDAC 111

4.4.2 Perturbation of PDAC tumour with radiotherapy and combination immunotherapy 115

5. Local and systemic immune response to *Kras* oncogene expression and progression from pre-invasive pancreatic intraepithelial neoplasia to invasive carcinoma 120

5.1 Introduction 120

5.2 Aims 122

5.3 Results 123

5.3.1 PanIN lesion progression in the KC PDAC murine model allows longitudinal assessment of immune cell contribution to *Kras* oncogene expression 123

5.3.2 The myeloid immune response to PanIN lesion progression 126

5.3.3 MDSC involvement at the transition to high-grade PanIN lesion. 128

5.3.4 The lymphoid immune response to PanIN lesion progression 132

5.3.5 Immune infiltrate proximity to PanIN lesions shifts throughout lesion progression 135

5.3.6 CD19+ B-cell involvement during early, low-grade PanIN lesion development 139

5.4 Discussion 142

6. Drivers of immune cell recruitment during early development of pre-invasive pancreatic intraepithelial neoplasia 151

6.1 Introduction *151*

6.2 Aims *153*

6.3 Results *153*

6.3.1 Systemic cytokine profiling during PanIN lesion progression 153

6.3.2 IL-35 cytokine profiling early during PanIN lesion progression 157

6.3.3 Downregulation of IL-35 subset *EBI3* and *IL12A* found in KC HET organoids 161

6.4 Discussion *163*

7. General Discussion and Conclusion 170

7.1 Future work *178*

7.2 Conclusion *179*

8. Supplementary 180

Appendix 199

Bibliography 202

List of Figures

Figure 1.1: Anatomy of the pancreas. 2

Figure 1.2: Spectrum of histological patterns in PDAC. 5

Figure 1.3: Pancreatic intraepithelial neoplasia histology. 14

Figure 1.4: Histological and molecular alterations during precursor lesion progression into pancreatic ductal adenocarcinoma. 18

Figure 1.5: Tumour immune microenvironment. 25

Figure 1.6: The immune network in PDAC. 31

Figure 2.1: Schematic of orthotopic treatment chart. 54

Figure 3.1: Spectral comparison between two versions of the 17-colour flow cytometry panel. 75

Figure 3.2: FOXP3-PE antibody titration on splenocytes. 77

Figure 3.3: PD-1-PeCy7 FMO control to determine fluorescence spread. 78

Figure 3.4: Quantification of the impact of collagenase and DNase treatment on antigen expression. 80

Figure 3.5: Gating strategy for analysis of cell subsets. 82

Figure 3.6: Immune profiling orthotopic syngeneic PDAC. 84

Figure 4.1: KPC genetic model is representative of late-stage PDAC tumour. 94

Figure 4.2: Comparison of the systemic immune microenvironment in established PDAC murine models. 97

Figure 4.3 Comparison of the local immune microenvironment in established PDAC murine models. 100

Figure 4.4: Fractionated low-dose radiotherapy and combination immunotherapies reduce tumour volume in an orthotopic mouse. 103

Figure 4.5: Modulation of local tumour immune infiltrate following fractionated low-dose radiotherapy and combination immunotherapies in an orthotopic mouse. 106

Figure 4.6: IF spatial resolution of local tumour immune infiltrate following fractionated low-dose radiotherapy and combination immunotherapies in an orthotopic mouse. 111

Figure 5.1: KC mouse model displays PanIN lesion progression. 125

Figure 5.2: Local and systemic myeloid immune response during PanIN lesion progression. 128

Figure 5.3: *Ex vivo* T-cell suppression to elucidate MDSC status during PanIN lesion progression. 132

Figure 5.4: Local and systemic lymphoid immune response during PanIN lesion progression. 135

Figure 5.5: Proximity between immune infiltrate and PanIN lesions during lesion development. 138

Figure 5.6: Spatiality of B-cells during PanIN lesion development. 142

Figure 6.1: Systemic cytokine levels during PanIN lesion progression. 157

Figure 6.2: KC HET organoids are representative of low-grade PanIN lesions. 159

Figure 6.3: IL-35 profiling of PanIN lesion progression and late-stage PDAC using a commercially available ELISA. 160

Figure 6.4: IL-35 and IL-35 receptor expression in B-cells and KC organoids. 162

Figure 7.1: Proposed model of the immune microenvironment during PanIN lesion progression. 177

Supplementary 8.1: Antibody titrations. 183

Supplementary 8.2: FMO controls to determine fluorescence spread. 188

Supplementary 8.3: Modulation of systemic immune populations following fractionated low-dose radiotherapy and combination immunotherapies in an orthotopic mouse. 189

Supplementary 8.4: PD1 expression of immune populations following fractionated low-dose radiotherapy and combination immunotherapies in an orthotopic mouse. 191

Supplementary 8.5: CCR5 expression of immune populations following fractionated low-dose radiotherapy and combination immunotherapies in an orthotopic mouse. 193

Supplementary 8.6: Association between E-cadherin and NK, activated NK, CD4 and CD8 T-cells. 194

Supplementary 8.7: Optimisation of ex vivo T-cell suppression. 195

Supplementary 8.8: CD19 antibody IHC optimisation. 196

Supplementary 8.9: Systemic cytokine response during PanIN lesion progression. 198

List of Tables

Table 1.1: Overview of benign and pre-malignant pancreatic neoplasms 15

Table 1.2: Novel therapies for advanced PDAC in clinical trial. 32

Table 2.1: List of chemical reagents. 37

Table 2.2: List of buffers and their composition. 38

Table 2.3: Pancreas dissociation Buffer. 39

Table 2.4: Tumour dissociation Buffer. 39

Table 2.5: List of qPCR primers. 39

Table 2.6: Primary and secondary antibodies for immunohistochemistry. 40

Table 2.7: Primary and secondary antibodies for immunofluorescence. 40

Table 2.8: Primary and secondary antibodies used for Western blotting. 41

Table 2.9: Antibodies used for CFSE assay. 41

Table 2.10: Antibodies used in 17-colour flow cytometry panel. 42

Table 2.11: List of cell lines. 43

Table 2.12: Cell culture reagents and supplements. 43

Table 2.13: Cell culture reagents and supplements for Mouse Complete Feeding Media for organoid culture. 44

Table 2.14: Thermocycler reaction conditions for RT PCR. 51

Table 2.15: Details of antibody titration. 61

Table 3.1: Rationale for antigen choice.....71

Table 3.2: Cell identification table. 72

Table 3.3: Antigen identification table. 73

List of Abbreviations

AAH	Atypical adenomatous hyperplasia
ACD	Acid citrate dextrose
ADM	Acinar-to-ductal metaplasia
APC	Antigen presenting cells
APD	Avalanche photodiodes
aPD1	Anti-Programmed cell death protein 1
ATM	Ataxia telangiectasia mutated
BCA	Bicinchoninic acid
BM	Bone marrow
BMDM	Bone marrow derived macrophages
BRCA1	Breast cancer gene 1
BRCA2	Breast cancer gene 2
BSA	Bovine Serum Albumin
BTLA	B- and T-lymphocyte-associated
CA125	Cancer antigen 125
CA19-9	Carbohydrate antigen 19-9
CAF	Cancer-associated fibroblast
CCL5	C-C chemokine ligand 5
CCR1	C-C chemokine receptor 1
CCR3	C-C chemokine receptor 3
CCR4	C-C chemokine receptor 4
CCR5	C-C chemokine receptor type 5
CCR5i	C-C chemokine ligand 5 inhibitor
cDC	Conventional dendritic cells
cDC1	Conventional type-1 dendritic cells
CDKN2A	Cyclin Dependent Kinase Inhibitor 2A
cDNA	Complementary DNA
CFSE	Carboxyfluorescein succinimidyl ester
CO_2	Carboxylate
CT	Delta-delta Cycle Threshold
CTLA-4	Cytotoxic T-lymphocyte-associated antigen
CXCL12	C-X-C motif chemokine ligand 12
CXCR2	C-X-C motif chemokine receptor 2

CyTOF	Cytometry by time-of-flight
DAB	3,3'-Diaminobenzidine
DC	Dendritic cells
dH_2O	Deionised water
DMEM	Dulbecco's Modified Eagle Media
DMSO	Dimethyl Sulfoxide
DNA	Deoxyribonucleic Acid
DPX	Di-N-Butyl Phthalate
DTT	Diothiothreitol
EBI3	Epstein-Barr virus-induced gene 3
EDTA	Ethylenediaminetetraacetic acid
ELISA	Enzyme-linked immunosorbent assay
ERK	Extracellular signal-regulated kinase
FBS	Foetal bovine serum
FC	Flow cytometry
FFPE	Formalin fixation and paraffin embedding
FMO	Fluorescence minus one
FOXP3	Forkhead box P3
GAP	Guanine activating protein
GAPDH	Glyceraldehyde-3-Phosphate Dehydrogenase
GEF	Guanine exchange factor
GEMM	Genetically engineered mouse model
GNLY	Granulysin
gp130	Glycoprotein 130
Gy	Grays
GZMA	Granzyme A
GZMB	Granzyme B
GZMH	Granzyme H
H&E	Haematoxylin and eosin
H_2O	Water
HET	Heterozygous
HRAS	Harvey rat sarcoma retrovirus
HRP	Horseradish Peroxidase
iDC	Immature dendritic cells
IDO	Indoleamine-pyrrole 2,3-dioxygenase
IF	Immunofluorescence

IFN-α	Interferon alpha
IFN-γ	Interferon gamma
IHC	Immunohistochemistry
iKC	Inducible KC (*Kras$^{LSL.G12D}$; Ptf1a-CreER™)*
IL	Interleukin
iNOS	Inducible nitric oxide synthase
IPMN	Intraductal Papillary Mucinous Neoplasm
IR	Irradiation
IVC	Individually Ventilated Cage
Kb	Kilobase
KC	*Kras$^{LSL.G12D+-}$; Pdx-1-Cre*
KDa	Kilodalton
KPC	*Kras$^{LSL.G12D+-}$; Trp53$^{LSL.R17H+-}$; Pdx-1-Cre*
KRAS	Kirsten Rat Sarcoma
LAG-3	lymphocyte-activation gene 3
LN	Liquid nitrogen
LSL	Lox-STOP-Lox
LUAD	Non-small cell lung adenocarcinoma
LUSC	Non-small cell lung squamous cell carcinoma
M-MDSC	Monocytic myeloid derived suppressor cells
MDM2	Mouse double minute 2 homologue
MDSC	Myeloid derived suppressor cells
MEK	Mitogen activated protein kinase
MEN1	Multiple Endocrine Neoplasia, Neurofibromatosis 1
MeOH	Methanol
MFI	Median florescence intensity
mg	Milligram
MHC	Major histocompatibility complex
ml	Millilitre
MLH1	MutL homolog 1
mm	Millimetre
mM	Millimolar
MRI	Magnetic resonance imaging
mRNA	Messenger RNA
MSH2	MutS homolog 2
MSH6	MutS homolog 6

mW	Milliwatt
NBF	Neutral buffered formalin
NK	Natural Killer cells
NKT	Natural Killer T cells
NRAS	Neuroblastoma RAS viral oncogene homolog
PanIN	Pancreatic intraepithelial neoplasia
PBMC	Peripheral blood mononuclear cells
PBS	Phosphate-buffered saline
PCR	Polymerase Chain Reaction
PD-1	Programmed cell death protein 1
PD-L1	Programmed death-ligand 1
PDAC	Pancreatic ductal adenocarcinoma
PDX1	Pancreatic and Duodenal Homeobox 1
Pen-Strep	Penicillin/Streptomycin
PFT1	Pancreas transcription factor 1
PIK3CA	Phosphatidylinositol-4,5-bisphosphonate 3-kinase catalytic subunit α
PMN-MDSC	Polymorphonuclear myeloid derived suppressor cells
PMT	Photomultiplier tubes
PNET	Pancreatic neuroendocrine tumour
PRF1	Perforin 1
PRSS1	Protease serine 1
QC	Quality control
qPCR	Quantitative polymerase chain reaction
RAS	Ras Proto-Oncogene
RBC	Red blood cell lysis
RNA	Ribonucleic acid
ROS	Reactive oxygen species
rpm	Revolutions per minute
RPMI	Roswell Park Memorial Institute 1640 medium
RT-PCR	Reverse transcriptase polymerase chain reaction
RTP	Room temperature and pressure
SA-PE	Streptavidin phycoerythrin
SARRP	Small animal radiation research platform
SD	Standard deviation
SDS-PAGE	Sodium dodecyl sulfate–polyacrylamide gel electrophoresis
SI	Stain index

SMA	Smooth muscle actin
SMAD4	Mothers against decapentaplegic homolog 4
SPINK1	Serine protease inhibitor Kazal-type 1
STK11	Serine/threonine kinase 11
TAM	Tumour-associated macrophage
TGFβ	Transforming growth factor beta
Th1	T-helper cell 1
TIGIT	T cell immunoreceptor with Ig and ITIM domains
TIM-3	T cell immunoglobulin and mucin-domain containing-3
TLR	Toll-like receptor
TLS	Tertiary lymphoid structure
TMB	Tetramethylbenzidine
TNF	Tumour necrosis factor
TP53	Tumour protein p53
Tregs	T-regulatory cells
VEGF	Vascular endothelial growth factor
VEGFA	Vascular endothelial growth factor A
VHL	Von Hippel-Lindau disease
WT	Wild type
XCL1	X-C motif chemokine ligand 1
µg	Microgram
µl	Microlitre
µm	Micrometre

1.Introduction

1.1 Pancreatic cancer

1.1.1 Biology of the pancreas

Anatomically, the pancreas is structurally divided into the head, body and tail and located in the upper abdomen, posterior to the lower half of the stomach. The head of the pancreas is surrounded by the duodenum, with the tail extended towards the spleen. The physiological function of the pancreas consists of both endocrine and exocrine portions (Figure 1.1). Endocrine secretion of hormones, including insulin, proinsulin, amylin, C-peptide, somatostatin, pancreatic polypeptide and glucagon is performed by the islets of Langerhans to regulate blood sugar levels and glandular secretion (Karpińska and Czauderna, 2022). Around 80-85% of the pancreatic mass is dedicated to the exocrine function within the acinus and ductal system (Henderson et al., 1981). Acinar cells allow synthesis, storage and secretion of digestive enzymes. These include proteolytic enzymes trypsin, chymotrypsin, carboxypeptidase and elastase, lipolytic enzymes lipase, phospholipase and esterase, and glycolytic enzymes lactase and amylase. Transportation of digestive enzymes requires water and ions to pass through the acinar lumen into the intralobular ducts and subsequently drain into the main pancreatic duct for entry into the duodenum. Distinct multipotent progenitors, Pancreatic and duodenal homeobox 1 (PDX1), Pancreas transcription factor 1 (PFT1), c-Myc and Carboxypeptidase A1 (CPA1), reside at the tip of the pancreatic ductal tree to allow the formation of endocrine and exocrine cells in the pancreas (Zhou et al., 2007).

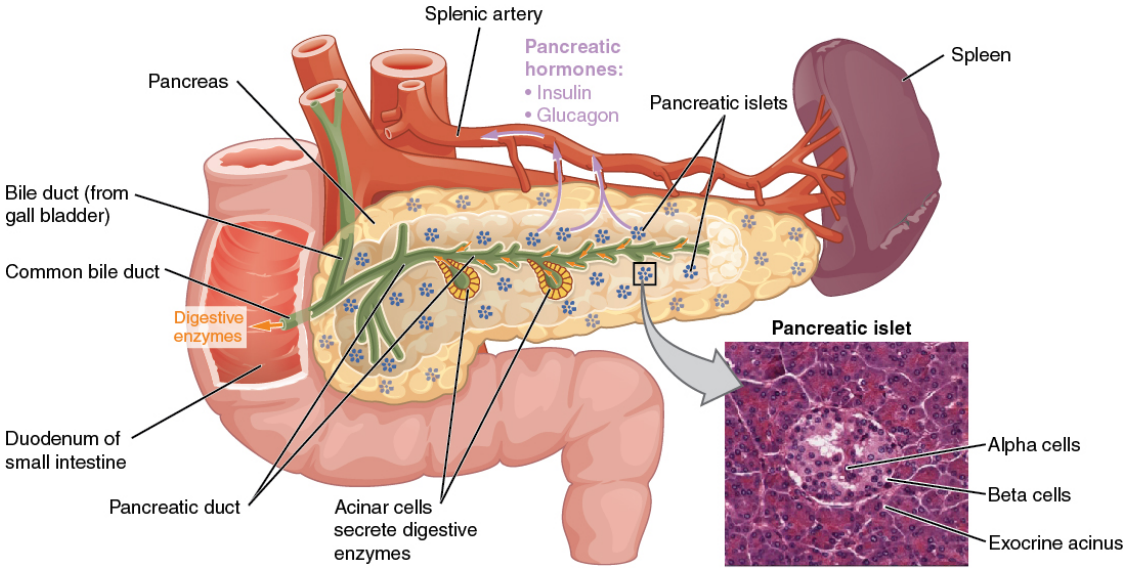


Figure 1.1: Anatomy of the pancreas.
The pancreas has both endocrine and exocrine functions. The endocrine portion consists of Islets of Langerhans to allow the secretion of insulin, produced by beta cells, and glucagon, produced by alpha cells, within the pancreatic islets (grey arrow). Both insulin and glucagon regulate the rate of glucose metabolism in the body. The exocrine portion consists of digestive enzymes, which are secreted by the acini and pass through the ductal system to the duodenum. Figure taken from Anatomy and Physiology (Biga et al., 2018) and is open access under the Creative Commons Attribution Licence.

1.1.2 Types of pancreatic cancer

Rare cancers of the pancreas include pancreatoblastoma and pancreatic sarcoma. Pancreatoblastoma represent malignant epithelial neoplasms of the pancreas (Horie et al., 1977). They share similarities to the molecular pathogenesis of hepatoblastomas and found to be genetically distinct from more common pancreatic cancers (Abraham et al., 2001). In addition, their occurrence in patients with Beckwith-Wiedemann syndrome and familial adenomatous polyposis has been reported (Koh et al., 1986; Giardiello et al., 1996; Cetta et al., 1997; Kohda et al., 2000). Primary sarcomas of the pancreas, including leiomyosarcomas and carcinosarcomas, are extremely rare and thought to represent 0.1% of all pancreatic cancers (Baylor and Berg, 1973; Darvishian et al., 2002; Zhang et

al., 2010). While rare, pancreatic sarcomas are typically more aggressive with a worse prognosis (Ambe et al., 2011).

Pancreatic cancers are more typically exocrine or endocrine in origin. Pancreatic neuroendocrine tumours (PNETs) represent 1-2% of pancreatic cancers (Mullan et al., 2001; Hallet et al., 2015). While PNET endocrinopathies are typically sporadic, hereditary diseases can also cause PNET formation such as Multiple Endocrine Neoplasia, Neurofibromatosis 1 (MEN1; Recklinghausen's syndrome), von Hippel-Lindau disease (VHL) and tuberous sclerosis (Anlauf et al., 2007; Falconi et al., 2016).

Rarer exocrine malignancies include cystic tumour of the pancreas. Pancreatic cysts can be benign or malignant and classified as retention cysts, pseudocysts and cystic neoplasms (Garud and Willingham, 2012; Karoumpalis and Christodoulou, 2016). Cystic pancreatic lesions have been associated with cystic fibrosis, VHL and MEN1 (Hammel et al., 2000; Maisonneuve et al., 2007; Kimura et al., 2010). Acinar cell carcinoma is thought to represent 1% of adult and 15% of paediatric pancreatic neoplasms, with a better prognostic outcome in paediatric patients (Klimstra et al., 1992; Klimstra, 2007; Ban et al., 2010). Elevated α-fetoprotein has been characterised in some patients; however, the causation of acinar carcinoma is still relatively unknown (Itoh et al., 1992; Nojima et al., 1992; Xing-Mao et al., 2018).

Pancreatic ductal adenocarcinoma (PDAC) represents approximately 90% of all pancreatic cancers, arising from the exocrine portion of the pancreas. As the most prevalent form, the nomenclature of PDAC is often used interchangeably with pancreatic cancer. PDAC is a highly aggressive disease and is the seventh leading cause of cancer-related death worldwide (Sung et al., 2021). Incidence of disease is increasing, with projections of a 6% rise in the UK by 2035 (Smittenaar et al., 2016). Furthermore, PDAC is expected to become the second leading cause of cancer-related death in Germany and the United States of America by 2030 (Rahib et al., 2014; Quante et al., 2016). Indeed,

survival is dismal; a 25.4% one-year survival, a 7.3% five-year survival and only a 5% ten-year survival in England (CRUK, 2013-2017). Histomorphological features of PDAC consist of atypical tubular glands resembling pancreatic ducts with heterogeneity (Figure 1.2). As an invasive neoplasm of mucin production and gland formation, histological features, including nuclear pleomorphisms, luminal necrosis, incomplete glandular lumina, haphazard arrangement of glands adjacent to muscular vessels, lymphovascular invasion and perineural invasion, can aid diagnosis (Kamisawa et al., 2016). Furthermore, PDAC is divided into three grades based on glandular formation: well-differentiated (G1), moderately-differentiated (G2) and poorly-differentiated (G3) (Garcia et al., 2013). Heterogeneity within PDAC tumours can include non-tubular components, including clear-cell, cribriform or gyriform component. Colloid carcinoma is defined as G1 (Figure 1.2H). Conventional PDAC is typically defined as G2 or G3 (Figure 1.2A), cribriform and clear-cell combined PDAC are G2 (Figure 1.2B-C), gyriform, papillary, micropapillary, adenosquamous and complex combined PDACs are predominantly G3 tumours (Figure 1.2D-G, I) (Schlitter et al., 2017).

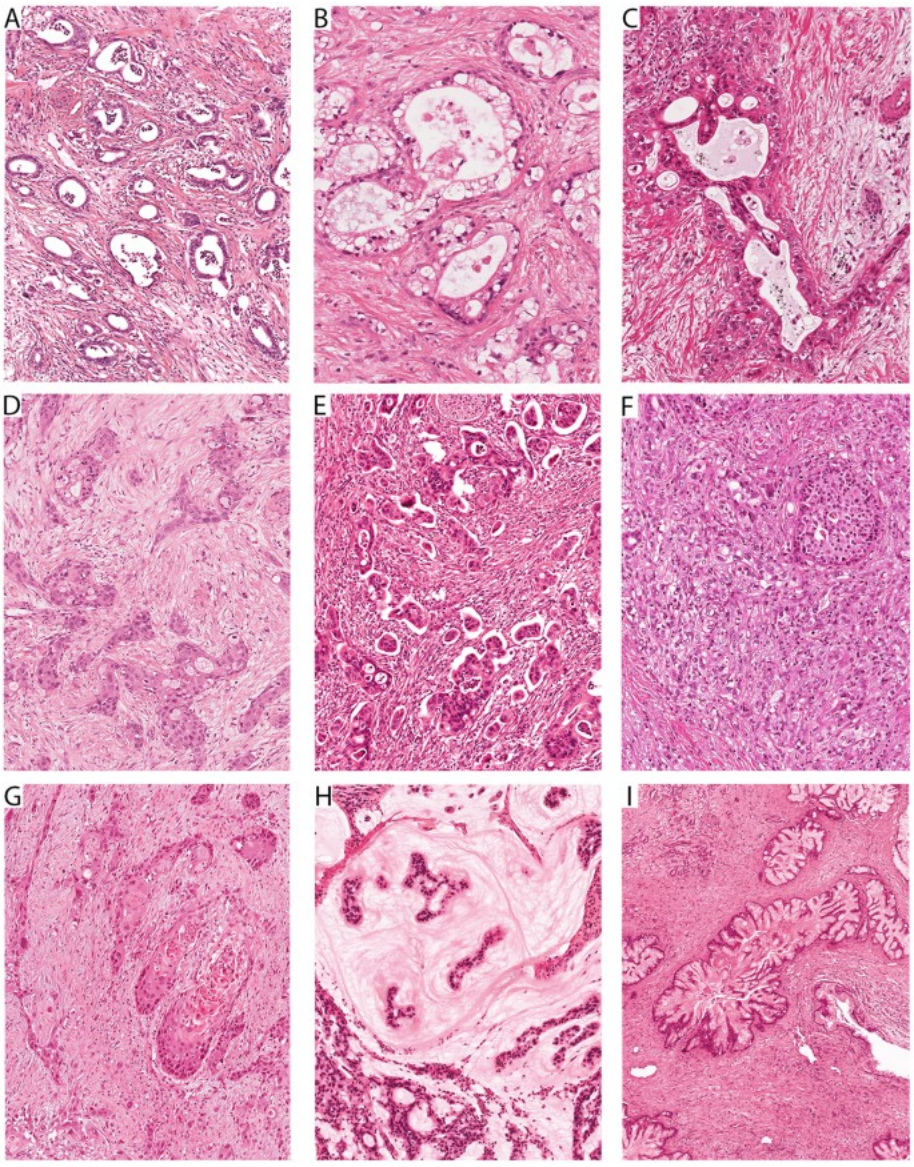


Figure 1.2: Spectrum of histological patterns in PDAC.
(A) Conventional PDAC. (B-F) Combined PDACs with a dominant histological component: (B) Clear-cell component. (C) Cribriform component. (D) Gyriform component. (E) Micropapillary component. (F) Complex component. (G) Adenosquamous carcinoma. (H) Colloid carcinoma. (I) Papillary carcinoma. Figure taken from (Schlitter et al., 2017) and is open access under the Creative Commons CC BY Licence.

Advances in transcriptomics have allowed sub-classification of PDAC. Classical, quasi-mesenchymal and exocrine like molecular subtypes were initially found (Collisson et al., 2011). Separation of the stroma and pancreas from PDAC further identified classical and basal-like subsets (Moffitt et al., 2015). Bailey et al revealed four distinct subtypes: squamous, pancreatic progenitor, immunogenic and aberrantly differentiated endocrine exocrine (Bailey et al., 2016). These studies suggest that squamous, quasi-mesenchymal

and basal-like subtypes are likely to be the same subtype considering they share molecular similarity and reveal worse prognosis and response to chemotherapy compared to classical or pancreatic progenitor subtypes (Mizrahi et al., 2020). Further characterisation of the PDAC microenvironment has revealed desmoplastic, immune classical and stroma activated subsets (Puleo et al., 2018). Classification of PDAC subtypes will aid clinical outcomes for patients to stratify treatment regimen and prognosis, although further investigation is warranted.

1.2 Epidemiology and etiology of pancreatic cancer

Pancreatic cancer diagnosis has doubled in the last two decades (1990-2017) (Pourshams et al., 2019). This is thought to largely be due to an aging population as age was the strongest risk factor, while death rates increase throughout the lifespan (Pourshams et al., 2019). Indeed, the median age of diagnosis of PDAC is 71 years (Ben-Aharon et al., 2019). Incidence of disease is also 50% higher in men compared to women (Kamisawa et al., 2016). Additional risk factors have been attributed to cigarette smoking, alcohol consumption and obesity (Lynch et al., 2009; Arslan et al., 2010; Bracci, 2012; Lucenteforte et al., 2012). Diseases such as diabetes, chronic pancreatitis, periodontal disease and Helicobacter pylori infection have also been associated with an increased risk of PDAC development (Everhart and Wright, 1995; Trikudanathan et al., 2011; Bosetti et al., 2014; Munigala et al., 2015; Maisonneuve et al., 2017).

Heritable genetic risk towards pancreatic cancer has been estimated to be 21.4% in which causative mutations cause predisposition (Chen et al., 2019). Peutz-Jeghers syndrome, a familial cancer syndrome, is associated with PDAC risk due to tumour suppressor *STK11* mutations (Giardiello et al., 1987). Similarly, hereditary breast-ovarian cancer syndrome also carries an increased risk due to *BRCA1* and *BRCA2* mutations. While *BRCA1* mutation carries relatively low risk, *BRCA2* mutation is the most frequently inherited risk factor associated with PDAC (Brose et al., 2002; Couch et al., 2007).

Germline mutations to *CDKN2A* cause atypical mole melanoma and have an associated pancreatic cancer risk (Goldstein et al., 1995). Additional risk of PDAC has been associated with germline mutations to genes involved in DNA damage response (*ATM*; ataxia telangiectasia) and DNA mismatch repair (*MLH1*, *MSH2*, *MSH6*; Lynch syndrome) (Kastrinos et al., 2009; Roberts et al., 2012).

Chronic pancreatitis has long been associated with the risk of pancreatic cancer, thought to be due to repeated cycles of inflammation. Hereditary pancreatitis syndromes are associated with a 40% lifetime risk of the disease, due to mutations in *SPINK1* and *PRSS1* (Lowenfels et al., 1997). Patients harbouring germline mutations to *CFTR* also carry PDAC predisposition (McWilliams et al., 2010). Similarly, this is thought to be due to an increased risk of pancreatitis.

1.3 PDAC diagnosis

Diagnosis of PDAC typically occurs at later stage of disease, predominantly due to non-specific symptoms such as weight loss, nausea, bloating, new-onset diabetes, changes in bowel habits, back and shoulder pain, jaundice and changes in bowel habits (Keane et al., 2014). Symptoms that do present are often associated with advanced, invasive stages of disease.

Diagnostic imaging, using multidetector CT angiography or MRI, is recommended for accurate and timely diagnosis of PDAC and to assess staging and resectability (Diehl et al., 1998; Sandrasegaran et al., 2013; Al-Hawary et al., 2014). Endoscopic ultrasound can be used in combination for either identification of regional lymph nodes or to guide fine needle aspiration for tissue confirmation (Agarwal et al., 2004).

Serum biomarkers are also used in PDAC diagnosis. PDAC expression of molecular markers include carbohydrate antigen (CA)19-9, carcinoembryonic antigen (CEA) and cancer antigen 125 (CA125, also known as MUC16). (CA)19-9 has been validated as a serum biomarker for PDAC (sensitivity: 79-81%; specificity: 82-90%) (Ballehaninna and Chamberlain, 2012). Additionally, (CA)19-9 is used to monitor systemic treatment, both neoadjuvant and metastatic, response (Wong et al., 2008; Bauer et al., 2013; Tzeng et al., 2014). CEA and CA125 have also shown elevation in patient serum (Chan et al., 2014).

1.4 PDAC treatment

Surgical resection remains the only treatment that offers curative potential for patients (Millikan et al., 1999). A pancreatoduodenectomy, distal pancreatectomy or total pancreatectomy is typically performed depending on tumour location and type. However, only 15% of patients that present with PDAC have the potential to undergo surgery (Sohn et al., 2000; Ansari et al., 2015). Unresectable tumour at the time of diagnosis is often due to non-specific symptomology that lends itself to late-stage diagnosis. Furthermore, the vast majority of patients who underwent potentially curative surgery developed recurrence in the abdominal cavity (Van den Broeck et al., 2009). Around 50% of patients present with metastatic disease at the time of diagnosis, largely due to the late-stage of diagnosis (Adamska et al., 2017).

Several randomised, controlled trials have led to adjuvant chemotherapy recommendation following surgery (Kalser and Ellenberg, 1985; Neoptolemos et al., 2004; Regine et al., 2008; Neoptolemos et al., 2010; Oettle et al., 2013). First introduced in 1997, the nucleoside analogue gemcitabine has provided minimal survival benefit as a monotherapy (Burris et al., 1997; Kim and Gallick, 2008). When given in combination with capecitabine, gemcitabine provided a survival benefit from 25.5-month to 28-month median survival (Oettle et al., 2007; Neoptolemos et al., 2010; Neoptolemos et al., 2017). Fluorouracil with

leucovorin, oxaliplatin and irinotecan (FOLFIRINOX) further increased median overall survival from 35 to 54.4-months compared to gemcitabine monotherapy alone (Conroy et al., 2018). Neoadjuvant therapy uses systemic therapies to treat progressive disease with the aim to achieve surgical resection following therapy. However, a recent phase 3 study found neoadjuvant chemo-radiation combined with gemcitabine, compared to immediate surgery for resectable and borderline resectable tumour, had no significant survival benefit (Versteijne et al., 2020). Despite this, chemoradiation improved resection rate and prolonged disease-free survival (Versteijne et al., 2020). The benefit of radiotherapy to PDAC treatment regimen is still unclear. Currently, a phase 2 clinical trial, SCALOP-2, is testing the role of radiotherapy dose escalation with or without radiosensitiser nelfinavir following gemcitabine or nanoparticle albumin bound-paclitaxel (nab-paclitaxel) chemotherapy (Strauss et al., 2019).

Around one third of patients present with locally advanced disease at diagnosis, typically due to vascular involvement that prevents surgical resection (Mizrahi et al., 2020). Systemic chemotherapy regimens include gemcitabine combined with nab-paclitaxel or FOLFIRINOX (Marthey et al., 2015; Philip et al., 2020). Successful response to chemotherapy may allow for subsequent surgical resection.

For metastatic patients, systemic chemotherapy remains the primary treatment modality for palliative care and to prolong life (Mizrahi et al., 2020). Combination of gemcitabine with FOLFIRINOX or nab-paclitaxel in phase 3 clinical trials improved survival from 6.8 to 11.1 months and 6.7 to 8.5 months respectively (Conroy et al., 2011; Von Hoff et al., 2013). Gemcitabine monotherapy is still offered to patients whose comorbidities would make combination therapy unfavourable.

Other targeted therapeutic strategies could offer benefit to PDAC patients. Inhibition of PARP, an enzyme required for single-stranded DNA repair, demonstrated significant activity and prolonged survival in *BRAC1* or *BRAC2*-mutated metastatic PDAC (Golan et

al., 2019). Ongoing phase 2 trials will determine the role of PARP inhibition as an adjuvant therapy in PDAC patients with *BRAC1*, *BRAC2* and *PALB2* mutations (APOLLO; NCT04858334). PDAC with *ATM* mutation are also sensitive to combination PARP and ATR inhibition. Early-phase clinical trials testing ATR inhibition with chemotherapy (NCT04514497), or PARP inhibition are ongoing (NCT036822)

Oncogenic *KRAS* mutations occur in the majority of PDAC cases. The development of RAS inhibitors has proved challenging due to lack of high-affinity binding, inhibitor accessible pockets (Liu et al., 2019). The first efficacious $KRAS^{G12C}$ inhibitor demonstrated a 30% reduction in disease burden at 4.3 months median follow-up (Hong et al., 2020). Preclinical data has also demonstrated pre-clinical *in vivo* tumour reduction following $KRAS^{G12D}$ inhibition (Wang et al., 2022c). Given $KRAS^{G12D}$ is the most prevalent KRAS mutation, its inhibition could have beneficial implications (Bamford et al., 2004).

Targeting the interaction between the PDAC and the tumour microenvironment it resides in can offer another line of therapeutic strategy. Targeting immune checkpoint, such as PD-1/PD-L1 and CTLA-4, has offered durable clinical efficacy in a range of malignancies, including solid tumours (Gandhi et al., 2018; Larkin et al., 2019; Rini et al., 2019; Schmid et al., 2020). Unfortunately, the same clinical benefit has not been translated to PDAC (O'Reilly et al., 2019). It is thought that a lack of clinical efficacy may be due to reduced antigenicity and immunogenicity and an immunosuppressive microenvironment. Targeting of immune specific subsets associated with the PDAC immune microenvironment, and any ongoing trials, are discussed in further detail in Section 1.10.8.

A dense, desmoplastic stroma is also prominent in the PDAC microenvironment and thought to act as a physical barrier to immune cell tumour infiltration. The stroma consists of a multitude of extracellular matrix, fibroblasts, immune cells and pancreatic stellate cells (Neesse et al., 2015). Targeting the dense stroma would allow an increase in vascular perfusion and drug delivery to the tumour. While an angiotensin-receptor blocker was

shown to decrease collagen and hyaluronan production in the PDAC stroma, with improved drug delivery in murine models, no clinical efficacy was found in metastatic PDAC patients (Chauhan et al., 2013; Kasi et al., 2021). Overall, further investigation and understanding of the complex tumour microenvironment is required to viably target PDAC with meaningful clinical significance.

1.5 Molecular biology of PDAC

1.5.1 *KRAS* mutations

Oncogenic Kirsten rat sarcoma retrovirus (*KRAS*) mutations are found in around 90% of PDAC tumours (Jones et al., 2008; Biankin et al., 2012; Sausen et al., 2015; Waddell et al., 2015; Witkiewicz et al., 2015). *KRAS*, Harvey rat sarcoma retrovirus (HRAS) and neuroblastoma RAS viral oncogene homolog (NRAS) are members of the RAS family (Harvey, 1964; Kirsten and Mayer, 1967; Hall et al., 1983). RAS family members are frequently mutated in cancers (Prior et al., 2012; Waters and Der, 2018). KRAS is a small GTPase, that cycles between an active GTP-bound form, regulated by guanine exchange factor (GEF), and an inactive GDP-bound state, regulated by GTPase activating protein (GAP). Following extracellular stimulation of receptor tyrosine kinases, RAS becomes activated (RAS-GTP) to engage effector proteins, such as RAF1, to regulate downstream signal transduction of mitogen activated protein kinase kinase (MEK) and subsequent extracellular signal-related kinase (ERK 1/2) (Moodie et al., 1993; Vojtek et al., 1993). This in turn activates a number of downstream signalling pathways associated with migration, apoptosis, proliferation, differentiation and cell-cycle (Eblen, 2018).

RAS missense mutations encoding a single amino acid substitution predominantly occur at three mutational points: glycine-12 (G12), glycine-13 (G13) or glutamine-61 (Q61) rendering RAS constitutively active in its GTP-bound active form. In PDAC, the most frequent *KRAS* mutations are Glycine-to-Aspartate (G12D) or Glycine-to-Valine (G12V)

(Prior et al., 2012). G12D mutation has been associated with advanced PDAC as an independent prognostic marker (Bournet et al., 2016).

1.5.2 Other genetic mutations in PDAC

Aside from activating *KRAS* mutations, mutations to tumour suppressor genes tumour protein p53 (*TP53*), mothers against decapentaplegic homolog 4 (*SMAD4*) and cyclin dependent kinase inhibitor 2A (*CDKN2A*) can occur in PDAC. The protein p53, encoded by *TP53*, functions as a tumour suppressor transcription factor and acts as a 'guardian to the genome' considering its role in prevention of emergence and progression of many cancer types (Lane, 1992). Around 50-75% of PDAC harbours *TP53* mutations, of which mutations are predominantly missense and allow stabilisation and accumulation of mutant p53 (Scarpa et al., 1993). *SMAD4* is inactivated in around 60% of PDAC tumours. SMAD4 mutation results in signalling via pathways independent to transforming growth factor beta (TGFβ), leading to a decrease in TGFβ cell cycle arrest, apoptosis and promotion of epithelial to mesenchymal transition (Hahn et al., 1996; Bailey et al., 2016). *CDKN2A* is a tumour suppressor gene encoding cell-cycle checkpoint protein $p16^{INK4A}$. It negatively regulates cell cycle progression at G1 to S-phase by preventing the complex formation between cyclin dependent kinases CDK4/6 and cyclin D (Serrano et al., 1993). *CDKN2A* also encodes $p14^{ARF}$ ($p19^{ARF}$ in mice) via an alternative reading frame, which interacts with mouse double minute 2 homologue (MDM2) and prevent MDM2 interaction with p53. This subsequently stabilises p53 (Quelle et al., 1995; Stott et al., 1998). *CDKN2A* loss of function mutation occurs in 90% of PDAC via point mutation, homozygous deletion, loss of heterozygosity and promoter hypermethylation (Schutte et al., 1997; Lin et al., 2020a).

As previously discussed in Section 1.2 familial syndrome germline mutations to *ATM*, *STK11*, *SPINK1*, *BRAC1*, *BRAC2*, *MLH1*, *MSH2* and *MSH6* have also been associated with PDAC, albeit less common.

1.6 Pancreatic precursor lesions

PDAC is associated with early precursor lesions, that become more neoplastic over time, eventually culminating in invasive carcinoma. Evidence to support incremental progression from ductal hyperplasia to subsequent non-papillary, papillary and atypical hyperplasia, prior to invasive adenocarcinoma, was based on histological analysis of patient pancreatic cancer samples with morphometry and multivariant analysis (Sommers et al., 1954; Kozuka et al., 1979; Furukawa et al., 1994; Brat et al., 1998; Brockie et al., 1998). These pre-malignant lesions were later defined as Pancreatic Intraepithelial Neoplasia (PanIN) lesions (Klimstra and Longnecker, 1994; Brat et al., 1998).

Evidence would suggest that these PanIN lesions arise from a process known as acinar-to-ductal metaplasia (ADM). Genetic mutations, such as oncogenic KRAS expression in acinar cells, in conjunction with inflammation, have been shown to induce transdifferentiation into duct-like cells, representing regions of high proliferation and precursor potential with ductal marker expression (Klimstra and Longnecker, 1994; Aichler et al., 2012; Rooman and Real, 2012). Macrophage secretion of CCLR and TNFα has been shown to induce ADM via activation of nuclear factor κB (NFκB) (Liou et al., 2013). KRAS hyperactivation can enhance epidermal growth factor receptor signalling, which can subsequently activate Notch signalling downstream to drive ADM via prevention of acinar cell differentiation and maintenance of pancreatic precursor cells (Esni et al., 2004; De La et al., 2008; Liou et al., 2015a).

PanIN lesions typically measure around 0.5 cm and are morphologically classified into three grades: PanIN-1, PanIN-2 and PanIN-3. PanIN-1 lesions consist of tall, columnar cells in the ductal epithelium, that would normally be cuboidal, with basal location of round nuclei and no atypia. PanIN-1A lesions are defined as flat (Figure 1.3A), while PanIN-1B have papillary or are basally pseudostratified (Hruban et al., 2001). Abnormalities of the nucleus becomes more complex in PanIN-2 lesions, including loss of polarity,

pleomorphism, crowding, pseudostratification and hyperchromasia (Figure 1.3B). Additionally, PanIN-2 lesions are mucinous with papillary structure (Hruban et al., 2001). PanIN-3 lesions are the most neoplastic, in which papilla and cribriform structures form and epithelial structures can 'bud off' into the ductal lumen. Cytological structure of PanIN-3 includes enlarged, pleomorphic and poor orientation of nuclei (Figure 1.3C). In contrast to PDAC, PanIN-3 lesions do not invade the basement membrane (Hruban et al., 2004; Hruban et al., 2007). In more recent years, reclassification of precursor lesions has termed PanIN-1 and PanIN-2 as low-grade and PanIN-3 as high-grade PanIN lesions to better fit clinical need for histological assessment (Basturk et al., 2015).

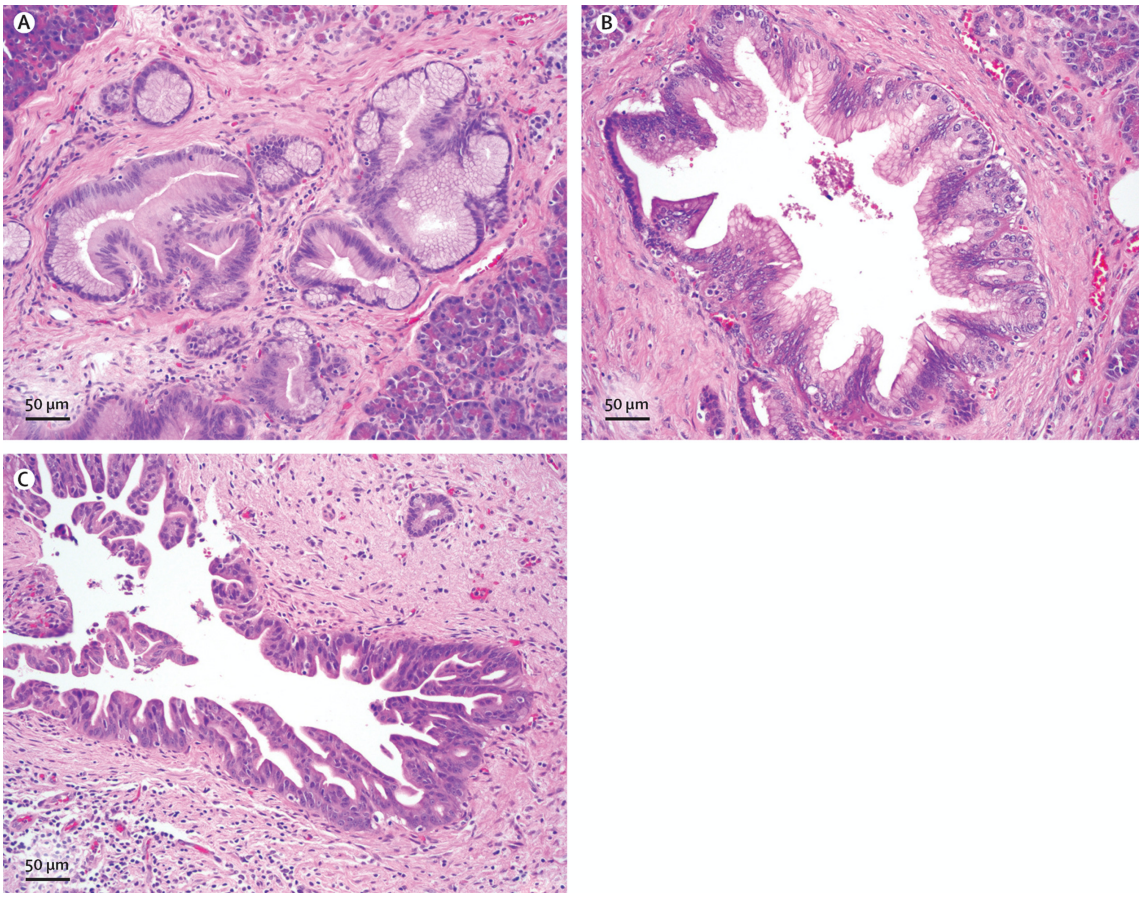


Figure 1.3: Pancreatic intraepithelial neoplasia histology.
(A) PanIN-1 consists of flat or papillary lesion composed of uniform columnar cells with round basal nuclei and supranuclear mucin. (B) PanIN-2 lesions are flat or papillary with moderate nuclear atypia such as enlargement, hyperchromasia and loss of polarity. (C) PanIN-3 is flat or papillary with severe architectural atypia such as budding, cribriforming and luminal necrosis. Severe cytological atypia including enlargement, hyperchromasia, loss of polarity, prominent nucleoli. Figure taken from(Kamisawa et al., 2016). Reprinted with permission from Elsevier. License Number: 5454131317126

While PanIN lesions are the most common pancreatic precursor neoplasm, other non-invasive neoplasia includes mucinous cystic neoplasm (MCN) and intraductal mucinous neoplasm (IPMN). Additional benign and pre-malignant pancreatic lesions are detailed in Table 1.1. IPMNs are found in around 25% of surgically resected pancreatic neoplasms (Kosmahl et al., 2004). They produce mucin from a cystic mass originating from the pancreatic ductal system (Crippa et al., 2010; Tanaka et al., 2012). Nomenclature of IPMNs are based on site origin: IPMNs of the main duct (MD-IPMN), IPMNs from the ductal branch (BD-IPMN) and IPMNs originating from both (mixed-IPMN) (Tanaka et al., 2012). Further to this, IPMNs are also divided into a unifocal, single cystic mass or multiple multifocal cystic masses. (Crippa et al., 2010; Tanaka et al., 2012). In contrast, MCNs are not part of the pancreatic ductal system and primarily occur in the pancreatic body or tail (Lüttges et al., 2002; Tanaka et al., 2012). Architecturally, MCNs are thick-walled and focally lined by columnar mucinous epithelium (Masia et al., 2011). Similar to PanIN lesions, IPMNs and MCNs can exhibit low and high-grade dysplasia (Basturk et al., 2015). Unlike PanIN lesions, that require histological assessment of biopsies, IPMNs and MCNs can be diagnosed via radiological examination (Basturk et al., 2015; Ren et al., 2019).

Table 1.1: Overview of benign and pre-malignant pancreatic neoplasms

Group	Entity
Benign	Acinar cell cystadenoma
	Serous cystadenoma
	Pyloric gland adenoma
Pre-malignant	Pancreatic intraepithelial neoplasia
	Intraductal papillary mucinous neoplasm
	Intraductal tubulopapillary neoplasm
	Mucinous cystic neoplasm

1.6.1 PanIN incidence and molecular association

Although precancerous pancreatic neoplasms, such as PanIN lesions, are common and increase in prevalence with age, they are rarely detected incidentally (Andea et al., 2003; Schwartz and Henson, 2007; Matsuda et al., 2017). Incidence of PanIN lesions, particularly high-grade, are more common in invasive carcinoma than chronic pancreatitis. Concurrently, they are more common in chronic pancreatitis pancreata than healthy control (Andea et al., 2003). PanINs were identified in 16% of healthy controls but increased to 60% in chronic pancreatitis (4% with PanIN-3) and 82% in pancreatic cancer (40% with PanIN-3) (Schwartz and Henson, 2007; Hruban et al., 2008). A more recent study estimated the likelihood, and time of onset, for PanIN lesion progression, from low to high-grade, and subsequent PDAC formation using data from the National Cancer Institute Surveillance, Epidemiology and End Result program and published data on PanIN incidence by age (Peters et al., 2018). The study found PanIN-3 lesions were associated with a higher probability of progression to invasive PDAC than PanIN-1 or PanIN-2 lesions. The probability of progression from PanIN-1 lesions to PDAC was estimated to be around 1.5%, taking around 35.3 years (Peters et al., 2018). Of note, their model found a long latency from PanIN-3 development to PDAC formation of around 12.3 years (Peters et al., 2018). This window of time may allow for a window of detection. Indeed, these findings were in agreement with the literature, in which 40% of PanIN-1 will not advance to PDAC, whereas 30-50% of pancreata with invasive behaviour contain PanIN-3 (Hruban et al., 2004; Hruban et al., 2007). However, the findings of Peter et al assumed an average-risk population despite several environmental and mutational risk factors for PDAC development. Despite this, the transition to high-grade PanIN-3 lesion would indicate loss of control due to its association with later PDAC development.

The progression and dysplastic activity of PanIN lesions is associated with a greater mutational burden (Figure 1.4) . *KRAS* mutations are frequently found in early PanIN-1

lesions, and remain a prominent mutation throughout PanIN progression (Löhr et al., 2005). Furthermore, oncogenic *KRAS* is found in more than 90% of all PDAC cases (Biankin et al., 2012). The role of *KRAS* as an initiator mutation for PDAC was confirmed through murine models in which *Kras* was constitutively activated under spatial control in the pancreas (Tuveson et al., 2004). Following *KRAS* mutation during early PanIN-lesions, telomere shortening can occur. This is followed by *CDKN2A* inactivation, typically during PanIN-2 progression, and subsequent inactivation of *TP53* and *SMAD4* during PanIN-3 high-grade lesion (Moskaluk et al., 1997; Lüttges et al., 2001; van Heek et al., 2002; Rosty et al., 2003). Aside from familial germline mutations, *BRCA2* is also mutated in around 10% of sporadic PDAC cases (Murphy et al., 2002).

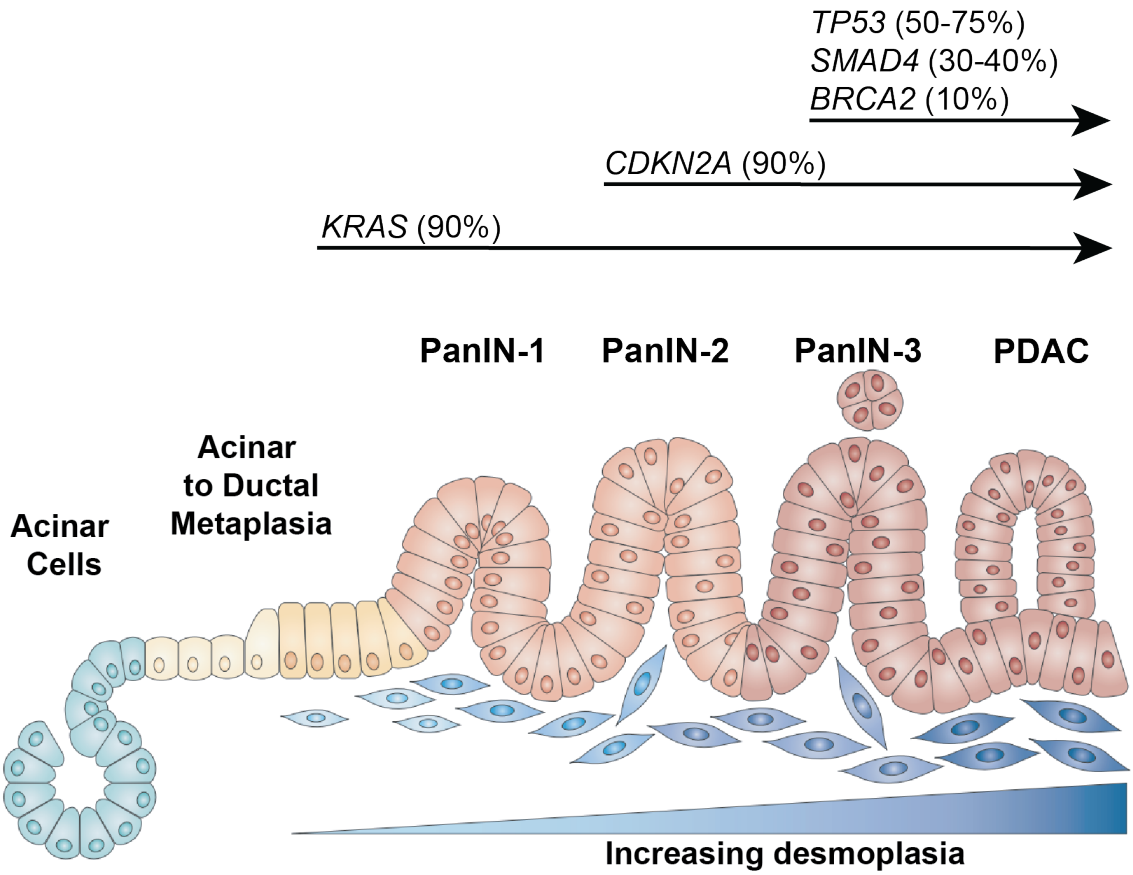


Figure 1.4: Histological and molecular alterations during precursor lesion progression into pancreatic ductal adenocarcinoma.
Each PanIN lesion stage is associated with an accumulation of genetic and epigenetic alterations throughout tumorigenesis that enable progression to PDAC. 90% of PDAC tumours harbour *KRAS* mutations at the point of transformation into invasive adenocarcinoma. Inactivation of *CDKN2A* occurs during PanIN-2 staging and is present in 90% of PDAC tumours. Inactivation of *TP53* and *SMAD4* occur during PanIN-3 staging and occur in 50-75% and 20-40% of PDAC tumours respectively. *BRCA2* mutations occur during PanIN-3 lesions and are present in around 10% of sporadic PDAC cases. Figure adapted from (Morris et al., 2010). Reprinted with permission from Springer Nature, license number: 5452490900634

1.7 Precursor lesions in other cancers

Preneoplastic lesions are found in other cancers, including breast, colorectal and lung. Low-grade precursor lesions include atypical ductal hyperplasia, flat epithelial atypia and lobular neoplasia (Sinn et al., 2010). Subsequent high-grade lesions, ductal carcinoma in situ occurs prior to breast cancer formation (Abdel-Fatah et al., 2008). Studies have suggested that 50% of patients with high-grade lesions go on to develop invasive breast cancer (Page et al., 1982; Pinder and Ellis, 2003). Similar to pancreatic cancer, their

stepwise progression ultimately results in low-grade invasive carcinoma of the breast (Allred et al., 2001; Abdel-Fatah et al., 2007). By definition, atypical ductal hyperplasia has atypical ductal epithelia with micropapillae not completely filling the duct (Abdel-Fatah et al., 2008). Flat epithelial atypia is comprised of acini ectasia of terminal ductal-lobular units with a lining of columnar cells, occasionally with small tufts but not micropapillae. In addition, nuclei display loss of polarity (Schnitt and Vincent-Salomon, 2003; O'Malley et al., 2006). Lobular neoplasia occur when acini, in affected terminal duct lobular units, are distended by cellular proliferation (O'Malley, 2010). Precancerous lesions have been associated with oestrogen receptor positivity and significant *TP53* mutation present in high-grade lesions, similar to pancreatic high-grade PanIN lesions (Clarke et al., 1997; Tan et al., 2002)

The World Health Organisation defined three preneoplastic lesions of the bronchial epithelium. Squamous dysplasia is thought to be a precursor to squamous cell carcinoma, atypical adenomatous hyperplasia (AAH), thought to be a precursor for adenocarcinoma, and diffuse idiopathic pulmonary neuroendocrine cell hyperplasia, which may progress to carcinoid tumour (Kerr, 2001; Greenberg et al., 2002). Non-small cell lung cancer consists of two histological subtypes, adenocarcinomas (LUAD) and squamous cell carcinoma (LUSC). No precursor lesions have been identified for small-cell lung carcinoma, rather extensive damage to the hyperplastic bronchial epithelium is characteristic of tumour (Wistuba et al., 2000). AAH consist of focal proliferation of alveolar cells with mild nuclear atypia although histological criteria are poorly defined (Mori et al., 2001). They are the only known precursor lesion in the development of LUAD and, similar to PanIN lesions, have been associated with *KRAS* and *EGFR* mutations and *CDKN2A* hypermethylation (Mori et al., 2001; Sakamoto et al., 2007; Selamat et al., 2011).

Established evidence has found adenomas and dysplasia precursor lesions can result in colorectal adenocarcinoma. Adenomas consist of clonal lesions with enlarged, hyperchromatic and elongated nuclei in a stratified arrangement along the basement

membrane and may show mucin depletion and increased apoptotic activity (Fleming et al., 2012). Adenomas can be further subclassified into tubular, tubulovillous and villous based on architectural components. Inflammatory bowel disease, similar to chronic pancreatitis in PDAC, is a known risk-factor for the development of dysplasia and colorectal carcinoma (Blackstone et al., 1981). Lesions may be flat or raised and classified as low or high-grade. High-grade dysplasia has cytological atypia, increased glandular density with crowded glands, loss of nuclear polarity and necrotic debris within the lumen of dysplastic glands (Fleming et al., 2012). Colorectal carcinoma is associated with adenomatous polyposis coli, *KRAS* and *TP53* mutations (Ogino and Goel, 2008). Similar to PDAC, mutational load and frequency increase with precancerous lesion development towards invasive carcinoma (Fearon and Vogelstein, 1990). Loss of function mutations to adenomatous polyposis coli precede constitutive activation to *KRAS*, present in around 61.9% of adenomas, and *BRAF* (Powell et al., 1992; Davies et al., 2002; Zauber et al., 2013). Similar to the pancreatic cancer mutational load, the adenoma-carcinoma sequence also includes mutations to *SMAD4* and *TP53* as well as phosphatidylinositol-4,5-bisphosphonate 3-kinase catalytic subunit alpha (*PIK3CA*) (Baker et al., 1990; Takagi et al., 1996; Kato et al., 2007). Similar to low-grade PanIN lesions the risk of adenomas transitioning into invasive carcinoma is around 2.5-5.6% (Brenner et al., 2007).

Considering a low carcinoma transition rate is common amongst low-grade precursor lesions in various cancers, this would suggest that the microenvironment, in which low-grade neoplastic lesions reside in, may be crucial to the resolution of these lesions or further neoplastic transition into invasive carcinoma.

1.8 Murine models to study PDAC

Due to the propensity of PDAC late-diagnosis in humans and difficulty in obtaining low-grade tumour, genetic mouse models (GEMM) have been used to study disease. In 2003, Hingorani et al developed the KC GEMM, which targeted the expression of oncogenic *Kras* to pancreatic progenitor cells. The construct Lox-STOP-Lox (LSL) was inserted upstream of exon 1 into the *Kras* locus and designed to create a G to A transition at codon 12. AdenoCre was used to remove the STOP element and homologous recombination allowed endogenous expression of oncogenic $Kras^{G12D}$ in murine lung adenocarcinoma and later utilised by Hingorani et al to generate the KC GEMM (Jackson et al., 2001; Hingorani et al., 2003). Cross-breeding with mice that expressed bacterial Cre recombinase from pancreatic-specific promoters *Pdx-1* or *Ptf1a/P48* resulted in the KC GEMM ($Kras^{G12D/+}$*;Pdx-1-Cre*) (see Chapter 5) (Kawaguchi et al., 2002; Hingorani et al., 2003). This model expressed oncogenic *Kras* in all pancreatic lineages during embryogenesis and was subsequently able to recapitulate PanIN lesion progression, similar to the human condition (Hingorani et al., 2003). At 2.25 months, around 20% of ducts contained PanIN-1A lesions. Ducts became more neoplastic with age as PanIN lesion formation and progression occurred. At 7-10 months, 82% of the ducts were neoplastic and high-grade PanIN-3 lesions were observed (Hingorani et al., 2003). A median survival of 14-months with later PDAC development provided evidence for the initiator capability of *Kras* mutation towards the development of pancreatic cancer (Hingorani et al., 2003). Of note, *Pdx1-Cre* expression is considered ‘leaky’ as *Pdx1* is not exclusive towards the pancreas. Expression is observed in other tissues such as the skin, oral mucosa, perianal, gastric and adrenal regions and can result in off-site papilloma and lymphoma (Hingorani et al., 2003; Rachagani et al., 2012). Unlike *Pdx1*, *Ptf1a* expression in the developing gut is restricted towards pancreatic progenitors (Kawaguchi et al., 2002; Magnuson and Osipovich, 2013).

To capture the widely invasive and metastatic nature of PDAC, the KPC GEMM was later developed by Hingorani et al in 2005 (Hingorani et al., 2005). To investigate tumour progression, and considering *Tp53* mutations are present in around 75% of PDAC tumours, *Trp53*^{R172H}, an orthologue of the most common *TP53* mutation in human PDAC, was targeted for endogenous expression in progenitor cells of the murine pancreas (Olivier et al., 2002; Hingorani et al., 2005). Targeting of endogenous *Kras*^{G12D} was carried out as conducted in the KC GEMM (Hingorani et al., 2003). Conditional mutant *Trp53* alleles were generated by introducing LoxP flanked transcriptional STOP cassette into intron 1 of *Trp53*. Site directed mutagenesis introduced Argenine-to-Histidine mutation at codon 172 (Olive et al., 2004; Hingorani et al., 2005). Endogenous mutation of both oncogenic *Kras* and *Tp53* was directed to the pancreas through interbreeding with *Pdx1-Cre* transgenic mice to generate the KPC GEMM (*LSL-Kras*$^{G12D/+}$*;LSL-Trp53*$^{R172H/+}$*;Pdx-1-Cre*) (see Chapter 4) (Hingorani et al., 2005). The KPC model faithfully recapitulated human disease, including poor vascularity, fibrosis and metastatic spread, and clinical features of PDAC, including ascites, bowel and biliary obstruction and cachexia. (Hingorani et al., 2005; Beatty et al., 2011; Provenzano et al., 2012). While the pancreata are devoid of neoplasia at birth, the full spectrum of PanIN lesions were present at 10-weeks. By 16-weeks, most mice developed spontaneous, locally invasive PDAC accompanied by a dense stromal reaction (Hingorani et al., 2005). In comparison to xenograft and implantation models, KPC and KC GEMMs are immunocompetent and provide an important platform to study the interaction between the immune system and tumour. Similar to the human condition, KPC GEMMs display significant inflammatory infiltrate and paucity of effector T-cells within the tumour microenvironment (Beatty et al., 2011; Bayne et al., 2012; Beatty et al., 2015).

More recently, inducible PDAC GEMMs have been developed to recapitulate the acquisition of pancreatic cancer postnatally rather than mutagenic activation during embryogenesis. In 2020, Mallya et al crossed Lox-STOP-Lox *KRAS*^{G12D} with *Ptf1a-*

CreER^{TM} mice to generate an inducible KC murine model (iKC; (*Kras*$^{LSL.G12D}$*; Ptf1a-CreER*™) (Mallya et al., 2020). Tamoxifen was used to activate Cre and induce mutant *Kras* expression in acinar cells at 16-weeks. Low-grade PanIN lesions were present 4-weeks post-tamoxifen treatment, with high-grade PanIN lesion development 30-weeks post treatment. An abundance of desmoplasia and PDAC was observed 40-50 weeks post-treatment, hence the iKC model was found to recapitulate clinical PanIN formation and PDAC development (Mallya et al., 2020).

Syngeneic orthotopic PDAC models have been generated in recent years, due to the variable nature of tumour latency and invasive progression observed in GEMMs, while still maintaining their immune repertoire unlike immunocompromised models (Tseng et al., 2010; Qiu and Su, 2013). These models are generated via the injection of syngeneic tumour cells into the healthy pancreas of a wild-type mouse (see Chapter 3 and 4). These models develop rapidly, with local invasion, poorly defined borders and liver metastasis frequently found (Tseng et al., 2010). The extent of desmoplasia and patterns of fibrosis, typically found in GEMMs and human PDAC, is not as prominent in orthotopic models, likely due to their accelerated nature (Tseng et al., 2010; Majumder et al., 2016). In addition, variability in recruitment and activation of B-cell immune infiltrate within the tumour locale was found between PDAC GEMMs and orthotopic models, hypothesised to be due to the short-time frame of orthotopic generation (Spear et al., 2019).

1.9 Cancer immunology

The immune system serves to protect against foreign pathogen, while maintaining a balance of self-tolerance. Evidence regarding immunosurveillance, by which the immune system recognises and destroys malignancy, was first provided over 60 years ago (Prehn and Main, 1957; Klein et al., 1960). Later, the term ‘tumour immunoediting’ was coined,

based on Rag2-deficient (immune-deficient) and wild-type murine studies (Shankaran et al., 2001; Dunn et al., 2002). Crosstalk between the tumour and the immune system resulted in three outcomes: tumour elimination, equilibrium or tumour escape from immune control (Shankaran et al., 2001; Matsushita et al., 2012). Considering high mutational burden in the setting of an evolving tumour, the immune system is able to eradicate some early tumours in this stage (Raval et al., 2014). The equilibrium phase is characterised by immunoediting in which tumour proliferation and mutation attempt to reduce tumour antigenicity and subsequent immune recognition and response (Dunn et al., 2004). A reduction in antigenicity can occur due to mutation of immunogenic tumour antigen or dysfunction of antigen presentation including loss of major histocompatibility complex (MHC) expression or loss of antigen processing machinery (Schreiber et al., 2011). However, despite immunosurveillance, certain tumours may evade this state of balance and escape to form clinically significant cancer (Dunn et al., 2004). Tumour evasion of the immune system is now recognised as a hallmark of cancer (Hanahan and Weinberg, 2011). The complex interplay between the immune system and crosstalk between the immune system and the tumour is detailed in Figure 1.5.

By understanding mechanisms involved, a new age of immunotherapies has been developed in the oncology space, harnessing the body's own immune system as an anti-cancer tool (Zhang and Chen, 2018). Tumours can utilise inhibitory checkpoint pathways, typically involved in limiting T-cell activation and duration of immune response, therefore evading immune-mediated eradication (Sharpe, 2017). Inhibitors against cytotoxic T-lymphocyte-associated antigen (CTLA-4) and Programmed cell death protein 1 (PD-1) checkpoints have been beneficial in the treatment of metastatic melanoma, lung, bladder, head and neck cancers and haematological malignancies (Weber et al., 2015; Weinstock and McDermott, 2015; Chow et al., 2016; Lesokhin et al., 2016; Lim et al., 2016). Other immune checkpoints include lymphocyte activation gene 3 (LAG-3), T-cell immunoglobulin and mucin domain 3 (TIM-3), T cell immunoglobulin and ITIM domain

(TIGIT) and V-domain Ig-containing suppressor of T-cell activation (VISTA) (Meyers et al., 2005; Yu et al., 2009; Goldberg and Drake, 2011; Lines et al., 2014).

Overexpression of TIM-3, VISTA and PD-L1 in PDAC confers low immunogenicity (Wang et al., 2011; Knudsen et al., 2017; Peng et al., 2017). Despite this overexpression, PDAC has had little response to anti-PD1 immunotherapy (Kabacaoglu et al., 2018).

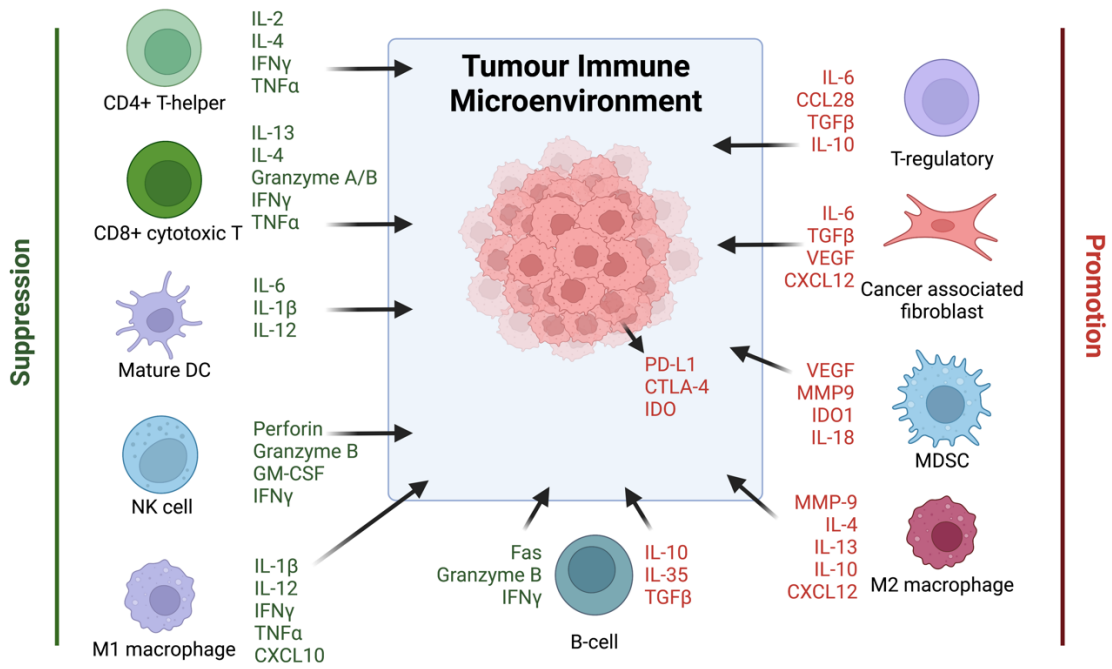


Figure 1.5: Tumour immune microenvironment.
Schematic detailing a broad overview of the tumour immune microenvironment including factors associated with suppression and promotion of the tumour. Solid tumours establish both pro-tumoral and immunosuppressive microenvironments depending on the context of the immune environment. Complex combinations of factors, cytokines and chemokines can influence this microenvironment. Immune cells and factors typically involved in tumour suppression (green) and tumour promotion (red) are depicted. Immune components associated with tumour suppression include CD4+ T-helper cells, CD8+ cytotoxic T-cells, Mature dendritic cells (DC), natural killer (NK) cells and M1 macrophages. Components associated with tumour promotion include T-regulatory cells, cancer associated fibroblasts, myeloid-derived suppressor cells (MDSCs) and M2 macrophages. Programmed death-ligand 1 (PD-L1), cytotoxic T-lymphocyte-associated antigen 4 (CTLA-4) and T-cell immunoglobulin and Indoleamine 2,3-dioxygenase (IDO) immune checkpoint inhibition can lead to immunosuppression, and subsequent immune exclusion. The context of whether immune cells are involved in suppression or promotion of the tumour depend on the tumour microenvironment and cancer type. B-cells have been shown to elicit tumour suppression (green) and tumour promotion (red) as an example of immune cell plasticity in the context of the tumour microenvironment.

1.10 PDAC immune microenvironment

Typically, PDAC is considered a non-immunogenic malignancy considering its multiple means of immune evasion. A low mutational rate is thought to confer low antigenicity and poor immunogenicity in PDAC (Matsushita et al., 2012; Vogelstein et al., 2013). However, other solid tumour malignancies, such as renal and bladder, displayed responsiveness to immunotherapy despite their low mutational burden (Matsushita et al., 2012; Vogelstein et al., 2013). The reduced immunogenicity of PDAC is hypothesised to be due to cancer-cell intrinsic mechanisms, and an immunosuppressive tumour microenvironment (TME) (Figure 1.6). The frequency and variation of immune cell subsets within the PDAC microenvironment has consequential effects on overall prognosis and survival (Kiryu et al., 2021). Understanding drivers of immune cell variation is key to improving outcomes for PDAC patients.

1.10.1 Stromal barrier

The dense desmoplastic stroma accounts for around 50-80% of the total tumour volume and can promote growth, metastasis as well as a physical barrier to immune infiltration (Kleeff et al., 2007; Haqq et al., 2014; Whatcott et al., 2015; Carstens et al., 2017). A reduction in immune infiltrate, and worse patient prognosis, was found in stroma-activation and basal-like tumour PDAC subtypes compared to other subtypes of PDAC (Moffitt et al., 2015; Mahajan et al., 2018; Puleo et al., 2018). As part of the stroma, cancer-associated fibroblasts (CAFs) exist in three distinct subtypes: myofibroblastic CAF (myCAF), inflammatory CAF (iCAF) and antigen-presenting CAFs (apCAFs) (Bernard et al., 2019; Hosein et al., 2019; Dominguez et al., 2020). CAFs have been shown to produce transforming growth factor beta TGFβ, vascular endothelial growth factor (VEGF), interleukin-6 (IL-6) and CXC-chemokine ligand 12 (CXCL12) to confer tumour growth, angiogenesis and immunosuppressive cell recruitment (Matsuo et al., 2009; Ikenaga et

al., 2010; Lonardo et al., 2012; Jacobetz et al., 2013; Wu et al., 2017; Stylianou et al., 2018).

1.10.2 Tumour-associated macrophages

The immunosuppressive microenvironment is dominated by tumour-associated macrophages (TAMs), which can be polarised into M1 or M2 phenotypes (Helm et al., 2014; Zhu et al., 2017; Candido et al., 2018). Toll-like receptor (TLR) ligand or interferon gamma (IFNγ) can stimulate M1-activation, which typically act against intracellular pathogen and drive an anti-tumour response (Helm et al., 2014). Alternatively activated M2 macrophages are elicited by IL-4, IL-10 and IL-13 and can initiate tumorigenesis via promotion of angiogenesis, inflammation and invasion (Kurahara et al., 2011). M2 macrophage involvement has been associated with worse prognosis whereas M1 macrophages were associated with a survival advantage (Ino et al., 2013; Komura et al., 2015). While TAMs have typically been attributed towards an M2 phenotype, macrophage polarisation is plastic and, in this setting, influenced by the tumour microenvironment. Nonetheless, M2-type TAMs have been shown to produce factors including IL-10, TGFβ, IL-6, CCL2, CCL17 and prostaglandin E to inhibit immune cell activity, such as CD8 T-cells, and suppress an inflammatory response (Principe et al., 2016; Daley et al., 2017; Eriksson et al., 2019).

1.10.3 Myeloid Derived Suppressor Cells

Often found in autoimmune disease and various cancers, myeloid derived suppressor cells (MDSCs) are characterised by their myeloid origin and capacity to suppress an inflammatory immune response. Phenotypic and structural characteristics similar to TAMs and neutrophils further subdivide their nomenclature into monocytic-MDSC (M-MDSC) and polymorphonuclear-MDSCs (PMN-MDSC) respectively (Thyagarajan et al., 2019). MDSCs facilitate immunosuppression through secretion of reactive oxygen species

(ROS), Arginase 1 and inducible nitric oxide synthase (iNOS), which inhibits T-cell proliferation, effector T-cell function and IFNγ production (Schmielau and Finn, 2001; Rodriguez et al., 2005; Rodriguez et al., 2007). Mechanisms to suppress T-cell function include inhibition of T-cell JAK3 and STAT5, prevention of MHC II expression and T-cell apoptosis (Bingisser et al., 1998; Rivoltini et al., 2002; Harari and Liao, 2004). Stromnes et al found that selective depletion of MDSCs in PDAC GEMMs allowed restoration of the adaptive immune response to target tumour cells (Stromnes et al., 2014). Clinically, PMN-MDSC were found to be the dominant phenotype in PDAC compared to healthy and chronic pancreatitis patient controls (Khaled et al., 2014). Furthermore, MDSC elevation in the blood and tumour of PDAC patients has been associated with poor survival (Gabitass et al., 2011; Khaled et al., 2014).

1.10.4 T-regulatory cells

Poor patient prognosis, advanced disease presentation and a lower probability of surgical resection, with a poor resection survival rate, is strongly associated with the presence of T-regulatory cells in the PDAC tumour (Ikemoto et al., 2006; Clark et al., 2007b; Hwang et al., 2016; Kiryu et al., 2021). T-regulatory cells can suppress an adaptive immune response, as demonstrated via an inverse relationship between the presence of T-regulatory cells and a reduction in CD8+ effector T-cells in the PDAC tumour, contributing towards poor clinical prognosis (Carstens et al., 2017). In orthotopic PDAC models, chemokine ligand 5 (CCL5) and TGFβ have been shown to recruit T-regulatory cells and facilitate their differentiation from CD4+CD25- naïve T-cells (Moo-Young et al., 2009; Tan et al., 2009; Wang et al., 2017). Experimentally, T-regulatory cell secretion of cytokines, including TGFβ and IL-10, result in inhibition of effector T-cell function, promotion of T-regulatory cell proliferation, inhibition of dendritic cell (DC) antigen presentation, reduction of natural killer (NK) cell function and promotion of M2 macrophage development (Ghiringhelli et al., 2005; Gao et al., 2017; Kelly et al., 2018; Pu et al., 2018b).

1.10.5 CD8 T-cells

Infiltration of CD8+ effector T-cells is associated with positive prognosis in PDAC patients (Fukunaga et al., 2004; Carstens et al., 2017; Kiryu et al., 2021). Variation in T-cell heterogeneity within the PDAC microenvironment has been associated with variation in patient prognosis and survival (Carstens et al., 2017; Kiryu et al., 2021). While effector T-cell cytotoxic activity can eliminate malignant cells via IFNγ-mediated macrophage activity, mechanisms of effector T-cell exhaustion in PDAC prevent can prevent such activity (Nathan et al., 1983; Schreiber et al., 1983). Elevation of inhibitory receptors PD-1, TIGIT and CTLA-4 was detected on tumour-infiltrating lymphocytes in the PDAC tumour (Meng et al., 2016; Steele et al., 2020). Binding of cognate receptor, present on cancer cells or immunosuppressive cells, elicits a reduction in effector T-cell function and proliferation (Rahn et al., 2019; Saka et al., 2020)

1.10.6 B-cells

To date, the role of B-cells in the PDAC microenvironment has been contradictory. Infiltration of CD20+ B-cells has been associated with improved survival and prognosis in PDAC patients (Tewari et al., 2013). Through an effective adaptative immune response against tumour, B-cells can facilitate antigen presentation, prime T-cells and generate anti-tumour antibodies (Donepudi et al., 2003; Schilbach et al., 2004). Murine models of PDAC have also demonstrated B-cell activation through germinal centre entry, B-cell memory and plasma cell differentiation and tumour-infiltrating B-cell upregulation of proinflammatory CXCL1, CXCL2 and CXCL5 (Spear et al., 2019). However, elevation in B-cell activation factor has been associated with PDAC metastasis (Koizumi et al., 2013). Indeed, B-cells have been shown to contribute towards tumorigenesis through promotion of M2 macrophage differentiation and inhibiting T-cell response against tumours (Shah et al., 2005; Andreu et al., 2010; Gunderson et al., 2016; Lee et al., 2016b). In recent years, investigation regarding B-regulatory cell secretion of immunosuppressive TGFβ and IL-10

has demonstrated immunoregulatory functions of this B-cell subtype (Blair et al., 2010; Carter et al., 2011; Nouël et al., 2015). Elevation of plasma IL-18 has been shown in PDAC patients (Guo et al., 2016). Subsequently, elevated IL-18 was shown to induce B-regulatory cell proliferation, IL-10 secretion and PD-1 expression to promote decreased T-cell effector functions in PDAC (Zhao et al., 2018).

1.10.7 Other immune subsets

A reduction in circulatory NK cells, as well as NK activating receptors CD226 and CD96, were found in PDAC patients compared to healthy controls (Bang et al., 2006; Peng et al., 2016). Subsequent analysis of these circulatory NK cells revealed dysfunction in C-X-C Motif Chemokine Receptor 2 (CXCR2), hypothesised to prevent PDAC tumour infiltration (Lim et al., 2019). Furthermore, CAFs in the PDAC stroma have shown to decrease expression of IFNγ, perforin and granzyme B in NK cells upon *in vitro* co-culture (Huang et al., 2019). These studies would suggest NK dysfunction and may be involved in promotion of PDAC.

Circulating dendritic cells (DC) in the peripheral blood of PDAC patients are decreased in frequency and impairment of function (Yanagimoto et al., 2005; Tjomsland et al., 2011). In addition, reports of a positive correlation between DC infiltration, infiltration of CD4/CD8 T-cells and a positive prognosis in PDAC (Fukunaga et al., 2004).

Other immune cells associated with poor prognosis include tumour-associated neutrophils (TANs), mast cells, Th2 CD4 T-cells, while the association between γδ T-cells and PDAC is still unclear (Protti and De Monte, 2013; Felix and Gaida, 2016; Hwang et al., 2016; Seifert et al., 2020). Studies have shown contradictory roles for Th17 CD4 T-cells. They have been associated with advanced patient disease, while opposing studies have shown increased survival in PDAC murine models (Gnerlich et al., 2010; He et al., 2011).

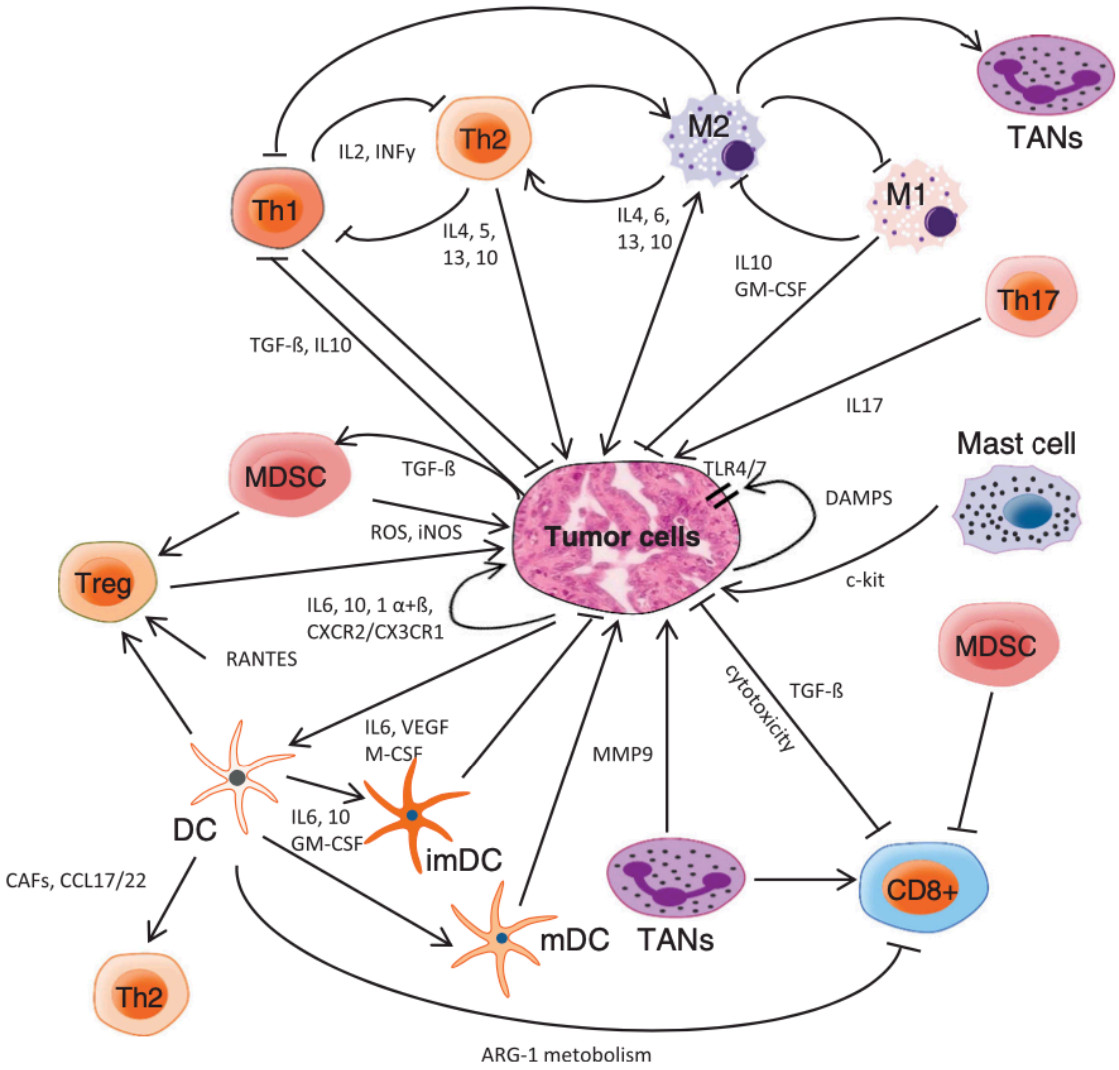


Figure 1.6: The immune network in PDAC.
The immune network in pancreatic cancer is dynamic and complex. Tumour-infiltrating immune cells act in complex, synergistic and opposing ways with other immune cells and tumour cells. The immune response is influenced by cytokines and chemokines derived from PDAC tumour cells (e.g., IL-6, IL-1, IL-10) or other immune cells (e.g., IL-4, IL-5, IL-13, IFNγ). Figure taken from (Wörmann et al., 2014). Reprinted with permission from Springer Nature, license number: 5454170356406.

1.10.8 Immunotherapeutic perturbations

While immunotherapeutic interventions have been beneficial in other cancers, very little benefit has been translated to PDAC due to its complex immune microenvironment. Clinical trials for therapies targeting the tumour microenvironment are detailed in Table 1.2.

Table 1.2: Novel therapies for advanced PDAC in clinical trial.

Clinical Trial ID	Mechanism	Study Agents	Setting
NCT02907099	CXCR4 antagonist. Inhibition of macrophage and MDSC suppression by blocking CXCL12 binding to CXCR4.	Motixafortide	Combination with PD-1 inhibitor.
NCT04060342	Myeloid cell recruitment	GB1275	Combination with PD-1 inhibitor, gemcitabine and nab-paclitaxel
NCT03214250	CD40 agonist. Promotes DC priming of T-cells through CD40/CD40 ligand binding.	Sotigalimab	Combination with PD-1 inhibitor, gemcitabine and nab-paclitaxel
NCT03006302	IDO1 inhibitor.	Epacadostat	Combination with pembrolizumab, CRS-207 +/- C/GVAX
NCT04262388	Adenosine antagonist by A2AR blockade. Inhibits suppression of immune cells through CD73 binding	Oleclumab	Combination with durvalumab.
NCT04104672	Adenosine antagonist by CD73 inhibition.	AB680	Combination with gemcitabine and nab-paclitaxel, AB122
NCT03766295	Mast cell inhibition.	Masitinib	Combination with gemcitabine with or without masitinib.

IDO1; indoleamine 2,3-dioxygenase 1, A2AR; adenosine 2 A receptor, CRS-207; attenuated listeria bacteria, C/GVAX; cyclophosphamide/GVAX vaccine.

1.11 Immune microenvironment of PanIN lesions

Oncogenic KRAS elicits early neoplasia by driving ADM and early PanIN lesion formation through the engagement of inflammatory pathways such as STAT3 signalling in KC GEMMs (Corcoran et al., 2011). In a pancreas-specific, inducible murine model of oncogenic $Kras^{G12D}$, IL-6 proinflammatory cytokine was found to synergise with oncogenic KRAS to activate reactive oxygen species and downstream MAPK/ERK signalling to further PanIN progression (Zhang et al., 2013b). Murine studies have demonstrated the role of inflammatory macrophages in the initiation and development of PanIN lesions (Liou et al., 2013; Liou et al., 2015b; Liou and Storz, 2015). In caerulein-induced murine models of pancreatitis and $p48^{cre}$;LSL-$Kras^{G12D}$ murine models of PDAC, macrophage secretion of TNF and CCL5 and matrix-metalloproteinase 9 facilitated ADM (Liou et al., 2013; Liou et al., 2015b). Furthermore, oncogenic *KRAS* low-grade ADM/PanIN-1 secrete IL-13 to polarise macrophages from an inflammatory to an alternatively activated (M2) phenotype in a $p48^{cre}$;LSL-$Kras^{G12D}$ murine model of PDAC (Liou et al., 2017a).

Pylayeva-Gupta et al showed oncogenic $KRAS^{G12D}$-depedent upregulation of GM-CSF was found in PDAC GEMM and human PanIN lesions and subsequently found to recruit myeloid cells, including macrophages, *in vivo* (Pylayeva-Gupta et al., 2012). Macrophages are present during early PanIN lesion development and are a major source of IL-6 in PanIN lesions of KC GEMMs (Clark et al., 2007a; Lesina et al., 2011).

Type 1 conventional dendritic cells (cDC1s) are professional antigen presenting cells for effective T-cell priming (Böttcher and Reis e Sousa, 2018). Lin et al found cDC1 dysfunctionality during PanIN lesion progression, prior to invasive carcinoma, in a KPC GEMM (Lin et al., 2020b). Apoptosis of systemic cDC1s was driven through elevated IL-6 in the serum, resulting in impairment to CD8 T-cell priming at early stages of neoplasia (Lin et al., 2020b). Similar paucity of cDC1s has also been documented in later-stage

PDAC in a *p48-Cre*;*Kras*$^{LSL\text{-}G12D}$;*Trp53*$^{fl/+}$;*R26*$^{tm1(LSL\text{-}OG)}$ murine model (Hegde et al., 2020). However, patient PDAC samples containing higher levels of cDCs had better disease-free survival and overall survival (Plesca et al., 2022). T-cells from cancer patients, including PDAC, have shown peptide recognition of oncogenic KRAS (Linard et al., 2002; Gjertsen et al., 2003; Kubuschok et al., 2006; Wang et al., 2016). However, it is unclear whether this peptide recognition occurs at early stages of PanIN progression, upon initial *KRAS* mutation, and whether this is confined to patients that have functional cDC1s for effective antigen presentation.

Together, these studies demonstrate the role oncogenic *KRAS* may have in eliciting immune-stimulatory pathways early in PanIN lesion progression, thus influencing the immune landscape that may allow further progression.

During the transition from low to high-grade PanIN lesions, *TP53* mutation frequently occurs during PanIN-3 lesion acquisition in human PDAC tumour samples (Maitra et al., 2003). KPC GEMMs, containing *Kras*^{G12D} and *Trp53*^{R172H} mutations, alongside p53-deficient tumours, showed similar STAT3-dependent immune evasion, resulting in tumour growth (Wörmann et al., 2016). Tumour cells had an accumulation of reactive oxygen species, reduced phosphatase SHP2 and prolonged JAK2 phosphorylation compared to KC GEMMs with functional *Tp53* (Wörmann et al., 2016). (Cooks et al., 2013). This *TP53* mutant restructuring of the immune microenvironment can increase tumour-infiltrating macrophages, neutrophils, T-regulatory cells, while simultaneously reducing CD8+ effector T-cells, through JAK-STAT signalling in KC mice and patient pancreatic tumour stroma (Wörmann et al., 2016). In addition, loss of p53 has been shown to activate NF-κB signalling to stimulate cancer cell production of pro-inflammatory cytokines, such as TNFα, in other human cancer cell lines and murine models (Cooks et al., 2013; Schwitalla et al., 2013). These studies indicate loss of p53 function may elicit dynamic changes to the PanIN lesion immune microenvironment, further perpetuating tumorigenesis.

Additional studies surrounding immune-infiltrate during PanIN lesion progression has also contributed towards better understanding of this immune-neoplasia axis. CD19+CD1d^{high}CD5+ B-cells were associated with PanIN lesions in the pancreata of human patient and murine KC GEMM samples. They were found to instigate tumorigenesis and through production of IL-35 (Pylayeva-Gupta et al., 2016). Additional studies are required to better understand B-cell functionality and the point at which they become involved in PanIN progression. These studies may elucidate previous, contradictory reports regarding the pro-tumorigenic and anti-tumorigenic roles B-cells play in later PDAC.

Overall, a better understanding of the immune microenvironment surrounding PanIN lesion progression is required to further understanding of these interactions, how the immune microenvironment may contribute towards neoplasia, and later carcinoma, and ultimately aid intervention strategies earlier in malignancy.

1.12 Aims of this study

1. Develop and optimise a 17-colour flow cytometry panel to examine peripheral blood and tumour immune infiltrate in established models of PDAC

2. Perturb the immune microenvironment of established PDAC murine models using combination of immunotherapies and radiotherapy to elucidate whether this alters PDAC tumour volume and the tumour immune microenvironment.

3. Investigate the immune microenvironment surrounding low and high-grade PanIN lesion development, in response to oncogenic *Kras* mutation, in a KC murine model.

4. Understand MDSC involvement during precursor PanIN lesion development towards PDAC.

5. Evaluate systemic immune drivers of PanIN progression.

2. Materials and Methods

2.1 Materials

2.1.1 Mouse strains

Genetically modified *Kras*$^{LSL.G12D+-}$*; Pdx-1-Cre* (KC) mice were previously described (Hingorani et al., 2003). Male KC mice and female *Pdx-Cre* only mice were kindly provided by Dr Paul Miller from Prof Xin Lu's laboratory (Ludwig Cancer Research Institute, University of Oxford) for crossbreeding. Genetically modified *Kras*$^{LSL.G12D+-}$*; Trp53*$^{LSL.R17H+}$*; Pdx-1-Cre* (KPC) were previously described (Hingorani et al., 2005). KPC mice were kindly provided by Dr Edward O'Neill from Dr Bart Cornelissen's laboratory (Oxford Institute for Radiation Oncology). For the generation of the orthotopic PDAC model (Section 2.6), C57BL/6J mice were acquired from The Jackson Laboratory and acclimatised for 1 week prior to orthotopic generation.

All animal studies were performed, in accordance with the UK Animals (Scientific Procedures) Act of 1986, under a project license (PF0F1EF6E) approved by the UK Home Office and with the University of Oxford ethical review committee. Animals were housed in environmentally enriched IVC cages. This included activity wheel or crawl ball, nesting material and chew sticks with a group of 5 mice per cage. The animal house was maintained in a 12-hour day-night cycle facility at 22°C and in 50% humidity. All mice had *ad libitum* access to certified food and tap water.

2.1.2 General laboratory reagents

All chemicals were purchased from Sigma-Aldrich or Thermo Fisher, unless stated otherwise, and used according to manufacturer's guidelines. Tissue culture plastic was purchased from Corning and Sarstedt. Glassware was purchased from VWR and Thermo Fisher.

Table 2.1: List of chemical reagents.

Name	Provider and Catalogue Number
Benzonase® Nuclease	Merck Millipore; 9025-65-4
Bovine Serum Albumin (BSA)	Sigma-Aldrich UK; A3059-100G
Citrate Buffer	Sigma-Aldrich UK; C9999
cOmplete™ protease cocktail inhibitor tablets	Roche; 4693116001
Dimethyl sulfoxide (DMSO)	Sigma-Aldrich UK; D8418-250
Diothiothreitol (DTT)	Merck Millipore; 73021
Ethanol (EtOH)	Fisher Scientific; 10437341
Ethylenediaminetetraacetic acid (EDTA)	Thermo Fisher; AM9261
Glycine	Fisher Scientific; 10754724
Lithium carbonate	Sigma-Aldrich UK; 554-13-2
Methanol (MeOH)	Fisher Scientific; M-4000-17
Milk Powder	Sigma-Aldrich UK; M7409-1BTL
Neutral buffered formalin (NBF)	Sigma-Aldrich UK; HT501128-4L
NuPAGE® MOPS SDS Running Buffer (20X)	Thermo Fisher; NP000102
PageRuler™ Prestained Protein Ladder	Thermo Fisher; 26620
Phosphate buffered saline (PBS) tablets	Oxoid; BR0014G
PhosSTOP™ phosphatase inhibitor cocktails	Roche; 4906845001
RIPA Lysis and extraction buffer	Thermo Fisher; 89900
Tris base	Fisher Scientific; 10103203
Tween-20	Sigma-Aldrich UK; 9005-64-5

2.1.3 Buffers and solutions

Table 2.2: List of buffers and their composition.

Buffer	Composition
1X Citrate buffer	10X Citrate buffer in dH_20 with 0.05% Tween-20 [10X = sodium citrate dihydrate (0.825 M), citric acid (0.175 M) to pH 6 with HCL]
PBS	10 PBS tablets in 1 litre dH_20, pH ~ 7.4 [1X concentration]
PBS-T	PBS with 0.1% (v/v) Tween-20
PBS-T (0.05%)	PBS with 0.05% (v/v) Tween-20
1X Running buffer [Western blotting]	20X NuPAGE® MOPS SDS running buffer in dH_20
1X Transfer buffer [Western blotting]	10X Tris/Glycine buffer in dH_20 with 20% (v/v) methanol [10X = Tris (250 mM), glycine (1.92 M), pH 8.3]
1X Washing buffer [Immunohistochemistry]	1X PBS with 0.05% (v/v) Tween-20
ACD buffer	0.5M D(+)-glucose, 0.5M Trisodium citrate, 0.5M citric acid in dH_20
Acid Alcohol	1% (v/v) HCL in 70% (v/v) ethanol
Blocking buffer and antibody incubation buffer [Western blotting]	5% (w/v) milk powder in PBS-T
FACS buffer [Flow-cytometry]	2% FBS, 1 mM EDTA in PBS
Lithium carbonate	0.5% (v/v) lithium carbonate in dH_20
MACS buffer	2mM EDTA, 0.5% BSA in PBS
Protein lysis buffer	1X RIPA lysis buffer, 1X protease inhibitor cocktail, 1X phosphatase inhibitor cocktail, Benzonase® Nuclease (1:1000)

Table 2.3: Pancreas dissociation Buffer.

All dissociations were made up in HBSS media (Gibco).

Enzyme	Supplier	Concentration
Collagenase P	Worthington	1:100
DNase	ThermoFisher	1:400

Table 2.4: Tumour dissociation Buffer.

All dissociations were made up in HBSS media (Gibco).

Enzyme	Supplier	Concentration
Collagenase I	Worthington	1:100
Collagenase II	Worthington	1:100
Collagenase IV	Worthington	1:100
DNase	ThermoFisher	1:400

2.1.4 qPCR primers

Table 2.5: List of qPCR primers.

Target	5' → 3' Sequence	Provider
Ebi3	Forward: CCCTACATGCTAAATGTCAC Reverse: ACTTGAGAGAGAAGATGTGT	Sigma Aldrich
Gapdh	Forward: CATCACTGCCACCCAGAAGACTG Reverse: ATGCCAGTGAGCTTCCCGTTCAG	Invitrogen
Il12a	Forward: GAAGACATCGATCATGAAGAC Reverse: CTCTTGTTGTGGAAGAAGTC	Sigma Aldrich
Il12rb2	Forward: CCTCTAAGCTACATCTCTCTG Reverse: ATGGATTCAGACTCTTCCAG	Sigma Aldrich
Gp130	Forward: ACATACGAAGACAGACCATC Reverse: CGTACAGATCTATATTCCTGC	Sigma Aldrich

2.1.5 Antibodies

Table 2.6: Primary and secondary antibodies for immunohistochemistry.

Square brackets indicate antibody species and clone.

Primary Antibody	Provider	Catalogue number	Dilution	Antigen retrieval (Boiling/Sub-boiling temperature)
CD19 [Rabbit; EPR23174]	Cell Signalling Technology	86916	1:800	125°C, 2-minutes/ 90°C, 1-minute/
Ly-6G/Ly6C (GR-1) [Rat; RB6-8C5]	R&D	MAB1037-100	1:100	125°C, 2-minutes/ 90°C, 1-minute
Secondary Antibody	**Provider**	**Catalogue number**		
HRP-labelled polymer ant-Rabbit	Dako EnVision+ System	K4003		

Table 2.7: Primary and secondary antibodies for immunofluorescence.

Primary Antibody	Provider	Catalogue number	Dilution	Opal fluorophore pairing
Ly6G	Abcam	ab238132	1:2000	Opal 480
NK1.1	Abcam	ab234107	1:2000	Opal 520
CD8	Cell Signalling	98941	1:800	Opal 570
LARP6	Invitrogen	PA5-24317	1:400	Opal 620
SMA	Abcam	ab5694	1:1000	Opal 690
CD68	Abcam	ab125212	1:500	Opal 780
TIGIT	Biorbyt	orb692212	1:2000	Opal 690
NKG2D	Abcam	ab203353	1:600	Opal 520
CD161	Abcam	ab234107	1:20000	Opal 620
CD3	Abcam	ab5690	1:600	Opal 570
CD8	Cell Signalling	98941	1:800	Opal 570
E-Cadherin	Cell Signalling	3195	1:500	Opal 780

Table 2.8: Primary and secondary antibodies used for Western blotting.
Square brackets indicate antibody species and/or clone.

Primary antibody	Provider	Catalogue number	Dilution
αTubulin [Rabbit]	Cell Signalling Technology	4370	1:1000
p44/42 MAPK (Erk1/2) [Mouse; L34F12]	Cell Signalling Technology	97166S	1:1000
pERK (T202/Y204) [Rabbit; D13.14.4E]	Cell Signalling Technology	4370S	1:1000
p53 [Mouse; 1C12]	Cell Signalling Technology	2524	1:1000
Secondary Antibody	**Provider**	**Catalogue number**	**Dilution**
Donkey anti-rabbit 800CW	LI-COR	926-32213	1:5000
Donkey anti-mouse 680CW	LI-COR	926-68072	1:5000

Table 2.9: Antibodies used for CFSE assay.

Antigen	Clone	Fluorochrome	Supplier	Catalogue number	Concentration
Live/Dead	-	LIVE/DEAD Near-IR	Thermo Fisher	L10119	1:200
CD45	30-F11	BV421	BioLegend	103133	1:200
CD8	SK1	PeCy7	BioLegend	344712	1:200
CD3	17A2	APC	Thermo Fisher	17-0032-82	1:200

Table 2.10: Antibodies used in 17-colour flow cytometry panel.

*Indicates antibody not used in final optimised panel

Antigen	Clone	Fluorochrome	Supplier	Catalogue number	Concentration
*Live/Dead	-	Zombie Yellow	ThermoFisher	L34968	1:2000
Live/Dead	-	LIVE/DEAD Blue	ThermoFisher	L23105	1:1000
CD45	30-F11	AF532	ThermoFisher	58-0451-80	1:50
CD19	1D3	SB436	ThermoFisher	62-0193-80	1:50
CD3	17A2	eF450	BioLegend	48-0032-80	1:50
NK1.1	PK136	BV650	BioLegend	108735	1:25
CD8a	53-6.7	BV570	BioLegend	100739	1:25
CD4	RM4-5	BV510	BD Biosciences	100553	1:100
CD25	7D4	AF647	BD Biosciences	563598	1:100
FOXP3	FJK-16s	PE	ThermoFisher	12-5773-80	1:20
CD206	C068C2	BV785	BD Biosciences	141729	1:25
F4/80	T45-2342	BV480	BD Biosciences	565635	1:100
CD80	REA983	APC	Miltenyi Biotech	130-116-46	1:100
CD279 (PD-1)	J43	PE-Cy7	ThermoFisher	25-9985-82	1:25
CD195 (CCR5)	REA354	VB-FITC	Miltenyi Biotech	130-105-141	1:20
CD11b	M1/70	AF700	BioLegend	101222	1:100
Ly6C	HK1.4	PE-Dazzle	BioLegend	128043	1:200
Ly6G	1A8	BV421	BioLegend	127627	1:25

2.1.6 Cell lines and cell culture reagents

Table 2.11: List of cell lines.

Table indicates mutation status of *Kras* and *Tp53*.

Name	Tissue Origin	Source	*Kras*	*Tp53*
KPC	Mouse pancreatic ductal adenocarcinoma	Prof Jennifer Morton, Beatson Institute of Cancer Research, University of Glasgow	G12D	R172H
L929	Mouse fibroblasts derived from adipose tissue	Dr Keaton Jones, Department of Oncology, University of Oxford	-	-

Table 2.12: Cell culture reagents and supplements.

Name	Provider
2-mercaptoethanol	Sigma-Aldrich
DMEM	Life Technologies
Foetal bovine serum	Sigma-Aldrich
GlutaMAX™	Thermo Fisher Scientific
Glutamine	Life Technologies
Penicillin/Streptomycin	Life Technologies
Recombinant Mouse IL-2 Protein	BioLegend
RPMI	Life Technologies
Trypsin-EDTA	Life Technologies

Table 2.13: Cell culture reagents and supplements for Mouse Complete Feeding Media for organoid culture.

Component	Provider	Final Concentration
1M HEPES (100X)	Sigma-Aldrich	1X
A83-01 (TGF-β inhibitor)	TOCRIS	0.5 µM (0.21 µg/mL)
Advanced DMEM/F-12	Thermo Fisher	Life Technologies
B27 supplement 50X (serum-free)	Thermo Fisher	1X
EGF Recombinant Mouse Protein	Thermo Fisher	0.05 µg/mL
Gastrin I	TOCRIS	0.01 µM (0.21 µg/mL)
GlutaMAX Supplement (100X)	Thermo Fisher	1X
mNoggin	Peprotech	0.1 µg/mL
N-Acetylcysteine	Sigma-Aldrich	1.25 µM (0.2 µg/mL)
Nicotinamide	Sigma-Aldrich	10 mM (1.22 mg/mL)
Penicillin/Streptomycin (100X)	Thermo Fisher	1X
R-spondin-conditioned media	TREVIGEN®	10%
Recombinant FGF	Peprotech	0.1 µg/mL

2.2 Cell culture

KPC pancreatic cancer cells and L929 fibroblasts (Table 2.11) were cultured in Dulbecco's Modified Eagle Medium (DMEM) supplemented with 10% Foetal Bovine Serum (FBS), 2 mM Glutamine, and Penicillin/Streptomycin (100 U/ml) [Complete DMEM]. Cells were incubated at 37°C and 5% CO_2. Cells stored in liquid nitrogen (LN) were defrosted by placing them in a 37°C water bath for 2-minutes. Once thawed, cells were resuspended in Complete DMEM. To remove leftover Dimethyl sulfoxide (DMSO) from freezing media, cells were centrifuged at 400 x g for 5-minutes at room temperature and pressure (RTP). Unless stated otherwise, all centrifugations were carried out under these conditions. Cell

pellets were resuspended in 10 mL of Complete DMEM and seeded into a T75 flask. To passage cells, sub-confluent cultures were washed in PBS and incubated with 0.25% Trypsin-EDTA solution. Detached cells were resuspended in Compete DMEM and reseeded into new tissue culture flasks at a 1:10 ratio. Cells stocks were routinely generated and stored in the vapour phase of a LN tank. In preparation, cells were resuspended in freezing media [90% (v/v) FBS, 10% (v/v) DMSO] in aliquots (>1x10^6 cells in 1 mL freezing media) in Cryovials (Corning®). Cryovials were placed in a Mr Frosty (Nalgene®) containing 200 mL isopropanol at RTP and frozen at -80°C for 24 hours before transferring to LN for long-term storage. All cell culture procedures, including primary cell culture (Section 2.2.1), organoid cell culture (Section 2.2.2), bone-marrow derived myeloid suppressor cell (Section 2.2.3), KC myeloid derived suppressor cells (Section 2.2.4) and CFSE assay (Section 2.2.5), were conducted under sterile conditions in a Class II Biological Safety Cabinet.

2.2.1 Primary cell culture

A single cell suspension of splenocytes was isolated from dissected spleens (Section 2.7 by using a 40 µM cell strainer (Gibco) and pressure applied using the plunger of a 5 mL-syringe (BD). The cell strainer was washed with 30 mL PBS and centrifuged at 300 x g for 10-minutes at RTP. Splenocytes were counted by mixing 0.4% trypan blue solution (Thermo Fisher) with cell suspension at a 1:1 ratio before transferring to a Countess® Cell Counting Chamber Slide (Thermo Fisher). Cells were counted using a Countess® Automated Cell Counter (Thermo Fisher). Unless stated otherwise, all cell counting was carried out using this method. Further cell isolations were conducted using the EasySep™ Mouse B-cell Isolation Kit (StemCell™) or EasySep™ Mouse CD8+ T-cell Isolation Kit (StemCell™) using an EasySep™ magnet (StemCell™). B-cells were taken for RNA extraction (Section 2.4). CD8+ T-cells were then used for CFSE assays (Section 2.2.5).

Isolated bone marrow (BM) (Section 2.7) was centrifuged at 300 x g for 10-minutes and resuspended in either complete DMEM supplemented with 15% L929 supernatant[1] for BM-derived macrophage (BMDM) polarisation, or complete DMEM supplemented with IL-6 (2.5 µg/mL; Peprotech) and GM-CSF (2.5 µg/mL; Peprotech) for myeloid-derived suppressor cell (MDSC) generation. Cells suspensions were plated into non-TC treated Nunc™ plates (Thermo Fisher) at the appropriate cell density and polarised for 5 days at 37°C and 5% CO_2. Cells were then taken for CFSE assay (Section 2.2.5), RNA (Section 2.4) or protein (Section 2.3.1) isolation.

2.2.2 Organoid culture

Organoids were previously isolated from heterozygous KC mice (Het; *Kras$^{LSL.G12D+-}$; Pdx-1-Cre+)* and wild-type *(WT; Kras$^{LSL.G12D-/-}$; Pdx-1-Cre+)* by Dr Fiona Bangs and Dr Asmita Thapa and stored in LN. Organoids were passaged by removing media and isolating organoids suspended in Matrigel® (Corning) using ice-cold Advanced DMEM/F-12 supplemented with 1 M (w/v) HEPES, GlutaMAX and Penicillin/Streptomycin (100 U/mL) [Splitting media] and mechanical disruption using a pipette tip. Organoids were centrifuged at 150 x g for 5-minutes at 4°C and resuspended using a 23-guage needle (BD) attached to a 5 mL syringe to dislodge any remaining Matrigel®. Organoids were resuspended in ice-cold splitting media and centrifuged at 150 x g for 5-minutes at 4°C. The organoid pellet was then resuspended in ice-cold Matrigel® and pipetted onto a 24-well plate. The Matrigel® dome was left to harden at 37°C for 5 – 15-minutes and 250 µL warmed Complete Feeding Media (Table 2.13) was added to the well. Media was supplemented with Rho Kinase Inhibitor Y-27632 (Sigma-Aldrich) at a final concentration

[1] L929 supernatant was used as a source of macrophage colony stimulating factor (M-CSF)

of 10.5 μM for WT organoids or for two passages post-thaw. Organoids were cultured at 37°C and 5% CO_2.

2.2.3 Bone-marrow derived myeloid suppressor cells

BM was isolated and polarised into BMDM or MDSCs as previously described (Section 2.7, 2.2.1). Five days after BM isolation and polarisation, BMDM and MDSCs were detached using 0.25% Trypsin-EDTA for 10-minutes at 37°C and scraped using a sterile, disposable rubber scraper (Sarstedt). Cells were counted and 40,000 cells for each condition were plated in triplicate with CD8+ T-cells (Section 2.2.5).

2.2.4 KC myeloid derived suppressor cells

KC and KPC spleens were dissected and splenocytes isolated as previously described (Section 2.2.1). Gr-1^{high}Ly6G+ and Gr-1^{dim}Ly6G- myeloid cells were isolated from cell suspensions using the Myeloid-Derived Suppressor Cell Isolation Kit (Miltenyi) following manufacturer's instructions. In brief, cells were counted and centrifuged at 300 x g for 10-minutes at 4°C; all centrifugations were carried out under these conditions for this protocol. Cells were resuspended in MACS buffer (Table 2.2), blocked with FC-block for 10-minutes at 4°C and incubated with Anti-Ly6G-Biotin for 10-minutes at 4°C, washed with MACS buffer and centrifuged; MACS buffer was used for all subsequent washes. Cells were resuspended in MACS buffer and incubated with Anti-Biotin Microbeads for 15-minutes at 4°C, washed and applied to an LS-column (Miltenyi) for positive selection using a MidiMACS™ magnetic separator (Miltenyi). Columns were washed three times, removed from the magnet, and flushed with MACS buffer to isolate the Gr-1^{high}Ly6G+ fraction. The elution was centrifuged, resuspended in MACS buffer, and incubated with Anti-Gr-1-

Biotin for 10-minutes at 4°C, washed and resuspended in MACS buffer and incubated with Steptavadin Microbeads for 15-minutes at 4°C. Cells were washed, centrifuged, and placed into MS-columns (Miltenyi) for a second positive selection on a MiniMACS™ magnetic separator. Columns were washed three times, removed from the magnet, and flushed with MACS buffer to isolate the Gr-1^{dim}Ly6G- fraction. Cells were then used in the CFSE assay (Section 2.2.5).

2.2.5 *Ex vivo* CFSE assay

CD8+ T-cells, previously isolated from splenocytes (Section 2.2.1), were counted and centrifuged. A fraction of T-cells was incubated with CellTrace™ CFSE Proliferation Kit (Thermo Fisher) [PBS: CFSE; 1:1000] in the dark at 37°C, 5% CO_2 for 20-minutes. Roswell Park Memorial Institute (RPMI) 1640 medium supplemented with 10% heat-inactivated[2] FBS, 2mM Glutamine, 50 μM 2-mercaptoethanol, 2 mM Glutamine, Penicillin/Streptomycin (100 U/mL) and recombinant mouse IL-2 (500 U/mL) [T-cell media], was then added, at five times the volume, and incubated for a further 10-minutes under the same conditions. CFSE+ and CFSE- CD8+ T-cells were then centrifuged and resuspended in fresh T-cell media and seeded into a TC-treated, low-evaporation, 96-well plate (VWR), that was had previously been coated with anti-CD3 (2.5 μg/mL; BD) and anti-CD28 (2.5 μg/mL; BD) (overnight at 4°C), at the either 20,000 cells/well or 40,000 cells/well. T-cells were then co-cultured with either BM-derived MDSCs (Section 2.2.3) or Gr-1^{high}Ly6G+/Gr-1^{dim}Ly6G- myeloid cells isolated from KC or KPC splenocytes (Section 2.2.4). Plates were incubated in the dark at 37°C, 5% CO_2 for 3 days and then processed for flow cytometry (FC) (Section 2.12).

[2] Heat inactivation was carried out at 56°C for 30-minutes to deactivate complement proteins

2.3 Western blotting

2.3.1 Protein extraction

BMDM and MDSCs were detached using 0.25% Trypsin-EDTA for 10-minutes at 37°C and scraped using a sterile, disposable rubber scraper. BMDM, MDSCs and KPC cells were washed twice with ice-cold PBS and cell pellets were lysed on ice for 30-minutes with protein lysis buffer (Table 2.2), vortexing every 10-minutes. Lysates were then spun down at 16,000 x g for 15 minutes at 4°C and supernatants were transferred to fresh Eppendorf tubes.

Organoids embedded in the Matrigel® dome were washed twice in ice-cold PBS and 500 µL of Cell Recovery Solution (Corning) was added onto the dome and dislodged via gentle pipetting. The cell suspension was transferred to 2 mL Eppendorf's and left on ice at 4°C for 1 hour to allow the release of organoids from the Matrigel®. Cell suspensions were then centrifuged at 3000 x g for 3-minutes at 4°C and washed in ice-cold PBS twice. Protein lysis buffer was then added to the organoid pellets and lysis was carried out as previously detailed.

Protein concentration of the lysates was determined using the Pierce BCA (bicinchoninic acid) Protein Assay Kit (Thermo Fisher) using manufacturer's instructions. In brief, 4mg/mL Bovine Serum Albumin (BSA) was diluted with protein lysis buffer to produce an 8-fold standard dilution from 2000 – 62.5 µg/mL. Protein lysis buffer was used as the blank sample. Lysates and standards were pipetted into a 96-well plate in triplicate with the addition of Reagent A and B (A:B; 50:1). The plate was incubated at 37°C for 30-minutes in the dark and absorbance was measured using a POLARstar Omega plate reader at 562 nm. A standard curve was produced using Microsoft Excel and a linear equation was used to determine total protein concentration of each sample with their relative absorbance.

2.3.2 SDS-polyacrylamide gel electrophoresis (SDS-PAGE)

Protein lysates (25-50 μg) were diluted in 4X NuPAGE™ LDS sample buffer (Thermo Fisher), 100 mM DTT and volumes equalised using dH_20. Samples were heated to 95°C for 10-minutes before loading equal protein concentrations onto a NuPAGE® 10% Bis-Tris Gel 1.5 mm (Life Technologies) alongside a Protein Ladder in 1X Running buffer (Table 2.2) and run at 150 V for 1.5 hours.

2.3.3 Immunoblotting

Following SDS-PAGE, proteins were transferred to a nitrocellulose membrane (0.45 μm pore size; *Bio-Rad*) at 100 V for 1.5 hours in 1X Transfer buffer (Table 2.2). Membranes were incubated with Blocking buffer (Table 2.2) for 1 hour at RTP to prevent non-specific binding before incubation with primary antibodies in antibody incubation buffer (Table 2.2) overnight at 4°C. αTubulin was used as the loading control. Information on the primary antibodies used is listed in Table 2.8. Following overnight incubation, membranes were washed in PBS-T three times at 10-minute intervals and incubated with secondary antibodies (Table 2.8) for 1 hour at RTP and washed as previously described. Protein detection was performed using an Odyssey® Infrared Imaging System (LI-COR; software v3.0.30). The bands of interest were selected, and the background border was chosen at width 2. The intensity represented the background-corrected total intensity of the pixels enclosed in the selected area multiplied by the area of the shape. Normalisation was carried out by calculating the ratio between the intensity value for each sample and the corresponding control intensity value.

2.4 RNA isolation and quantitative polymerase chain reaction (qPCR)

RNA isolation was performed on organoid (Section 2.2.2, 2.3.1) and B-cell (Section 2.2.1) samples using the ReliaPrep™ RNA Miniprep Systems (Promega) following manufacturer's instructions. In brief, cells were lysed in BL buffer and TG buffer (4M Guanidine thiocyanate, 0.01M Tris (pH 7.5), 1% 1-Thioglycerol) with 100% isopropanol and lysate nucleic acid bound to ReliaPrep™ Minicolumns by centrifugation at 14,000 x g for 30 seconds. Further incubation with DNase I Solution[3] and subsequent washes with RNA wash solution were performed and RNA eluted from the column with nuclease-free water (Thermo Fisher). RNA concentration was quantified using a NanoDrop 1000 (Thermo Fisher) by measuring the sample absorbance at a wavelength of 260 and 280 nm. Samples were then stored at -80°C or cDNA synthesis was directly performed using the LunaScript® RT SuperMix Kit (NEB). 1 μg of RNA was added to LunaScript RT SuperMix and nuclease-free water for a final volume of 20 μL. Samples were transferred to a thermocycler (My Cycler, Bio-Rad). Reaction conditions are detailed in Table 2.14.

Table 2.14: Thermocycler reaction conditions for RT PCR.

Cycle Step	Temperature	Time	Cycles
Primer Annealing	25°C	2-minutes	1
cDNA Synthesis	55°C	10-minutes	
Heat Inactivation	95°C	1-minute	

cDNA samples were frozen at -20°C or target gene expression was directly assessed using LunaScript® qPCR Master Kit (NEB). A final reaction concentration 100ng of cDNA

[3] To digest contaminating genomic DNA

was added to 1X Luna Universal qPCR Master Mix, 0.25 μM forward and reverse primers (Table 2.5), made up to a final volume of 10 μL with nuclease-free water. All reactions were performed in duplicate and ran for 45 cycles. Fold change in target mRNA expression was calculated based on the delta-delta cycle threshold (CT) method (Livak and Schmittgen, 2001) after normalisation to GAPDH expression.

2.5 Genotyping

Mouse genotypes from ear biopsies were determined using real time PCR (RT-PCR) with specific probes designed for each gene, *Cre* and *Kras*^{G12D}, by commercial vendor Transnetyx (Cordova, TN).

2.6 Establishment of an orthotopic model

C57BL/6 mice was anaesthetised with 4% Isoflurane/Oxygen. The mouse was then transferred to the nose cone, and Isoflurane reduce to 2%. Eye drops (Viscotears) were applied, and analgesic (5 mg/kg Metacam and 0.1 mg/kg Vetergesic) was administered by subcutaneous injection at the scruff of the neck. The lower right-hand quadrant of the abdomen was shaved using hair clippers. An incision of approximately 2 cm was made in the right abdominal side, and the spleen and attached pancreas were exteriorised using forceps. NKPCB-NBC12.1F (KPC-F) cells, derived from a KPC mouse (LSL-KrasG12D; LSL-Trp53R172H; Pdx1Cre), were generated and kindly donated by Professor Jennifer Morton (Beatson Institute, Glasgow). A total of 500 cells in a volume of 5 μL, 94% Matrigel® and 6% DMEM (Gibco) were injected via 26-guage syringe (Hamilton). Successful injection was verified by the appearance of a wheal at the injection site with

no leakage through the pancreatic capsule. KPC-F cells were injected at similar passages (P9-11) between surgeries to assure better orthotopic reproducibility. The spleen and pancreas were gently moved back into the peritoneal cavity and the peritoneum was sutured with absorbable 4.0 Vicryl suture (Ethicon) and skin was closed with a 7 mm wound clip applier. The mouse was kept in a 37°C recovery chamber and placed back to IVC upon fully waking up. The mouse was monitored closely after surgery.

2.6.1 MRI scanning

Tumour growth was monitored via MRI one-week post-surgery. The mouse was anaesthetised with 1.5-3% Isoflurane/Oxygen and positioned into a custom-made, 3D printed, multimodality cradle. The MRI scanning was performed using a 4.7 T 310 mm horizontal bore Biospec AVANCE III HD preclinical imaging system equipped with 114 mm bore gradient insert (Bruker BioSpin GmbH, Germany). Murine body temperature was maintained at 36°C by monitoring rectal temperature using an optical system (ACS-P4-N-62SC and OTP-M, Opsens Inc., Quebec, Canada). Respiration was monitored using a pneumatic balloon (VX010, Viomedex Ltd, UK) and maintained at 40-60 breaths/minute. The balloon was placed against the animals chest and coupled to a pressure transducer. A threshold-based respiration gating control signal was generated on a custom-built gating device. The gating method allowed an additional duration of ~150 ms after the completion of each breath to allow acquisition of MRI slices during inter-breath periods. This allowed efficient multi-slice MRI scanning with reduced sensitivity to respiratory motion of the free breathing animal (Kinchesh et al., 2019). Tumour size never exceeded the maximum licence capacity of 600mm^3, typically culled when tumours were 400-500mm^3 or at an experimental endpoint. Tumour volume was calculated using ITK-SNAP (Yushkevich et al., 2006).

2.6.2 *In vivo* drug and radiation treatments

Mice were orthotopically challenged with pancreatic tumours and monitored as previously described (Section 2.6). Twelve days post-surgery, orthotopic mice began a treatment regimen as detailed in Figure 2.1

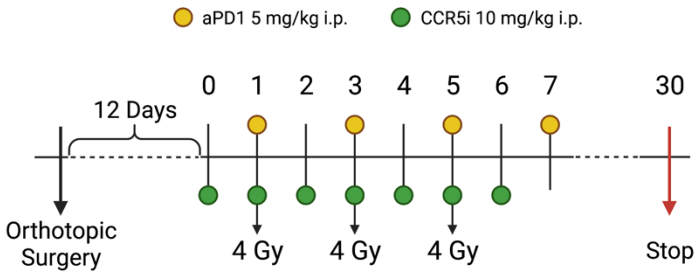


Figure 2.1: Schematic of orthotopic treatment chart.

Depending on treatment group, mice were anaesthetised and locally irradiated with 4 Gy using a combination of MRI scanning (Section 2.6.1) and the small animal radiation research platform (SARRP). Maraviroc (R&D), a CCR5 antagonist (described as CCR5i) was administered (10 mg/kg in PBS) via intraperitoneal (IP) injection daily from day 0 until day 6. Monoclonal Ultra-LEAF™ purified anti-PD1 antibody (BioLegend) was administered (5 mg/kg in PBS) via IP injection on alternate days from day 1 until day 7. Mice were culled at 30 days or if maximum tumour volume was reached.

2.7 Collection of murine blood and tissue

Mice were euthanised by approved schedule 1 methods. If blood was collected, mice were euthanised through exsanguination via cardiac puncture under anaesthesia (3-3.5% Isoflurane/Oxygen) using a 25-guage syringe (Thermo Fisher) coated with anticoagulant ACD buffer (Table 2.2) (100μL ACD buffer; ≤ 1mL blood). Transverse sections of

orthotopic tumour and/or pancreas were taken to preserve architecture. Sections were taken for FC (stored in PBS on ice) (see Section 2.11), for formalin fixation and paraffin embedding (FFPE) and/or stored in 10% neutral buffered formalin (NBF) (Section 2.8). Spleens were stored in PBS on ice prior to FC processing (Section 2.11.1), cell isolation (Section 2.2.1) or stored in 10% NBF for FFPE (Section 2.8). BM was harvested by dissecting the femur and tibia bones. Under sterile conditions bones were cut on each end using scissors and BM was flushed using a 21-guage needle filled with PBS. For further culture of BM derived cells see Section 2.2.3.

2.7.1 Plasma isolation

Following collection, blood was left to homogenate on a rotator for 5-minutes and then centrifuged at 100 x g for 10-minutes at RTP. Without disturbing the buffy coat, plasma supernatant was collected and centrifuged again at 3000 x g for 5-minutes at RTP. Supernatant was collected, avoiding contamination with the pellet if present, and immediately frozen at -20°C.

2.8 Formalin fixation and paraffin embedding (FFPE)

Following sacrifice, tissues were collected and fixed in 10% NBF for 24 hours at RTP and transferred to 70% ethanol overnight at 4°C. Tissues collected included pancreas, tumour and spleen. Fixed tissues were transferred to processing/embedding cassettes (Simport) in 70% ethanol and stored at 4°C for up to 7 days before processing.

Overnight processing was performed using the STP120 Spin Tissue Processor (Thermo Fisher Scientific). This involved tissue dehydration using a series of increasing concentrations of ethanol followed by tissue clearing in Citroclear (TCS Biosciences) and Histoplast PE paraffin wax (Thermo Fisher/Epredia) infiltration. Using the HistoStar™ Embedding Workstation, tissues were removed from cassettes and transferred to plastic

moulding plates. Paraffin wax was added to the moulds, which were then topped with the corresponding cassette lid before setting on the cold plate. Tissue blocks were cut into sections (4 μm thickness) using a Leica RM2125 microtome and mounted onto SuperFrost Ultra Plus™ Adhesion slides (Thermo Fisher Scientific).

2.9 Histological analysis

Tissue sections were deparaffinised in Citroclear twice and rehydrated in an ethanol gradient (100%, 100%, 70%, 50%) for 3-minutes each, followed by two washed in PBS. Slides were stained for haematoxylin and eosin (H&E), immunohistochemistry (IHC) or multiplex-immunofluorescence (IF). After staining, slides were dehydrated in an ethanol gradient (50% 70%, 100%, 100%) for 30 seconds each followed by tissue clearing in xylene (Thermo Fisher) twice for 1-minute each. Slides were mounted with dibutylphthalate polystyrene xylene (DPX; Sigma-Aldrich), dried for 24 hours and scanned using an Aperio ScanScope CS digital slide scanner (Leica Biosystems) at 20X magnification. Digital images were analysed using the Aperio ImageScope or QuPath software platforms.

2.9.1 Haematoxylin and eosin staining (H&E)

Rehydrated slides were stained in freshly filtered Harris Haematoxylin (VWR) for 1-minute, then washed in running tap water for 8-minutes. Sections were differentiated with 2 dips in 1% Acid Alcohol solution (Table 2.2) followed by 10 dips in dH_20. Sections were blued by 10 dips in Scott's Tap water (VWR), 10 dips in dH_20 and 10 dips in 0.5% lithium carbonate. Slides were washed under running tap water for 5-minutes and then dehydrated via 10 dips across an ethanol gradient (50%, 70% 100%). Dehydrated slides were then placed in eosin (Sigma-Aldrich) for 30 seconds. Excess eosin was removed by

4 washes in 90-100% ethanol (30 seconds each) and the dehydrated slides were then cleared, mounted and scanned as previously described (Section 2.9).

2.9.2 Immunohistochemical staining (IHC)

Antigen retrieval was performed using 1X Citrate buffer (Table 2.2) using a pressure cooker at 125°C for 2-minutes, 90°C for 1-minute. Samples were left in the pressure cooker until the temperature reached 80°C, and then cooled on ice for 1 hour prior to washing in PBS-T (0.05%) (Table 2.2). Sections were blocked for 1 hour using the Dual Enzyme Block as part of the Dako EnVision®+ Dual Link System-HRP (DAB+) Kit (Agilent). Tissues were incubated with primary antibody (Table 2.6) overnight in a moist chamber at 4°C. Slides were washed with PBS-T (0.05%) and incubated with secondary antibody (Table 2.6) for 30-minutes in a moist chamber at RTP and washed as previously described. If the primary antibody species was Rat, slides were incubated with Rabbit Anti-Rat IgG (Abcam; 1:1000) for 30 minutes at RTP prior to incubation with secondary antibody. For visualisation, tissues were stained with diaminobenzidine (DAB; Dako, Agilent) diluted 50-fold in DAB+ substrate buffer (Dako, Agilent) (incubation time dependent DAB visualisation of positive control sample) and counterstained for 20-seconds with Gill's haematoxylin (Sigma-Aldrich). Slides were washed in running tap water for 5-minutes prior to dehydration, tissue clearing mounting and scanning as previously described (Section 2.9).

2.10 Multiplex immunofluorescence

Multiplex immunofluorescence staining was carried out on 4 μm thick FFPE sections by the Translation Histopathology Laboratory (THL, University of Oxford). In brief, sections

were stained using the OPAL™ protocol (AKYOA Biosciences) on a Lecia BOND RX^{m} Auto-Stainer (Lecia, Microsystems). Six consecutive staining cycles were performed using primary antibody-Opal fluorophore pairings detailed in Table 2.7. Primary antibodies were incubated for 30-minutes and detected using the BOND™ Polymer Refine Detection System (Lecia Biosystems) as per manufacturer's instructions. In brief, sections were baked, dewaxed with BOND™ dewax solution, rehydrated with alcohol and incubated with Epitope Retrieval Solution 1 or 2 (ER1, ER2) (Lecia Biosystems) at 100°C for 20-minutes. ER1 was used for Ly6G and SMA, ER2 was used for all other antibodies. ER1 or ER2 was performed before each primary antibody was applied. Sections were washed three times with BOND™ wash, blocked with peroxidase block (3 – 4% (v/v) hydrogen peroxide) for 5-minutes and subsequently washed three times with BOND™ wash. Primary antibodies were incubated for 30-minutes, washed as before, and incubated with Anti-Rabbit Poly-HRP-IgG for 8-minutes. Sections were washed twice in BOND™ wash, once in deionised water prior to Opal antibody incubation for 10-minutes. Sections were washed three times in deionised water and finally incubated with spectral DAPI (Akoya Biosciences) and slides mounted with VECTASHIELD® Vibrance™ Antifade Mounting Medium (Vector Laboratories). Whole slide multispectral images were obtained on the AKOYA Bioscience Vectra® Polaris™ (scanned at 20X magnification). Batch analysis and spectral unmixing of the tissues was performed with inForm 2.4.11 software. Batched analysed multispectral images were fused in QuPath to produce a spectrally unmixed reconstructed whole tissue image.

2.11 17-colour spectral flow cytometry

The optimised antibody panel can be seen in Table 2.10. Panel development is detailed in Chapter 3. For each assay, reference controls were obtained by running single-stained and unstained samples to provide individual fluorescence spectra necessary to unmix the

data. Compensation beads, including UltraComp eBeads™ (Thermo Fisher), Anti-Mouse Ig, κ/Negative Control Compensation Particles Set (BD), Anti-Rat and Anti-Hamster Ig κ/Negative Control Compensation Particles Set (BD) and Anti-REA MACS® Comp Bead Kit (Miltenyi), were used for single-stained controls. Cells were heat-shocked at 95°C for 10-minutes, placed on ice for 20-minutes and used for the Live/Dead single-stained control. The assay cell-type was used for the unstained sample.

2.11.1 Tissue dissociation

Spleens harvested from a C57BL/6 mouse, were longitudinally cut into two sections. One section was processed as described in Section 2.2.1 and 2.11.1. The other half was micro-dissected with curved scissors, incubated with pancreatic or tumour dissociation buffer (Table 2.3, 2.4) relative to spleen weight (25 mL/g) and placed on an Eppendorf ThermoMixer (Thermo Fisher) at 850 rpm for 45-minutes at 37°C. The dissociation was pipetted vigorously and incubated for a further 50-minutes under the same conditions. The dissociation was passed through a 70 μM cell strainer (Gibco) and neutralised with DMEM + 10% FBS. Both samples were labelled and acquired according to Section 2.11.1 and 2.11.4.

2.11.2 Antibody titration

Spleens were harvested from wild-type (WT) C57BL/6 female mice and a single cell suspension of splenocytes was generated as previously described (Section 2.2.1). Splenocyte suspensions were centrifuged and washed twice in PBS before lysing in 5 mL 1X Red Blood Cell (RBC) lysis buffer (BioLegend) and incubated on ice for 5-minutes. The buffer was diluted in 30 mL PBS, centrifuged, and resuspended in 10 mL FACS buffer

(Table 2.2). Splenoytes were counted to a cell density of $0.5x10^6$ cells per well in 50 μL FACS buffer and blocked with Mouse BD Fc-Block™ (BD) for 10-minutes at 4°C. Cells were washed twice in FACS buffer before pipetting into a 96-well plate (Thermo) to be stained with the appropriate concentration of antibody (Table 2.15), using antibodies detailed in Table 2.10, for a 30-minute incubation at 4°C in the dark. Reference controls were also stained. All incubations for this method were carried out under these conditions unless stated otherwise. Cells and reference controls were centrifuged at 500 x g for 2-minutes at RTP and washed prior to incubation with FOXP3 Fixation/Permeabilization buffer (Thermo) followed by three Permeabilization buffer (Thermo) washes. If FOXP3 staining was required, the appropriate well was incubated with antibody. Samples were centrifuged at 500 x g for 2-minutes at RTP and washed with Permeabilization buffer twice, before resuspension in 200 μL FACs buffer and storage in the dark at 4°C overnight. Acquisition was carried out according to Section 2.11.4. The stain index was calculated as:

$$Stain\ Index\ (\Delta) = \frac{MFI\ positive\ population - MFI\ negative\ population}{2\ X\ robust\ Standard\ Deviation\ negative\ population}$$

Table 2.15: Details of antibody titration.
Counterstains detailed if used, concentration range stated for staining in splenocytes. Concentration range based on manufacturers recommendations.

Antibody	Counterstain	Concentrations tested
Live/Dead	-	1:500 – 1:16000
CD45	-	1:25 – 1:800
CD3	-	1:25 – 1:800
NK1.1	-	1:25 – 1:800
CD19	-	1:25 – 1:800
F4/80	-	1:100 – 1:3200
CD11b	-	1:100 – 1:3200
CD4	CD3	1:25 – 1:800
CD8a	CD3	1:25 – 1:800
CD80	F4/80	1:25 – 1:800
CD206	F4/80	1:100 – 1:3200
Ly6C	CD11b	1:100 – 1:3200
Ly6G	CD11b	1:25 – 1:800
CD25	CD4	1:100 – 1:3200
PD-1	CD8	1:25 – 1:800
CCR5	CD8	1:25 – 1:800
FOXP3	CD4, CD25	1:100 – 1:3200

2.11.3 Fluorescence minus one (FMO)

Splenocytes were acquired and processed as previously described (Section 2.2.1, 2.12.1). One tube contained the full 17-colour panel (Table 2.10), one tube contained unstained splenocytes and then a series of tubes each omitting one antibody at a time.

50µL of Brilliant Violet Dye Buffer (BD) was also added to each tube. Acquisition was carried out according to Section 2.11.4.

2.11.4 17-colour spectral flow cytometry assay

700µL of blood samples was lysed with 12 mL 1X RBC lysis, incubated for 10-15-minutes on a rotator, centrifuged, and washed with FACS buffer. Tumour and pancreas samples were micro-dissected and processed as previously described (Section 2.7). Both blood and tumour samples were counted to a cell density of $1x10^6$ and stained in 100 µL as previously described (Section 2.11.2) and acquired. Samples were acquired on a 4-laser Aurora (Cytek) with SpectroFlo software (Cytek) version 2. Gating strategies are shown in Chapter 3, Figure 3.5. Unless stated otherwise, a minimum of 10,000 events were acquired for reference control samples and 100,000 CD45-gated events were acquired per tube. Cytometer performance was checked prior to each experiment using SpectroFlo QC Beads (Cytek). All FC analysis in this thesis was carried out using FlowJo software (BD) version 10.5.3 unless stated otherwise.

2.12 CFSE flow cytometry

The protocol for CFSE FC acquisition had previously been optimised by Dr Keaton Jones (Department of Oncology, University of Oxford). Plates were processed for FC on day zero, one and three. An undivided peak was fixed based on CFSE intensity at the time of staining (Day 0, CD8+ T-cells only) and after natural decay (Day 1, CD8+ T-cells only). On the day of acquisition, Plates were spun down at 500 x g for 2-minutes and washed twice in FACS buffer. Cells were blocked with Mouse BD Fc-Block™ (BD) for 10-minutes at RTP in the dark, centrifuged and washed as previously described. Cells were then

incubated with antibodies detailed in Table 2.9 for 20-minutes in the dark at RTP. For each assay, compensation samples were run as single-colour controls using Anti-Mouse Ig, κ/Negative Control Compensation Particles Set (BD), Arc™ Amine Reactive Compensation Bead Kit (Thermo Fisher), CFSE+ T-cells and unstained T-cells. Cells and compensation samples were centrifuged and washed as previously described in this method and resuspended in 90 µL of FACS buffer for acquisition. Samples were acquired on a 4-laser CytoFLEX (Beckman Coulter) with CytExpert software (Beckman Coulter) version 2.5. A minimum of 10,000 events were acquired for compensation samples and all cells in the 90 µL sample was acquired. Cytometer performance was checked prior to each experiment using CytoFLEX Daily QC Fluorospheres (Beckman Coulter).

2.13 Multiplex cytokine array

Previously acquired frozen plasma samples (Section 2.7.1) were analysed for IL-1α, IL-1β, IL-3, IL-7, IL-11, IL-12p40, IL-12p70, IL-23, IL-27, IL-33, IFN-β, GM-CSF and TSLP using the LEGENDplex™ Mouse Cytokine Array (BioLegend) according to manufacturer's instructions. In brief, each plasma sample was diluted 1:2 with LEGENDplex™ Assay Buffer. Diluted plasma sample and an 8-fold standard, formulated from LEGENDplex™ Mouse Cytokine Panel 2 Standard Cocktail, was pipetted in duplicate into a V-bottom plate (BioLegend) with LEGENDplex™ Matrix C, LEGENDplex™ Mouse Cytokine Panel 2 Premixed Beads and LEGENDplex™ Detection Antibodies. The plate was placed on an Eppendorf ThermoMixer at 700 rpm for 2 hours at RTP protected from the light. SA-PE was added to each well and incubated under the same conditions for 30-minutes. The plate was centrifuged at 1000 x g for 5-minutes at RTP, supernatant was removed, and cells washed with 1X LEGENDplex™ Wash Buffer twice, resuspended in 300 µL Wash Buffer and acquired. Samples were acquired on a 3-laser LSRFortessa (BD) with *FACSDiva*™ Software (BD) version 9.0. LEGENDplex™ Setup Beads 3 (BioLegend)

were used to set PMT voltages of the classification channel APC, reporter channel PE and FITC channel. A minimum of 5000 singlet events were acquired for each sample. Cytometer performance was checked prior to each experiment using CS&T Beads (BD). Data was analysed using the LEGENDplex™ Data Analysis Software Suite.

2.14 ELISA

2.14.1 Plasma samples

Frozen plasma samples, previously acquired (Section 2.7.1), were analysed for IL-35 with the Mouse IL-35 ELISA Kit (Assay Genie) according to manufacturer's instructions. In brief, plasma samples were thawed and diluted 1:4 in Sample Dilution Buffer. A lyophilised standard was reconstituted with Sample Dilution Buffer over an 8-fold dilution (1000 pg/mL – 15.625 pg/mL). Pre-coated plates were washed twice in 1X Wash Buffer prior to the addition of diluted sample and standard plated in duplicate and incubated at 37°C for 90-minutes. The contents of the plate were discarded, washed twice, and incubated with Biotin-detection antibody at 37°C for 60-minutes. The contents of the plate were discarded and washed three times and incubated with Tetramethylbenzidine (TMB) substrate at 37°C in the dark for 10 – 20-minutes until a blue colour became visible. Stop solution was added to each well and optical density absorbance was measured at 450 nm on a POLARstar Omega plate reader. A standard curve was produced using Microsoft Excel and a linear equation was used to determine total protein concentration of each sample with their relative absorbance.

2.14.2 Organoid supernatant

Organoid supernatant (Section 2.2.2) aliquots were taken and frozen at -20°C. On the day of analysis samples were thawed and analysed for IL-35 using the LEGEND MAX™ Mouse IL-35 Heterodimer ELISA Kit (BioLegend). In brief, lyophilised mouse IL-35 standard was reconstituted with Assay Buffer F over an 8-point dilution (30 ng/mL – 0.47 ng/mL). The precoated plate was washed four times in 1X Wash Buffer prior to the addition of Assay Buffer F to each well and either undiluted organoid supernatant or standard pipetted in triplicate. The plate was sealed and placed on an Eppendorf ThermoMixer at 700 rpm for 2 hours at RTP. Plate contents were discarded and washed four times. Mouse IL-35 Detection Antibody Solution was added to each well and incubated under the same conditions for 1 hour. Plate contents were discarded and washed four times. Avidin-HRP D Solution was added to each well and incubated under the same conditions for 30-minutes. Contents were discarded and the plate was washed five times to minimise background. Substrate Solution F was added to each well and incubated for 15-minutes in the dark at RTP. The reaction was stopped with the addition of Stop Solution and the plate absorbance was read immediately at 450 nm and 570 nm on a POLARstar Omega plate reader (absorbance at 570 nm subtracted from absorbance at 450 nm). A standard curve was produced using Microsoft Excel and a linear equation was used to determine total protein concentration of each sample with their relative absorbance.

2.15 Statistical analysis

Pancreatic Intraepithelial Neoplasia (PanIN) lesions were identified based on cytological and architectural features as described in Chapter 1, Section 1.6. Percentage frequency and standard deviation (SD) values were generated by FlowJo (software 10.5.3). Western

blot analysis was performed on ImageStudio Lite (software 5.2.5; LI-COR). H&E and IHC analysis was performed on QuPath (software 0.3.2).

All data are presented as mean ± SD or mean with 95% confidence intervals and significance visualised as *($p<0.01$), **($p<0.001$) or ***($p<0.0001$). Testing for Gaussian distribution was performed using Shapiro-Wilk normality test. If data fit a normal distribution, either ordinary univariate analysis of variance (ANOVA) or Brown-Forsythe and Welch ANOVA was performed depending on the assumption of equal standard deviations. Post-hoc analysis was performed using Tukey multiple comparisons test. If data did not fit a normal distribution, the non-parametric Kruskal-Wallis test was performed followed by Dunn's multiple comparisons test. A two-way ANOVA was performed if data fit a normal distribution, followed by Šídák's multiple comparisons test for post-hoc analysis. Unpaired two-tailed Student's t-test (parametric) or Mann Whitney test (non-parametric) performed depending on data fit to Gaussian distribution. Simple linear regression was performed in which the r^2 value was a measure of how well the linear regression model fit the data. Graphs and statistical analysis were performed using GraphPad Prism 9.

Results I

3. Panel design and optimisation for high-dimensional immune-phenotyping of PDAC mouse models using spectral flow cytometry

3.1 Introduction

Several methods for quantifying immune infiltrate are available, but vary depending on their accuracy, reliability and cost-effectiveness. Their individual advantages and disadvantages are briefly described to highlight the rationale for the use of spectral flow-cytometry in this thesis, to broadly identify immune populations in murine PDAC.

Historically semi-quantifiable immunohistochemistry (IHC) and quantifiable immunofluorescence (IF) have been used by pathologists to characterise immune infiltrate within solid tumour (Hendry et al., 2017). Multiplex IHC/IF elucidates the spatial resolution and relationship among individual cell types but is limited by the number of colours available and high cost (PerkinElmer TSA Opal™; 7-colours) (Tan et al., 2020; Sun et al., 2021).

In recent years characterisation of immune infiltrate via RNA-sequencing, using computational approaches based on expression signatures or specific gene markers, has shed light on immune response mechanisms in the tumour milieu (Finotello and Trajanoski, 2018). However, these can be hampered by the robustness of the deconvolution algorithm when considering unknown tumour content and multicollinearity; particularly when expression of low-abundance cell types are masked by expression of the same gene in more abundant cell subsets (Shen-Orr and Gaujoux, 2013). When comparing multiparametric FC to next-generation sequencing for monitoring of acute myeloid

leukaemia, FC was found to have improved sensitivity in disease monitoring and more cost-effective for sample number (McGowan et al., 2022).

The use of high-dimensional cytometry by time-of-flight (CyTOF) mass cytometry has also emerged as a technique for broad immune profiling, using antibodies conjugated to rare heavy metal isotopes not typically found in biological samples (Bandura et al., 2009). Although equivalence between FC and CyTOF immunophenotyping has been detailed in several studies, longer acquisition times, caution to avoid cross-contamination with heavy metals during sample preparation and high cost should be considered when using CyTOF (Gadalla et al., 2019; Ferrer-Font et al., 2020a). While neither technique is superior, challenging CyTOF data analysis, where prior bioinformatics knowledge is required, may also act as a hindering factor (Li et al., 2017).

Flow cytometry (FC) has become a pivotal tool for the identification and quantification of immune subsets across various diseases including cancers of both haematological and solid malignancy. Multi-colour FC has been used on the tumour locale in the context of murine breast cancer and several syngeneic murine tumour models (Yu et al., 2018; Almeida et al., 2021). The relatively low sample volume and low cost make it ideal to screen large sample numbers containing low cell numbers, such as tumour infiltrate (Ferrer-Font et al., 2020a; Niewold et al., 2020). However, conventional FC is restricted by overlapping emission spectra of two or more fluorochromes and exacerbated further by larger panels, limiting the parameters for cell identification (Chuah and Chew, 2020). Spectral FC allows the complete fluorescence spectrum of individually labelled cells to be captured across multiple detectors to capture the full emission across a defined wavelength range (Nolan and Condello, 2013). This allows two fluorochromes of similar emission to be used if their spectral signatures are unique, resulting in the ability to design much larger panels than conventional FC. As with all cytometry, longitudinal studies require reproducible and standardised workflow for accurate

spectral FC results, therefore panel design and optimisation is imperative (Laskowski et al., 2020).

Larger spectral FC panels have been used to elucidate the tumour immune infiltrate in lung adenocarcinoma, but not PDAC (Johnson et al., 2020). Several groups have begun to define the immune contribution to PDAC via conventional multi-colour FC, but these have often been limited in panel size and therefore immune population identification (Kenkel et al., 2017; Lanfranca et al., 2018; Pu et al., 2018a; Qiu et al., 2019). Other studies have characterised the spleen or peripheral blood rather than the local microenvironment itself (Yang et al., 2019; Takahashi et al., 2021). Some studies have defined the immune infiltrate within the tumour, but the parameters used to define the immune scope of PDAC were limited (Clark et al., 2007a). To our knowledge, no other spectral FC panel specific to PDAC has been published.

3.2 Aims

The studies described in this chapter aim to design and optimise a 17-colour spectral FC panel, capable of accurately quantifying B-cells, CD8 cytotoxic T-cells, T-regulatory cells, NK and NKT cells, M1 and M2 macrophages, and granulocytes (PMN-MDSC) or monocytes (M-MDSCs). This FC panel aims to detect the immune compartment only, both systemically in the peripheral blood and locally within the pancreatic microenvironment in the context of pancreatic cancer. Detection of the stroma, CAFs and the tumour are not included in this analysis.

Considering the hypocellular nature of leukocytes within tumour, or low volume acquisition of murine blood, all optimisations detailed in this chapter were carried out in splenocytes as a representative sample of both blood and solid tumour.

3.3 Results

3.3.1 Panel design for spectral flow cytometry

Initial antigen combination was based on the previous work of Dr Kelly McKelvey (University of Sydney) on systemic whole-blood of C57BL/6 mice (McKelvey et al., 2020). This panel was further adapted to include the addition of transcription factor FOXP3, necessary for enhanced classification of T-regulatory cells (Tregs) (Fontenot et al., 2003; Hori et al., 2003). The functionality of each antigen was carefully considered (Table 3.1) prior to finalisation of panel design. The lineage for cell identification (Table 3.2) and antigen co-expression was also considered prior to panel finalisation. Identification of MDSCs from CD11b+Ly6C+ (monocytic MDSCs; M-MDSC) and CD11b+Ly6C+Ly6G+ (polymorphonuclear MDSCs; PMN-MDSCs) was based on standardisation recommendations in the field of MDSC classification (Bronte et al., 2016). Due to the discrepancies in MDSC identification within the field, owing to no unique MDSC marker, M-MDSCs are also identified as monocytes and PMN-MDSCs are also defined as granulocytes in all analyses (Cassetta et al., 2019). CD279 (PD-1) and CD195 (CCR5) were included in the panel design as an additional parameter of analysis for an *in vivo* drug study; combination of anti-PD-1, CCR5 inhibitor and radiotherapy in an orthotopic PDAC mouse model (Chapter 4).

Table 3.1: Rationale for antigen choice

Name	Function
Live/Dead	Dye reacts with free amines on compromised membranes. Dye reactivity in viable cells is restricted to cell-surface amines, yielding weaker fluorescence
CD45	Pan-leukocyte protein with tyrosine phosphatase activity involved in regulation of signal transduction in haematopoiesis
CD19	BCR co-receptor, B-cell activation and differentiation
CD3	T-cell co-receptor, present at all stages of T-cell development
NK1.1	Type II integral membrane glycoprotein, role in NK cell activation/differentiation, IFNγ production and cytotoxic granule release. NK1.1 only expressed in a subset of murine strains including C57BL/6 (Giorda et al., 1992).
CD8a	TCR co-receptor in antigen recognition of MHC I and subsequent CD8 T-cell activation
CD4	TCR co-receptor in antigen recognition of MHC II and subsequent CD4 T cell activation
CD25	Interleukin-2 receptor alpha chain, combines with beta chain and common gamma chain to form high-affinity IL2 receptor
FOXP3	Master transcriptional regulator of the regulatory pathway involved in development and function of regulatory T cells
CD206	Mannose receptor 1, a C-type lectin involved in phagocytosis and antigen presentation in macrophages
F4/80	Murine homologue of protein EMR1, widely used to characterise murine tissue macrophage populations
CD80	Type I membrane protein, part of the immunoglobulin superfamily found on surface of antigen-presenting cells to aid costimulatory signalling
CD279	Cell surface Programmed cell death protein 1 is an immune checkpoint, negatively regulating TCR signalling to downregulate immune response
CD195	Seven transmembrane spanning G protein-associated molecule, also known as chemokine receptor 5 (CCR5). Regulates lymphocyte chemotaxis and trans-endothelial migration during inflammatory response.
CD11b	One protein subunit that forms heterodimeric integrin alpha-M beta-2 with CD18. Mediates inflammation by regulating leukocyte adhesion/migration.
Ly6C	Murine differentiation antigen expressed on developing macrophages and DC, granulocytes and subpopulations of lymphocytes. Used for initial definition of MDSCs (Bronte et al., 2016)
Ly6G	GPI-anchored protein, transiently expressed on monocytes in the bone marrow, neutrophils, eosinophils, plasmacytoid dendritic cells. Used for initial definition of MDSCs (Bronte et al., 2016)

Table 3.2: Cell identification table.

Name	Lineage
NK cells	CD45+ NK1.1+ CD3-
NKT cells	CD45+ NK1.1+ CD3+
CD4+ T cells	CD45+ CD3+ CD4+
CD8+ T cells	CD45+ CD3+ CD8a+
T-regulatory cells	CD45+ CD3+ CD4+ CD25+ FOXP3+
B-cells	CD45+ CD19+
M1 macrophage	CD45+ F4/80+ CD80+
M2 macrophage	CD45+ F4/80+ CD206+
Granulocytes (PMN-MDSC)	CD45+ CD11b+ F4/80^{hi} Ly6C+ Ly6G+
Monocytes (M-MDSC)	CD45+ CD11b+ F4/80^{hi} Ly6C+ Ly6G-

The combination of fluorophores was developed in collaboration with Dr Helen Ferry (Nuffield Department of Medicine, University of Oxford) and Cytek Bioscience. The expected antigen density (Table 3.3; low, medium, high) was combined with fluorochromes of varying degrees of fluorescent intensity. In general, high antigen expression was paired with fluorochromes of lower fluorescent intensity using dyes with unique spectral signatures. Initial panel design had included a Live/Dead Zombie Yellow™ stain. Dyes with similar spectral signatures risk the introduction of spreading error, which can be mitigated if used with markers that are not co-expressed (Ferrer-Font et al., 2020b).

Table 3.3: Antigen identification table.

Name	Provider	Antigen density	Fluorochrome	Laser
CD45	30-F11	High	Alexa Fluor® 532	Blue
CD19	1D3	High	Super Bright 436	Violet
CD3	17A2	High	eFluor® 450	Violet
NK1.1	PK136	Medium	BV650	Violet
CD8a	53-6.7	High	BV570	Violet
CD4	RM4-5	High	BV510	Violet
CD25	7D4	Low	Alexa Fluor® 647	Red
FOXP3	FJK-16s	Low	PE	Blue
CD206	C068C2	Low	BV785	Violet
F4/80	II/41	Medium	BV480	Violet
CD80	REA983	Low	APC	Red
CD279	J43	Low/medium	PE-Cy™7	Blue
CD195	REA354	Low/medium	VioBright™ FITC	Blue
CD11b	M1/70	High	Alexa Fluor® 700	Red
Ly6C	HK1.4	Medium	PE-Dazzle594	Blue
Ly6G	1A8	Medium	BV421	Violet

SpectroFlo™ software (Cytek Biosciences) allows the quantification of panel fluorochrome Similarity™ Index, as a measure of dye pair uniqueness on a scale (0-1); values close to 1 indicate signature similarity, whereas values close to 0 indicate spectral uniqueness. Similarity™ indices for panel variations containing Zombie Yellow™ (Figure 3.1A) and LIVE DEAD Blue (Figure 3.1B) show dye similarity between BV421 (Ly6G) and Super Bright 436 (CD19), APC (CD80) and Alexa Fluor® 647 (CD25), eFluor® 450 (CD3) and Super Bright 436 (CD19). However, as their antigen conjugates weren't co-expressed these combinations of dyes were considered acceptable. Similarity between Zombie Yellow™ (live cells) and both BV510 (CD4) and BV570 (CD8a) was observed (Figure 3.1A). The Complexity™Index, an

overall measure of dye uniqueness in a full spectral panel, was calculated. A lower value, as observed with LIVE/DEAD Blue (Figure 3.1B), indicates a lower overall spread of dyes. Higher values indicate a more challenging panel where overall spread is higher. Well-designed larger panels (≥10) will generate a complexity index of 40-5[4]. Further visual inspection of full-spectrum signatures for both panel variations (Figure 3.1C/D) concluded that LIVE/DEAD Blue was optimal for the continual use of the optimised panel, but that prior optimisations (Section 3.3.2, 3.3.4) were still correct considering minimal spectral spread into the LIVE/DEAD blue dye.

[4] According to Cytek Bioscience website: spectrum.cytekbio.com

A

	Alexa Fluor 532	Super Bright 436	eFluor 450	BV650	BV570	BV510	Alexa Fluor 647	PE	BV785	BV480	APC	PE-Cy7	VioBright FITC	Alexa Fluor 700	PE-Dazzle594	BV421	LIVE DEAD Yellow
Alexa Fluor 532	1	0.02	0.02	0.01	0.05	0.02	0	0.6	0	0.01	0	0.01	0.67	0	0.48	0.02	0.03
Super Bright 436	0.02	1	0.94	0.1	0.17	0.22	0	0.01	0.07	0.36	0	0	0.01	0	0.01	0.97	0.1
eFluor 450	0.02	0.94	1	0.08	0.15	0.27	0	0.01	0.07	0.46	0	0	0.01	0	0.01	0.85	0.12
BV650	0.01	0.1	0.08	1	0.26	0.16	0.16	0.06	0.15	0.07	0.33	0.04	0	0.14	0.17	0.1	0.24
BV570	0.05	0.17	0.15	0.26	1	0.58	0	0.48	0.03	0.27	0.03	0.01	0.04	0	0.37	0.16	0.8
BV510	0.02	0.22	0.27	0.16	0.58	1	0	0.23	0.03	0.84	0.02	0.01	0.05	0.01	0.18	0.17	0.89
Alexa Fluor 647	0	0	0	0.16	0	0	1	0	0.01	0	0.93	0.02	0	0.53	0	0	0
PE	0.6	0.01	0.01	0.06	0.48	0.23	0	1	0	0.11	0.01	0.01	0.23	0	0.69	0.01	0.32
BV785	0	0.07	0.07	0.15	0.03	0.03	0.01	0	1	0.02	0.04	0.3	0	0.1	0.02	0.07	0.02
BV480	0.01	0.36	0.46	0.07	0.27	0.84	0	0.11	0.02	1	0	0	0.09	0.01	0.07	0.28	0.6
APC	0	0	0	0.33	0.03	0.02	0.93	0.01	0.04	0	1	0.03	0	0.51	0.03	0	0.03
PE-Cy7	0.01	0	0	0.04	0.01	0.01	0.02	0.01	0.3	0	0.03	1	0	0.07	0.05	0	0.01
VioBright FITC	0.67	0.01	0.01	0	0.04	0.05	0	0.23	0	0.09	0	0	1	0.01	0.17	0.01	0.05
Alexa Fluor 700	0	0	0	0.14	0	0.01	0.53	0	0.1	0.01	0.51	0.07	0.01	1	0	0	0.01
PE-Dazzle594	0.48	0.01	0.01	0.17	0.37	0.18	0	0.69	0.02	0.07	0.03	0.05	0.17	0	1	0	0.27
BV421	0.02	0.97	0.85	0.1	0.16	0.17	0	0.01	0.07	0.28	0	0	0.01	0	0	1	0.07
LIVE DEAD Yellow	0.03	0.1	0.12	0.24	0.8	0.89	0	0.32	0.02	0.6	0.03	0.01	0.05	0.01	0.27	0.07	1

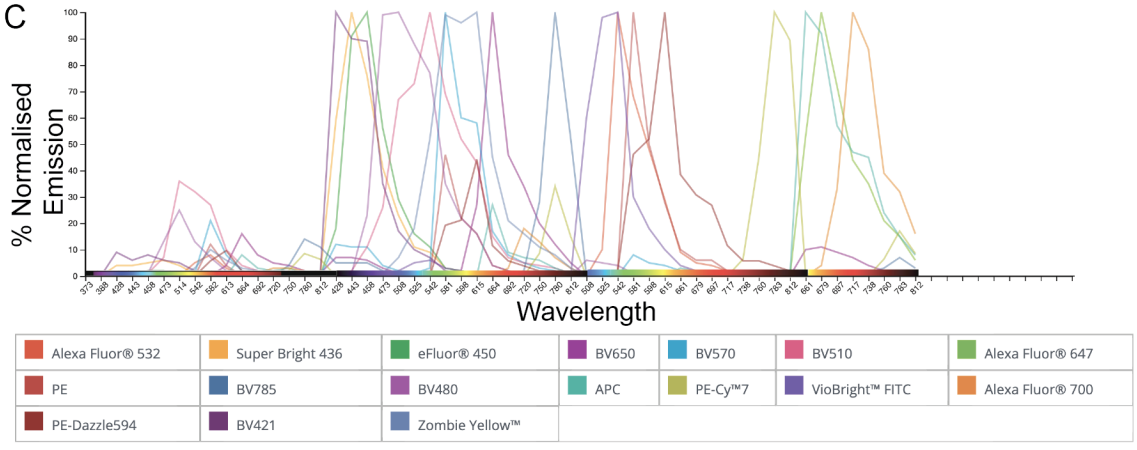
Complexity™ Index: 20.76

B

	Alexa Fluor 532	Super Bright 436	eFluor 450	BV650	BV570	BV510	Alexa Fluor 647	PE	BV785	BV480	APC	PE-Cy7	VioBright FITC	Alexa Fluor 700	PE-Dazzle594	BV421	LIVE DEAD Blue
Alexa Fluor 532	1	0.02	0.02	0.01	0.05	0.02	0	0.6	0	0.01	0	0.01	0.67	0	0.48	0.02	0.02
Super Bright 436	0.02	1	0.94	0.1	0.17	0.22	0	0.01	0.07	0.36	0	0	0.01	0	0.01	0.97	0.25
eFluor 450	0.02	0.94	1	0.08	0.15	0.27	0	0.01	0.07	0.46	0	0	0.01	0	0.01	0.85	0.21
BV650	0.01	0.1	0.08	1	0.26	0.15	0.16	0.06	0.15	0.07	0.33	0.04	0	0.14	0.17	0.1	0.03
BV570	0.05	0.17	0.15	0.26	1	0.58	0	0.48	0.03	0.27	0.03	0.01	0.04	0	0.37	0.16	0.04
BV510	0.02	0.22	0.27	0.16	0.58	1	0	0.23	0.03	0.84	0.02	0.01	0.05	0.01	0.18	0.17	0.2
Alexa Fluor 647	0	0	0	0.16	0	0	1	0	0.01	0	0.93	0.02	0	0.53	0	0	0.01
PE	0.6	0.01	0.01	0.06	0.48	0.23	0	1	0	0.11	0.01	0.01	0.23	0	0.69	0.01	0.01
BV785	0	0.07	0.07	0.15	0.03	0.03	0.01	0	1	0.02	0.04	0.3	0	0.1	0.02	0.07	0.01
BV480	0.01	0.36	0.46	0.07	0.27	0.84	0	0.11	0.02	1	0	0	0.09	0.01	0.07	0.28	0.2
APC	0	0	0	0.33	0.03	0.02	0.93	0.01	0.04	0	1	0.03	0	0.51	0.03	0	0.01
PE-Cy7	0.01	0	0	0.04	0.01	0.01	0.02	0.01	0.3	0	0.03	1	0	0.07	0.05	0	0
VioBright FITC	0.67	0.01	0.01	0	0.04	0.05	0	0.23	0	0.09	0	0	1	0.01	0.17	0.01	0.01
Alexa Fluor 700	0	0	0	0.14	0	0.01	0.53	0	0.1	0.01	0.51	0.07	0.01	1	0	0	0
PE-Dazzle594	0.48	0.01	0.01	0.17	0.37	0.18	0	0.69	0.02	0.07	0.03	0.05	0.17	0	1	0	0.01
BV421	0.02	0.97	0.85	0.1	0.16	0.17	0	0.01	0.07	0.28	0	0	0.01	0	0	1	0.26
LIVE DEAD Blue	0.02	0.25	0.21	0.03	0.04	0.2	0.01	0.01	0.01	0.2	0.01	0	0.01	0	0.01	0.26	1

Complexity™ Index: 19.27

C



D

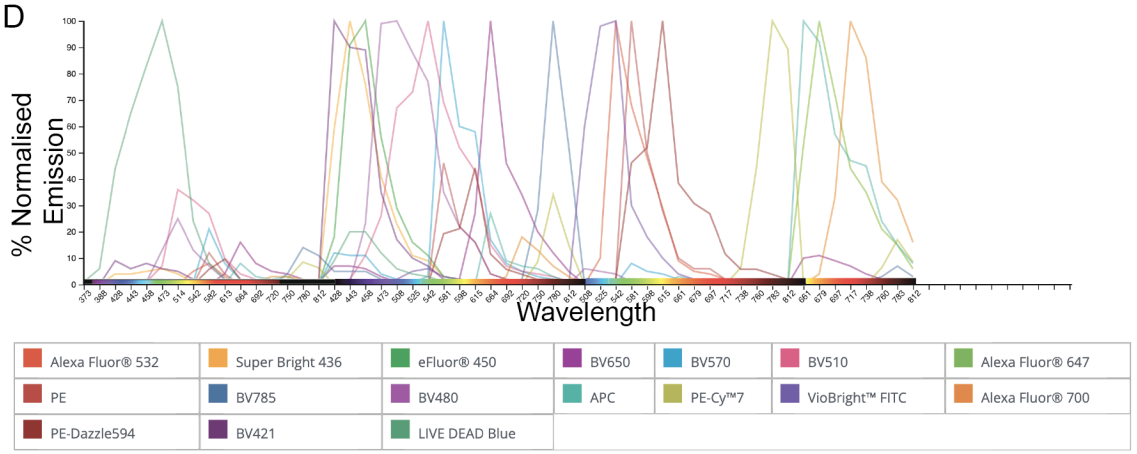


Figure 3.1: Spectral comparison between two versions of the 17-colour flow cytometry panel.

Comparison of the two versions of the FC panel with a 4-laser configuration (16UV-16Violet-14Blue-8Red). Similarity™ Index for both panel variations containing Zombie Yellow™ (A) or LIVE DEAD Blue (B) as a measure of dye pair uniqueness (Scale 1 – 0). Combinations depicted in blue indicate values closer to 1 and similar dye signatures. Complexity™ Index, as a measure of overall uniqueness of all dyes in full spectrum cytometry panel, are shown for both panel versions. Lower values indicate lower overall spread and better panel design. The full wavelength spectrum for each fluorochrome in both panel variations containing Zombie Yellow™ (C) or LIVE DEAD Blue (D).

3.3.2 Antibody titration

Similar to conventional FC, titration of conjugated-antibodies is imperative to minimise background staining, reducing the amount of antibody required and reducing non-specific binding to allow accurate comparison between samples (Hulspas, 2010). Antibodies were titrated sequentially, allowing optimised antibody-conjugates to be used as anchoring stains for rarer populations that require multi-lineage staining (Figure 3.2A, Table 3.2). Antibodies were titrated over a 5-point dilution above and below manufacturer's recommendations (Figure 3.2B). For each antibody, a large separation between median florescence intensity (MFI) of the positive and negative populations (Figure 3.2C, 3.2E) and a high stain index (Figure 3.1C) were used to determine optimal concentration; stain index was used to determine the relative brightness of a fluorophore on a given instrument (Nguyen et al., 2013). See Supplementary 8.1 for all further antibody titrations.

Considering the tumour dissociation protocol may cleave immune antigen, the lowest optimal titration was not always taken for the final antibody concentration (Supplementary 8.1 for remaining titrations, Table 2.9 for optimised concentration). Best practises also recommend against titration below saturation for functional readouts considering saturating concentrations avoid variability, ensuring accurate detection between samples (Cossarizza et al., 2017).

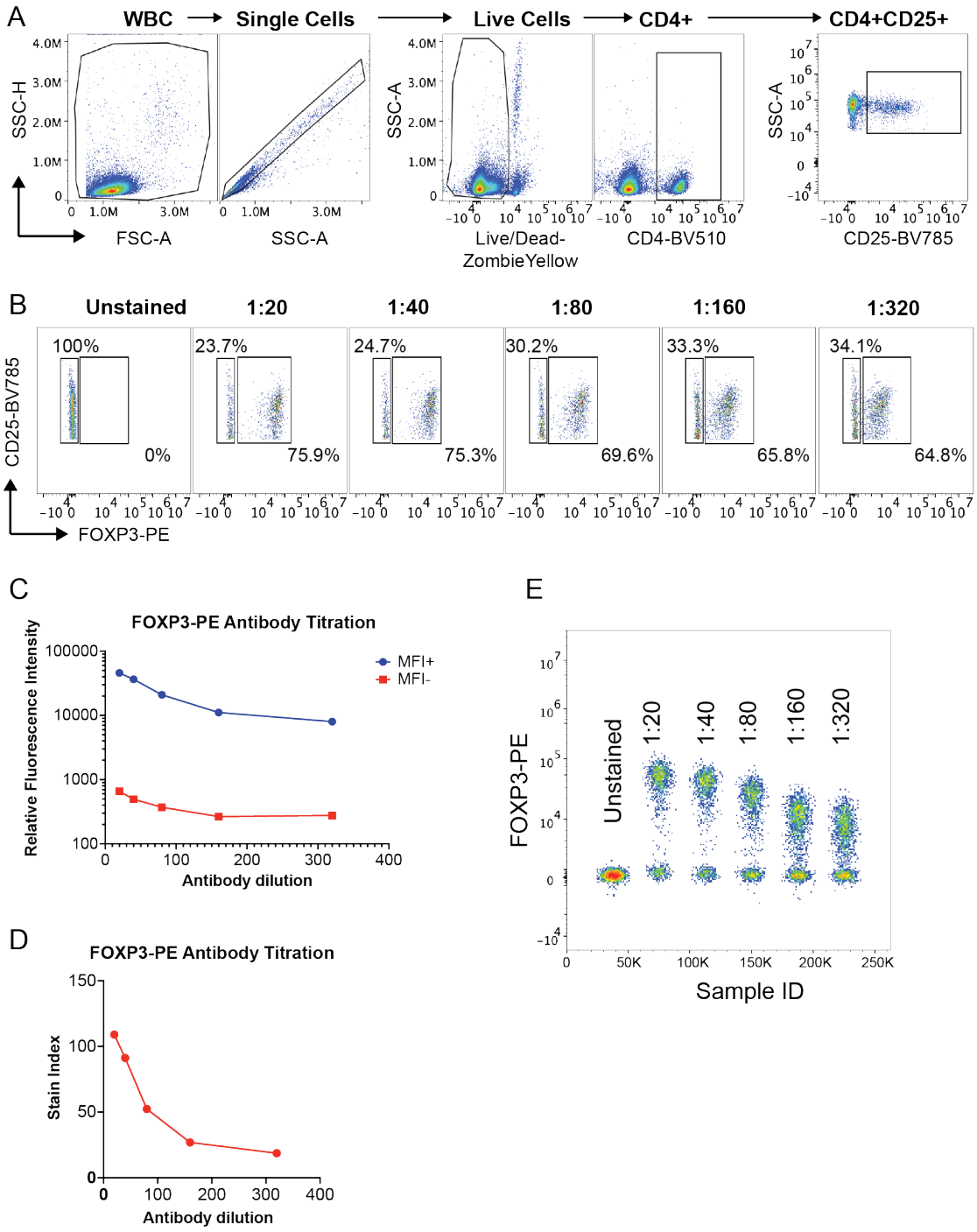


Figure 3.2: FOXP3-PE antibody titration on splenocytes.
(A) Gating Strategy for FOXP3-PE titration. Splenocytes isolated from C57BL/6 naïve mouse were counterstained with Live/Dead-Zombie Yellow (1:2000), CD4-BV510 (1:100) and CD25-AF647 (1:100) (determined from previous titration). (B) Cells were titrated with FOXP3-PE 1:2 over a 5-point dilution (concentration of titration and percentage of positive and negative gating shown on dot plot). (C) Relative Fluorescence Intensity of MFI+ and MFI- gating and (D) Stain Index was determined. (E) Visual inspection of sample concatenation.

3.3.3 Fluorescence minus one control

Following antibody titration, fluorescence minus one (FMO) controls were used to measure the spread of fluorescence from the other staining parameters into the channel of interest, required to determine the threshold of positive staining (Cossarizza et al., 2019). Subsequent gating boundaries were established between positive and negative populations, particularly for low expressed antigen and background. Figure 3.3 details a representative FMO control (BV421-Ly6G). Clear separation was identified for all populations and gating boundaries used for all further FC analysis (See Supplementary 8.2 for all further FMO controls).

A

Tube	Full Panel	BV421-FMO
BV421	+	-
Alexa Fluor® 532	+	+
Super Bright 436	+	+
eFluor® 450	+	+
BV650	+	+
BV570	+	+
BV510	+	+
Alexa Fluor® 647	+	+
PE	+	+
BV785	+	+
BV480	+	+
PE-Cy™7	+	+
VioBright™ FITC	+	+
Alexa Fluor® 700	+	+
PE-Dazzle594	+	+
Zombie Yellow™	+	+
APC	+	+

B

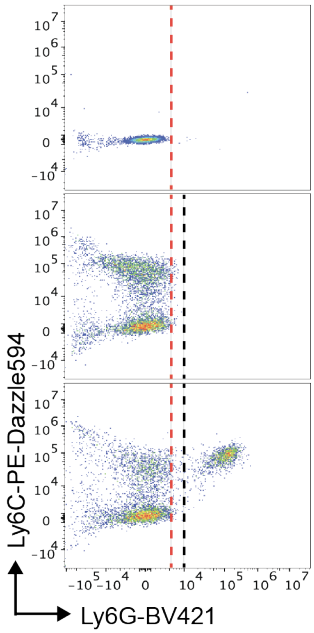


Figure 3.3: PD-1-PeCy7 FMO control to determine fluorescence spread.

(A) Table to show FMO matrix. (B) Dot plots of multicolour flow cytometry showing fluorescence spread into the BV421 channel compared to an unstained control. Unstained control (top plot), BV421-FMO (middle plot), fully stained panel (bottom plot). Black dotted line represents FMO gating boundary compared to unstained boundary in red.

3.3.4 Determining whether tissue dissociations buffers cleave immune antigen

To identify immune infiltrate within the tumour, preparation of a single cell suspension for FC acquisition was required. Tissue dissociation was optimised to yield high-viability and minimise alteration to cell surface antigen, typically found in enzymatic dissociation, for effective phenotyping (Autengruber et al., 2012). Enzymatic dissociation protocols were taken from Quatromoni et al and Carter et al, for respective tumour and pancreas dissociation, considering they showed higher cell-viability in comparison to mechanical dissociation and lower concentrations of collagenase maintained immune expression (Carter et al., 2009; Quatromoni et al., 2015). Collagenases were used to digest extracellular matrix via collagen peptide bond cleavage, while DNase-I degraded free-DNA and prevented cell aggregation (Reichard and Asosingh, 2019). Mincing tissue prior to enzymatic incubation increased surface area between tissue and enzymes to allow more efficient and complete digestion of tissue (Reichard and Asosingh, 2019). Variation of surface expression on splenocytes was observed with pancreatic (Collagenase P) and tumour (Collagenase I, II, IV) dissociation in comparison to untreated splenocytes (Figure 3.4A-C). Despite variation in surface expression with both dissociation buffers, no immune antigen was completely cleaved and regarded as suitable for further analyses.

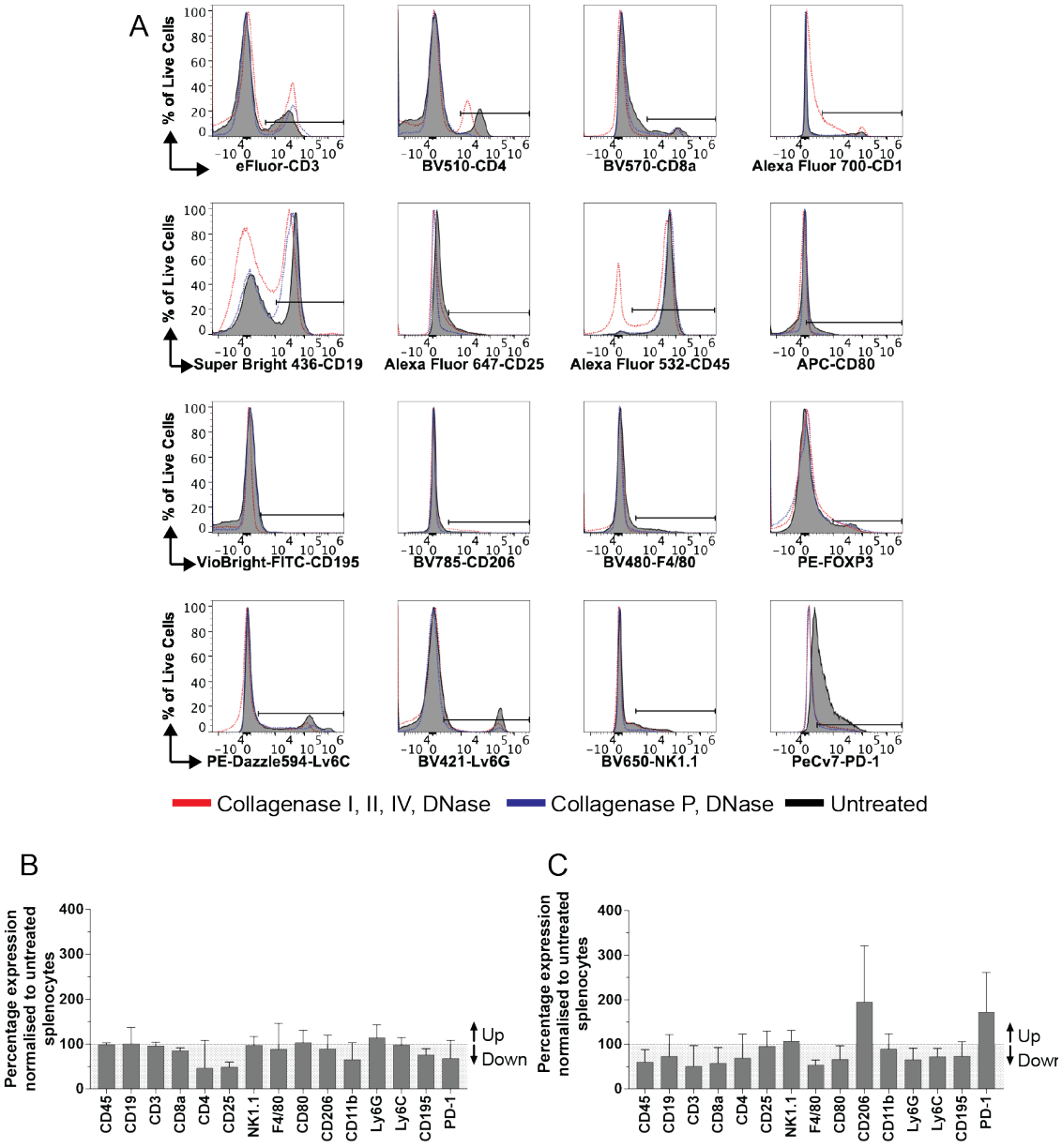


Figure 3.4: Quantification of the impact of collagenase and DNase treatment on antigen expression.

C57BL/6 naïve spleens were digested with either collagenase P and DNase or collagenase I, II, IV and DNase and antigen expression levels were compared to matched untreated splenocytes as an internal control. (A) Histograms show representative results obtained for every antigen-fluorochrome conjugate as a percentage of live cells. Gating based on FMO control. (B) Quantification of the impact of enzymatic digestion on antigen expression for Collagenase P and (C) Collagenase I, II, IV. Percent expression after digestion was normalised to antigen expression on sample-matched untreated splenocytes, which was defined as 100% (n=3).

3.3.5 Immune-phenotyping peripheral blood and tumour infiltrate in an orthotopic PDAC model

Following optimisation, characterisation of splenocyte immune populations was captured using the FC panel, with maximal separation and minimal background staining (Figure 3.5A, 3.5B).

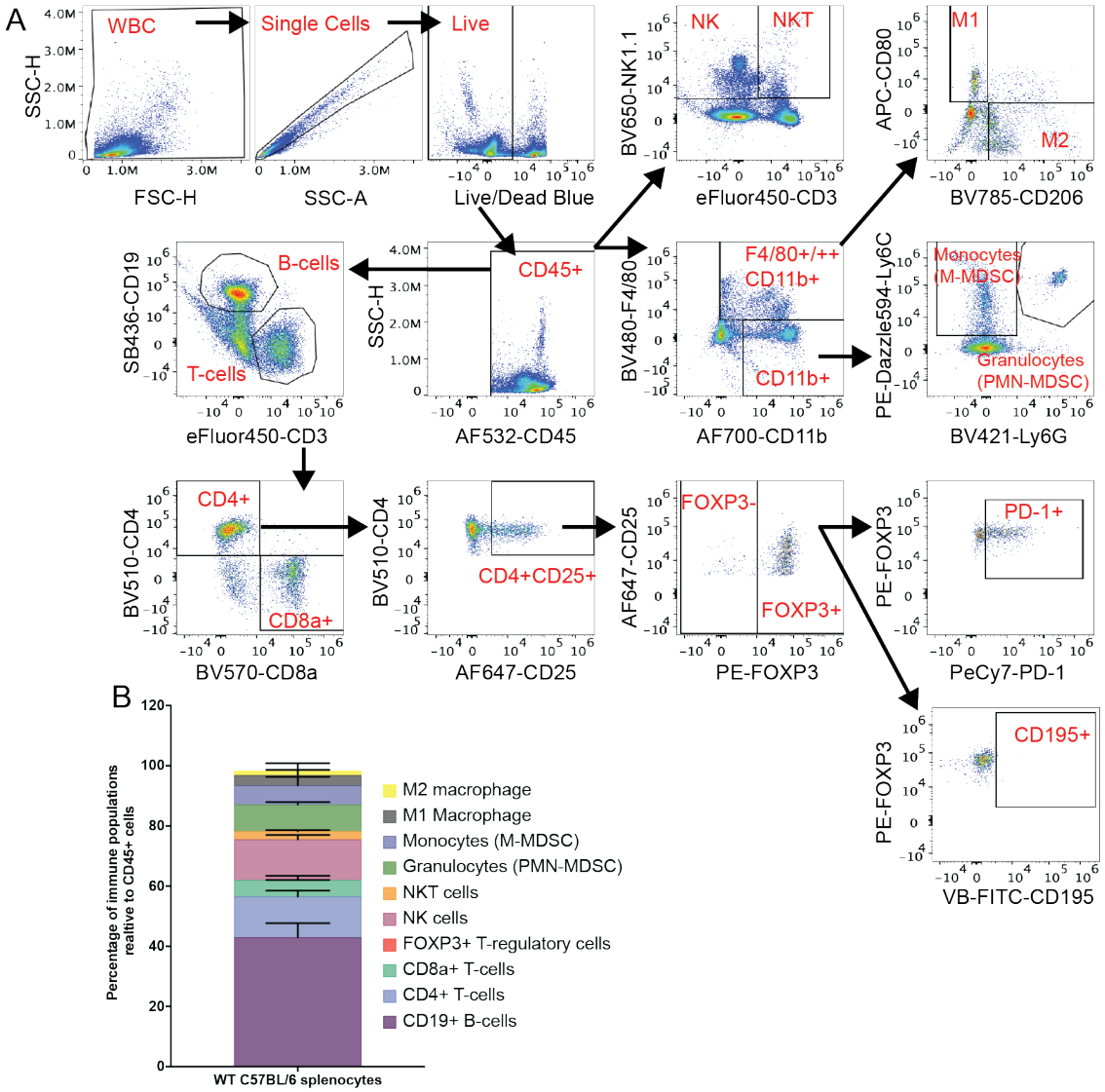


Figure 3.5: Gating strategy for analysis of cell subsets.
(A) Gating strategy on representative C57BL/6 wild type splenocyte sample. Fluorochrome abbreviations: Super Bright436 (SB436), Alexa Fluor532 (AF532), Alexa Fluor700 (AF700), Alexa Fluor 647 (AF647), VioBright-FITC (VB-FITC). (B) Graph showing mean percentage of immune cells ± SD for each population relative to CD45+ cells. B-cells (CD19+), T-helper lymphocytes (CD3+CD4+), cytotoxic T-lymphocytes (CD3+CD8a+), T-regulatory cells (CD3+CD4+CD25+FOXP3+), NK (NK1.1+) and NKT (CD3+NK1.1+), monocytes (CD11b+Ly6C+), granulocytes (CD11b+Ly6C+Ly6G+), M1 (F4/80+/+CD11b+CD80+) and M2 (F4/80+/+CD11b+CD206+) macrophages in splenocyte samples from C57BL/6 wild-type (WT) mice (n=3).

Following this, further analysis sought to determine whether the optimised panel could identify immune populations in a murine model of PDAC. To do so, an orthotopic PDAC model, with tumours around 400-600mm^3, was employed. Orthoptic tumour latency and progression are less variable than a genetic model, but still maintain their immune

repertoire compared to an immune-compromised mouse (Qiu and Su, 2013). Previous optimisation, including formation of the orthotopic tumour and MRI monitoring of tumour size, had previously been established in collaboration with Professor Jennifer Morton (Beatson Institute), Dr Simone Lanfredini (Department of Oncology), and the Department of Oncology Imaging Core. NKPCB.NBC.12.1F KPC cells were chosen for orthotopic implantation based on their epithelial and mesenchymal expression (Vimentin and E-Cadherin, Figure 3.6B), and comparable tumour growth (Figure 3.6D), which was monitored by MRI (Figure 3.6C). Generation of the orthotopic model is detailed in Figure 3.6A.

CD45+ leukocytes were identified in both the blood and tumour infiltrate (Figure 3.6C) with an expected significant difference in the percentage of tumour infiltrating leukocytes ($p>0.0001$). With the ability to identify infiltrating leukocytes, we sought to identify major immune populations in an orthotopic PDAC model (Figure 3.6D). Within the myeloid compartment we were able to discern M1 and M2 macrophages, monocytes (M-MDSC) and granulocytes (PMN-MDSC) with higher proportions in the tumour locale than the blood on average (M1 and M2 macrophages; $p=0.0152$, $p=0.0022$ respectively). The majority of the lymphoid compartment showed the opposite trend; on average higher proportions of B-cells ($p=0.0022$), cytotoxic T-cells, NK and NKT cells were present in the blood compared to tumour infiltrate. T-regulatory cells showed a marginal significant increase in infiltrate compared to the blood ($p=0.0335$). The data presents the panel's ability to capture major immune populations within the tumour microenvironment of a PDAC mouse. Moreover, this data has established the FC panel as a key tool to discern and interrogate shifting immune populations based on treatment perturbations (Chapter 4) and immune contribution to emerging lesions of PDAC (Chapter 5 and 6).

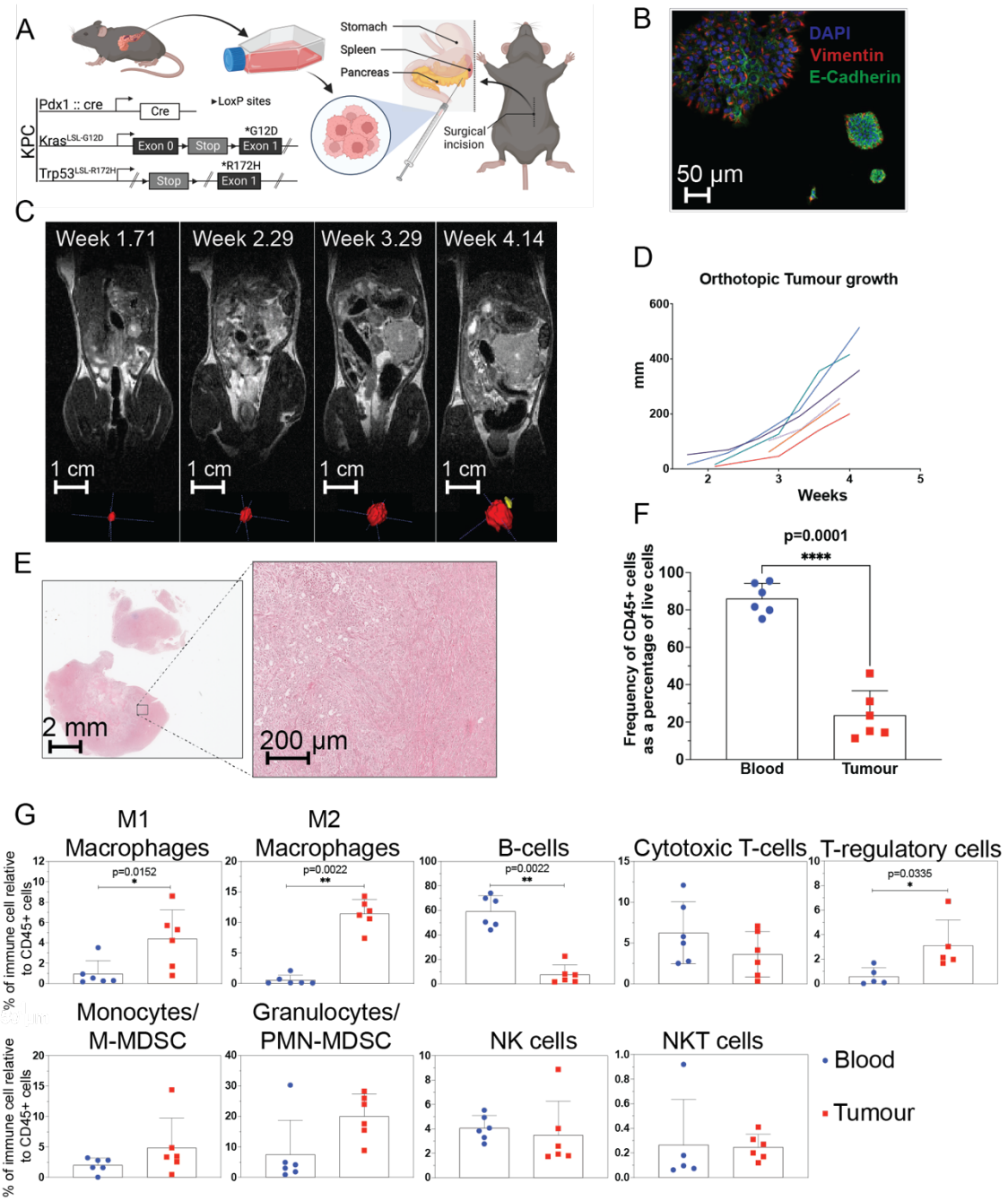


Figure 3.6: Immune profiling orthotopic syngeneic PDAC.
(A) Schematic representation of orthotopic model generation. (B) IF image of NKPCB.NBC.12.1F (KPC-F) cells derived from a KPC mouse stained with Vimentin (red), E-Cadherin (green) and DAPI (blue). Scale bar = 100 µm. (C) Cross-sectional anatomy of mouse abdomen, obtained through respiratory gated MRI, to monitor growth of orthotopically injected KPC-F cells over time. Scale bar = 1 cm. (D) Tumour growth of orthotopically injected KPC-F, 0 – 4 weeks, n = 6. Image and analysis for (B, C, D) were produced by Dr Simone Lanfredini. (E) Representative H&E stained KPC-F orthotopic tumour. Scale bar = 2 mm (left image), 200 µm (right image). (F) Total leukocyte population of blood and tumour of an orthotopic PDAC mouse, stained with the 17-colour FC panel. CD45 positivity was taken as a percentage relative to live cells and represented as a mean ± SD. Statistical significance denoted by * ($p<0.01$), ** ($p<0.001$) and *** ($p<0.0001$) and performed using two-tailed Student's t-test (n=6). (G) Graphs showing percentage of immune cells relative to CD45+ cells within an orthotopic PDAC mouse in both blood (blue) and tumour locale (red). Populations include M1 and M2 macrophages, B-cells, Cytotoxic T-cells, T-regulatory cells, monocytes (M-MDSC), granulocytes (PMN-MDSC), NK and NKT cells (n=6).

3.4 Discussion

As the field of immuno-oncology advances, better tools are required to interrogate the immune systems involvement and possible contribution to cancer manifestation. This chapter details the design and optimisation of a 17-colour FC panel for high-dimensional immunophenotyping PDAC in a murine model using spectral FC in both the peripheral blood and tissue locale.

Based on its ability to optimise larger panels for comprehensive immune cell identification, spectral FC was chosen to study the immune component of PDAC and its earlier precancerous lesions. The rationale for specific cell identification was based on previous reports in the literature regarding immune cell infiltrate within the PDAC niche. Identification of cytotoxic T-cells (CD8a+) and T-helper cells (CD4+), with additional parameters for T-regulatory cell identification, were chosen based on reports of survival benefit or detriment in PDAC patients characterised by their CD8:CD4 ratio (Carstens et al., 2017). The controversial involvement of B-cells in the PDAC microenvironment, including concurrent reports of tumour promotion and increased patient survival benefit, were included in the panel to interrogate further. (Castino et al., 2016; Minici et al., 2020). A growing body of literature has recently highlighted the potential contribution of NK and NKT cells to the PDAC milieu (Janakiram et al., 2017; Lim et al., 2019). Their inclusion in the panel sought to better understand their involvement during PDAC development and progression (Chapter 4, 5, 6).

Previously the literature has shown extensive TAM infiltration in the PDAC microenvironment, with increased infiltrate associated with poor outcome (Kurahara et al., 2011; Ino et al., 2013). TAMs have typically been associated with an M2-macrophage phenotype, but debate in the field is still ongoing given the plasticity of macrophage

polarisation (Helm et al., 2014). M1 (CD80) and M2 (CD206) markers of macrophages were included in the panel to observe their change in ratio over time and shift depending on therapies. Finally, markers for MDSCs were included considering their association with shorter survival amongst PDAC patients via T-regulatory cell induction (Siret et al., 2019; Trovato et al., 2019). Gold-standard identification of MDSCs is based on their functionality via T-cell suppression assays and interrogated further in Chapter 5.

The FC panel design captured broad immune populations rather than specifying immune cell cytokine profiles, or additional parameters for more niche cell classifications. Although this limited the panel with regard to cell specificity, for instance immunosuppressive cytokines such as IL-10 to further characterise MDSCs, at the initial stage of design it was unknown which cell types would be of interest and require greater focus. Detection of a cytokine response is limited by the size of the cell population examined and the robustness of the cytokine response, which may prove difficult in non-lymphoid tissue (Kovacs et al., 2021). Arrest of intracellular protein transport, using inhibitors such as Brefeldin A, can enhance detection of intracellular cytokines, but require injection into the animal hours prior to euthanasia and sample acquisition. When considering the complexity and length of procedure, and given Brefeldin A inhibits the secretory pathway, and therefore doesn't assess the release of members of the IL-1 family stored in the cytosol, cytokine analysis wasn't included in panel design (Dinarello, 2018; Kovacs et al., 2021). Further inflammatory cytokine analysis was broadly inspected in the plasma samples of mice profiled for FC analysis (Chapter 6) to give a global understanding of their cytokine profiling, combined with immune populations quantified by FC, in a multi-faceted approach.

When considering fluorochrome conjugation, spectral FC allows fluorochromes of similar wavelengths, with unique spectral signatures, to be included in the same panel. The combination of similar fluorochromes would require extensive optimisation, or may not be possible, with conventional FC. In addition, avalanche photodiodes (APDs) in spectral

cytometers have greater quantum efficiency at wavelengths >650 nm contributing to better signal-to-background distinction in comparison to photomultiplier tubes (PMTs) used in many conventional cytometers (Lawrence et al., 2008). This benefitted APC, Alexa® Fluor 647 and Alexa® Fluor 700 within the panel. The majority of fluorophores in the panel were excited by the violet laser, yet this had minimal impact on the Similarity™ indices for both panel variations.

Antibody titrations were carried out in accordance with standardised protocols in the literature (Hulspas, 2010). Chosen titrations were based on stain index and visualisation of separation between positive and negative populations. If the MFI of an antibody-conjugate was too high, replacement with a dimmer fluorophore, a lower titration concentration could reduce spread into other channels (Mahnke and Roederer, 2007). No replacement fluorophores were used in this instance, rather lower titrations were chosen. Subsequently FMO controls were carried out and gating parameters chosen for all further analyses.

As the panel required both immune identification in the blood and the tissue infiltrate, tissue dissociation was optimised. Despite varying degrees of antigen cleavage observed after pancreatic dissociation and tumour dissociation, no antigen was completely cleaved. Limitations to this study include the lack of additional enzymatic buffers and or varying concentrations tested. The enzymatic cocktails were chosen based on best preservation of similar immune antigen and cell viability, from a range of cocktails, in the literature (Carter et al., 2009; Quatromoni et al., 2015). Although mechanical dissociation does not result in antigen cleavage, its diminished cell viability can hinder downstream staining if dying cells are lost to sample processing (Grange et al., 2011). Similar to conclusions drawn by Quatromoni et al, no enzymatic cocktail is perfect with regard to every parameter. Despite some antigen cleavage, similar quantification was observed between orthoptic PDAC immune infiltrate in this chapter and orthotopic reports in the literature

(Spear et al., 2019). Therefore, the cocktails were deemed acceptable and used for all further analyses.

Previous studies have begun to define the immune microenvironment surrounding PDAC in orthotopic murine models but have been limited to tissue acquisition or the immune cell types identified (Lanfranca et al., 2018; Siret et al., 2019; Spear et al., 2019). Following panel optimisation, we were able to capture the relative immune population composition of leukocytes in splenocyte tissue, in agreement with other age-matched studies strengthening confidence in the panel's capabilities (Pinchuk and Filipov, 2008; Menees et al., 2021). Interrogation of an orthotopic PDAC model further revealed the scope of the FC panel, with successful identification of immune populations within the blood and tumour microenvironment. This study reports similar proportions of total leukocytes, in both blood and tumour, as previously observed in orthotopic and KPC models highlighting the reproducibility of the panel in identifying tumour infiltrate (Zhu et al., 2017; Spear et al., 2019). To this end, localised T-regulatory and cytotoxic-T cells, NK and NKT cells, M1 and M2 macrophage, granulocyte (PMN-MDSC) and monocyte (M-MDSC) infiltrate were identified, which agreed with similar reports in both murine and human PDAC samples (Liou et al., 2017a; Wang et al., 2017; Trovato et al., 2019).

CD19+ B-cell infiltrate characterised, similar to data reported by Spear et al, in which B-cells were responsible for 10% of tumour infiltrate (Spear et al., 2019). There is some discrepancy in the field regarding B-cell involvement, likely due to different models used. It has been indicated that KPC models better reflect human PDAC, with longer disease progression and pronounced stromal content allowing B-cell infiltrate, including memory and expansion (Spear et al., 2019). Spear et al determined B-cells were largely absent from the orthotopic model, likely due to accelerated progression of dominant malignant cells in comparison to the stroma (Hingorani et al., 2005; Tseng et al., 2010; Majumder et al., 2016; Spear et al., 2019). Compared to age-matched C57BL/6 WT mice, a higher percentage of B-cells was captured in the blood of the orthotopic mice (average of ~35%

vs 59.13% respectively) (Pinchuk and Filipov, 2008). However, our data agrees with previous reports of CD45+CD19+ B-cell frequency in the peripheral blood of established murine PDAC (average of ~60%) (Spear et al., 2019).

A recent study by Yang et al used the CyTOF to interrogate KPC PDAC immune infiltrate (Yang et al., 2022). While there are differences in panel design, and given the variance between genetic KPC and orthotopic models, the percentage of infiltrating cells captured in late stage tumour were similar to those identified with our panel including T-regulatory cells, cytotoxic T-cells, granulocytes (PMN-MDSC), monocytes (M-MDSC); analysis of NK and NKT wasn't included in their study (Yang et al., 2022).

Overall, the FC panel can identify major immune populations with maximal separation and minimal background staining. Importantly, we were able to optimise the panel with the capability to immune profile PDAC blood and tumour samples, with the intention to also determine immune infiltrate in models of earlier precursor lesions. The optimised FC panel aims to detect the change in the immune compartment over time, hypothesised to change over the course of PanIN lesions progression towards PDAC.

Results II

4. High-dimensional immune-phenotyping of established PDAC mouse models and dynamic perturbation of the immune microenvironment using combination immunotherapy and radiotherapy

4.1 Introduction

The acquisition of tissue after surgical resection has made it possible to investigate the immunological response to advanced disease. In tandem, it has also allowed the differentiation between treatment responders and non-responders in accordance with their immunological repertoire (Castino et al., 2016; Carstens et al., 2017; Wartenberg et al., 2018). However, it is still unclear as to why patient immune response varies and how an immunologically beneficial or detrimental microenvironment may be established in response to tumour earlier in disease pathogenesis.

Given the propensity of PDAC late-diagnosis, obtaining early low-grade patient tumour is difficult. To circumvent this challenge, genetic mouse models (GEMM), such as KPC mice, have been used to study disease. Given KPC tumours arise spontaneously, they are useful for mapping the immune response to disease over time. Several studies have utilised the model for characterisation of immune component and immunotherapy response (Feig et al., 2013; Beatty et al., 2015; Yang et al., 2022).

KPC cell lines derived from KPC GEMMS allow faithful representation of their genetic mutations in orthotopic murine models (Torres et al., 2013). Data in the literature has suggested that, as KPC cells have similar growth rates in immunodeficient and

immunocompetent mice, their immunogenicity align with an immune exhausted and/or extruded PDAC microenvironment (Lo et al., 2015; He et al., 2020). Syngeneic murine models can be established by injection of tumour cells orthotopically into the pancreatic capsule or subcutaneously in the superficial fascia. However, subcutaneous models lose their biological relevance given the tumours are situated away from the primary site of tumour development and their failure to metastasise (Fung et al., 2015). In addition, their immunological relevance is called into question given the differences in immune microenvironment and surrounding lymphatic system between pancreas and superficial fascia (Devaud et al., 2014; Zhao et al., 2017). KPC GEMM tumour did not respond to anti-PD1 and CTLA-4 treatment, whereas subcutaneous KPC GEMM had a complete response to checkpoint blockade (Ben-David et al., 2017; Christmas et al., 2018). With this in mind, subcutaneous models are better suited to non-immunological based treatments (Rubio-Viqueira et al., 2006). Similarly, discrepancies between orthotopic and GEMM PDAC immune contribution have highlighted the need for expansive, model-specific immune characterisation in both models (Spear et al., 2019).

Considering murine models are vital to assess new PDAC therapeutics, further documentation of the immune contribution allows for a greater understanding of the microenvironment in each model and subsequent therapeutic targeting. Logistical challenges can also influence therapeutic assessment in murine models. KPC GEMM tumour size and onset are often inconsistent and can act as a barrier to assay therapeutic effect. Conversely, growth kinetics of the orthotopic model provide reliability in tumour onset and size while maintaining immunological context (Qiu and Su, 2013). More importantly, its reliability allows for efficient screening of drug treatments within a short time span, from onset until full disease progression.

Currently PDAC treatment poses a challenge considering 50% of patients are diagnosed at an advanced stage and 80-85% of tumours are surgically unresectable at the time of diagnosis (Vincent et al., 2011; Park et al., 2021). Metastasis or primary lesion contact

with the aorta, superior mesenteric artery or portal vein, without the possibility of vascular reconstruction, renders the tumour unresectable according to the National Comprehensive Cancer Network[5] (Elbanna et al., 2020; Gemenetzis et al., 2021).

Adjuvant chemotherapies have provided the next line of treatment for unresectable disease or reoccurrence of tumour following resection (Herman et al., 2008; Van Laethem et al., 2010; Ducreux et al., 2015). However, these therapies haven't provided a substantial improvement in survival since their introduction some 30 years prior. Given PDAC is a cancer of unmet need, different therapeutic modalities are being assessed for greater survival benefit. Radiation treatment has provided favourable outcomes in several cancers, but its use in PDAC is controversial (Hammel et al., 2016; Landau and Kalnicki, 2018). Similar to neoadjuvant chemotherapy, radiotherapy aims to reduce the tumour border, particularly with vasculature involvement, to allow tumour resection in borderline cases. However, given high incidence of radio-resistance, radiotherapy has not offered consistent advantage in PDAC (Zhang et al., 2022).

In recent years, immunotherapy has heralded a new generation of cancer therapeutics. Unfortunately, the success of immunotherapy has not translated into the PDAC setting. This has been hypothesised to be due to low antigenicity, a low mutational burden and an immunosuppressive landscape (Ino et al., 2013; Stromnes et al., 2015; Tamborero et al., 2018). Furthermore, effector immune cells are rare within the PDAC tumour (Vonderheide and Bayne, 2013). Despite this, studies in recent years have shown combination of radiotherapy with immunotherapy has provided some benefit *in viv*o (Golden et al., 2015; Gajiwala et al., 2018). An increasingly understood phenomena, known as the 'abscopal effect', allows the benefit of radiation to go beyond the specified treatment site and is thought to be orchestrated by the systemic immune response to local radiation (Mole, 1953; Siva et al., 2015; Hu et al., 2017b). Radiation has been shown to release tumour-

[5] National Comprehensive Cancer Network (2021) Pancreatic adenocarcinoma https://www.nccn.org/patients/guidelines/content/PDF/pancreatic-patient.pdf

specific antigens from the targeted tumour via necrotic or apoptotic cell death and caspase cascade signalling (Golden et al., 2014). This, coupled with an upregulation of cytokine production at the site of radiation, is thought to alter the systemic immune response for further immune-mediated tumour destruction.

4.2 Aims

The studies described in this chapter aim to explore the immune microenvironment of orthotopic and genetic PDAC models, in the context of an established tumour, using the optimised high-dimensional FC panel for immunophenotyping. These studies also aim to investigate the perturbation of PDAC tumour using combination immunotherapies and radiotherapy, and whether this alters the immune microenvironment and subsequent tumour growth.

4.3 Results

4.3.1 Characterisation of the immune microenvironment in established PDAC models at late-stage disease.

In recent years, the immune contribution to genetic KPC and syngeneic orthotopic PDAC models has been documented in the literature (Stromnes et al., 2014; Siret et al., 2019; Wang et al., 2022a). Comparative studies between the two established models have also highlighted their discrepancies, particularly the paucity of B-cell infiltrate within the orthotopic tumour, attributed to the lack of clonal expansion due to the relatively short time-frame of orthotopic generation (4 weeks) in comparison to KPC (5-month median survival) (Spear et al., 2019). While these studies have provided an insight surrounding immune contribution to disease, analysis has predominantly focused on T-cell subsets and MDSCs locally, with a more detailed exploration lacking.

To explore the discrepancy between the genetic KPC and orthotopic tumour in greater detail, advancement of disease was first confirmed histologically. KPC tumour displayed invasive ductal carcinoma, with an abundant desmoplastic stroma and areas of luminal necrosis, characteristic of advanced disease (Figure 4.1C) (Hingorani et al., 2005). Similar histological analysis was identified in syngeneic orthotopic tumour, confirming the suitability of both models for the characterisation of advanced, high-grade disease (Chapter 3, Figure 3.6E). In lieu of an appropriate control for both KPC and orthotopic mice (control littermates; *Pdx-1-Cre+; Kras*$^{G12D+/+}$*; LSL-Trp53*$^{R172H+/+}$ and Matrigel-only orthotopic mice respectively), age-matched WT C57BL/6 mice were used as a control group for comparison of healthy pancreatic tissue against PDAC tumour (Figure 4.1B).

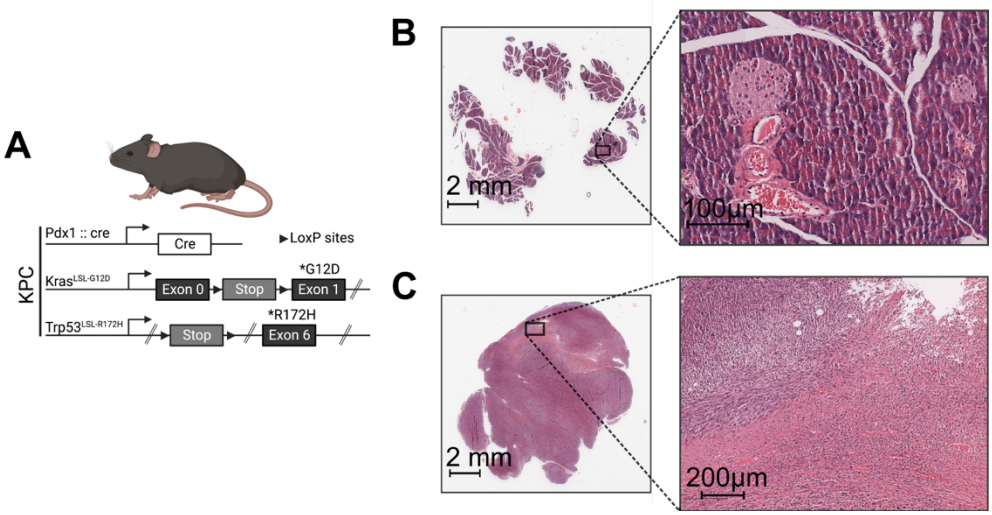


Figure 4.1: KPC genetic model is representative of late-stage PDAC tumour.
(A) Schematic diagram representing an activating point mutation (G12D) in *Kras* and a dominant negative mutation in *Trp53* (R172H) are conditionally activated in a mouse pancreas by breeding *LSL-Kras*$^{G12D/+}$*; LSL-Trp53*$^{R172H/+}$ mice to *Pdx-1-Cre* mice that express Cre recombinase under the expression of a pancreas-specific *Pdx-1* promoter. LSL = Lox-STOP-Lox. (B) Representative images of H&E staining on a C57BL/6 WT mouse pancreas (n=5) Scale bar = 2 mm (left image), 100 μm (right image). (C) Representative images of H&E staining on a KPC mouse tumour (n=4). Scale bar = 2 mm (left image), 200 μm (right image).

To investigate the systemic immune response during advancement of PDAC in greater detail, peripheral blood was taken from orthotopic mice with 400-600mm^3 tumours, and KPC mice aged between 23 – 27 weeks with palpable tumours. Orthotopic analysis,

previously detailed in Chapter 3, is presented again in this chapter for comparison to the KPC genetic model. Samples were subsequently stained with the 17-colour FC panel for immune cell identification. Myeloid populations profiled were consistently more abundant in KPC mice compared to WT control and orthotopic PDAC, including M1 and M2 macrophages, monocytes and granulocytes (Figure 4.2A/B). As expected, a significant increase in circulating monocyte/M-MDSC ($p=0.0002$) and granulocyte/PMN-MDSC ($p=0.0179$) fractions was observed in the genetic KPC model periphery (Figure 4.2B). However, these findings were not evident when comparing the orthotopic model against WT control for circulating myeloid populations analysed (Figure 4.2A/B). Instead, M1 macrophages ($p=0.0140$), M2 macrophages ($p=0.0016$) and monocytes/M-MDSCs ($p<0.0001$) were significantly increased in the KPC compared to the orthotopic model.

No difference was found for CD8a+ cytotoxic T-cells in circulation between either model of PDAC against WT control, consistent with treatment naïve PDAC patient blood samples (Steele et al., 2020; Brouwer et al., 2022). In comparison, CD4+ T-helper cells were increased above WT control for both tumour settings, but this did not translate to the T-regulatory compartment in either case (Figure 4.2D/E). Of interest, variability between the PDAC models was observed with systemic NK and NKT populations, with a significant decrease in orthotopic circulation compared to WT (Figure 4.2C; $p=0.0340$ and $p=0.0106$ respectively). While no significant difference was observed between KPC and WT control, NK ($p=0.0080$) and NKT ($p=0.0459$) cells were significantly increased in KPC GEMMs compared to orthoptic. Similarly, discrepancies between genetic and orthotopic B-cell infiltrate have previously been reported but lacked comparison in the blood (Spear et al., 2019). Interestingly a significant decrease in KPC circulating B-cells was found compared to orthotopic tumour ($p=0.003$) and WT control ($P=0.0001$) (Figure 4.2F).

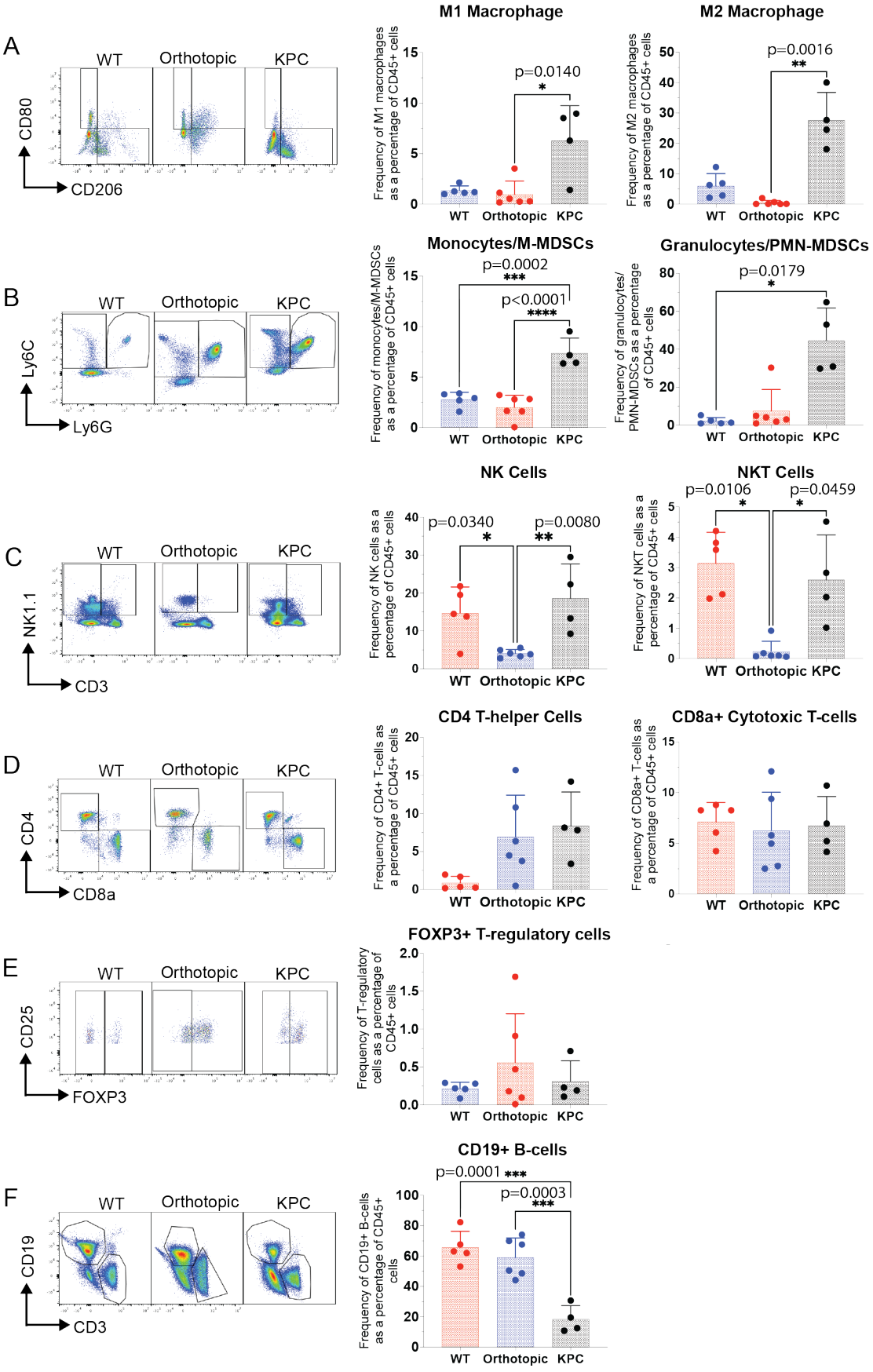

A
WT
Orthotopic
KPC
CD80
CD206
M1 Macrophage
Frequency of M1 macrophages as a percentage of CD45+ cells
p=0.0140
*
M2 Macrophage
Frequency of M2 macrophages as a percentage of CD45+ cells
p=0.0016
**
B
Ly6C
Ly6G
Monocytes/M-MDSCs
Frequency of monocytes/M-MDSCs as a percentage of CD45+ cells
p=0.0002
***
p<0.0001
****
Granulocytes/PMN-MDSCs
Frequency of granulocytes/ PMN-MDSCs as a percentage of CD45+ cells
p=0.0179
*
C
NK1.1
CD3
NK Cells
Frequency of NK cells as a percentage of CD45+ cells
p=0.0340
*
p=0.0080
**
NKT Cells
Frequency of NKT cells as a percentage of CD45+ cells
p=0.0106
*
p=0.0459
*
D
CD4
CD8a
CD4 T-helper Cells
Frequency of CD4+ T-cells as a percentage of CD45+ cells
CD8a+ Cytotoxic T-cells
Frequency of CD8a+ T-cells as a percentage of CD45+ cells
E
CD25
FOXP3
FOXP3+ T-regulatory cells
Frequency of T-regulatory cells as a percentage of CD45+ cells
F
CD19
CD3
CD19+ B-cells
Frequency of CD19+ B-cells as a percentage of CD45+ cells
p=0.0001 ***
p=0.0003
***

Figure 4.2: Comparison of the systemic immune microenvironment in established PDAC murine models.
(A) Representative gating strategy on FC dot plots for M1 and M2 macrophages (left). Quantification of M1 (CD45+F4/80+CD80+) macrophages in WT, Orthotopic and KPC blood (centre). Quantification of M2 (CD45+F4/80+CD206+) macrophages in WT, Orthotopic and KPC blood (right). (B) Representative gating strategy on FC dot plots for monocytes and granulocytes (left). Quantification of monocytes/M-MDSCs (CD45+CD11b+Ly6C+) in WT, Orthotopic and KPC blood (centre). Quantification of granulocytes/PMN-MDSCs (CD45+CD11b+Ly6C+Ly6G+) in WT, Orthotopic and KPC blood (right). (C) Representative gating strategy on FC dot plots for NK and NKT cells (left). Quantification of NK cells (CD45+NK1.1+) in WT, Orthotopic and KPC blood (centre). Quantification of NKT cells (CD45+NK1.1+CD3+) in WT, Orthotopic and KPC blood (right). (D) Representative gating strategy on FC dot plots for T-helper and cytotoxic T-cells (left). Quantification of T-helper cells (CD45+CD3+CD4+) in WT, Orthotopic and KPC blood (centre). Quantification of cytotoxic T-cells (CD45+CD3+CD8a+) in WT, Orthotopic and KPC blood (right). (E) Representative gating strategy on FC dot plots for T-regulatory cells (left). Quantification of T-regulatory cells (CD45+CD3+CD4+CD25+FOXP3+) in WT, Orthotopic and KPC blood (centre). (F) Representative gating strategy on FC dot plots for B-cells (left). Quantification of B-cells (CD45+CD19+) in WT, Orthotopic and KPC blood (centre). All quantifications were a frequency of CD45+ cells represented as a mean ± SD. Statistical significance denoted by * ($p<0.01$), ** ($p<0.001$) and *** ($p<0.0001$) and performed using a Welch and Brown-Forsythe ANOVA for parametric data or Kruskal-Wallis test for non-parametric data. Post-hoc analysis was performed using Tukey multiple comparisons test (parametric data) or Dunn's multiple comparison test (non-parametric data). WT (n=5), Orthotopic (n=6), KPC (n=4). WT; C57BL/6 wild-type

Following identification of immune subsets systemically, the localised immune infiltrate within the tumour was characterised from matched biological samples. Transverse sections of tumour, or pancreas for WT control samples, were dissected and dissociated with collagenase buffer prior to staining with the 17-colour FC panel for immune identification. Tumour-associated macrophages (TAMs) have typically been associated with an M2-like phenotype, but recently the literature has suggested greater plasticity between M1 and M2 in the tumour milieu (Murray et al., 2014; Chávez-Galán et al., 2015; Zhu et al., 2017). With this in mind, both subtypes of macrophages were profiled. M1 macrophages were significantly increased in genetic KPC tumour ($p=0.0202$) (Figure 4.3A). As expected, KPC tumours had significantly more infiltrating M2 macrophages compared to WT control ($p=0.0011$), but also to orthotopic tumour ($p=0.0046$) representing an abundant immune population present within the heterotypic tumour. Infiltrating granulocytes/PMN-MDSCs were present in both established tumour models in significant number compared to WT control (Figure 4.3B; KPC $p=0.0352$; orthotopic $p=0.0030$). By contrast, a decline in monocytic/M-MDSC infiltrate in both orthotopic

(p=0.0077) and KPC was observed in comparison to healthy WT pancreas, but no difference between the tumour types themselves.

Paucity of T-cell subsets has often been described in the context of murine and human PDAC tumour (Brouwer et al., 2022; Yang et al., 2022). While this was evident within the KPC tumour, this finding was not as apparent in the orthotopic setting; significant T-helper (p=0.0337), and T-regulatory infiltrate (p=0.0114) was found (Figure 4.3D/E).

The presence of NK cells and their contribution to the pathogenesis of PDAC remains unclear. Very low frequencies of NK and NKT cells were previously found in human PDAC tumour samples, thought to be attributed to low chemokine receptor CXCR2 expression (Lim et al., 2019; Marcon et al., 2020). Similar to this, no change in NKT infiltrate was observed compared to WT (Figure 4.3C). Lower frequencies of NK infiltrate were observed in both established tumour models compared to WT, but with discrepancies' between the two; a reduction in orthotopic NK infiltrate was observed (Figure 4.3C; p=0.0227). Similar discrepancies' were observed with CD19+ B-cell infiltrate (Figure 4.3F).

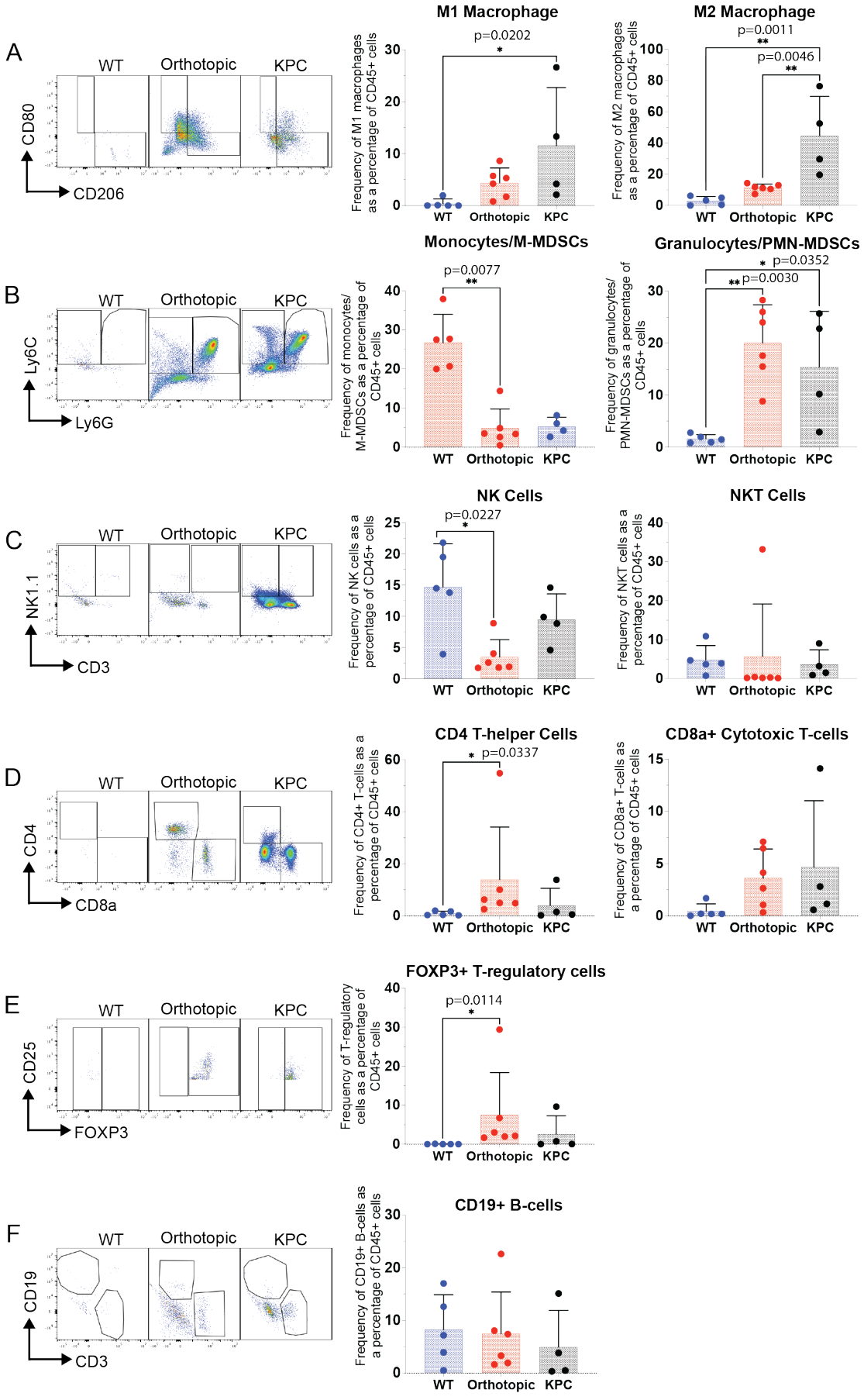

A
WT
Orthotopic
KPC
CD80
CD206
M1 Macrophage
p=0.0202
*
Frequency of M1 macrophages as a percentage of CD45+ cells
M2 Macrophage
p=0.0011
**
p=0.0046
**
Frequency of M2 macrophages as a percentage of CD45+ cells
B
Ly6C
Ly6G
Monocytes/M-MDSCs
p=0.0077
**
Frequency of monocytes/ M-MDSCs as a percentage of CD45+ cells
Granulocytes/PMN-MDSCs
* p=0.0352
** p=0.0030
Frequency of granulocytes/ PMN-MDSCs as a percentage of CD45+ cells
C
NK1.1
CD3
NK Cells
p=0.0227
*
Frequency of NK cells as a percentage of CD45+ cells
NKT Cells
Frequency of NKT cells as a percentage of CD45+ cells
D
CD4
CD8a
CD4 T-helper Cells
* p=0.0337
Frequency of CD4+ T-cells as a percentage of CD45+ cells
CD8a+ Cytotoxic T-cells
Frequency of CD8a+ T-cells as a percentage of CD45+ cells
E
CD25
FOXP3
FOXP3+ T-regulatory cells
p=0.0114
*
Frequency of T-regulatory cells as a percentage of CD45+ cells
F
CD19
CD3
CD19+ B-cells
Frequency of CD19+ B-cells as a percentage of CD45+ cells
WT
Orthotopic
KPC

Figure 4.3 Comparison of the local immune microenvironment in established PDAC murine models.
(A) Representative gating strategy on FC dot plots for M1 and M2 macrophages (left). Quantification of M1 (CD45+F4/80+CD80+) macrophages in WT, Orthotopic and KPC pancreas/tumour (centre). Quantification of M2 (CD45+F4/80+CD206+) macrophages in WT, Orthotopic and KPC pancreas/tumour (right). (B) Representative gating strategy on FC dot plots for monocytes and granulocytes (left). Quantification of monocytes/M-MDSCs (CD45+CD11b+Ly6C+) in WT, Orthotopic and KPC pancreas/tumour (centre). Quantification of granulocytes/PMN-MDSCs (CD45+CD11b+Ly6C+) in WT, Orthotopic and KPC pancreas/tumour (right). (C) Representative gating strategy on FC dot plots for NK and NKT cells (left). Quantification of NK cells (CD45+NK1.1+) in WT, Orthotopic and KPC pancreas/tumour (centre). Quantification of NKT cells (CD45+NK1.1+CD3+) in WT, Orthotopic and KPC pancreas/tumour (right). (D) Representative gating strategy on FC dot plots for T-helper and cytotoxic T-cells (left). Quantification of T-helper cells (CD45+CD3+CD4+) in WT, Orthotopic and KPC pancreas/tumour (centre). Quantification of cytotoxic T-cells (CD45+CD3+CD8a+) in WT, Orthotopic and KPC pancreas/tumour (right). (E) Representative gating strategy on FC dot plots for T-regulatory cells (left). Quantification of T-regulatory cells (CD45+CD3+CD4+CD25+FOXP3+) in WT, Orthotopic and KPC pancreas/tumour (centre). (F) Representative gating strategy on FC dot plots for B-cells (left). Quantification of B-cells (CD45+CD19+) in WT, Orthotopic and KPC pancreas/tumour (centre). All quantifications were a frequency of CD45+ cells represented as a mean ± SD. Statistical significance denoted by * ($p<0.01$), ** ($p<0.001$) and *** ($p<0.0001$) and performed using a Welch and Brown-Forsythe ANOVA for parametric data or Kruskal-Wallis test for non-parametric data. Post-hoc analysis was performed using Tukey multiple comparisons test (parametric data) or Dunn's multiple comparison test (non-parametric data). WT (n=5), Orthotopic (n=6), KPC (n=4). WT; C57BL/6 wild-type.

4.3.2 Combination of fractionated low-dose radiation and immunotherapy reduces tumour volume in a PDAC orthotopic model.

Following the generation and detailed immune characterisation of two advanced models of PDAC, analysis to determine whether alteration to the immune microenvironment could offer therapeutic benefit was carried out.

Blockade of checkpoint inhibitor PD1/PD-L1 axis has shown great success in the field of cancer immunotherapy, including melanoma, renal cell and non-small cell lung carcinoma (Iwai et al., 2002; Topalian et al., 2012; Hamid et al., 2013). Despite its expression in human PDAC samples, monotherapies against the PD1/PD-L1 have lacked efficacy due to the aforementioned reduction in immunogenicity and antigenicity with an

immunosuppressive landscape (Hutcheson et al., 2016). Yet when combined with radiotherapy, blockade of PD-L1 significantly enhanced orthotopic PDAC tumour response in a cytotoxic T-cell context (Azad et al., 2017).

The association between FOXP3+ T-regulatory cells and poor patient prognosis has suggested T-regulatory cell involvement in orchestrating an exhausted, immunosuppressed microenvironment in PDAC (Yamamoto et al., 2012). The expression of C-C chemokine ligand 5 (CCL5) by FOXP3+ T-regulatory cells was found to recruit T-regulatory cells from the periphery into the tumour vicinity both *in vitro* and *in vivo* (Wang et al., 2017). CCL5 is typically expressed by inflammatory cells, including T-cells and monocytes (Zeng et al., 2022). While CCL5 can bind to C-C chemokine receptor 1 (CCR1), C-C chemokine receptor 3 (CCR3) and C-C chemokine receptor 4 (CCR4), its highest affinity is towards C-C chemokine receptor 5 (CCR5) (Velasco-Velázquez et al., 2014; Aldinucci et al., 2020). CCR5, a G-protein-coupled receptor, is expressed on smooth muscle, T-cells, endothelial, epithelial and parenchymal cells (Schlecker et al., 2012).

Considering CCL5 was found to be upregulated by human and murine tumour cells, disruption of the CCL5/CCR5 signalling axis reduced T-regulatory cell migration into orthotopic PDAC tumour *in vivo* (Tan et al., 2009). Furthermore, our lab had previously collaborated on the randomised phase 2 SCALOP trial in which high levels of circulating CCL5 were found to be associated with low overall survival in PDAC patients and subsequently identified as a prognostic marker of locally advanced PDAC (Willenbrock et al., 2021).

Based on previous literature, and our collaboration, we sought to improve PDAC tumour response with a multi-faceted approach: (1) low-dose radiotherapy aimed to create an immunologically ‘hot’ microenvironment surrounding the tumour through the abscopal effect, (2) blockade of the PD-1/PD-L1 axis aimed to reignite previously exhausted and/or

excluded T-cells, (3) inhibition of CCR5 sought to reduce the immunosuppressive landscape in a T-regulatory cell-dependent manner. Considering homogenous orthotopic PDAC offered a reproducible tumour microenvironment to assess treatment response, it was chosen for the purposes of this study.

To investigate the combination of radiotherapy and immunotherapy on PDAC tumour in an *in vivo* setting, a syngeneic PDAC orthotopic model was generated by injecting NKPCB.NBC.12.1F KPC cells in C57BL/6 WT mice. 12-days post-surgery, mice were treated with a combination or variation of 5 mg/kg aPD1, 10 mg/kg CCR5i and 4 Grays (Gy; 1 Gy = 1 Joule/kilogram) depending on treatment group according to Figure 4.4A. Tumour and blood was collected at 30 days, or when tumour volume reached 600 mm^3. Tumour volume was assessed via MRI following treatment induction. Radiation (depicted as IR) significantly reduced tumour volume in all variations of immunotherapy combination (Figure 4.4C). Considering non-IR treatment groups did not reduce tumour volume in comparison to untreated mock, IR-only treatment groups were analysed further. While no significant difference in tumour volume (Figure 4.4D) or cellularity (Figure 4.4E) was observed between combination treatment groups, CCR5i+aPD1+IR treated mice had a reduction of p53 positive cells within the tumour ($p=0.0194$), indicating fewer malignant cancer cells (Figure 4.4F) (Ando et al., 2015). Additionally, an increase in necrosis was observed with combination CCR5i+aPD1+IR treatment (Figure 4.4G).

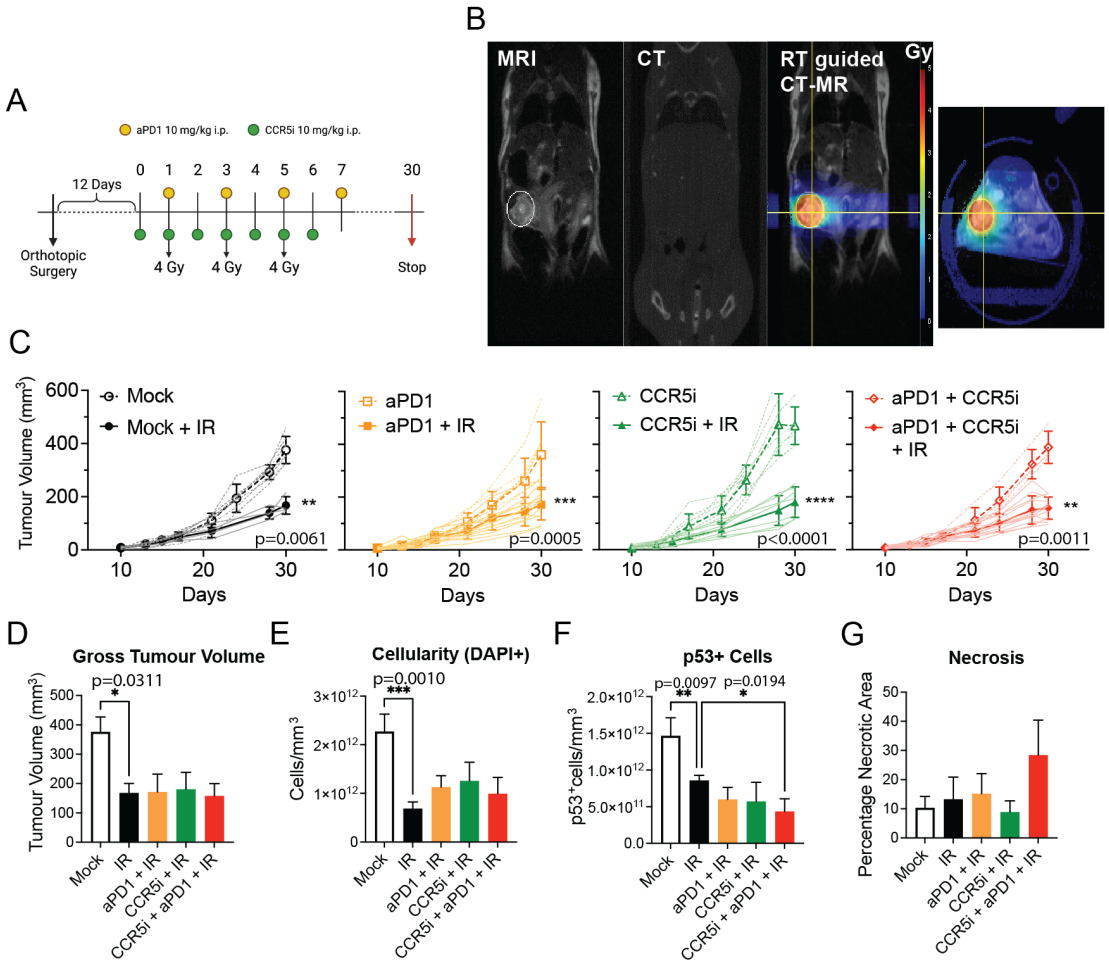


Figure 4.4: Fractionated low-dose radiotherapy and combination immunotherapies reduce tumour volume in an orthotopic mouse.
(A) Schematic of treatment schedule. (B) Representative images of cross-sectional anatomy of a mouse abdomen, obtained through respiratory gated MRI (left), SARRP (centre; labelled CT), and an overlay of the MRI and CT images for tumour-specific dosage of 4 Gy (right). (C) Tumour volume of orthotopic tumour, quantified from MRI images, for treatment groups Mock+/- IR (black), aPD1+/- IR (yellow), CCR5i+/- IR (green) aPD1+CCR5i+/- IR (red). (D) Gross orthotopic tumour volume in treatment groups. Data represented as mean tumour volume ± SD. (E) Quantification of DAPI positive cells within the tumour for each treatment group. Data represented as mean DAPI positive cells per mm^3 ± SD (F) Quantification of p53 positively stained cells via IHC within the tumours of each treatment group. Data represented as p53 DAB positive cells per mm^3 ± SD (G) Percentage of visual, histological necrotic area within each treatment group. Data represented as mean percentage positive cells ± SD. Statistical significance denoted by * (p<0.01), ** (p<0.001) and *** (p<0.0001) and performed using an unpaired T-test for parametric data or a Mann-Whitney test for non-parametric data for tumour volume at 30 days (C) or a Welch and Brown-Forsythe *ANOVA* for parametric data or Kruskal-Wallis test for non-parametric data for all further analysis. Post-hoc analysis was performed using Tukey multiple comparisons test (parametric data) or Dunn's multiple comparison test (non-parametric data). Mock (n=6), IR (n=3), aPD1 (n=8), aPD1+IR (n=8), CCR5i (n=3), CCR5i+IR(n=8), aPD1+CCR5i (n=5), aPD1+CCR5i+IR (n=8). Quantification of tumour volume and histological quantification was carried out by Dr Simone Lanfredini.

4.3.3 Immune response in orthotopic tumour following combination fractionated low-dose radiation and immunotherapy.

In parallel to the quantification of tumour volume, the impact of radiotherapy in combination with immunotherapies on the immune system was evaluated. Transverse sections of orthotopic tumour, from mice treated with IR, aPD1+IR, CCR5i+IR or aPD1+CCR5i+IR, were quantified for immune infiltrate using the 17-colour FC panel. Mock samples were also evaluated as an untreated control tumour setting. Peripheral blood was taken for systemic immune quantification and stained using the same 17-colour FC panel in tandem (Supplementary 8.3).

Upon aPD1+IR treatment, CD8+ cytotoxic T-cell, T-helper cell and NK cell subsets were increased in the tumour locale (Figure 4.5A/B/D, NK; p=0.0360). Intriguingly, aPD1+IR significantly reduced tumour infiltrating B-cell (p=0.0061) and reduced M1 macrophages (Figure 4.5F).

Consistent with aPD1+IR, CCR5i+IR increased CD8 cytotoxic T-cells, but also allowed greater NKT cell infiltrate into the tumour vicinity (Figure 4.5A/E). CCR5i+IR conferred a significant increase in T-helper (p=0.0224) and NK cell tumour infiltrate (p=0.0360) compared to IR and allowed a greater expansion of these subsets compared to any other treatment regimen (Figure 4.5B/D). In addition, CCR5i+IR reduced B-cell, M1 macrophage and granulocyte/PMN-MDSC tumour infiltrate compared to IR alone (Figure 4.5F/G). Despite this finding, an expansion of tumour-promoting monocytes/M-MDSC and M2 macrophage was found (Figure 4.5H/J).

aPD1+CCR5i+IR combination did not significantly increase any immune cell infiltrate beyond that of aPD1+IR or CCR5i+IR. Interestingly combination treatment and CCR5i+IR, but not aPD1+IR, conferred an expansion of NKT cell infiltrate (Figure 4.5E). Conversely

a significant reduction in circulating NKT was observed with these treatments compared to IR alone (Supplementary 8.3E, CCR5i+IR; p=0.485, aPD1+CCR5i+IR; p=0.0045). This data would suggest an NKT infiltration axis, from the blood to the tumour, occurs upon addition of CCR5i to treatment regimen, while aPD1 had no effect. Although aPD1+IR significantly reduced B-cell infiltrate, this effect was lost upon addition of CCR5i to the combination treatment (Figure 4.5F). Within the blood, radiotherapy increased the number of B-cells compared to untreated mock, but no difference between immunotherapy was found (Supplementary 8.3F).

Despite what had previously been shown in the literature, FOXP3+ T-regulatory cells significantly infiltrated the tumour regardless of immunotherapy compared to IR treatment alone (Figure 4.5C, aPD1+IR; p=0.0001, CCR5i+IR; p=0.0117, aPD1+CCR5i+IR; p=0.0460). Yet all immunotherapy treatment groups were comparative with untreated mock (IR-) mice. This rather contradictory result was unexpected, particularly when CCR5i was included in the treatment regimen. A significant increase in FOXP3+ cells was observed in the blood following aPD1+IR and CCR5i+IR treatment compared to IR alone (Supplementary 8.3C, aPD1+IR; p=0.0050, CCR5i+IR; p=0.0359).

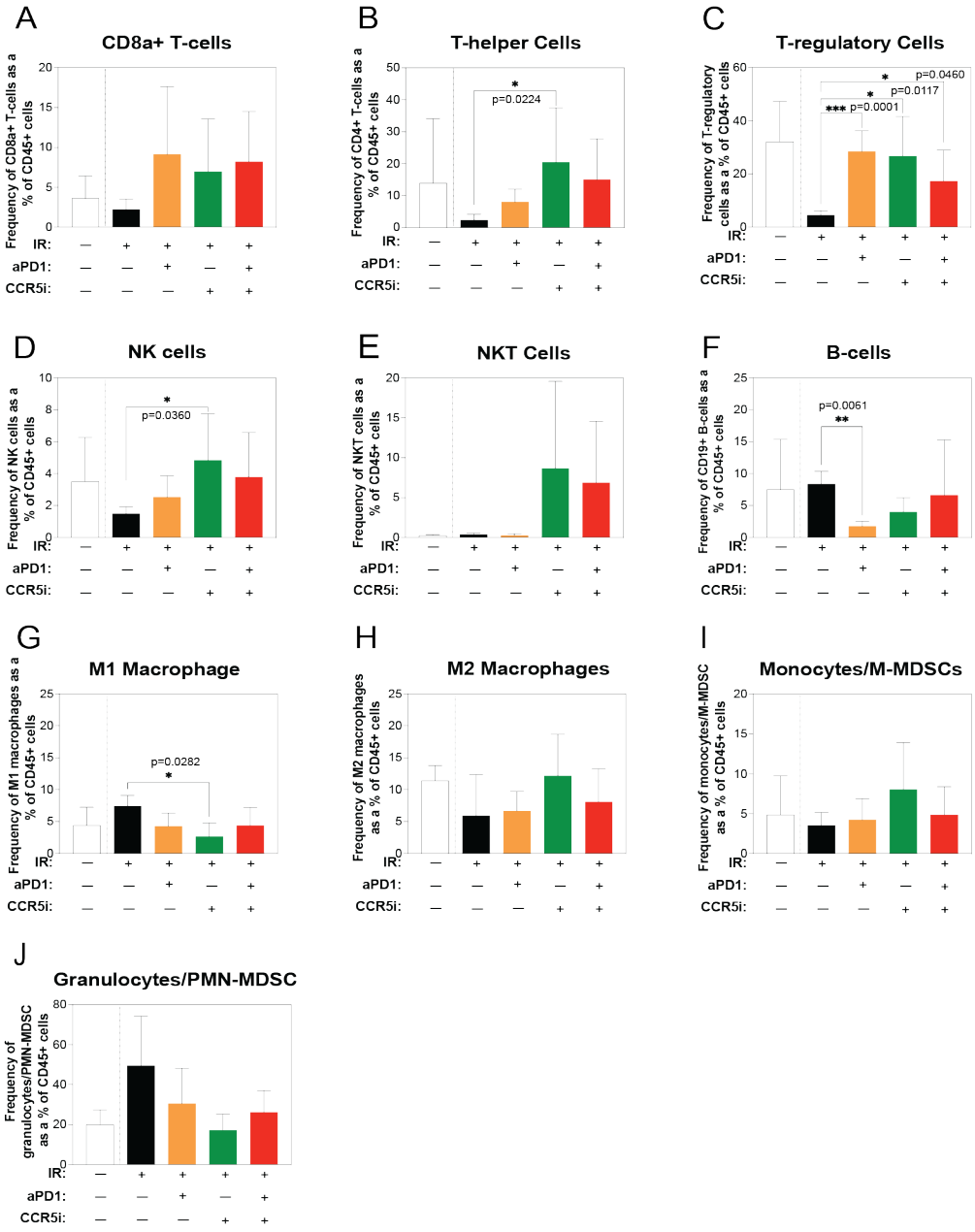


Figure 4.5: Modulation of local tumour immune infiltrate following fractionated low-dose radiotherapy and combination immunotherapies in an orthotopic mouse.

Graphs showing percentage of immune cells relative to CD45+ cells within an orthotopic PDAC murine tumour following treatment. Mock untreated (white), IR (black), aPD1+IR (yellow), CCR5i+IR (green), aPD1+CCR5i+IR (red). Immune cells characterised include (A) CD8+ T-cells, (B) CD4+ T-helper cells, (C) T-regulatory cells, (D) NK cells, (E) NKT cells, (F) B-cells, (G) M1 macrophages, (H) M2 macrophages, (I) Monocytes/M-MDSCs and (J) Granulocytes/PMN-MDSCs. Data represented as mean percentage positive cells ± SD. Statistical significance denoted by * ($p<0.01$), ** ($p<0.001$) and *** ($p<0.0001$) and performed using a Welch and Brown-Forsythe ANOVA for parametric data or Kruskal-Wallis test for non-parametric data. Post-hoc analysis was performed using Tukey multiple comparisons test (parametric data) or Dunn's multiple comparison test (non-parametric data). Mock (n=6), IR (n=3), aPD1+IR (n=8), CCR5i+IR (n=8), aPD1+CCR5i+IR (n=8).

Across the myeloid cell tumour infiltrate, differences were observed in the extent of infiltrate suppression. While CCR5i+IR treatment resulted in a significant reduction of infiltrating M1 macrophages (Figure 4.5G; p=0.0282), neither immunotherapy nor combination had much effect on M2 macrophages (Figure 4.5H). While no immunotherapy appeared to alter the monocyte/M-MDSC or granulocyte/PMN-MDSC infiltrate (Figure 4.5I/J), fractionated radiotherapy increased CD11b+Ly6C+Ly6G+ granulocyte presence within the tumour. This result may be due to the presence of PMN-MDSCs, given their increase in response to chronic inflammation as a result of fractionated radiotherapy. This is also supported by the fact that this increase in CD11b+Ly6C+Ly6G+ granulocytes/PMN-MDSCs was attenuated with the addition of immunotherapies. Immune population expression of PD1 (Supplementary 8.4) and CCR5 (Supplementary 8.5) was not significantly altered with immunotherapy treatment.

4.3.4 Spatial resolution reveals a non-activated NK cell signature associated with CD8 T-cell infiltration and reduction in tumour volume following combination treatment.

The observed differences between radiotherapy alone and combination with aPD1 and CCR5i suggest implications for CD8a+ cytotoxic T-cell, NK and NKT cell tumour infiltration when treatments were combined. However, considering FC requires tumour cell dissociation in a single-cell suspension, the spatiality of immune infiltrate within the tumour was unknown. It was not possible to discern the penetration of immune infiltrate towards the centre of the tumour, or whether these cells remained excluded at the periphery. Tertiary lymphoid structures have been characterised in clinical PDAC tumours and found to be prognostic for improved survival in treatment naïve patients (Gunderson et al., 2021).

FC alone is not able to discern lymph node presence as a potential source of infiltrating immune cells within the analysed samples.

With this in mind, we utilised the 7-colour Vectra Polaris for immunofluorescent (IF) staining on transverse tumour sections. Formalin-fixed paraffin embedded (FFPE) tumour samples were sectioned to a thickness of 4 μm for evaluation by IF. Optimisation of the IF panel and staining was carried out by the Transitional Histopathology Lab, University of Oxford (THL) (Figure 4.6A). Quantification of staining was blinded and carried out by Simei Go (O'Neill lab). aPD1+IR treatment samples showed inconsistent staining, therefore excluded from analysis (data not shown). TIGIT staining also showed variable inconsistency, and similarly excluded from further analysis (data not shown). Staining was characterised as tumour (E-cadherin+) or immune infiltrate for CD4 (CD3+CD8-CD161-), CD8 (CD8+CD161-) and activated NK cells (CD161+NKG2D+) (Figure 4.6C). Although these immune cells were shown to infiltrate the tumour via FC, data acquired showed little or no significance due to variability within the data. When considering visualisation of immune infiltrate, tumours were classified as responder or non-responder depending on reduction of tumour; a pre-determined 20% threshold was used to classify responder (<20% E-Cadherin of total cells) and non-responder (>20% E-Cadherin of total cells) (Figure 4.6C).

The number of tumour infiltrating CD8+ T-cells increased when orthotopic mice were treated with CCR5i and radiotherapy and further enhanced with the addition of aPD1 to the treatment regimen (Figure 4.6B). While this data was non-significant, variability of the response can be attributed to responder and non-responder E-Cadherin staining (Figure 4.6C). The desmoplastic stroma acts as a physical barrier to immune cell penetrance within PDAC tumour (Provenzano et al., 2012). Further understanding regarding how treatment affected the degree of immune infiltrate towards the central tumour core was sought. Each tumour section, stained with the IF panel, was partitioned into five concentric circles of arbitrary distance, based on tumour diameter, from the tumour periphery to the

central core (1 indicating central core of tumour, 5 indicating tumour periphery). Both CD8+ T-cells and activated NK cells were analysed (Figure 4.6D). Both cell types were greater in cell number towards the tumour periphery compared to the central core, decreasing in number towards the core. While variability and non-significance were evident, the combination of aPD1+CCR5i+IR did evoke an increase in effector-cells at the central core of tumour compared to CCR5i+IR, IR alone or untreated tumour. Again, this could be attributed to the variability in responder vs non-responder per treatment group (Figure 4.6C). Given the homogeneity of the orthotopic model, specifically chosen for consistency of PDAC tumour, we wanted to understand the discrepancies in E-cadherin response and whether this was immune cell specific. Immune cells were stratified against tumour response (<20% E-Cadherin) or non-response (>20% E-cadherin) irrespective of treatment. No difference was observed between CD4+ T-cells, CD8+ T-cells, total NK cells or activated NK cells. Interestingly, a significant increase in non-activated NK cells ($p=0.0444$) was observed in tumours with low E-cadherin (Figure 4.6E). An association between non-activated NK cells and low E-cadherin (<20%) was found, predominantly following CCR5i+IR and aPD1+CCR5i+IR treatment (Figure 4.6F, $r^2=0.4761$, $p=0.0031$). In addition, significant positive correlation between non-activated NK cells and higher CD8+ T-cell infiltrate was also found in the same treatment groups (CCR5i+IR and aPD1+CCR5i+IR) (Figure 4.6G, $r^2=0.3937$, $p=0.0093$). Association between E-cadherin and CD4, CD8, activated NK cells or total NK cells was analysed (Supplementary 8.6), but yielded lower r^2 values implying that those cells were less predictive of E-cadherin outcome. This data indicates that tumour response may be associated with non-activated NK cells and CD8 T-cells. However, further work is required to confirm this relationship given the weak association and, if so, why a differential response to combination immunotherapy and radiotherapy was observed in orthotopic PDAC tumour.

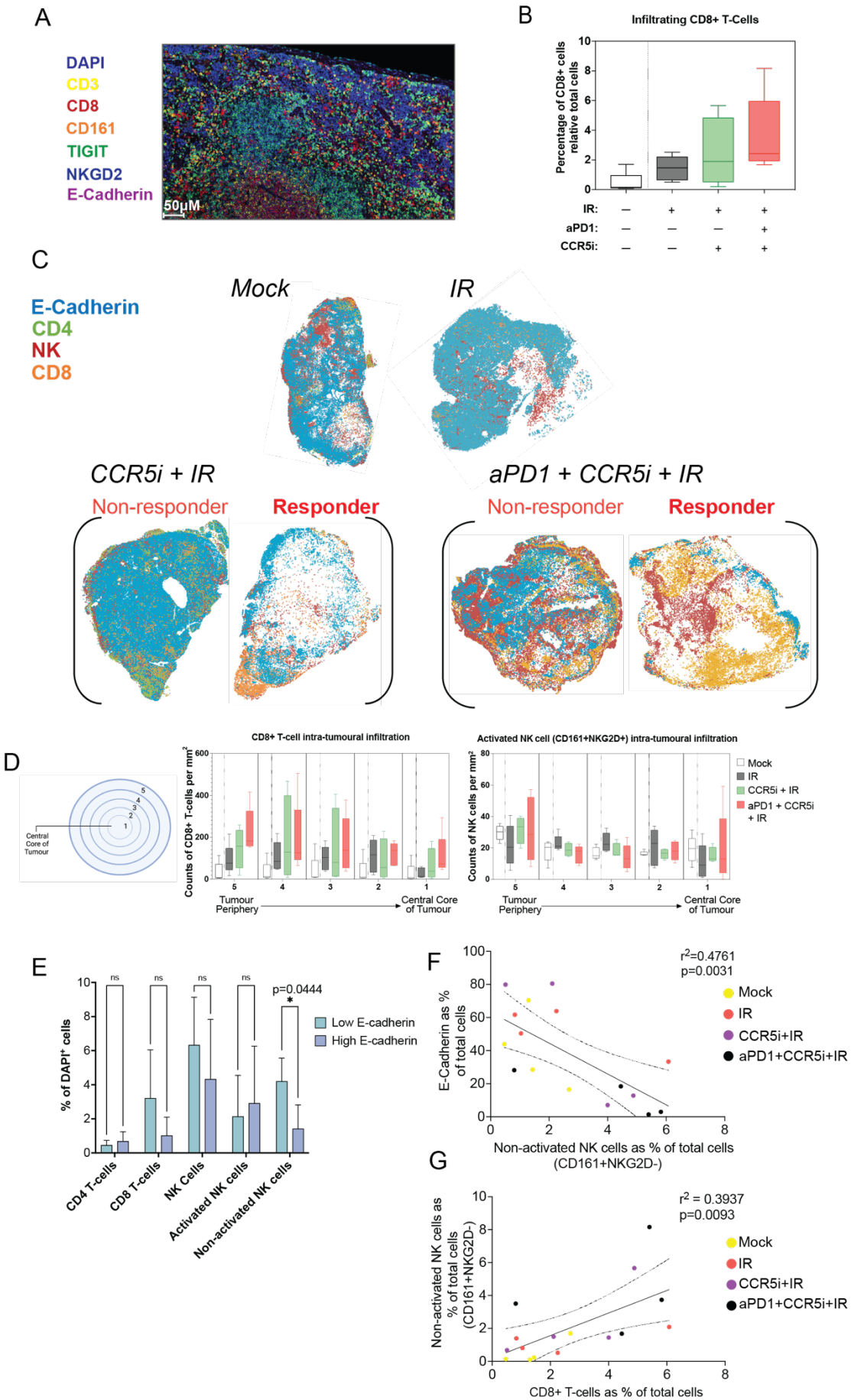

A
DAPI
CD3
CD8
CD161
TIGIT
NKGD2
E-Cadherin
50µM
B
Infiltrating CD8+ T-Cells
Percentage of CD8+ cells relative total cells
IR:
aPD1:
CCR5i:
C
E-Cadherin
CD4
NK
CD8
Mock
IR
CCR5i + IR
aPD1 + CCR5i + IR
Non-responder
Responder
Non-responder
Responder
D
Central Core of Tumour
CD8+ T-cell intra-tumoural infiltration
Counts of CD8+ T-cells per mm²
Tumour Periphery
Central Core of Tumour
Activated NK cell (CD161+NKG2D+) intra-tumoural infiltration
Counts of NK cells per mm²
Mock
IR
CCR5i + IR
aPD1 + CCR5i + IR
E
% of DAPI+ cells
ns
p=0.0444
Low E-cadherin
High E-cadherin
CD4 T-cells
CD8 T-cells
NK Cells
Activated NK cells
Non-activated NK cells
F
r²=0.4761
p=0.0031
E-Cadherin as % of total cells
Non-activated NK cells as % of total cells (CD161+NKG2D-)
Mock
IR
CCR5i+IR
aPD1+CCR5i+IR
G
r² = 0.3937
p=0.0093
Non-activated NK cells as % of total cells (CD161+NKG2D-)
CD8+ T-cells as % of total cells
Mock
IR
CCR5i+IR
aPD1+CCR5i+IR

Figure 4.6: IF spatial resolution of local tumour immune infiltrate following fractionated low-dose radiotherapy and combination immunotherapies in an orthotopic mouse.
(A) Representative image of immunofluorescent panel optimisation on C57BL/6 spleen tissue sample. DAPI (blue), CD3-Opal 480 (yellow), CD8-Opal 570 (red), CD161-Opal 620 (orange), TIGIT-Opal 690 (green), NKG2D-Opal 520 (purple), E-cadherin-Opal 780 (pink). Scale bar = 50 μm. (B) Graphs showing percentage of CD8+ T cell infiltrate relative to total DAPI+ cells following treatment. Mock untreated (white), IR (black), CCR5i+IR (green), aPD1+CCR5i+IR (red). Data represented as mean percentage positive cells ± SD. (C) Representative images of whole tissue sections of pancreata stained with the immunofluorescent panel detailing E-cadherin (blue; E-cadherin+), CD4 (green; CD3+CD8-CD161-), NK (red; CD161+NKG2D+) and CD8 (yellow; CD8+CD161-). (D) Intra-tumoural infiltration of CD8+ T cells (left graph) and activated NK cells (CD161+NKG2D+, right graph) following Mock untreated (white), IR (black), CCR5i+IR (green) or aPD1+CCR5i+IR (red) treatment. Data represented as mean percentage positive cells ± SD. Infiltrate was determined based on 5 concentric circles of arbitrary distance from the tumour periphery (5) to the central core (1), detailed by the schematic. (E) Graph showing immune cell stratification against low E-cadherin (<20%, green) (n=7) and high E-cadherin (>20%, blue) (n=15) as a percentage of DAPI+ cell. Data represented as mean percentage positive cells ± SD. Statistical significance denoted by * ($p<0.01$), ** ($p<0.001$) and *** ($p<0.0001$) and performed using a two-way ANOVA. Post-hoc analysis was performed using Šídák's multiple comparisons test. (F) Graph showing correlation between non-activated NK cells (CD161+NKG2D-) and E-cadherin as a percentage of total cells and (G) correlation between non-activated NK cells (CD161+NKG2D-) and E-cadherin as % of total cells for Mock (yellow), IR (red), CCR5i+IR (purple), and aPD1+CCR5i+IR (black), treatment groups. Data points represent biological replicates. Sold line displays simple linear regression with 95% confidence intervals (dotted black lines). Mock (n=4), IR (n=3), CCR5i+IR (n=4), aPD1+CCR5i+IR (n=4). Analysis was conducted by Simei Go and Professor Eric O'Neill.

4.4 Discussion

4.4.1 Immune microenvironment surrounding advanced models of PDAC

Murine models have provided a useful tool to investigate the immunology of PDAC and provide insight into disease management and therapeutic options. However, differences in immunological contribution to the tumour locale between genetic heterozygous and orthotopic homogenous murine models have prompted further investigation. Difference in mechanistic properties and stromal content between these PDAC models has been well documented. Longer disease progression and significant stromal content is present in both KPC and human PDAC (Hingorani et al., 2005). Differentially, orthotopic models display an accelerated disease progression in which a homogenous malignant cell content

is dominant (Tseng et al., 2010; Majumder et al., 2016). These differences are likely to alter their immunological microenvironment, given the stroma is a pivotal component of PDAC (Kadaba et al., 2013). Indeed, differential immune populations have been associated with different stromal compartments (juxtatumoral stroma and panstromal) that correlate with patient survival (Ene-Obong et al., 2013). In this chapter, KPC and orthotopic PDAC mice, representing homogenous and heterogenous clonal expansion of tumour at the advanced stage, were used to further understand differences in the immunological repertoire on a broader scale compared to previous literature. Furthermore, characterisation was applied to both systemic blood and localised tumour for thorough understanding of these differences.

The data revealed varying frequencies of immune populations, both in circulation and tumour infiltration, between the two models. In agreement with the literature, an increase in circulating and tumour infiltrating granulocytes/PMN-MDSC within the KPC model was evident (Stromnes et al., 2014). Percentages of both monocytes/M-MDSC and granulocytes/PMN-MDSC were consistent with treatment naïve patient peripheral blood mononuclear cells (PBMC) prior to surgical resection, indicating suitable recapitulation of human disease for these populations (Karakhanova et al., 2015; Brouwer et al., 2022). Expansion of circulatory MDSCs within PDAC patients has been associated with poor prognosis and correlates with stage and grade of disease (Gabitass et al., 2011; Mundy-Bosse et al., 2011; Porembka et al., 2012). Inconsistent with the circulatory KPC myeloid response, frequencies of these populations were relatively unaffected in the systemic orthotopic setting. While similar percentages for circulatory monocytes/M-MDSC was detailed in the literature for orthotopic PDAC, granulocytes/PMN-MDSCs frequencies were lower than previous reports (Nielsen et al., 2021). Similarly, M1 and M2 macrophages were increased both systemically and locally in the genetic model, but not abundant in orthotopic circulation. Recently Zhu et al reported two subsets of TAMs within PDAC tumour, originating from either Ly6C+ monocytes peripherally or tissue-resident

macrophages of embryonic origin (Zhu et al., 2017). Further studies have shown Ly6C+ monocytes switch from a pro-inflammatory to immunosuppressive macrophages with time and PDAC progression (Yang et al., 2022). Although the data does not account for macrophage origin, a reduction of orthotopic circulatory monocytes, compared to KPC, may account for subsequent reduction in both circulatory and infiltrating orthotopic macrophages. This could be attributed to the shorter timeframe of disease generation compared to typical PDAC progression but would require further investigation.

Caution was taken regarding characterisation of MDSCs given their functionality, and therefore confirmation of their presence, could not be quantified using the FC panel alone. However, given MDSCs play a role in establishing an immunosuppressive microenvironment, at the tumour and systemic level, it is likely that this data may be, at least in part, representative of this cell type rather than granulocytes and monocytes alone.

Unusually monocytes/M-MDSC infiltrate was lower in both murine models, with significance in the orthotopic setting. In the human setting, no significant difference between human control and PDAC tumour for equivalent monocytic myeloid cells (CD14+CD33+HLA-DR^{low}) was found (Brouwer et al., 2022). Caution should be taken when interpreting KPC and orthotopic data against patient monocyte/MDSC infiltrate due to this difference. One possible implication of this data, in combination with data produced by Brouwer et al, is that monocytes/M-MDSCs may not have as significant a role in driving immunosuppression as granulocytes/PMN-MDSCs given the difference in frequency in the tumour locale. However, further investigation is warranted.

Interestingly both advanced PDAC models have comparative circulating T-cell population, which were similar in percentage to control, suggesting these cell populations are not discriminatory or prognostic of advanced disease. Similar to myeloid infiltrate, frequencies of CD8 cytotoxic T, CD4 T-helper, T-regulatory cell and B-cells agreed with late-stage KPC tumour analysed via CyTOF (Yang et al., 2022). CD8 cytotoxic T-cell and T-

regulatory tumour infiltrate was also indicative of human patient data, but surprisingly not B-cell infiltrate (Brouwer et al., 2022). Brouwer et al found a significant increase compared to adjacent non-malignant pancreatic tissue (16% B-cells of CD45+ cells on average), while data in this chapter showed lower infiltrate (4.92% of CD45+ cells). Discrepancies between orthotopic and KPC B-cell infiltrate have previously been documented (Spear et al., 2019). While frequency of orthotopic infiltrate was similar to those reports, data in this chapter showed KPC B-cell infiltrate at a lower frequency. It has been indicated KPC models better reflect human PDAC with longer disease progression and pronounced stromal content allowing B-cell infiltrate, including memory and expansion. This is largely absent from the orthotopic model, likely due to accelerated progression of dominant malignant cells in comparison to the stroma (Hingorani et al., 2005; Tseng et al., 2010; Majumder et al., 2016). However, with a small KPC sample size, caution must be applied, as the findings might not be representative and do not recapitulate the literature. Within circulation, a significant decrease in circulating B-cells was also observed in KPC mice. While unexpected, this phenomena was also found by Steele et al in the blood of PDAC patients compared to healthy controls (Steele et al., 2020). There still remains controvosy in the field regarding B-cell contribution to PDAC, and whether this is supportive of tumour progression or survival (Castino et al., 2016; Pylayeva-Gupta et al., 2016). Investigation into early B-cell contribution to PDAC progression may offer insight regarding clonal expansion and memory in response to disease.

Similar discrepencies between both murine model NK subsets, in circulation and infiltration, was found. Similar to KPC data, Marcon et al found comparable levels of NK cells in the blood to healthy donors, but that peripheral NK cells had a reduction in NKG2D and NKp30 activating surface receptor in PDAC samples. (Lim et al., 2019; Marcon et al., 2020). The lack of activation markers associated with immune subsets is a limitation of data acquired for established PDAC in this chapter. Regarding the reduction of orthotopic NK cells in circulation, NK lymphopenia has been prognostic of shorter survival in other

cancer types (Imai et al., 2000; Xie et al., 2021). While a reduction in orthotopic NK cell infiltrate may be due to discrepancies in model generation, similar to B-cell infiltrate, circulatory NK lymphopenia may also be indicative of rapid cancer progression associated with shorter survival.

T-regulatory cells have been associated with worse patient survival by conferring an immunosuppressive microenvironment, preventing cytotoxic T-cell recruitment into the tumour vicinity. While present in the tumour, T-regulatory cells were not found at significant levels compared to healthy pancreas. Although this phenomenon has also been found in the context of KPC murine tumour, the opposite is true in human PDAC (Lee et al., 2016a; Spear et al., 2019; Brouwer et al., 2022; Yang et al., 2022). The data reported here appear to support the assumption that T-regulatory cell infiltrate into PDAC is not replicated between murine models and human tumour. Considering the data is supported by other murine studies, care should be taken when extrapolating murine studies onto patient data.

4.4.2 Perturbation of PDAC tumour with radiotherapy and combination immunotherapy

Dynamic characterisation of the immune repertoire in advanced PDAC is important to understand how perturbations to this microenvironment may alleviate disease. This chapter also detailed the response to combination low-dose radiotherapy and immunotherapies, within an orthotopic system, and the consequential effect on the immune landscape and overall tumour growth.

Tumour volume was significantly reduced when treatment regimen included fractionated, targeted IR (4 Gy). However, aPD1+IR, CCR5i+IR or aPD1+CCR5i+IR did not yield further reduction in tumour size. Despite this, aPD1+CCR5i+IR caused an increase in necrosis, albeit non-specific against IR alone. Similar to clinical studies, this study did not

differentiate between necrotic and metabolomic tumour within MRI volume quantification. Adjustment for tumour necrosis and volume change can more accurately predict patient survival (Kim et al., 2008). Recent supporting evidence demonstrates a similar IR-dependent reduction in tumour volume without additional immunotherapy benefit, despite using a higher dosage of IR (8 Gy) (Fujiwara et al., 2020). Our study delivered comparable results with lower dosage (4 Gy) using MRI-guided SARRP for precision, to prevent off-target radiotoxicity (Kersemans et al., 2017; Kinchesh et al., 2019).

Inconsistent with prior studies, the addition of aPD1 to IR conferred a reduction in granulocytes/PMN-MDSCs compared to IR alone, while the increase in CD4+ T-helper infiltrate was in agreement with some studies but not others (Azad et al., 2017; Fujiwara et al., 2020). Variance in data could be attributed to an increase in IR dosage compared to our study, considering B and T-helper cells are radiosensitive while T-memory, NKT and T-regulatory cells are radioresistant (Pouget et al., 2018; Fujiwara et al., 2020; Constanzo et al., 2021). Wider variance in data could also be attributed to the cellular differences used to generate the orthotopic PDAC models used; variation in KPC and Pan02 cells (Azad et al., 2017; Fujiwara et al., 2020). Care should be taken when comparing data against Pan02 models given the cellular genotype of Pan02 does not harbour *Kras* and *Trp53* mutation and phenotypically fails to recapitulate human disease (Wang et al., 2012).

Although IR treatment elicited a reduction in T-regulatory cell infiltrate, this response was abrogated upon the addition of both CCR5i and aPD1 to treatment regimen, comparable to untreated tumour. Wang et al showed a reduction in T-regulatory infiltrate following CCL5 inhibition (Wang et al., 2017). However, this study was based on subcutaneous tumour rather than orthotopic and may account for differences in our data. Evidence has shown T-regulatory cells are also mediated by additional chemokine axes; CCL28, CXCL12/CXCR4, CCL2/CCR2 (Bayry et al., 2008; Righi et al., 2011; Yang et al., 2012; Zhan et al., 2020). Lack of response could be due to a compensatory mechanism via

another chemokine axis in response to CCR5 inhibition, but further investigation is required to understand this. It is important to consider that the role of CCR5 in PDAC is still controversial, with evidence showing CCR5 benefit to PDAC eradication. Indeed, CCR5 polarised immunogenic macrophages to enable CD8 T-cell expansion in the tumour, while suppression of CCR5 reduced effector function of CD8 T-cell (Hundeyin et al., 2019; Mirlekar et al., 2020). While the role of CCR5 requires further evidence, our data did not show reduction in CD8+ tumour infiltrate with CCR5 inhibition, but rather the opposite. Similarly, Wang et al demonstrated combined inhibition of CCR2, CCR5 and PD1 alongside IR enhanced CD8+ T-cell PDAC infiltration (Wang et al., 2022b). Nonetheless, further investigation is required to understand the discrepancies in T-regulatory cell response to immunotherapy and IR treatments.

B-cell contribution to PDAC pathogenesis remains controversial (Spear et al., 2019; Minici et al., 2020; Mirlekar et al., 2020). While clinical studies have shown prognostic benefit, this has largely been attributed to plasma cell differentiation (Kroeger et al., 2016). It is thought that tumour samples with mature tertiary lymphoid structures have high-quality tumour neoantigen, which allows the formation of Ki67+ CD20+ germinal centres for B-cell somatic hypermutation and downstream plasma cell generation. This elicits an improved survival for patients via increased humoral immunity (Gunderson et al., 2021). Gunderson et al showed early-stage tertiary lymphoid structures had activated CD4+ memory cells, naïve CD19+IgM+IgD+ B-cells and NK cells in treatment naïve clinical samples. While B-cells were not characterised as a parameter for spatial IF staining to determine germinal centres within the orthotopic tumour, FC analysis showed a reduction of infiltrating CD19+ B-cells with combination immunotherapy. Although the panel did not distinguish between naïve and mature B-cells, frequencies were lower than untreated mock and IR-only treated orthotopic tumour. In addition, lymph node structures were not detected histologically via H&E (data not shown). In addition, aPD1+IR significantly reduced B-cell infiltrate, which could suggest that these cells were indeed B-regulatory

cells and blockade of their PD1 expression reduced their infiltration (Wang et al., 2019). Further characterisation of these potential B-regulatory cells, for instance IL-10 expression, is required.

aPD1 and CCR5i with IR conferred a variable increase in effector CD8+ cytotoxic T, CD4+ T-helper and NK cell infiltrate via FC. The combination of aPD1/aPD-L1 and varying dosage of fractionated IR has been previously documented in the literature. Our data corroborates previous findings, with consistent results in CD8+ T-cell tumour infiltrate (Azad et al., 2017; Fujiwara et al., 2020). Variation in immune infiltrate may be due to the difference in treatment responders and non-responders based on E-Cadherin staining. Another interpretation of this data may suggest variation in immune infiltrate is the cause of treatment responders and non-responders. One possible cause for this variation could be due to leakage at the site of orthotopic injection upon model generation. In situ injection is highly susceptible to peritoneal dissemination and variance in tumour growth kinetics (Wang et al., 2022a). Mice were excluded from the study if off-site tumour was detected via MRI, but nuance in growth kinetics may not have been captured in all mice. Previous data in this chapter, and the literature, have confirmed that these models aren't as representative of the human condition compared to GEMMs due to limited immune exposure over time (Spear et al., 2019). Despite this, it was chosen for its homogenous tumour microenvironment for analysis of treatment perturbation. We did observe differences in tumour response to treatment, prompting further investigation. Intriguingly, non-activated NK cells (CD161+NKG2D-) were associated with lower E-cadherin and treatment response, predominantly following CCR5i+IR and aPD1+CCR5i+IR treatment. In addition, non-activated NK cells had a positive correlation to increasing numbers of CD8+ T-cells in the tumour locale following combination treatment. Further investigation is required to understand how non-activated NK-cells and CD8 T-cells may be interacting, potentially though antigen presentation. Furthermore, differences in survival, or treatment

response, may provide supporting evidence to target this axis for PDAC immune perturbation in future *in vivo* experiments.

Overall, the data in this chapter has characterised the immunological microenvironment of two murine models of advanced PDAC. The data largely supports previously documented discrepancies between the homogenous orthotopic and heterogenic KPC models, due to differences in disease progression and subsequent immunological memory. However, the number of mice profiled in this study are limiting. A larger cohort of orthotopic and KPC mice should be included for all further investigation, to confirm whether differences to the literature are not due to outliers. Furthermore, correct controls for each model should be used for comparison rather than C57BL/6 WT mice. Control littermate *Pdx-1-Cre+; Kras*$^{G12D+/+}$*; LSL-Trp53*$^{R172H+/+}$and Matrigel-only orthotopic injection should be used for KPC and orthotopic PDAC comparison respectively. While the KPC model generally recapitulates the human condition, both systemically and locally, care should be taken when interpreting certain immune subsets, such as T-regulatory cell, when extrapolating data onto the human condition. Despite differences between the two models, a comprehensive characterisation of the surrounding advanced PDAC immune milieu serves as a baseline for comparison against the microenvironment of emerging lesions and pre-invasive carcinoma.

Furthermore, this chapter has highlighted a potential association between non-activated NK cells and tumour response through the reduction of E-cadherin following fractionated low-dose radiotherapy in combination with immunotherapies. This study was limited by biological replicates in some treatment groups (IR; n=3). Additional replicates are required to support the data and add clarity to any outliers, particularly for additional FC investigation. The non-activated NK:CD8 T-cell axis requires further investigation given the weak association to tumour response documented in this chapter. An increased window of treatment may allow further upregulation of these immune cells and lead to an increase in tumour response.

Results III

5. Local and systemic immune response to *Kras* oncogene expression and progression from pre-invasive pancreatic intraepithelial neoplasia to invasive carcinoma

5.1 Introduction

Similar to other carcinomas, invasive PDAC is thought to occur from sequential progression of intraepithelial neoplasia (Brat et al., 1998; Koorstra et al., 2008). Indeed, pancreatic intraepithelial neoplasia (PanIN) lesions were found in the vicinity of the tumour from resected pancreata, either from PDAC patients or those with familial history of pancreatic cancer (Cubilla and Fitzgerald, 1976; Andea et al., 2003; Brune et al., 2006; Shi et al., 2009b). Other pancreatic precursor lesions include intraductal papillary mucinous neoplasms (IPMN) and mucinous cystic neoplasms (MCN) (Uehara et al., 2008; Distler et al., 2013; Zamboni et al., 2013). Of these precursors, PanIN lesions were found to be the most common (Hruban et al., 2008).

Oncogenic *KRAS* mutations are detected in around 74% of early PanINs lesions (Shi et al., 2009a). PanIN lesions undergo multiple stages of progression over a period of years, prior to the formation of aggressive tumour (Hruban et al., 2004). Incidence of PanIN lesions is also associated with age. Typically, lesions are rare in patients under 40 years, but occur more commonly in those aged over 40 years (Matsuda et al., 2015). Autopsies of entire pancreatic parenchyma, in patients with no evidence of PDAC (mean age, 80.5 years), found PanIN-1, PanIN-2 and PanIN-3 lesions in 77%, 28% and 4% of examined cases respectively (Matsuda et al., 2017). Although PanIN lesions are present in patients

before the onset of PDAC, difficulties acquiring human biopsy samples prevent their analysis over time in this setting. To circumvent this issue, Hingorani et al developed the KC GEMM, the first murine model to successfully recapitulate human PDAC via endogenous expression of mutant *Kras*^{G12D} to progenitor cells of the murine pancreas using a *Pdx1* promoter (Hingorani et al., 2003). This GEMM displayed the full spectrum of PanIN lesions over time to allow PanIN lesion interrogation and mechanisms of disease pathogenesis.

Despite harbouring oncogenic *KRAS* mutations, PanINs themselves rarely progress onto PDAC (Brat et al., 1998; Brockie et al., 1998; Terhune et al., 1998). Rather additional factors are required to promote their progression to PDAC, but these factors remain poorly understood. It is thought that the microenvironment surrounding these PanIN lesions may be critical. PanIN lesions have previously been associated with inflammation in the literature. Low-grade lesions were found to progressively increase in pancreata of chronic pancreatitis and PDAC patients (Andea et al., 2003). Pancreatitis was shown to contribute towards tumorigenesis by revoking the senescence barrier of low-grade PanIN lesions (Guerra et al., 2011a). Inflammation not only delays repair of the pancreas, but also stimulates the expansion of PanIN lesions. In addition, chronic pancreatitis carries a 10-fold increased risk of developing PDAC (Lowenfels et al., 1993; Malka et al., 2002). Inflammatory immune cells, such as macrophages can induce the transdifferentiation of acinar cells to a more progenitor-like phenotype in the pancreas (acinar-to-ductal-metaplasia, ADM) via CCL5 and TNFα cytokine secretion (Liou et al., 2013). ADM was driven through nuclear factor κB (NFκB) and target genes involving survival, proliferation and extracellular matrix degradation, while remodelling of the microenvironment occurred via matrix-metalloproteinase-9 secreted from macrophages (Liou et al., 2013; Liou et al., 2015b). Following this, Liou et al showed IL-13 secretion from oncogenic *Kras* positive ADM and low-grade PanIN allowed polarisation of inflammatory to alternatively activated macrophages. Secretion of CCL2 and IL-1Rα promoted PanIN growth and fibrosis (Liou

et al., 2017b). Recent studies have explored factors relating to PanIN progression over time. Schlesinger et al used single-cell RNA-sequencing to analyse the pancreata of a *Kras* mutant murine model. However, macrophages were the only immune cell type detected at early time-points and represented the largest population of immune cells during later time-points, alongside NK, B and T-cells (Schlesinger et al., 2020).

While MDSCs have previously been identified in mice with PanIN lesions, this was on the basis of Gr-1+CD11b+ and taken at a 3-10 month time-point rather than sequentially during lesion progression (Clark et al., 2007a). Studies have shown B and T-regulatory cell presence in PanIN lesion-bearing mice but did not discriminate between PanIN lesion stage or grade (Clark et al., 2007a; Pylayeva-Gupta et al., 2016). It is not known at which stage of PanIN lesion development that the immunosuppressive environment is formed, or indeed the cells involved in this formation.

5.2 Aims

The studies described in this chapter aim to investigate the effect and consequence of oncogenic *Kras* mutation on the local and systemic immune response during the transition from low-grade, non-invasive neoplasia to high-grade invasive carcinoma. This *in vivo* investigation also aims to identify potential immune cells associated with loss of control and transition to high-grade lesions.

5.3 Results

5.3.1 PanIN lesion progression in the KC PDAC murine model allows longitudinal assessment of immune cell contribution to *Kras* oncogene expression

To understand how immune populations contribute to the progression of these lesions, a murine model capable of tracking lesion development was required. PanIN lesions can be observed in the pancreas of a KPC GEMM, containing both *Kras* and *Trp53* mutations from birth. However, inactivation of *TP53* occurs in human high-grade PanIN-3 lesions much later in progression (Redston et al., 1994). As a consequence of endogenous *Trp53* mutation, KPC mice form tumours quickly, making it difficult to characterise early lesion development that is physiologically representative of the human condition. For the purposes of this study, the *Kras*$^{LSLG12D/+}$*; Pdx1-Cre* (KC) GEMM was chosen considering oncogenic *Kras* mutation show a spread of neoplastic lesions over time (Figure 5.1A) (Hingorani et al., 2003).

To understand immunological contribution to PanIN lesion progression over time, KC pancreata were collected at 3-month intervals from 3 – 12 months. This timeframe was chosen based on the formation of PanIN lesions documented in this model and prior experience (Dr Asmita Thapa, O'Neill Group) (Hingorani et al., 2003). Pancreata were sectioned at 4 μm and stained with H&E. Histological assessment sought to confirm whether morphological and cytological PanIN features of the KC GEMMs used in this study agreed with the literature. Pancreatic regions affected by *Kras* mutation displayed reactive regions of ADM, where acinar cells appear to differentiate into ductal structures (Figure 5.1B). As previously described (Chapter 1), PanIN-1 lesions consisted of columnar cells with basal location of nuclei (Figure 5.1B). ADM and PanIN-1 lesions were observed at each time-point (3 – 12 months). PanIN-2 lesions were identified from 6-months

onwards, based on their papillary structure, moderate nuclear atypia and loss of nuclear polarity to allow nuclei migration from the basement membrane to the apical region. Advancement of PanIN-2 lesions was observed from 9-months (Figure 5.1B). In addition to advanced features observed in PanIN-2 lesions, PanIN-3 also displayed epithelial cell clusters 'budding off' into the lumen. PDAC presented invasion of the basement membrane with haphazard arrangement of ductal structures in the desmoplastic stroma. Both PanIN-3 and PDAC were distinguished at 12-months. Similar to a human condition PanIN-1 and 2 (3-6 months) were distinguished as low-grade and PanIN-3 to carcinoma (9-12 months) as high-grade. The spread of PanIN-1 to PanIN-3 lesions can be observed at 12-months.

Overall, the histological identification of neoplastic ADM/PanIN-1, PanIN-2, PanIN3/PDAC KC GEMM pancreas can be characterised at 3-month intervals. Although PanIN lesions are heterogenous in nature, this data allows further investigation at each time-point regarding immune contribution to multi-step progression of PanIN lesions into aggressive PDAC.

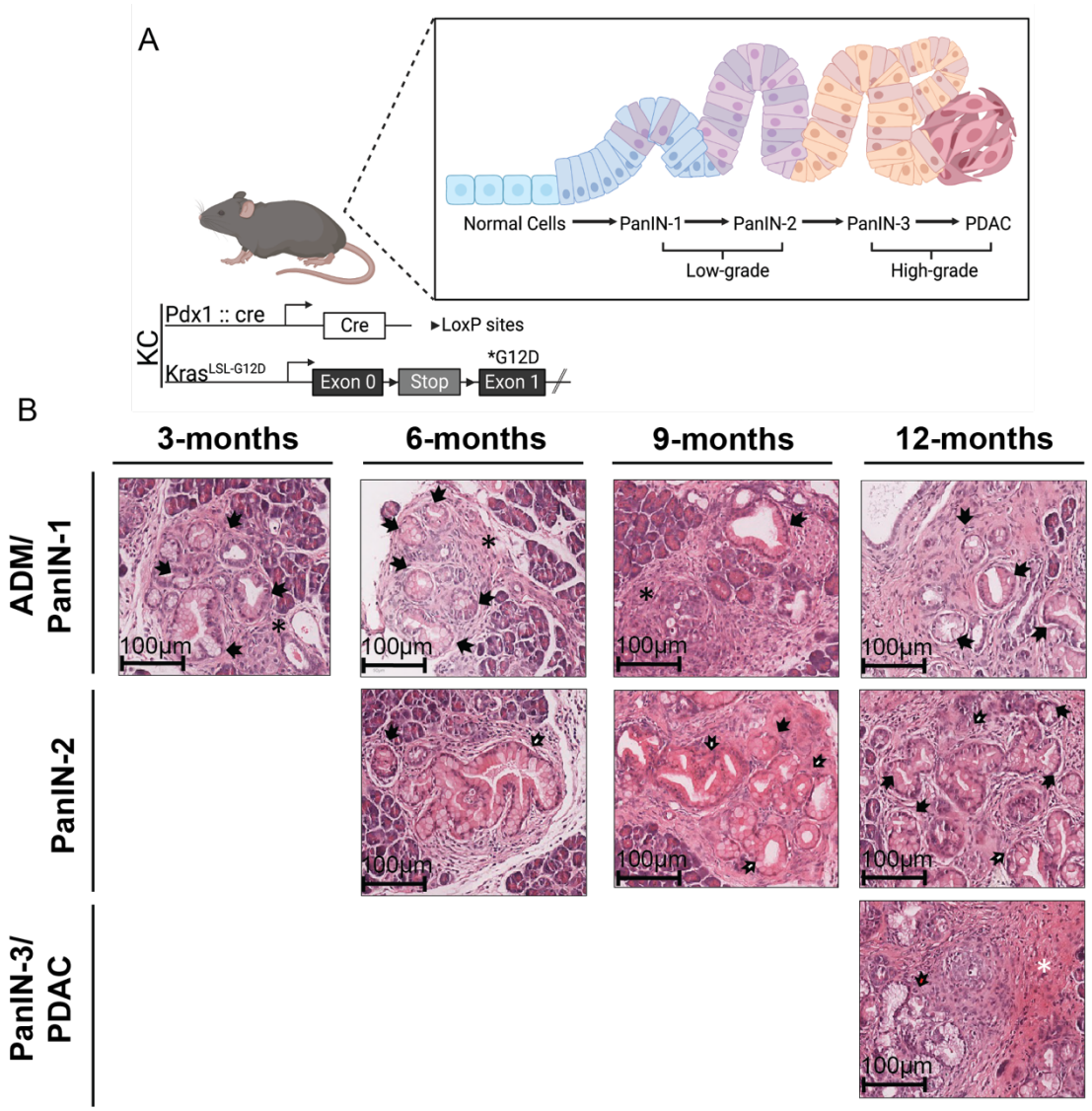


Figure 5.1: KC mouse model displays PanIN lesion progression.

(A) Schematic diagram representing the KC mouse model. An activating point mutation (G12D) in *Kras* is conditionally activated in a mouse pancreas by breeding *LSL-Kras*$^{G12D/+}$ mice to *Pdx-1-Cre* mice that express Cre recombinase under the expression of a pancreas-specific *Pdx-1* promoter. A multi-step progression of tumourigenesis in pancreas, including a series of Pancreatic Intraepithelial Neoplasia (PanIN) lesions representing specific architectural and cytological features. PanIN lesion classification has been revised from three-tier to two-tier system. PanIN-1 and PanIN-2 are grouped together as low-grade PanIN lesions, while PanIN-3 as high-grade lesions. LSL = Lox-STOP-Lox. (B) Representative images of H&E staining on KC mouse pancreata, taken at 3, 6, 9 and 12 months. Black Asterix = acinar-to-ductal metaplasia, black arrow = PanIN-1, white arrow = PanIN-2, red arrow = PanIN-3, white Asterix = PDAC (3-month; n=4, 6-months; n=5, 9-months; n=3, 12-months; n=3) Images shown at 10X magnification. Scale bar = 100 µm.

5.3.2 The myeloid immune response to PanIN lesion progression

To investigate the immune response during progression of PanIN lesions over time, peripheral blood was taken, and transverse sections of pancreas were dissected from KC *Kras$^{LSLG12D/+}$; Pdx1-Cre* mice (known as KC HET for the purposes of this chapter) and age-matched *Kras$^{LSLG12D+/+}$; Pdx1-Cre* control mice (known as KC WT for the purposes of this chapter) at 3, 6, 9 and 12-months. Samples were subsequently stained with the multicolour FC panel for immune identification.

When profiling the myeloid compartment, systemic macrophages were more abundant at later time-points representing an advancement of PanIN lesions (Figure 5.2A/B). Systemic M1 macrophages were significantly increased at 9-months ($p=0.0289$), representing the transition from low to higher-grade lesions. Surprisingly, this finding was not translated to the pancreatic setting. M1 macrophages did not infiltrate the pancreas at any time-point with significance (Figure 5.2A). Although a significance in pancreatic M2 macrophages was observed at 12-month ($p=0.0094$), compared to KC WT matched controls, the frequency of macrophages wasn't indicative of high KPC M2 macrophage infiltration (Chapter 4) (Figure 5.2B).

While no change in CD11b+Ly6C+ monocytes was observed systemically, an increasing proportion of monocytic infiltrate was found in the pancreas from 6 – 12-months (Figure 5.2C). Intriguingly, CD11b+Ly6C+Ly6G+ granulocytes were upregulated in the blood, compared to age-matched controls at 3-months (Figure 5.2D). A significant reduction in systemic KC granulocytes was observed over the course of PanIN lesion development, from 3-month low-grade lesions to 12-month high-grade lesions ($p=0.0063$). The opposite trend was found in the local pancreas. Infiltrating granulocytes were present in the pancreas at 3-months, during early PanIN lesion development, and remained present in the pancreas throughout PanIN progression at each stage. In addition, KC HET

granulocytes were significantly increased compared to age-matched KC WT at 6 (p=0.0317) and 12-months (p=0.0002).

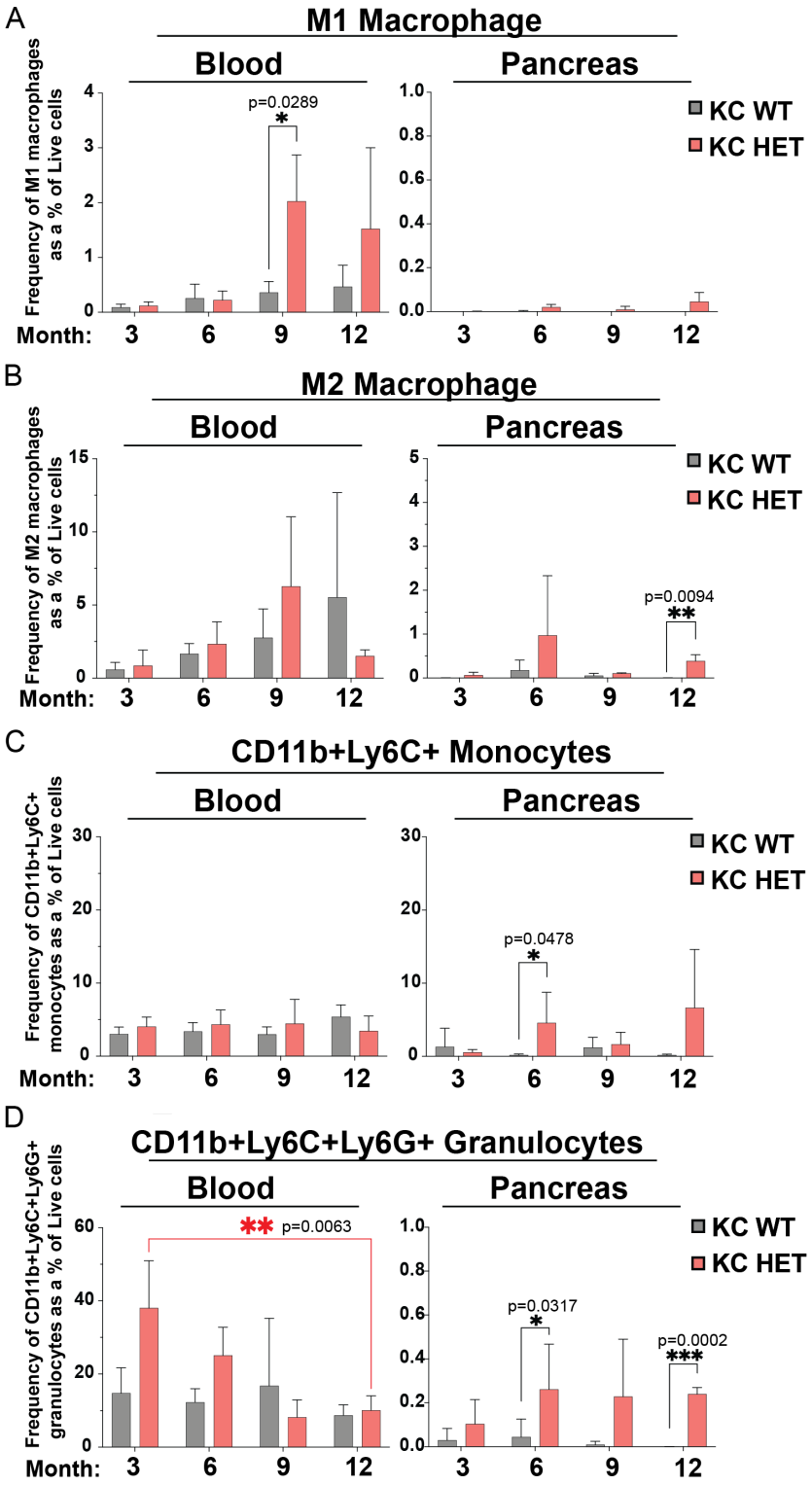


Figure 5.2: Local and systemic myeloid immune response during PanIN lesion progression.
Flow cytometry quantification of *Kras$^{LSL.G12D/+}$;Pdx-1-Cre* (KC) mouse blood and pancreata for (A) M1 (CD45+F4/80+CD80+) macrophages, (B) M2 (CD45+F4/80+CD206+) macrophages, (C) granulocytes (CD45+CD11b+Ly6C+Ly6G+) and (D) monocytes (CD45+CD11b+Ly6C+) over 3 – 12 months. All quantifications were a frequency of live cells represented as a mean ± SD. Statistical significance denoted by * ($p<0.01$), ** ($p<0.001$) and *** ($p<0.0001$) and performed using a Welch and Brown-Forsythe ANOVA for parametric data or Kruskal-Wallis test for non-parametric data (red), or unpaired T-test for parametric data or Mann-Whitney test for non-parametric data (black). When ANOVA statistical analysis was conducted post-hoc analysis was performed using Tukey multiple comparisons test (parametric data) or Dunn's multiple comparison test (non-parametric data). 3-month KC HET and KC WT (n=4), 6-month KC HET and KC WT (n=5), 9-month KC HET and KC WT (n=3), 12-month KC HET and KC WT (n=3). KC WT; *Kras$^{LSL.G12D+/+}$;Pdx-1-Cre,* wild-type. KC HET; *Kras$^{LSL.G12D/+}$;Pdx-1-Cre,* heterozygous.

5.3.3 MDSC involvement at the transition to high-grade PanIN lesion.

Currently, identification of MDSCs from CD11b+Ly6C+ (monocytic MDSCs; M-MDSC) and CD11b+Ly6C+Ly6G+ (polymorphonuclear MDSCs; PMN-MDSCs) is based on standardisation recommendations in the field of MDSC classification (Bronte et al., 2016). However, owing to no unique MDSC marker, suppressive M-MDSCs and PMN-MDSCs are indistinguishable from inflammatory monocytes and granulocytes based on surface marker alone (Cassetta et al., 2019). Instead, an *ex vivo* MDSC: T-cell suppression assay is used as the gold standard for distinction and subsequent identification of MDSCs (Bronte et al., 2016).

MDSCs have previously been associated with late-stage PDAC disease (Bayne et al., 2012; Siret et al., 2019). Indeed, their association and involvement span multiple cancer types and autoimmune diseases (Hoechst et al., 2008; Vuk-Pavlović et al., 2010; Greten et al., 2011; Gabrilovich et al., 2012; Jiao et al., 2013; Iacobaeus et al., 2018). By nature, MDSCs allow dampening of chronic inflammation (Movahedi et al., 2008; Gabrilovich et al., 2012). Considering the association between PanIN lesions and inflammation, with chronic development over time, it was hypothesised that MDSCs may contribute to the process of PanIN lesion development at the transition between low-grade and high-grade

lesion (Fukuda et al., 2011; Guerra et al., 2011a; Loncle et al., 2015). In addition, CD11b+Ly6C+ 'monocytes' were found to infiltrate the pancreas at 6 and 12-months (Figure 5.2C), while infiltrating CD11b+Ly6C+Ly6G+ 'granulocytes' increased in abundance from 3 – 12-months (Figure 5.2D).

To investigate whether these infiltrating monocytes and granulocytes were truly MDSCs and, if so at what stage of lesion development are they upregulated, an *ex vivo* T-cell suppression assay was conducted. Gr-1^{high}Ly6G+ (granulocyte/PMN-MDSC) and Gr-1^{dim}Ly6G- (monocyte/M-MDSC) were isolated from the spleens of KC HET or KC WT mice using positive selection via magnetic isolation. Isolated cells were co-cultured with CFSE stained CD8+ T-cells, stimulated with plate bound CD3 and CD28 antibodies (Figure 5.3A-C), previously isolated from C57BL/6 mice. T-cell proliferation was analysed on day 3. Isolation of Gr-1^{high}Ly6G+ and Gr-1^{dim}Ly6G- populations from the pancreas was not possible given low cell numbers were inadequate for the suppression assay. Initial assay optimisation was carried out using MDSCs derived from C57BL/6 BM (Supplementary 8.7). Concentrations of GM-CSF and IL-6, for MDSC differentiation, was taken from the literature (Lee et al., 2018b).

At 12-months, with high-grade lesion and carcinoma presence, KC HET Gr-1^{high}Ly6G+ and Gr-1^{dim}Ly6G- populations significantly reduced the percentage of CD8 T-cell proliferation in comparison to age-matched KC WT (Figure 5.3D, Gr-1^{high}Ly6G+ 1:1 ratio; p=0.0022, Gr-1^{high}Ly6G+ 2:1 ratio; p=0.0009, Gr-1^{dim}Ly6G- 1:1 ratio; p=0.0197). This result indicates the presence of both PMN-MDSCs and M-MDSCs in circulation at the onset of carcinoma from high-grade lesion. This phenomenon was not as apparent at 9-months, but reduction in proliferation was still maintained with co-culture of both KC HET Gr-1^{high}Ly6G+ (2:1 ratio; p=0.0014) (Figure 5.3E). The significant reduction in proliferation elicited by Gr-1^{high}Ly6G+ co-culture would suggest greater PMN-MDSC involvement. Comparable levels of T-cell proliferation was evident at 6-months between KC HET and KC WT for both Gr-1^{high}Ly6G+ and Gr-1^{dim}Ly6G-, indicating these populations were

unlikely to be MDSCs (Figure 5.3F). Surprisingly, Gr-1^{high}Ly6G+ cells isolated form KC HET mice at 3-months prompted a significant increase in the proliferation of CD8+ T-cells in comparison to not only KC WT, but also CD8+ T-cell only control (Figure 5.3G, 1:1 ratio; p=0.0435). This data would suggest these Gr-1^{high}Ly6G+ cells are indeed granulocytes given their lack of suppression. Yet, more compellingly, these KC HET granulocytes, isolated during early PanIN lesion development, appear to have the capacity to mount a T-cell response through increased CD8+ proliferation during early lesion development. This data is additionally fascinating given the significant increase in KC HET circulatory granulocytes and presence of granulocytic infiltrate at 3-months (Figure 5.2D).

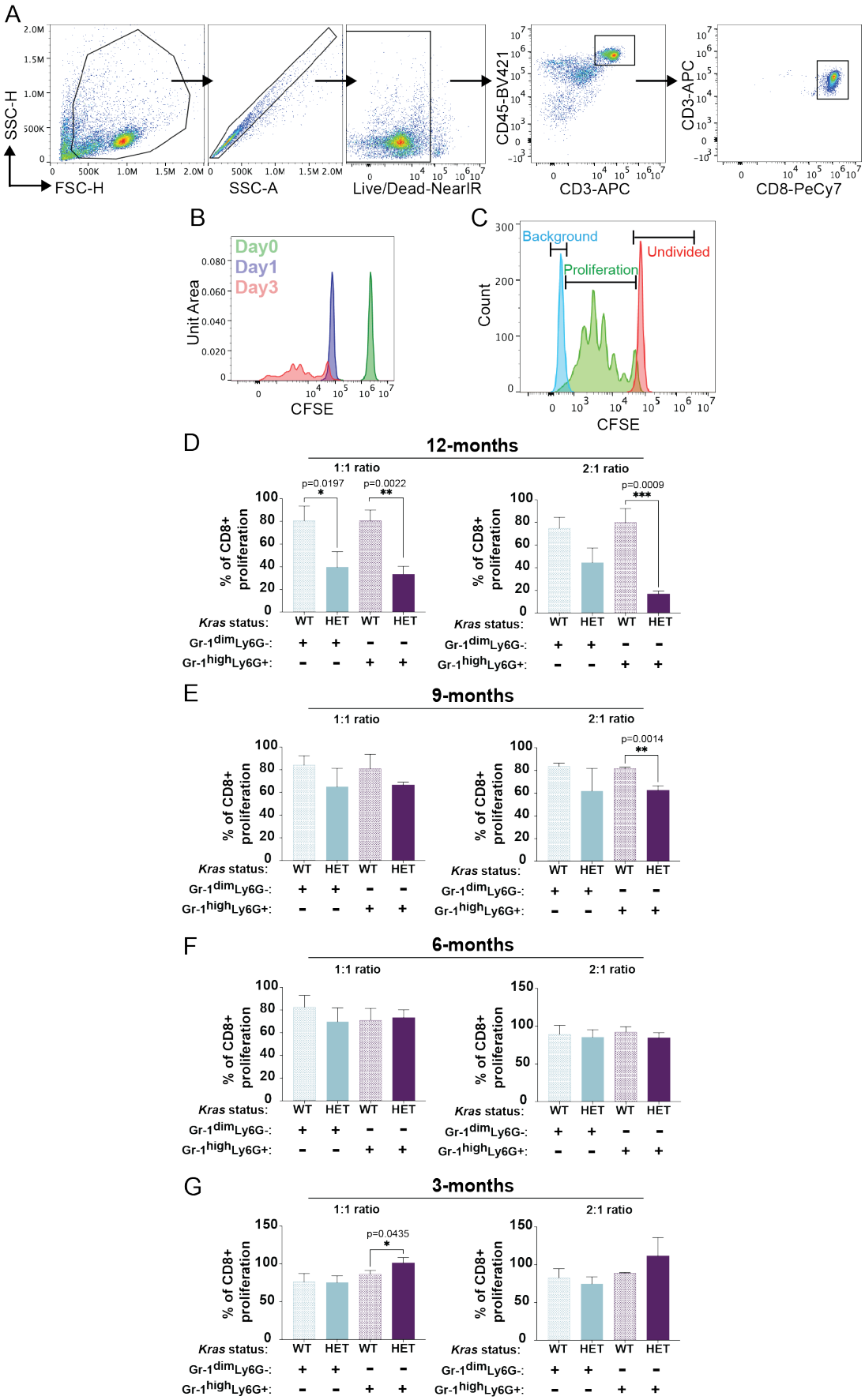

A
SSC-H
FSC-H
SSC-A
Live/Dead-NearIR
CD45-BV421
CD3-APC
CD3-APC
CD8-PeCy7
B
Day0
Day1
Day3
Unit Area
CFSE
C
Background
Undivided
Proliferation
Count
CFSE
D
12-months
1:1 ratio
2:1 ratio
p=0.0197
p=0.0022
p=0.0009
% of CD8+ proliferation
Kras status:
WT HET WT HET
Gr-1dimLy6G-:
Gr-1highLy6G+:
E
9-months
1:1 ratio
2:1 ratio
p=0.0014
F
6-months
1:1 ratio
2:1 ratio
G
3-months
1:1 ratio
2:1 ratio
p=0.0435

Figure 5.3: *Ex vivo* T-cell suppression to elucidate MDSC status during PanIN lesion progression.
Co-culture of Gr-1^{high}Ly6G+ and Gr-1^{dim}Ly6G- myeloid cells, isolated from *Kras$^{LSL.G12D/+}$;Pdx-1-Cre* (denoted by *Kras* HET status) and *Kras$^{LSL.G12D+/+}$;Pdx-1-Cre* (denoted by *Kras* WT status) murine spleens, and CD8+ T-cells isolated from C57BL/6 spleens. (A) Representative gating strategy on FC dot plots for CD8+ T-cells prior to CFSE analysis. (B) Representative CFSE signal decay with respect to time. Multi-peak distributions seen on Day 3 are indicative of CD8+ T-cell proliferation. (C) Example of modelling proliferation over cell generations. Peaks were broadly defined as 'Proliferation' for the purpose of analysis. Undivided peak was fixed based on CFSE intensity at time of staining (Day 0) and after natural decay (Day 1). Background peak was fixed based on 'no CFSE' T-cell sample control. Quantification of Gr-1^{high}Ly6G+ and Gr-1^{dim}Ly6G- T-cell suppression, in a 1:1 (myeloid cell: T-cell) or 2:1 (myeloid cell: T-cell) ratio at (D) 12-months, (E), 9-months, (F) 6-months and (G) 3-months. All quantifications were relative to CD8+ T-cell only controls, represented as mean ± SD. Statistical significance denoted by * ($p<0.01$), ** ($p<0.001$) and *** ($p<0.0001$) and performed using an unpaired T test (parametric data) or Mann-Whitney test (non-parametric data). KC (n=3) and WT (n=3) at each time point. Technical triplicates were averaged for each biological replicate data-point.

5.3.4 The lymphoid immune response to PanIN lesion progression

Similar to the characterisation of myeloid immune contribution to PanIN lesion development (Section 5.3.2), the lymphoid component was also investigated on the same biological specimens using the multicolour FC panel at the same time.

KC HET mice did not have a significant difference in circulating CD8+ cytotoxic T-cells or T-regulatory cells compared to age-matched controls (Figure 5.4A/B). However, a significant increase in infiltrating cytotoxic T-cells was observed in the pancreas at 6-months (Figure 5.4B). Interestingly this observation occurred at the transition from low to high-grade PanIN lesion. This effect was then mitigated at later time-points. Notably, T-regulatory cell pancreatic infiltrate was not detected at any time-point during PanIN lesion development (Figure 5.4B). Within the NK compartment, a significant increase in NK cells from KC HET mice was observed in both the blood and pancreatic infiltrate at 6-months, at the transition from low to high-grade PanIN lesions and eventual loss of lesion control (Figure 5.4C). NK cells were detected in the KC HET pancreas at 12-months, despite non-

significance. Contrary to this observation, infiltrating NKT cells from KC HET mice were detected but without significance (Figure 5.4D). However, NKT cells from KC HET mice were significantly increased in the peripheral blood at 3 – 6 months, when PanIN lesions are still classified as low-grade. Intriguingly, when profiling CD19+ B-cells in the blood, a significant reduction was observed in KC HET mice compared to KC WT at 3-months. This striking response was maintained with significance until 6-months (Figure 5.4E, $p<0.0001$). At the point of high-grade transition, at 9 – 12-months, this reduction was lost, and B-cells were comparable to the age-matched control baseline. Despite this compelling systemic reduction during early PanIN lesion development, only small numbers of infiltrating B-cells were detected in the KC HET pancreas. The frequency of B-cell infiltrate was further reduced at 9 and 12-months. No significant increase in pancreatic B-cell infiltrate was observed at any time-point of lesion development.

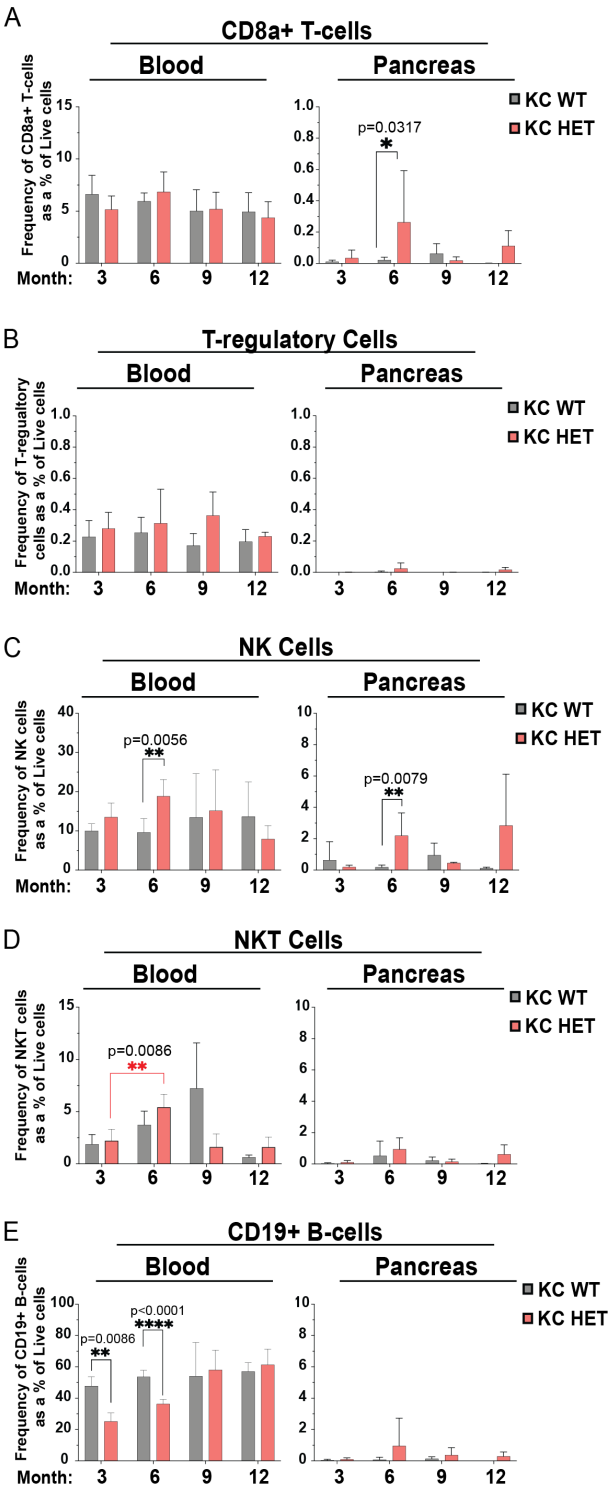

A
CD8a+ T-cells
Blood
Pancreas
Frequency of CD8a+ T-cells as a % of Live cells
p=0.0317
*
KC WT
KC HET
Month: 3 6 9 12
B
T-regulatory Cells
Blood
Pancreas
Frequency of T-regualtory cells as a % of Live cells
KC WT
KC HET
Month: 3 6 9 12
C
NK Cells
Blood
Pancreas
Frequency of NK cells as a % of Live cells
p=0.0056
**
p=0.0079
**
KC WT
KC HET
Month: 3 6 9 12
D
NKT Cells
Blood
Pancreas
Frequency of NKT cells as a % of Live cells
p=0.0086
**
KC WT
KC HET
Month: 3 6 9 12
E
CD19+ B-cells
Blood
Pancreas
Frequency of CD19+ B-cells as a % of Live cells
p=0.0086
**
p<0.0001
****
KC WT
KC HET
Month: 3 6 9 12

Figure 5.4: Local and systemic lymphoid immune response during PanIN lesion progression.
Flow cytometry quantification of *Kras$^{LSL.G12D/+}$;Pdx-1-Cre* (KC) mouse blood and pancreata for (A) cytotoxic T-cells (CD45+CD3+CD8a+), (B) T-regulatory cells (CD45+CD3+CD4+CD25+FOXP3+), (C) NK cells (CD45+NK1.1+), (D) NKT cells (CD45+NK1.1+CD3+) and (E) B-cells (CD45+CD19+) over 3 – 12 months. All quantifications were a frequency of live cells represented as a mean ± SD. Statistical significance denoted by * ($p<0.01$), ** ($p<0.001$) and *** ($p<0.0001$) and performed using a Welch and Brown-Forsythe ANOVA for parametric data or Kruskal-Wallis test for non-parametric data (red), or unpaired T-test for parametric data or Mann-Whitney test for non-parametric data (black). When ANOVA statistical analysis was conducted post-hoc analysis was performed using Tukey multiple comparisons test (parametric data) or Dunn's multiple comparison test (non-parametric data). 3-month KC HET (n=4) and KC WT (n=4), 6-month KC HET (n=5) and KC WT (n=5), 9-month KC HET (n=3) and KC WT (n=3), 12-month KC HET (n=3) and KC WT (n=3). KC WT; *Kras$^{LSL.G12D+/+}$;Pdx-1-Cre,* wild-type. KC HET; *Kras$^{LSL.G12D/+}$;Pdx-1-Cre,* heterozygous.

5.3.5 Immune infiltrate proximity to PanIN lesions shifts throughout lesion progression

Following the identification of immune populations within the pancreatic microenvironment during PanIN lesion progression, the spatiality of these populations, and proximity to the developing PanIN lesions themselves, was still unknown. To understand this in greater detail a collaboration with the Blagden Lab (Department of Oncology, University of Oxford) allowed the design of a 7-colour multiplex immunofluorescence panel (IF) using the parameters Ly6G (granulocytes), NK1.1 (NK cells), CD8 (cytotoxic T-cells), CD68 (macrophages), α-smooth muscle actin (SMA), La Ribonucleoprotein 6, Translational Regulator (LARP6) and 4′,6-diamidino-2-phenylindole (DAPI). These parameters were chosen based on prior FC data regarding pancreatic immune infiltrate and the Blagden Lab interest in SMA and LARP6. KC WT and KC HET pancreata, from the same biological samples taken for FC characterisation, were sectioned at 4 μm and stained with the IF panel. Five randomised sections were chosen for analysis from areas containing ADM and PanIN lesions for KC HET analysis from 1 biological sample. Five randomised sections were taken from the pancreata of 1 KC WT sample. Staining was carried out by the THL lab (Department of Oncology), and analysis was conducted by Kendra Perez Smith and Masooma Rajput (Blagden Lab). Optimisation of the IF panel was carried out

on sections of spleen prior to pancreatic staining (data not shown). LARP6 staining was included in panel visualisation but further quantification was not carried out for the purposes of this thesis.

At 3-months, during early lesion development, granulocytes and NK cells were observed within areas of ADM and developing PanIN-1, while rarer populations of CD8 T-cells were only resident at the perimeter of these lesions (Figure 5.5A-D). However, at 6-months the nature of this proximity shifted. CD8 T-cells were found to infiltrate regions of ADM and developing low-grade PanIN lesions (Figure 5.5A/D). Additionally, NK cells and macrophages were found in greater abundance in KC HET samples compared to KC WT. The dynamic relationship between immune infiltrate and PanIN lesion proximity was further altered at 9-months, upon the transition from low to high-grade lesion. A reduction in the frequency of NK and CD8 T-cell infiltrate was observed (Figure 5.5A/C/D). Some variation in KC WT NK infiltrate at 3-months, and KC WT CD8 infiltrate at 6-months, was observed (Figure 5.5C/D). While the overall frequency of macrophages was reduced at 9-months in KC HET, compared to 6-months, these macrophages were found in closer proximity to higher-grade PanIN lesions (Figure 5.5A/E). Variation in infiltrating pancreatic macrophages in KC WT mice was founds, particularly at 6-months (Figure 5.5E). At 12-months, when lesions became more neoplastic and invasive carcinoma was emerging, a relative paucity of immune infiltrate was observed around regions of neoplasia compared to earlier time-points. Indeed, macrophages were found in abundance, but primarily restricted to the lesion perimeter (Figure 5.5A/E). Greater frequencies of granulocytes were found at 12-months in KC HET compared to KC WT or prior time-points, with some infiltrate into the lesion locale (Figure 5.5A-B). Interestingly, NK cells were able to penetrate into the vicinity of high-grade lesions, despite their overall reduction in frequency compared to earlier time-points (Figure 5.5A/C). SMA, expressed by pancreatic stellate cells, is used as a marker for stromal activation (Erkan et al., 2008; Fujita et al., 2010a). Throughout PanIN lesion development, SMA was found in greater abundance in KC HET

samples compared to KC WT, although variation was found in KC WT samples, particularly at 3-6 months in comparison to 9-12-months (Figure 5.5F). Greater deposition of SMA was found at 12-months, as a potential source of immune paucity by preventing immune infiltrate towards high-grade lesions (Figure 5.5A). Yet SMA presence at 3-months was intriguing, given the relative low-grade nature of lesions beginning to develop.

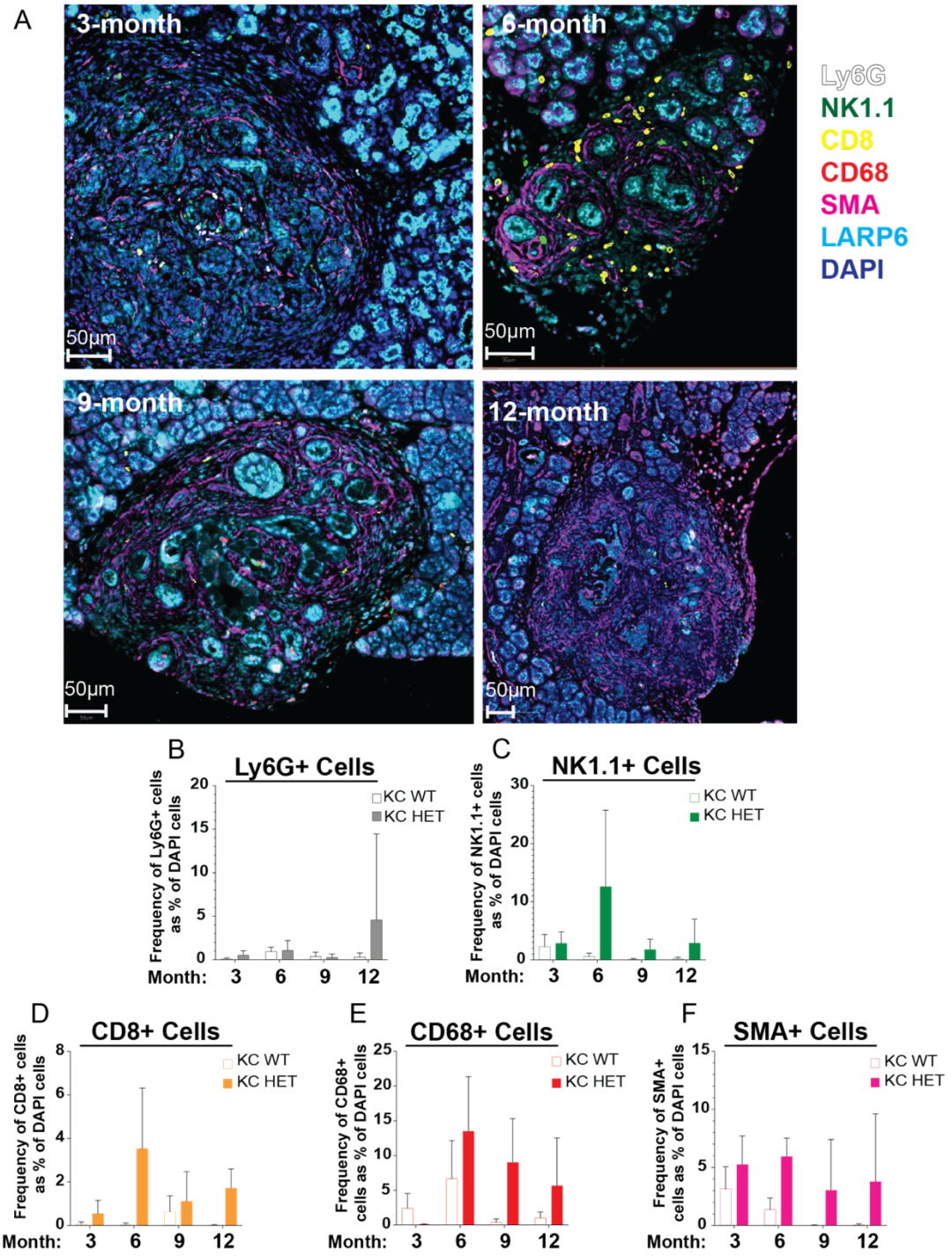


Figure 5.5: Proximity between immune infiltrate and PanIN lesions during lesion development.

Immunofluorescent staining of *Kras*$^{LSL.G12D/+}$*;Pdx-1-Cre* (KC HET) and *Kras*$^{LSL.G12D+/+}$*;Pdx-1-Cre* (KC WT) pancreatic tissue sections at 3, 6, 9 and 12-months. (A) Representative images of immunofluorescent staining on KC HET mouse pancreata at 3, 6, 9 and 12 months. Ly6G-Opal480 (white), NK1.1-Opal520 (green), CD8-Opal570 (yellow), CD68-Opal780 (red), SMA-Opal690 (magenta), LARP6-Opal620 (light blue) and DAPI. Scale bar = 50 µm. Quantification of immunofluorescent staining for (B) Ly6G, (C) NK1.1, (D) CD8, (E) CD68 and (F) SMA. All quantifications were a frequency of DAPI+ cells represented as a mean ± SD and performed using QuPath software. Data points are representative of 5 technical replicates. Tissue collected from n=1 KC HET and KC WT at each time-point.

5.3.6 CD19+ B-cell involvement during early, low-grade PanIN lesion development

Characterisation of B-cells was not included in the IF-panel, to analyse spatial proximity to PanIN lesions, due to finite parameters available on the multiplex system. Considering low frequencies of CD19+ B-cells were detected in the KC HET pancreas at 6-months, the spatial relationship between B-cell infiltration and PanIN lesion was warranted. In addition, uncertainty surrounding the role of B-cells during pancreatic tumorigenesis was still prevalent (Gunderson et al., 2016; Lee et al., 2016b; Pylayeva-Gupta et al., 2016; Brunner et al., 2020; Mirlekar et al., 2020; Delvecchio et al., 2022). Early lesion development (3-6 months) was associated with a significant reduction in circulating B-cells (Figure 5.4E). Yet it was unknown whether this reduction could be attributed to trafficking of B-cells into the pancreas, even in low numbers, in an attempt to resolve lesion development.

To investigate this in further detail, KC WT and KC HET pancreata, from the same biological samples taken for FC characterisation, were sectioned at 4 μm, stained with CD19 (EPR23174) antibody and positive signal was visualised by brown DAB stain. A nuclear counterstain was also included. A negative control with no primary antibody staining was performed on serial sections of pancreatic tissue and CD19 antibody staining on sections of C57BL/6 spleen was included as a positive control (data not shown). The CD19 antibody had previously been optimised on sections of C57BL/6 spleen (Supplementary 8.8). Visualisation of non-specific staining was observed in acinar cells surrounding PanIN lesions (Figure 5.6A, KC HET 6-months). For this reason, quantification of positive DAB signal was not possible. Further optimisation of the CD19 antibody for IHC, or IF staining for quantifiable analysis, is required to determine spatiality of B-cells within the pancreas of emerging PanIN lesions. From this preliminary data, no visual difference was observed between KC HET and KC WT sections.

As circulating B-cells were reduced in KC HET mice during low-grade lesion development, it was hypothesised that, instead of trafficking to the pancreas, they may be trafficking to the spleen for further B-cell development to elicit an immune response against emerging PanIN lesions (Loder et al., 1999). Dissection revealed enlarged KC HET spleens compared to age-matched control KC WT samples (Figure 5.6B). Furthermore, isolation of B-cells, using a pan-B-cell magnetic isolation kit, from whole spleens revealed a significant increase in the number of B-cells present in KC HET compared to age-matched KC WT at 3-months (Figure 5.6C, $p=0.0126$). To determine whether the increase in B-cells was maintained throughout PanIN development, spleens from KC WT and KC HET at 3, 6, 9 and 12-months were sectioned at 4 μm, stained with CD19 (EPR23174) antibody and positive signal was visualised by brown DAB stain. A nuclear counterstain was also included. A no primary antibody staining was performed on serial sections (data not shown). Quantification revealed a significant decrease in CD19+ B-cell presence in the KC HET spleen between 3 and 12-months (Figure 5.6D/E, $p=0.0468$). This reduction was also a significant finding considering the size of 12-month KC HET spleens was larger than age-matched controls (data not shown). Additionally, CD19+ B-cells were predominantly located in the red-pulp of the spleen sections at 3-months (Figure 5.6F). However, the spatial location of B-cells requires further investigation considering staining is apparent in the red pulp of the spleen. High-background and non-specific staining is also apparent in the KC HET spleen samples and should therefore be further optimised, similar to pancreatic samples.

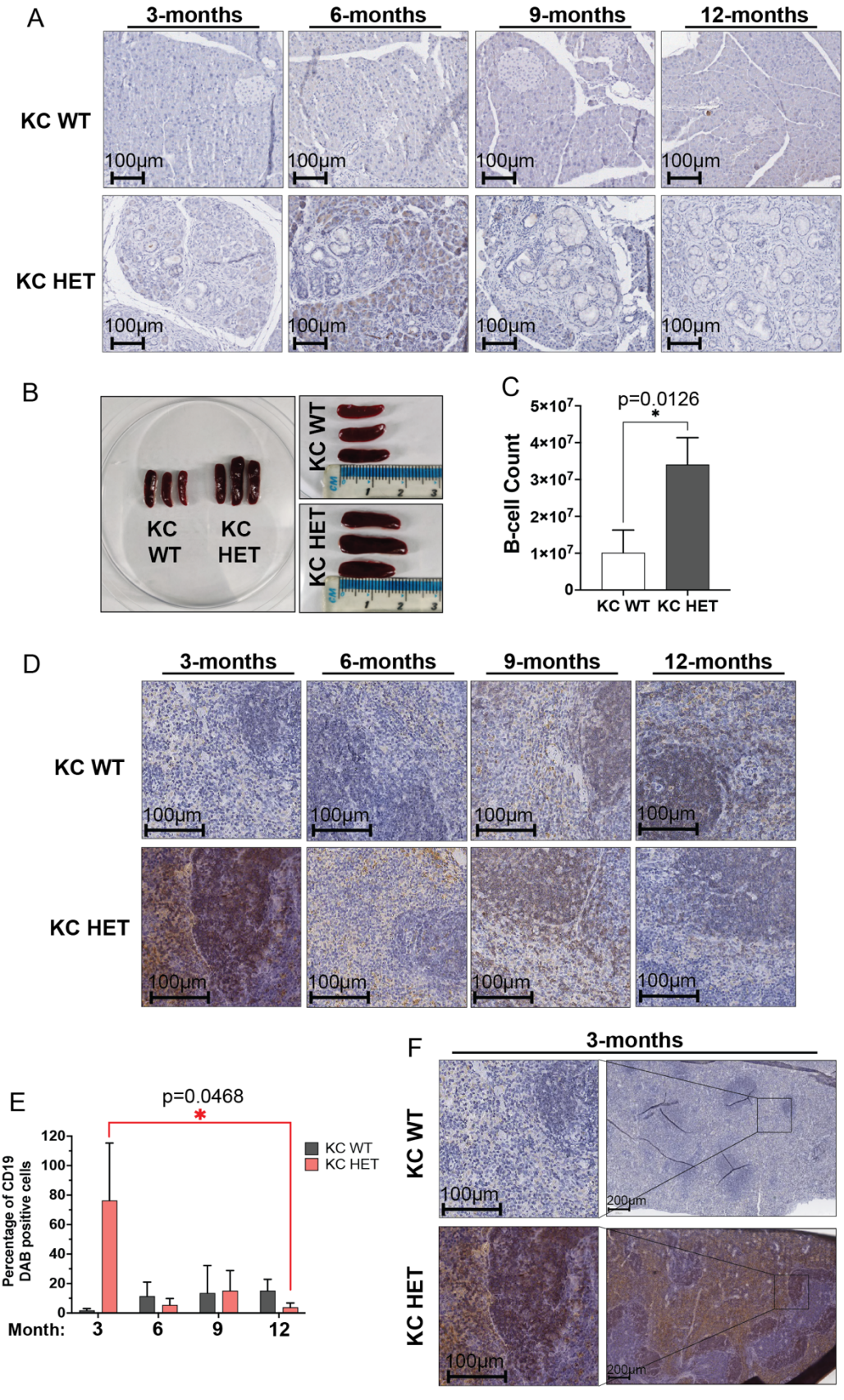

A
3-months
6-months
9-months
12-months
KC WT
KC HET
100µm
B
KC WT
KC HET
KC
WT
KC
HET
C
p=0.0126
*
B-cell Count
5×10^7
4×10^7
3×10^7
2×10^7
1×10^7
0
KC WT
KC HET
D
3-months
6-months
9-months
12-months
KC WT
KC HET
100µm
E
p=0.0468
*
Percentage of CD19 DAB positive cells
120
100
80
60
40
20
0
Month:
3
6
9
12
KC WT
KC HET
F
3-months
KC WT
KC HET
100µm
200µm

Figure 5.6: Spatiality of B-cells during PanIN lesion development.
(A) Representative images of IHC staining on *Kras$^{LSL.G12D+/+}$;Pdx-1-Cre* (KC WT) and *Kras$^{LSL.G12D/+}$;Pdx-1-Cre* (KC HET) mouse pancreata, taken at 3, 6, 9 and 12 months. Tissues were collected from n=3 mice per time-point and positive staining visualised by brown DAB staining corresponding to CD19 (EPR23174, 1:800). Sections were counterstained with haematoxylin. Scale bar = 100 μm. (B) Gross examination of KC WT and KC HET spleens. (C) Pan-B-cell isolation from KC WT (n=3) and KC HET (n=3) whole spleen tissue at 3-months. Data represented as mean cell count ± SD. Statistical significance denoted by * ($p<0.01$), ** ($p<0.001$) and *** ($p<0.0001$) and performed using an unpaired T-test. (D) Representative images of CD19 IHC staining on KC HET and KC WT spleen tissue, taken at 3, 6, 9 and 12-months. Images shown at 10X magnification. Scale bar = 100 μm. (E) Quantification of CD19 (1:800) IHC staining on KC HET (red) and KC WT (grey) spleen tissue samples. Tissues were collected from n=3 mice per time-point and positive staining visualised by brown DAB staining. Sections were counterstained with haematoxylin. Data represented as mean percentage positive cells ± SD for each marker and quantification performed using QuPath software. Statistical significance was performed using a Kruskal-Wallis test for non-parametric data. Post-hoc analysis was performed using Dunn's multiple comparison test (non-parametric data). (F) Representative images of CD19 IHC staining on KC HET and KC WT spleen tissue at 3-months. Images shown at 10X (left images) and 5X (right images) magnification. Scale bar = 100 μm (left images), 200 μm (right images).

5.4 Discussion

The current paradigm of PDAC formation is widely accepted as sequential precursor lesion formation, becoming more neoplastic over time, to eventually result in invasive carcinoma (Brat et al., 1998; Koorstra et al., 2008). Yet PanIN lesions themselves rarely progress onto PDAC alone, rather additional factors are thought to alter their ability to progress (Brat et al., 1998; Brockie et al., 1998; Terhune et al., 1998). ADM and early lesions are associated with inflammatory disease and PDAC is known to harbour an immune-suppressed microenvironment (Andea et al., 2003; Guerra et al., 2011a; Bailey et al., 2016; Liou et al., 2017b). Considering the microenvironment in which PanIN lesions reside in may be pivotal to their progression, this study aimed to understand the interplay of immune cells during PanIN lesion progression from early to late-stage lesion development.

The KC model represented longitudinal lesion development to document this progression. Although carcinoma was observed at 12-months, this was not near the percentage coverage of the KPC GEMM, in which carcinoma is dominant and the immunosuppressive

microenvironment is established. Data in this chapter focused on the local and systemic responses to *Kras* oncogene expression, rather than the emergence of cancer itself.

From this perspective, infiltrating macrophages were not observed at similar frequency compared to KPC GEMM, previously analysed in this thesis or the literature (Zhu et al., 2017; Yang et al., 2022). Indeed, infiltrating M2 macrophages, of suppressive capacity were observed in the pancreas at low levels from 6-months, while typically inflammatory M1 macrophages were not found to infiltrate with significance at any time-point, despite significant upregulation in circulation at the transition to high-grade PanIN. Using CD68, a pan-macrophage marker, macrophage presence was found at 6-months, but excluded to the periphery of high-grade PanIN lesions at 12-months. These findings disagree with Schlesinger et al and Liou et al. However, these studies found macrophage presence at 6 weeks compared to the 3-month time-point taken in this chapter (Liou et al., 2015b; Schlesinger et al., 2020). This data, alongside the literature, would suggest macrophage involvement at the initiator stage of ADM rather than later PanIN lesion progression. While Schlesinger et al found macrophages to be the most abundant immune population at 'late-stage', this was representative of a 3 – 9-month window of investigation, rather than shorter timeframes used in this study (Schlesinger et al., 2020).

A recent study has shown circulating Ly6C^{high} monocytes, alongside tissue-resident macrophages, are a source of infiltrating tumour associated macrophages in PDAC (Zhu et al., 2017). While an upregulation of circulating M1 and M2 macrophages was observed in the KC HET, no difference in circulating Ly6C+ monocytes was observed at any time-point. Yet a significant upregulation of infiltrating monocytes was observed at 6-months . While Zhu et al studied this phenomenon in the context of an established orthotopic KPC model, a similar occurrence between monocyte and M2 infiltration at the 6-month PanIN transition may be taking place. However, further investigation would be required to determine whether these M2 macrophages have a monocytic origin rather than tissue-resident polarisation. Indeed, these infiltrating CD11b+Ly6C+ were likely to be

inflammatory monocytes at this 6-month time-point, rather than suppressive M-MDSCs, as confirmed by the *ex vivo* MDSC suppression assay. However, splenic M-MDSC suppressive capacity was confirmed at 12-months, in which late-stage lesions and invasive carcinoma were present.

Granulocytic infiltrate was confirmed during early stages of ADM and PanIN-1 (3-months) through to high-grade lesion via FC and IF analysis. Although granulocytes were observed in prior studies, significance was not observed during PanIN progression taken globally at 3-10 months from KC GEMMs rather than sequential time-periods (Clark et al., 2007a).

MDSCs have been characterised in later-stages of PDAC tumour and thought to contribute to the immunosuppressive microenvironment niche (Gabitass et al., 2011; Mundy-Bosse et al., 2011; Porembka et al., 2012). However, it is unclear at which point of pathogenesis inflammatory counterparts phenotypically switch to MDSCs and whether these cells are functional or bystander in the creation of the immunosuppressive microenvironment seen in later disease. Granulocytes isolated in the spleens of KC HET mice were found to have significant T-cell suppressive capacity at 9 and 12-months. This data is similar to previous reports, but did not include the use of irradiation of granulocytes (60 Gy) in order to elicit suppressive capacity as was previously documented by Clark et al (Clark et al., 2007a). This data indicates that, at least in circulation, chronic inflammation induced the suppressive capacity of PMN-MDSCs. This data would suggest that the significant increase in granulocytes isolated from the 12-month KC HET pancreatic infiltrate have the potential to be PMN-MDSCs, but further analysis is required. It is also important to consider that Gr-1^{high}Ly6G+ and Gr-1^{dim}Ly6G- populations were positively selected through magnetic isolation. This method of isolation may have yielded impurities and contamination. In addition, other populations such as neutrophils, mast cells and monocytes are also characterised on the basis of Gr-1 and Ly6G staining. This potential contamination may have impacted the data if neutrophils or monocytes were present in the sample rather than MDSCs. Fluorescence-activated cell sorting could be used to

isolate PMN-MDSCs ($CD11b^{+}Ly6G^{+}Ly6Clo$) and M-MDSCs ($CD11b^{+}Ly6G^{-}Ly6C^{hi}$) and reduce any contamination using additional staining parameters unique to neutrophils (CD18+CD115-F4/80-) and monocytes (CCR2+CD49b+CD115+) to gate-out these populations (Bronte et al., 2016).

Parameters of this study were limited by the tissue location of MDSC isolation. As pancreatic granulocyte and monocyte cell numbers were insufficient for *ex vivo* study, the spleen, as a secondary lymphoid organ within proximity of the pancreas, was used instead. Although draining lymph nodes have been characterised in PDAC, their presence was not found histologically in the KC GEMM during PanIN lesion progression at 3 – 12 months and therefore could not be used for MDSC isolation (Fujita et al., 2010b; De Monte et al., 2016). The spleen has been reported to function as a reservoir for precursor monocytes and granulocytes that can mobilise from the spleen to sites of injury in the instance of myocardial infarction or chronic atherosclerosis (Leuschner et al., 2012; Robbins et al., 2012). A similar phenomena was observed in murine models of lung adenocarcinoma, with similar oncogenic *Kras* mutations and *Trp53* mutation to high-grade PanIN lesions and PDAC, with splenic precursors differentiating into TAMs or tumour associated neutrophils (TANs) (Cortez-Retamozo et al., 2012). Both TAMs and TANs are phenotypically similar to PMN-MDSCs and M-MDSCs respectively, MDSCs can be differentiated based on Ly6C expression, T-cell suppressive capacity and their plasticity to differentiate between monocytic and polymorphonuclear fractions (Youn et al., 2013; Wu and Zhang, 2020). While our own data, and other reports in the literature, would suggest MDSC presence in the spleen, the *ex vivo* experiment should be repeated in the pancreata of KC HET mice at 9 and 12-months to confirm MDSC presence (Clark et al., 2007a; Jordan et al., 2017; Spear et al., 2019). However, the findings of this study suggest that an immune-suppressed microenvironment is being set up at 9-months, upon the transition from low to high-grade PanIN lesion, based on splenic MDSC suppression.

Unexpectedly, 3-month splenic KC HET granulocytes, co-cultured with T-cells, significantly increased T-cell proliferation compared to age-matched WT control. In tandem, an increase in circulatory KC HET granulocytes was found, which significantly decreased at 12-months. Pylaeva et al recently demonstrated the dual role of neutrophils along cancer progression. In the absence of lymph node metastases, CD27+ neutrophils had an immune stimulatory role within tumour draining lymph nodes revealed through activation of T-cell proliferation in close proximity. Contrastingly, a metastatic microenvironment revealed immunosuppressive neutrophils through upregulation of PD-L1 and decrease in CD27 expression (Pylaeva et al., 2022). KC HET CD8 T-cell infiltrate was significantly upregulated at 6-months, in close proximity to PanIN lesions. This time-point appears to be the tipping point between granulocyte-stimulated T-cell proliferation at 3-months and the formation of PMN-MDSCs at 9-months. This raises the question as to whether these granulocytes are functioning through antigen presentation to T-cells. Neutrophils have been shown to cross-prime T-cells via MHC I and II pathways (Gosselin et al., 1993; Potter and Harding, 2001; Beauvillain et al., 2007). Further analysis of any granulocyte: T-cell interaction at 3 - 6-months is required to elucidate this further, including activated or exhaustive status of the T-cells. Additionally, to confirm whether granulocytes are attempting to control early lesions at this stage, perturbation of granulocytes in KC mice would determine whether PanIN lesion progression is accelerated *in vivo.* Interestingly, no significant difference in T-regulatory cells was observed at any time-point. This would suggest that MDSC are responsible for initial immune suppression of the microenvironment during lesion development. However, this finding was in contrast to previous reports in which T-regulatory cells were upregulated during PanIN lesion progression (Clark et al., 2007a). Considering contrasting findings have been observed between murine models and the human condition of late-stage PDAC, caution should be taken when interpreting these results in the KC HET GEMM (Lee et al., 2016a; Spear et al., 2019; Brouwer et al., 2022; Yang et al., 2022).

Similar to CD8+ T-cell infiltrate, NK cells were significantly upregulated in the pancreata containing low-grade PanIN lesions at 6-months. Similar findings were observed by Schlesinger et al, although NK cell localisation to PanIN lesion was observed in a window of 3-9 months. While NK cells have been shown to differentiate cancer stem cells via IFNγ, expansion, the killing capacity and secretion of IFNγ were defective in NK cells in mice with *Kras* mutations in the pancreas at a pre-cancerous stage (Kaur et al., 2018). The data presented in this chapter would suggest an attempt at PanIN lesion control, which is lost at 9-months with the upregulation of the MDSC immunosuppressive microenvironment and loss of NK and CD8 T-cell infiltrate.

B-cell contribution to the pathogenesis and later-stages of PDAC is controversial. CD20+ B-cell infiltrate was significantly upregulated in PDAC long-term survivors compared to short-term survivors (Brunner et al., 2020). Yet within late-stage murine models of PDAC their presence is associated with tumour progression and reduced survival (Gunderson et al., 2016; Lee et al., 2016b; Pylayeva-Gupta et al., 2016; Mirlekar et al., 2020; Delvecchio et al., 2022). In addition to these discrepancies, the role of B-cells in the context of early tumour development, rather than tumour progression, is less well characterised. Surprisingly data in this chapter showed a significant reduction of circulatory B-cells during low-grade PanIN progression but was restored to the age-matched control WT baseline at 9-months following transition to high-grade lesion and loss of control. Similar to this finding, absolute B-cell numbers were significantly reduced in the blood of acute and chronic pancreatitis patients compared to healthy controls (Wei et al., 2019). Despite these findings, minor upregulation of B-cell infiltrate was observed in the KC HET pancreata at 6-months. This observation could not be replicated using IHC staining of pancreatic sections to further elucidate spatiality. Considering non-specific binding of the CD19 antibody to acinar cells, this experiment should be further optimised for improved IHC or IF staining for quantifiable data. Lee et al found an upregulation of CD19+ B-cells in a similar 2-month *p48-Cre;LSL-Kras*^{G12D} mouse model (Lee et al., 2016b). Considering

this data, B-cells may play a role much earlier in development and therefore the experiment should be repeated at earlier time-points prior to 3-months.

Rather than infiltrating the pancreas, CD19+ B-cells were found to predominantly reside in the red pulp of KC HET spleens at 3 and 6-months in conjunction with a reduction in circulatory B-cells. However, further analysis will be required to better understand this spatiality. Additionally, considering non-specific binding and high background following CD19 IHC staining on KC HET spleen samples, further IHC optimisation or IF staining should be carried out to confirm these results.

Although tertiary lymphoid organs have been described as the location for B-cell maturation in several cancers including PDAC, the spleen was chosen for analysis considering tertiary lymphoid structures were not found during early PanIN progression of KC HET mice (Affara et al., 2014; Dieu-Nosjean et al., 2016; Spear et al., 2019). The KC HET spleens were larger with significantly greater total B-cells compared to age-matched controls. Spear et al showed a localised response in which germinal centre B-cells were only observed within or near the KPC GEMM tumour in draining lymph nodes, but not the spleen (Spear et al., 2019). Similarly, the data in this chapter did not present an increase in splenic B-cells at 12-months, but rather a significant decrease from 3-month B-cell infiltrate, when invasive carcinoma was present. However, plasma cell status, using CD138 staining, should be determined to understand whether plasma cell differentiation is taking place, particularly at the 3-6 months. Data from this study provoke further questioning. Does the predominant red-pulp localisation of B-cells indicate an arrest in differentiation? And more generally, are B-cells preventative or accelerating early lesion development?

When considering the data in this chapter more widely, a reciprocal reduction in circulatory B-cells occurs as circulatory granulocytes are increased in the KC HET model at time-points associated with inflammation. A coordinated production of leukocytes from the

bone marrow (BM) is crucial for effective innate and adaptive response (Ueda et al., 2005). Indeed, the BM has been shown to regulate production of granulocytes and neutrophils in response to inflammation (Terashima et al., 1996; Terashima et al., 1998). B-cell lymphopoiesis is also altered by inflammation. Sedger et al showed significantly lower B-cells in the BM of mice infected with influenza in a TNFα-dependent manner (Sedger et al., 2002). More interestingly, the reciprocal production of B-cells and granulocytes suggests that the progenitors of each compartment utilise a common developmental niche (Basu et al., 2000; Hirai et al., 2006). To understand this reciprocal relationship in greater detail, Ueda et al co-administered TNFα and IL-1β, which induced loss of lymphocytes from the BM while significantly enhancing granulopoiesis. The data suggested proinflammatory cytokines used were able to redirect haematopoiesis in favour of granulopoiesis (Ueda et al., 2005). They further demonstrated this preference was due to an inflammation-driven reduction in CXCL12 (Ueda et al., 2005). Furthermore, this CXCL12-CXCR4 axis is crucial for B-cell development in the BM (Tachibana et al., 1998; Egawa et al., 2001; Glodek et al., 2003; Tokoyoda et al., 2004). However, we do see a significant increase in splenic B-cells at these early inflammatory time-points. From the literature, and data detailed in this chapter, further analysis is required to understand whether a preferential selection for granulopoiesis over B-cell lymphopoiesis is occurring in the BM of KC HET mice at 3-months or earlier. Given cancer associated fibroblasts secrete CXCL12 in PDAC, it would be interesting to understand when CXCL12 secretion is restored during PanIN progression if it is indeed perturbed early on in development to favour granulopoiesis (Wehr et al., 2011; Feig et al., 2013).

Limitations to this study include the lack of biological replicates for IF analysis of immune spatiality towards PanIN lesions. Variation to immune infiltrate in KC WT mice was observed following IF staining, particularly for SMA and CD68+ macrophages. One interpretation could be attributed to aging in WT mice considering the reduction in CD68 and SMA in 9-12-month compared to 3-6-months KC WT mice. However, variation in this

IF experiment more widely is likely due to lack of biological replicates. Although initial data is promising, additional replicates should be carried out to confirm presence or absence of immune cells at each stage of lesion development.

As the biological replicates for all FC experiments were limiting in this chapter, due to breeding constraints, additional FC replicates should be carried out at each experimental time-point. While the shift in immune population between the 6 and 9-month experimental time points may represent an alteration in immune presence due to high-grade lesion transition, another interpretation may indicate technical experimental differences. Any experimental variation should be mitigated by including biological replicates from each time-point (3, 6, 9 and 12-months) in one experimental replicate in the future. *Trp53* mutational status was not characterised in high-grade lesions of development. Considering *Tp53* mutation is associated with high-grade PanIN-3 lesions, this should be characterised in the context of the KC HET GEMM (Redston et al., 1994).

Overall, this chapter has allowed greater insight into the chain of events that may be taking place over the course of lesion development. To the best of our knowledge, this is the first longitudinal study carried out in KC GEMMs to determine immune status during 3-month intervals of progression. Characterisation of granulocytes at 3-6-months may be protective and preventing lesion development by mounting a CD8 or NK cell response given their pancreatic infiltration at 6-months. However, the 6-9-month time point represents loss of control as lesions become more neoplastic. The presence of PMN-MDSCs occurs at this time-point with greater suppressive capacity at 12-months with the arrival of M-MDSCs. This data indicates a suppressive microenvironment is established at 9-months, even before invasive carcinoma is present. Greater understanding of the cells involved at these time-points will be crucial for perturbation of lesion development to prevent formation of invasive carcinoma. Further studies are required to understand B-cell characteristics during early lesion development and whether this could be attributed to anti or pro-development.

Results IV

6. Drivers of immune cell recruitment during early development of pre-invasive pancreatic intraepithelial neoplasia

6.1 Introduction

Inflammation and the development of PanIN lesions are closely associated. Oncogenic *Kras* has been shown to prevent resolution of inflammation, allowing low-grade PanIN lesion initiation (Liou et al., 2015b). But additional drivers of inflammation are required to prolong this signal for further neoplastic progression (Huang et al., 2014). Indeed NF-κB was found to amplify RAS signalling, allowing chronic inflammation and PanIN lesions (Daniluk et al., 2012). In addition, the association between chronic pancreatitis and development of PDAC in murine models has previously been documented (Guerra et al., 2007; Guerra et al., 2011b). Despite these findings, specific signals that drive immune cell recruitment and facilitate PanIN progression, in both a systemic and localised setting, are not sufficiently understood.

Cytokines are pivotal to the regulation of inflammatory responses. GM-CSF has multi-faceted roles in regulation of proliferation and maturation of monocytes, granulocytes, DC and MDSCs (Barreda et al., 2004; Lechner et al., 2010; Bayne et al., 2012). Under tumorigenic conditions, GM-CSF has also been shown to induce the expansion of Gr1+CD11b+ myeloid cells across multiple cancer types, including PDAC (Dolcetti et al., 2010; Marigo et al., 2010; Morales et al., 2010; Pylayeva-Gupta et al., 2012). It has been suggested that GM-CSF is a transcriptional target of oncogenic KRAS signalling given its upregulation in *Kras* mutant PDAC (Pylayeva-Gupta et al., 2012). However, further data is required to understand when transcriptional activation takes place during PanIN lesion

development, especially given that only 63% of ADM and 74% of low-grade PanIN lesions have oncogenic *Kras* mutations (Shi et al., 2009a).

Other factors have been shown to induce myeloid cell expansion across multiple cancer types, including IL-6 and IL-1β (Kranenburg et al., 2004; Ancrile et al., 2008; Coppé et al., 2008). Previous studies have shown myeloid-derived IL-6 activates STAT3 in cells undergoing ADM and PanIN lesions, which subsequently determines PanIN development (Corcoran et al., 2011; Lesina et al., 2011). IL-13 was found to drive differentiation of inflammatory macrophages in ADM towards an alternatively-activated macrophage phenotype, supporting tumorigenesis through IL-1Ra and CCL2 signalling (Liou et al., 2015b; Liou et al., 2017a).

Signalling axes driving the recruitment of other immune cell types have also been shown in PanIN progression. Oncogenic *Kras* induced IL-17 receptors on PanIN epithelial cells, thereby stimulating IL-17-secreting T_H17 and γδT-cells into the vicinity of the pancreatic stroma (McAllister et al., 2014). The combination of oncogenic *Kras* and chronic pancreatitis synergistically increased overall signalling of the IL-17 axis in murine models. Neutralising IL-17 signalling, with monoclonal antibodies against IL-17 and IL-17RA, significantly decreased Gr1+CD11b+ cells (McAllister et al., 2014). However, limitations to this study include the identification of these myeloid cells as MDSCs without taking their functional properties into account.

At later stages of PDAC progression, pro-tumorigenic B-cells were found to stimulate tumour proliferation via IL-35 secretion *in vivo* (Pylayeva-Gupta et al., 2016). IL-35 has been shown to facilitate the conversion of T-regulatory cells *in vivo*, thereby generating an immune-suppressive microenvironment (Collison et al., 2010; Wang et al., 2014; Mirlekar et al., 2018).

Taken together, these studies detail drivers of immune cell recruitment and differentiation within the pancreas during PanIN and PDAC development. However, further exploration

of the systemic immune response may yield further insight regarding the pathogenesis of PanIN lesion progression on a global scale.

6.2 Aims

The preliminary studies described in this chapter aim to investigate drivers of immune cell recruitment during early pre-invasive pancreatic intraepithelial neoplasia development in response to pancreatic epithelial *Kras* oncogene expression. This was carried out primarily at the systemic level; however, murine organoids of early PanIN lesions were additionally investigated to better understand and compare a localised PanIN-specific response.

6.3 Results

6.3.1 Systemic cytokine profiling during PanIN lesion progression

To investigate the systemic cytokine response during natural PanIN development over time, plasma was isolated from KC *Kras*$^{LSLG12D/+}$*; Pdx-Cre* mice (KC HET) and age-matched *Kras*$^{LSLG12D+/+}$*; Pdx-Cre* control mice (KC WT) at 3, 6, 9 and 12-months. Samples were subsequently stained with a 13-plex inflammatory cytokine array, profiling IL-1α, IL-1β, IL-6, IL-10, IL-12p70, IL-17A, IL-23, IL-27, CCL2 (MCP-1), IFNβ, IFNγ, TNFα, and GM-CSF. Plasma isolated from KPC (LSL-Kras$^{G12D/+}$;LSL-Trp53$^{R172H/+}$;Pdx-1-Cre), age-matched C57BL/6 (around 21 weeks) and orthotopic PDAC mice, previously detailed in Chapter 4, was also profiled with the cytokine array for comparison.

Studies have shown that IL-23, a member of the IL-12 family of cytokines associated with inflammation, is a critical modulator of inflammation in the tumour microenvironment of

several cancers (Qi et al., 2013; Chen et al., 2015; Hu et al., 2017a). IL-23 intra-sample variability was apparent, particularly within KC WT samples (Figure 6.1A). However, at 3-6 months, where low-grade PanIN progression is expected, a decrease in IL-23 was observed in KC HET compared to KC WT. This decrease in IL-23 was subsequently restored to the KC WT baseline at 12-months, when carcinoma begins to establish. Interestingly, IL-23 was significantly increased in the established late-stage orthotopic PDAC model ($p=0.0165$).

A similar phenomenon was observed for GM-CSF, in which early low-grade PanIN lesion time-points were associated with a decrease in circulating GM-CSF, restored to a KC WT baseline following transition to high-grade lesion, and significantly upregulated in KPC established tumour ($p=0.0089$) (Figure 6.1B).

Localised IL-1β secretion had previously been associated with PanIN lesion development in the literature (Fink et al., 1997; Liou et al., 2017b; Das et al., 2020). At the systemic level, IL-1β intra-sample variability was observed at different time-points of PanIN progression and later tumorigenesis, particularly due to one KC WT biological sample at 6-months (Figure 6.1C). High-grade PanIN lesions at 9-months saw a significant decline in circulatory IL-1β ($p=0.0220$). Yet a significant increase in IL-1β was observed in circulation for both late-stage models of PDAC (KPC; $p=0.0282$, orthotopic; $p=0.0315$).

IL-27 has been associated with anti- and pro-inflammatory roles in both autoimmune diseases and cancers. Indeed, IL-27 reduction in the serum of vitiligo and bladder cancer patients has suggested its anti-inflammatory role in these settings (Zhou et al., 2015; Hosseini et al., 2020). Interestingly, a significant decrease in systemic IL-27 was observed during low-grade PanIN development (6-months, $p=0.0151$), which rose after the transition to high-grade lesions (Figure 6.1D). Interestingly, late-stage established PDAC models were comparable to WT control samples. This data indicates that loss of IL-27, in the background of oncogenic pancreatic epithelial KRAS signalling, may act as a barrier

to high-grade lesion and subsequent tumour development. Conversely, loss of IL-27 may accelerate PanIN progression. Further investigation is required to better understand the implications of this data.

Further quantification of inflammatory cytokines did not reveal significant differences between KC WT and KC HET during PanIN progression (Supplementary 8.9). No difference in circulatory IFNγ, TNFα and IL-10 was observed during KC PanIN development, yet significant upregulation of the aforementioned cytokines was observed in tumour PDAC models (Supplementary 8.8B/C/G).

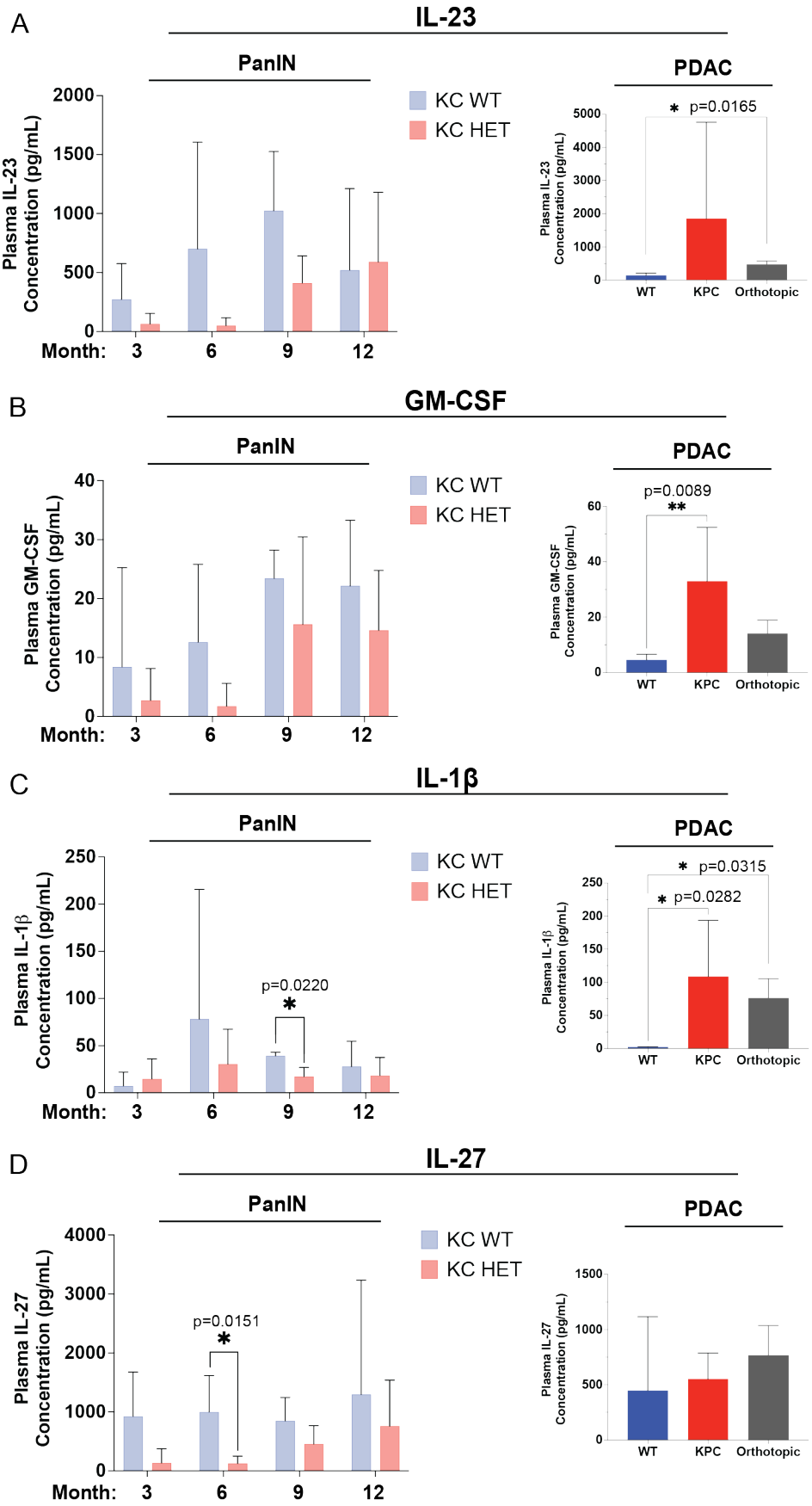

A
IL-23
PanIN
PDAC
KC WT
KC HET
Plasma IL-23 Concentration (pg/mL)
2000
1500
1000
500
0
Month: 3 6 9 12
* p=0.0165
5000
4000
3000
2000
1000
0
WT KPC Orthotopic
B
GM-CSF
PanIN
PDAC
KC WT
KC HET
Plasma GM-CSF Concentration (pg/mL)
40
30
20
10
0
Month: 3 6 9 12
p=0.0089
**
60
40
20
0
WT KPC Orthotopic
C
IL-1β
PanIN
PDAC
KC WT
KC HET
Plasma IL-1β Concentration (pg/mL)
250
200
150
100
50
0
p=0.0220
*
Month: 3 6 9 12
* p=0.0315
* p=0.0282
WT KPC Orthotopic
D
IL-27
PanIN
PDAC
KC WT
KC HET
Plasma IL-27 Concentration (pg/mL)
4000
3000
2000
1000
0
p=0.0151
*
Month: 3 6 9 12
1500
1000
500
0
WT KPC Orthotopic

Figure 6.1: Systemic cytokine levels during PanIN lesion progression.
13-plex inflammatory cytokine array on plasma of *Kras$^{LSL.G12D/+}$;Pdx-1-Cre* (KC HET), *Kras$^{LSL.G12D+/+}$;Pdx-1-Cre* (KC WT), C57BL/6 (WT), *LSL-Kras$^{G12D/+}$; LSL-Trp53$^{R172H/+}$*(KPC) and orthotopic PDAC mice. Quantification of (A) IL-23, (B) GM-CSF, (C) IL-1β and (D) IL-27. All quantifications were a concentration of each cytokine in pg/mL represented as a mean ± SD. Statistical significance denoted by * ($p<0.01$), ** ($p<0.001$) and *** ($p<0.0001$) and performed using an unpaired T-test for parametric data or Mann-Whitney test for non-parametric data (PanIN analysis) or one-way ANOVA for parametric data or Kruskal-Wallis test for non-parametric data (PDAC analysis). When ANOVA statistical analysis was conducted post-hoc analysis was performed using Tukey multiple comparisons test (parametric data) or Dunn's multiple comparison test (non-parametric data). 3-month KC HET and KC WT (n=4), 6-month KC HET and KC WT (n=5), 9-month KC HET and KC WT (n=3), 12-month KC HET and KC WT (n=4). C57BL/6 WT (n=4), KPC (n=4), Orthotopic (n=4). Data points representative of technical duplicates were averaged for each biological replicate.

6.3.2 IL-35 cytokine profiling early during PanIN lesion progression

IL-27 consists of p28 and (Epstein-Barr virus-induced gene 3) EBI3 subunits and belongs to two type I cytokine families: IL-6 and IL-12. IL-6 cytokines share a glycoprotein 130 (gp130) receptor subunit and are generally considered pro-tumorigenic (Hong et al., 2007; Taniguchi and Karin, 2014; Rose-John, 2018). The IL-12 family also share the gp130 receptor subunit but are considered more anti-tumorigenic (Broderick et al., 2006; Kilinc et al., 2006; Lasek et al., 2014). IL-27 engages a receptor comprised of gp130 and IL-27Rα with subsequent activation of JAK-STAT and MAPK signalling (Kastelein et al., 2007; Hunter and Kastelein, 2012). Despite its classification as an IL-12 family member, IL-35 shares similarities to the IL-6 family (Murakami et al., 2019). IL-30, originally identified as one of the IL-27 subunits, p28, was recently found to function independently of EBI3 (Dibra et al., 2012; Zhang et al., 2013a; Mitra et al., 2014). Due to receptor subunit competition between IL-27, IL-30 and IL-35, the balance between anti-tumour and pro-tumour responses may be affected owing to the differential roles each cytokine has (Figure 6.4A) (Kourko et al., 2019).

A significant reduction in circulatory IL-27 was observed during early PanIN development in tandem with a significant reduction in circulatory B-cells and sequestration of B-cells in the spleen at the same time-points (Chapter 5). Reports in the literature have shown IL-27 enhances germinal centre B-cell function, therefore its reduction could be preventing germinal centre function and driving B-cell accumulation in the spleen (Larousserie et al., 2006; Vijayan et al., 2016). Another interpretation of IL-27 reduction in the plasma could suggest that IL-27 is depleted because it is being used to enhance B-cell function in the germinal centre of the spleen.

Reports have detailed IL-35 involvement in B-regulatory cell development during PanIN progression and later PDAC (Pylayeva-Gupta et al., 2016; Mirlekar et al., 2020). As IL-27 and IL-35 compete for their shared receptor subunits, it was hypothesised that an upregulation of systemic IL-35 may be responsible for the reduction in systemic IL-27 (Collison et al., 2012; Shen et al., 2014; Kourko et al., 2019). Considering prostate and non-small cell lung cancer cells have been shown to secrete IL-35 *in vitro* and in patient tissue samples, we wanted to understand whether pancreata harbouring PanIN lesions were capable of IL-35 secretion (Zhu et al., 2020; Zhang et al., 2021).

To do so, organoids, previously isolated from *Kras*$^{LSL.G12D/+}$*;Pdx-1-Cre* (KC HET) and *Kras*$^{LSL.G12D/-}$*;Pdx-1-Cre* (KC WT) ducts, were used as a representative model of early PanIN lesion (Figure 6.2A). Indeed, when compared to KPC cell lines (KPC-A, KPC-F, KPC-G), derived from KPC GEMM late-stage tumours, KC HET organoids had weaker phosphorylated ERK (pERK), indicating reduced activation of the KRAS-mediated MAPK pathway (Figure 6.2B) (Moodie et al., 1993; Vojtek et al., 1993). Additionally, KPC cell lines displayed P53 upregulation, as a marker of high-grade PanIN and advanced disease, whereas KC HET organoids did not (Figure 6.2B) (Redston et al., 1994). Taken together, this data indicated that KC HET organoids were a suitable model for low-grade PanIN lesion characterisation.

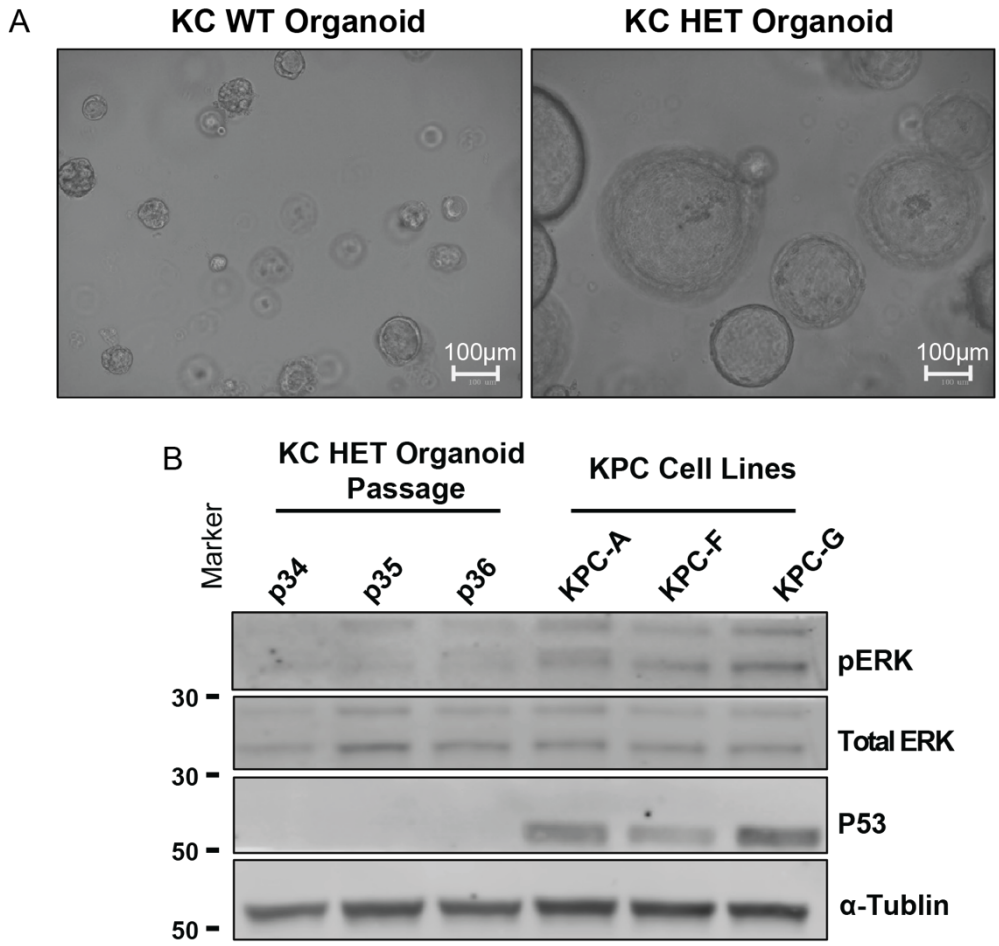


Figure 6.2: KC HET organoids are representative of low-grade PanIN lesions. (A) Representative brightfield images of organoids derived from *Kras*$^{LSL.G12D/+}$*;Pdx-1-Cre* (KC WT) and *Kras*$^{LSL.G12D/+}$*;Pdx-1-Cre* (KC HET) mice. Scale bar = 100 µm. Western blots of KC HET organoids (n=3) and KPC-A, KPC-F, KPC-G cell lysates (n=1). Total-ERK, p-ERK, P53 were determined including loading control (α-Tubulin).

Analysis was carried out on KC HET and KC WT plasma samples to determine systemic presence of IL-35. Supernatant from KC WT and KC HET organoid culture was also analysed to determine whether IL-35 was secreted locally. Initial IL-35 ELISA optimisation was conducted in plasma isolated from C57BL/6 WT and KPC. We hypothesised that circulatory IL-35 would be high in the KPC model considering IL-35 had previously been shown to promote KPC GEMM tumorigenesis and was upregulated in the serum of PDAC patients (Jin et al., 2014; Mirlekar et al., 2018). However, IL-35 was below the detection limit of any concentration using a BioLegend IL-35 ELISA kit (detection range: 0.47-30 ng/mL; sensitivity: 0.08 ± 0.04 ng/mL) (data not shown). Similarly, supernatant from KC

WT and KC HET organoid culture had undetectable levels of IL-35 (data not shown). IL-35 had previously been detected in the serum of PDAC patients using an ELISA with a lower range of detection (5.625-1000 pg/mL) (Jin et al., 2014). Therefore, plasma isolated from KC HET, KC WT, KPC and WT samples were analysed using the AssayGenie IL-35 ELISA kit with the same range of detection (sensitivity: 9.375 pg/mL). Although an upregulation was observed at 9-12-months in KC HET samples, control KC WT samples were variable (Figure 6.3A). Additionally, IL-35 was not detected in the plasma of KPC but rather the WT plasma, contradictory to previous reports (Figure 6.3B) (Jin et al., 2014). From this data, identification of sample IL-35 secretion was not possible due to sample and matched control variability. No other commercially available IL-35 ELISA could be acquired for further analysis.

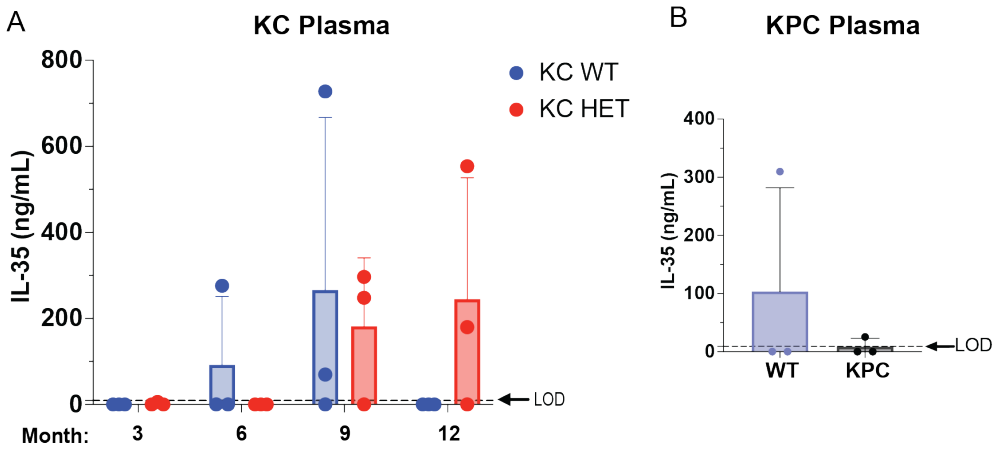


Figure 6.3: IL-35 profiling of PanIN lesion progression and late-stage PDAC using a commercially available ELISA.
(A) AssayGenie IL-35 ELISA on *Kras*$^{LSL.G12D/+}$*;Pdx-1-Cre* (KC WT) (n=3) and *Kras*$^{LSL.G12D/+}$*;Pdx-1-Cre* (KC HET) plasma (n=3) at 3, 6, 9 and 12-months. Data points are an average of technical duplicates. (B) AssayGenie IL-35 ELISA on C57BL/6 (WT) (n=3) and *LSL-Kras*$^{G12D/+}$*; LSL-Trp53*$^{R172H/+}$(KPC) (n=3) plasma. Data points are an average of technical duplicates. The limit of detection (LOD, 9.38 pg/mL) for the AssayGenie ELISA is displayed on both graphs as a dashed line.

6.3.3 Downregulation of IL-35 subset *EBI3* and *IL12A* found in KC HET organoids

Analysis of IL-35 concentration in the plasma and organoid supernatant using commercially available ELISA kits had presented technical issues yielding quantification impractical. To overcome technical issues and understand the role of IL-35 in early PanIN lesion development at the pancreatic and B-cell level, quantification was carried out at the mRNA level on organoids. As Pylayeva et al had previously shown $CD1^{high}CD5+$ B-cells secreted IL-35 in the KC pancreata, it was hypothesised that an accumulation of B-cells in the spleen of KC HET mice at 3-months may also have this capacity (Pylayeva-Gupta et al., 2016). In addition, IL-35 receptor subunit configuration differs according to cell type. B-cell IL-35 receptor consists of IL-12Rβ2 and WSX-1 (Wang et al., 2014). This further indicates potential for receptor competition between IL-27, IL-30 and IL-35.

RNA was isolated from 3-month KC WT and KC HET splenic B-cells and KC HET and KC WT organoids. Subsequently mRNA expression of IL-35 subsets *p35* and *Ebi3* and receptor subunits *Il12rb2* and *Gp130* were determined by qPCR. Surprisingly a significant reduction in *Ebi3* ($p=0.0375$) and *p35* ($p=0.0346$) expression was found in KC HET organoids (Figure 6.4B/C). No significant difference in IL-35 subunit expression was found for KC HET B-cells. No significant increase in *Il12rb2* and *Gp130* was found in KC HET B-cells compared to KC WT B-cells and no significant difference was found between KC HET and KC WT organoids (Figure 6.4D/E).

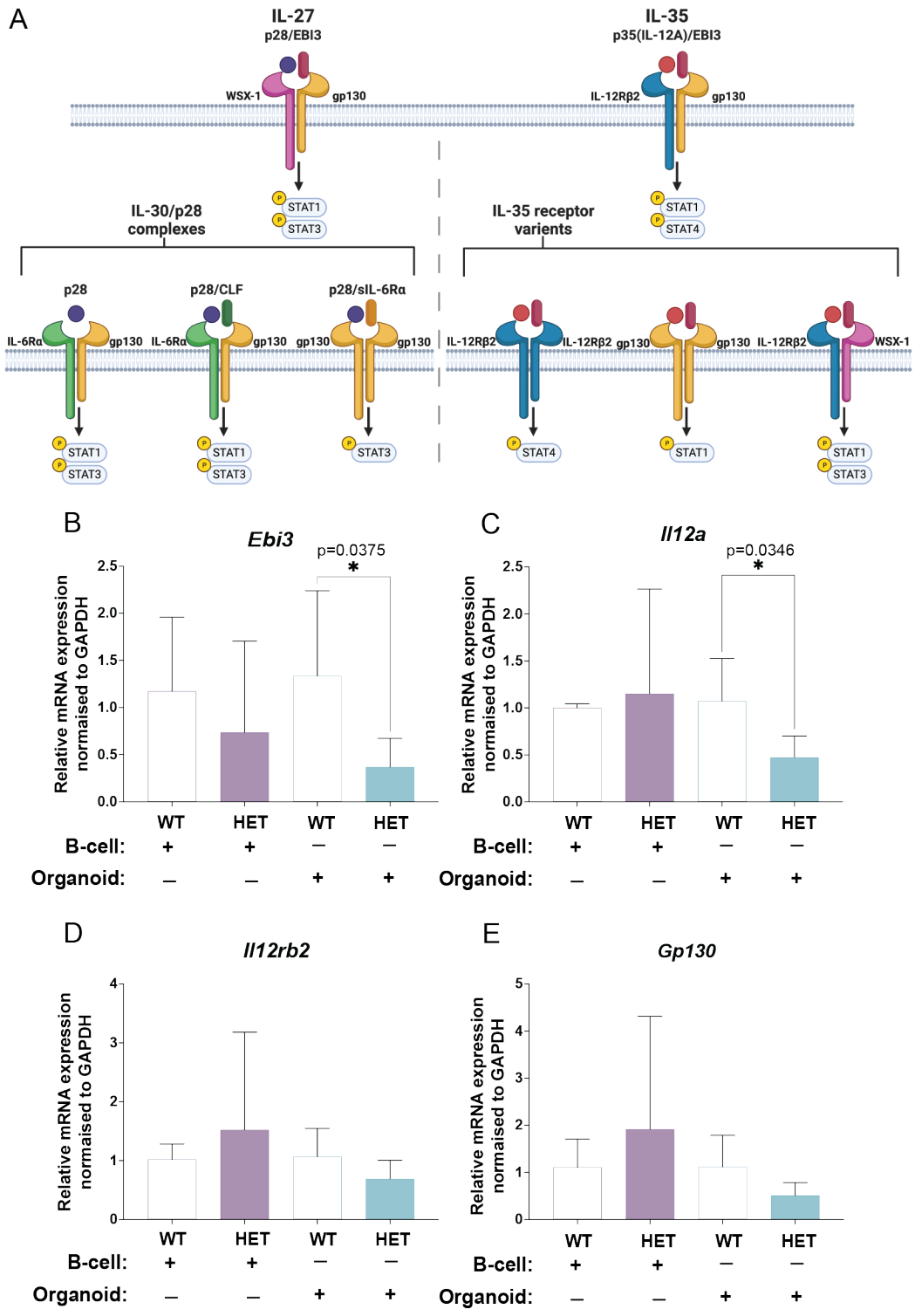


Figure 6.4: IL-35 and IL-35 receptor expression in B-cells and KC organoids.
(A) Schematic of receptor composition and shared receptor subunits between IL-27 and IL-35. B-cells were isolated using pan-B-cell magnetic separation from 3-month *Kras*$^{LSL.G12D+/+}$*;Pdx-1-Cre* (WT) (n=3) and *Kras*$^{LSL.G12D/+}$*;Pdx-1-Cre* (HET) spleens. Organoids were derived from *Kras*$^{LSL.G12D/-}$*;Pdx-1-Cre* (WT) (n=4) and *Kras*$^{LSL.G12D/+}$*;Pdx-1-Cre* (HET) (n=6). RNA was extracted from isolated B-cells and organoids. The fold-change in mRNA expression of (B) *Ebi3*, (C) *Il12*, (D) *Il12rb2* and (E) *Gp130* compared to WT controls was determined. Data points represent an average of technical duplicates. All quantifications were represented as a mean ± SD. Statistical significance denoted by * (p<0.01), ** (p<0.001) and *** (p<0.0001) and performed using an unpaired T-test.

6.4 Discussion

Early PanIN development has been associated with inflammation via association to inflammatory conditions such as pancreatitis or inflammatory immune cells such as macrophages (Guerra et al., 2007; Guerra et al., 2011b; Liou et al., 2015b; Liou et al., 2017b). While several studies have begun to elucidate local drivers of immune cell recruitment in this inflammatory setting, further exploration is required to understand how these contribute to the neoplastic lesions themselves and whether their contribution, both systemically and locally, expedites lesion progression. The preliminary studies in this chapter sought to characterise systemic factors associated with inflammation during lesion progression over time.

The data in this chapter implied that decreased levels of IL-23 was associated with early PanIN progression and may be involved in their promotion. Conflicting data has presented IL-23 as both anti and pro-tumorigenic. Its promotion of epithelial to mesenchymal transition has been associated with poor prognosis in oesophageal cancer (Chen et al., 2015). Yet adenoviral delivery of IL-23 in a fibrosarcoma tumour model significantly improved murine survival and decreased tumour volume (Reay et al., 2009). The role of IL-23 in PDAC has also been conflicting. Serum levels of IL-23 were significantly higher in later stage (III-IV) than early staged disease (I-II) (He et al., 2011). Similarly, data in this chapter found a significant increase in late-stage orthotopic PDAC models. This phenomenon had been associated with Th17 tumour infiltrate in the literature (He et al., 2011). Indeed IL-23 has previously been shown to stabilise transcription factor RORγT to allow Th17 and subsequent IL-17 release (Aggarwal et al., 2003; Ivanov et al., 2006). While not conducted in this thesis, Th17 cell characterisation in the KC GEMM may elucidate these findings further. Conversely, long-term PDAC survivors (>30-months) had higher IL-23 protein expression on resected tumour sections and shown to abrogate

macrophage-associated metastasis in concordance with TGFβ (Hussain et al., 2018). While the relationship between IL-23 and PDAC remains unclear, it was not significantly increased at later stages of high-grade PanIN lesions. Although systemic IL-23 and IL-17A were not significantly different to matched WT controls, recent studies have shown IL-17A, produced by Th17 and γδT-cells activated an IL-23/IL-17 neutrophil axis to promote acute pancreatitis (Yan et al., 2019; Hu et al., 2020). Indeed, granulocyte pancreatic infiltration was observed during early PanIN-1 lesion development (Chapter 5) Considering IL-17-secreting immune cells were found to induce stem-cell features of PanIN-1 cells during ADM to PanIN progression, the pro-tumorigenic IL-23/IL-17 axis warrants further investigation (Zhang et al., 2018b).

GM-CSF allows the development of granulocytes, monocytes and macrophages (Gough et al., 1984). In agreement with the literature, systemic GM-CSF was upregulated in established, late-stage PDAC (Bayne et al., 2012; Arnoletti et al., 2022; Ruffolo et al., 2022). Protein expression of GM-CSF in human and murine PanIN lesions, and upregulation of GM-CSF in orthotopic PDAC serum, had previously associated GM-CSF to PanIN progression (Pylayeva-Gupta et al., 2012). In this study systemic GM-CSF was down-regulated at low-grade lesions, compared to age-matched controls, but upregulated following high-grade transition at 9-12-months. This data also corresponds to splenic MDSC functionality at 9-12-months (Chapter 5). As GM-CSF is known to facilitate MDSC functionality, this data further suggests MDSC presence in the KC GEMM following high-grade transition of lesions to generate a local, immunosuppressive microenvironment (Barreda et al., 2004; Lechner et al., 2010; Bayne et al., 2012; Takeuchi et al., 2015). Tumour-derived GM-CSF, in pancreatic murine models, has been shown to drive Gr1+CD11b+ tumour infiltrate and suppressive CD8 T-cell capacity (Bayne et al., 2012). This perhaps rationalises why statistical upregulation of GM-CSF wasn't found systemically. Nonetheless, further investigation is required to determine whether systemic GM-CSF also facilitates MDSC expansion and contribution towards neoplasia, particularly

as prior studies have been conducted in an orthotopic model (Pylayeva-Gupta et al., 2012).

Inflammatory properties of IL-1β have been associated with poor prognosis in several cancers, promoting suppressive macrophage and MDSC infiltration (Apte et al., 2006; Jiang et al., 2015; Bent et al., 2018; Chen et al., 2018). Previous studies have found IL-1β association to pancreatitis, while elevated tumoral and serum IL-1β was associated with poor survival and chemoresistance in PDAC patients (Mayer et al., 2000; Maker et al., 2011; Mitsunaga et al., 2013; Zhang et al., 2018a). Data from this study agreed with the literature; significant upregulation of circulatory IL-1β was associated with established late-stage PDAC tumour. Pancreatic IL-1β secretion had previously been associated to PanIN lesion development (Fink et al., 1997; Liou et al., 2017b; Das et al., 2020). More recently, Das et al described a tolerogenic state in the PanIN microenvironment due to tumour-cell derived IL-1β. Cytokine production was mediated by TLR4-NLRP3 inflammasome and led to the accumulation of MDSCs, M2-macrophages, B-regulatory cells and Th17 (Das et al., 2020). However, this study carried out immune-infiltrate analysis in an orthotopic PDAC model, in the pancreata of *Il1β*receptor (*Il1r1*) null mice. This model is not suitable to capture the nuance of PanIN progression due to the outgrowth of PDAC tumour cells used. Variability in IL-1β KC HET plasma concentration was observed in this chapter. This data, along with the literature, would suggest IL-1β may have a localised role in the pancreas that doesn't translate to the systemic inflammatory profile until much later in carcinoma (Das et al., 2020; Takahashi et al., 2021).

Significant reduction in plasma IL-27 at time-points associated with low-grade PanIN lesions open a new line of questioning. Does the systemic loss of IL-27 have beneficial or detrimental implications for PanIN progression at during early development? IL-27 is produced by antigen presenting cells (APCs) and myeloid cells in response to toll-like receptor (TLR) activation (Guzzo et al., 2012; Petes et al., 2017; Petes et al., 2018). IL-27 secretion has also been shown to cause MHC I and II upregulation on myeloid and

epithelial cells (Feng et al., 2007; Feng et al., 2008). In the tumour setting, IL-27 has been shown to enhance the proliferation and cytotoxic activity of CD8 T-cells across several cancer types (Salcedo et al., 2004; Schneider et al., 2011; Liu et al., 2013). However, the role of IL-27 in cancer is multifaceted and some studies have implied its anti-tumour capability (Yoshimoto et al., 2015). In this study, a significant reduction in plasma IL-27 was found in concordance with a significant reduction of circulatory CD19+ B-cells and CD19+ B-cell accumulation in the spleen (Chapter 5). Reports in the literature have shown IL-27 enhances germinal centre B-cell function, therefore its reduction could be preventing germinal centre function and driving B-cell accumulation in the spleen (Larousserie et al., 2006; Vijayan et al., 2016). Contrary to this, another explanation regarding the depletion of IL-27 in the plasma could suggest that IL-27 is being used to enhance B-cell function in the germinal centres of the spleen. Considering non-specific and background CD19 IHC staining was observed in the KC HET spleen (Chapter 5), this interpretation of the data requires further investigation.

Plasma IL-27 returned to wild-type baseline at 9-months, upon the transition from low to high-grade PanIN lesion. Interestingly, Dibra et al found that lack of IL-27 signalling in mice that were heterozygous for mutant *Trp53* resulted in significantly reduced survival, increased osteosarcoma and increased $Trp53^{R17H}$ stability (Dibra et al., 2016). They suggested that IL-27 signalling may attenuate the oncogenic properties of mutant *Trp53* and that lack of signalling is associated with early mutant *Trp53* stability *in vivo.* When considering data in this chapter in relation to the literature, the reduction in systemic IL-27 may play a role in stabilisation of mutant *Trp53* later in disease progression. IL-27 returns to KC WT baseline upon transition to high-grade lesion and PanIN-3 formation, known to harbour *Tp53* mutation. While further investigation is required, including the *Tp53* and *Cdkn2a* mutational status of KC HET PanIN lesions, this may prompt a new line of questioning regarding the influence of the immune microenvironment on disease progression. Further investigation could include targeted gene delivery of IL-27, as

detailed by Figueiredo et al, to enhance the bioactivity of IL-27 *in vivo* (Figueiredo et al., 2020). This experiment may shed light on the role of IL-27 in PanIN progression; if enhanced IL-27 activity prevents PanIN formation, and if this influences the rescue of B-cells to confirm IL-27 involvement in splenic B-cell accumulation.

While IL-27 reduction should be considered as a potential instigator of systemic inflammation suppression, another plausible rationale was hypothesised to be due to receptor subunit competition with IL-35, known for its pro-tumorigenic properties (Wu et al., 2012; Zeng et al., 2013; Jin et al., 2014; Jin et al., 2015; Kourko et al., 2019). IL-35 is associated with increasing severity of malignancy across several cancers, including PDAC (Wu et al., 2012; Zeng et al., 2013; Jin et al., 2014; Jin et al., 2015). Indeed, recombinant IL-35 was found to enhance survival and proliferation of PDAC cell lines *in vitro* (Nicholl et al., 2014). Zou et al recently detailed IL-35-induced polarisation of neutrophils, towards a pro-tumour phenotype, by upregulating G-CSF and IL-6 to promote an immunosuppressive tumour microenvironment through neutrophil infiltration (Zou et al., 2017). In addition, IL-35 is produced by TAMs and tumour cells, further verifying its role in tumour promotion (Wang et al., 2013; Lee et al., 2018a).

Although IL-35 was not detected systemically in the plasma or organoid supernatant due to technical difficulties, the cytokine subunits, *Ebi3* and *Il12a*, were significantly reduced in KC HET organoids, indicating local secretion of IL-35 isn't taking place. No significant increase in IL-35 (*Ebi3*, *Il12a) or* IL-35 receptor subunits (*Il12rb2,Gp130)* were found in splenic B-cells isolated from KC HET 3-month mice. This data indicates that these splenic B-cells were unlikely to be a source of IL-35. However, a larger sample pool will be required to understand this in greater detail.

Mirlekar et al recently showed that IL-35 drives B-cell dysfunction in tumour-educated naïve B-cells through STAT3 and PAX5 in PDAC (Mirlekar et al., 2022). However, this data was generated in an orthotopic PDAC model and did not consider discrepancies in

B-cell immune generation between an orthotopic and genetic murine model of PDAC (Spear et al., 2019). Further exploration is required to understand whether splenic and intra-tumoral B-regulatory cells ($CD21^{hi}CD1d^{hi}CD5^{+}$) are present in the KC GEMM during later PanIN progression to high-grade lesions. In addition, whether IL-35 contributes towards B-regulatory cell generation to further progress lesion development by generating a *p35−/−* or *Ebi3−/−* cross with the KC GEMM.

Limitations of this preliminary study must also be considered. Splenic B-cells were only isolated from 3-month KC HET and KC WT mice. Isolation of B-cells from both the spleen, and the pancreas, should be carried out at 6, 9 and 12-months and prior to the 3-month time-point. The literature has suggested that the B-cell IL-35 receptor subunits consist of IL-12Rβ2 and WSX-1, therefore further examination of WSX-1 is required (Wang et al., 2014). IL-6Rα receptor subunit expression should also be analysed as shared competition for receptor subunits by IL-35, IL-27 and IL-30 may complicate interpretation of results regarding the responsible cytokine. A significant decrease in IL-35 cytokine subunits was found in KC HET organoids compared to controls. While organoids were representative of early PanIN lesions, mRNA expression would be better interpreted from KC HET pancreatic RNA lysates themselves at time-points associated with PanIN lesion progression. This would allow the interpretation of IL-35 response in association with lesion development.

Considering the association to pancreatitis, early PanIN stages were hypothesised to be associated with a systemic inflammatory microenvironment. However, the data in this chapter presented the inverse relationship. Systemically, early PanIN progression was not associated with upregulation of inflammatory cytokines, but rather upregulation of inflammatory IFNγ, TNFα, GM-CSF and IL-23 was associated with the transition to high-grade lesions and tumorigenesis. The data in this chapter, and supporting evidence in the literature, would suggest that the inflammatory microenvironment is sustained at the pancreatic level during early neoplasia rather than global inflammation systemically.

Subsequently, chronic pancreatic inflammation may influence immune-suppressive cell infiltration, such as MDSCs, and systemic inflammation during late-stage PDAC.

Initial data from this preliminary study suggests reduction of IL-27 in the plasma may hinder B-cell function considering IL-27 loss was observed in concordance with a decreased B-cell count in the blood and accumulation of splenic B-cells. Further investigation is required to elucidate this hypothesis in detail.

7. General Discussion and Conclusion

PDAC is considered a non-immunogenic malignancy, for the vast majority of patients, given the tumour microenvironment harbours reduced antigenicity and immunogenicity, alongside immunosuppressive cell involvement (Matsushita et al., 2012; Vogelstein et al., 2013; Kiryu et al., 2021). In addition, immunotherapeutic intervention has failed to deliver meaningful results to patient survival thus far, likely due to the various methods of immune evasion employed by the tumour (Kabacaoglu et al., 2018). ADM and early PanIN lesions have been associated with an inflammatory response (Corcoran et al., 2011; Liou et al., 2013; Zhang et al., 2013b; Liou et al., 2015b; Liou and Storz, 2015). The sequential alterations to the immune repertoire during lesion development, that ultimately lead to a non-immunogenic PDAC microenvironment, requires further understanding and may benefit future immunotherapeutic intervention.

The central purpose of this thesis sought to further understand the immunological repertoire associated with PDAC development over time. To support this aim, the immune microenvironment of PDAC in established models was characterised. This analysis sufficed as an immunological endpoint in which comparison could be made against the immune microenvironment associated with PanIN lesion development, from low to high-grade neoplasia and subsequent carcinoma. In doing so, the studies in this thesis aimed to understand the local and systemic immunological responses to *Kras* oncogene expression, how the immune system is perturbed and the point at which this supports an immunosuppressive microenvironment and tumour suppressor cells. Furthermore, this investigation aimed to identify systemic drivers associated with the dynamic immunological landscape altered by neoplastic development over time.

To answer these questions, a multicolour FC panel was generated to interrogate major immune populations systemically and in the tumour locale. While tissue dissociation of the pancreas and tumour resulted in some antigen cleavage, optimisation of enzymatic

dissociation aimed to mitigate this limitation. Although the multicolour FC panel captured a range of major immune populations for interrogation, the panel did not include DC markers. Future adaptions of the panel should include this, particularly for better understanding of antigen presentation within the PDAC and PanIN lesion microenvironment. Overall, the FC panel allowed immune evaluation at varying stages of PanIN progression, the established PDAC microenvironment and following immunotherapeutic perturbation at late-stage PDAC. Identification of immune populations associated with PDAC agreed with the literature and validated the reliability of the FC panel, aiding subsequent validation of novel findings during PanIN progression (Stromnes et al., 2014; Liou et al., 2017a; Wang et al., 2017; Zhu et al., 2017; Spear et al., 2019; Trovato et al., 2019; Yang et al., 2022). Furthermore, as the FC panel allowed the broad capture of major populations, we were able to define the importance of each population at each step of PanIN lesion pathogenesis. Future evaluation will now be able to interrogate these identified populations in greater depth with more nuance. Interrogation of suppressive, exhausted or activated capacity of immune cells, via cytokine release could be included. Rare cell subsets, such as γδ T or Th17 T-cells, could be included given recent findings have shown their involvement in PDAC (Yan et al., 2019; Das et al., 2020; Hu et al., 2020).

Therapeutic perturbation of the tumour microenvironment demonstrated the potential benefit of fractionated low-dose radiotherapy, in combination with immunotherapies, to significantly reduce tumour volume compared to untreated control. While combination therapy resulted in an increase of CD8 T and NK cell tumour infiltrate, this data was variable between biological replicates and did not significantly alter immune infiltrate at the central tumour core. Variation in immune infiltrate is likely due to the difference in treatment responders and non-responders within each treatment group based on E-Cadherin staining. Further investigation is required to understand these differences and whether they may be due to leakage of KPC cells at the site of orthotopic injection.

However, data in this thesis has highlighted a potential non-activated NK-CD8 axis that may be involved in treatment response. Non-activated NK cells, lacking NKG2D, correlated to treatment responders and an increase in CD8+ T-cells in the tumour locale following CCR5i+IR and aPD1+CCR5i+IR. Further investigation is required to understand if non-activated NK cells and T-cells are interacting via antigen presentation. Furthermore, future investigation regarding tertiary lymphoid structures within the tumour locale could shed light on DC antigen presentation to NK cells, but also plasma cell producing B-cells, as this was not captured by the FC or IF panels (Gunderson et al., 2021).

Evaluation of the established PDAC immune microenvironment, in both genetic and orthotopic settings, was conducted. Identification of immune populations largely agreed with the literature. The tumour locale of both models predominantly consisted of macrophages, particularly of an M2 phenotype, infiltration of granulocytes/PMN-MDSCs and cytotoxic T-cell exclusion (Stromnes et al., 2014; Liou et al., 2017a; Wang et al., 2017; Zhu et al., 2017; Spear et al., 2019; Trovato et al., 2019; Yang et al., 2022). In addition, B-cell infiltrate within the orthotopic tumour agreed with previous reports (Spear et al., 2019). Data in this thesis predominantly agreed with the literature regarding the differences between genetic and orthotopic murine models and further highlighted discrepancies in NK cells (Spear et al., 2019). This data further highlights the importance of utilising the correct model for the study of immune contribution towards disease pathogenesis over time, or specific immune cell interrogation with immunotherapy (Spear et al., 2019). Where data in this thesis differentiated from previous reports, these differences may be attributed to variation in the PDAC cell lines used for orthotopic generation. In addition, a greater number of KPC GEMM biological replicates may reduce this variation. These experiments should also be repeated with control littermate *Pdx-1-Cre+; Kras*$^{G12D+/+}$*; LSL-Trp53*$^{R172H+/+}$and Matrigel-only orthotopic injection should be used for KPC and orthotopic PDAC comparison respectively. However, data in this thesis added to the growing body of evidence regarding variation in FOXP3+ T-regulatory cell PDAC

infiltrate between human and GEMM (Lee et al., 2016a; Spear et al., 2019; Brouwer et al., 2022; Yang et al., 2022). Interpretation of this data would suggest caution be made when extrapolating murine analysis onto the human setting, particularly for immunotherapy studies, but further investigation is required. Overall, macrophage and granulocyte/PMN-MDSC dominated the systemic and local tumour microenvironment, while a reduction in infiltrating NK cells was observed in the tumour locale. This comprehensive characterisation of the surrounding advanced PDAC immune milieu served as a baseline for comparison against the microenvironment of emerging lesions and pre-invasive carcinoma.

Investigation surrounding the immune microenvironment of PanIN lesions has allowed greater insight into the chain of events that may be taking place over the course of lesion development (Figure 7.1). Data in this thesis revealed granulocyte infiltration during early ADM/PanIN-1 development at 3-months and remained present in the pancreata throughout lesion progression to carcinoma. Further analysis revealed splenic-derived granulocytes, isolated from KC GEMMs harbouring low-grade lesions (3-months), had the capacity to increase CD8 T-cell proliferation *ex vivo.* This raises the question as to whether these granulocytes are functioning through antigen presentation to T-cells early in lesion development given neutrophils have been shown to cross-prime T-cells via MHC I and II pathways (Gosselin et al., 1993; Potter and Harding, 2001; Beauvillain et al., 2007; Pylaeva et al., 2022). Although further analysis is required to understand whether this interaction is occurring, therapeutic intervention to amplify antigen-presentation later in PanIN development, to elicit PanIN eradication, may be plausible if a T-cell-granulocyte axis of eradication is indeed taking place at this stage of early pathogenesis.

In contrast, granulocytes isolated from KC spleens at the transition to high-grade PanIN lesions (9 and 12-months), significantly suppressed CD8 T-cell proliferation, thus classifying these cells as PMN-MDSCs. The suppressive capacity of splenic-M-MDSCs was identified at 12-months, upon carcinoma in situ, albeit with lower significance. Within

the established tumour of the KPC GEMM, monocytes/M-MDSCs did not significantly infiltrate the tumour compared to granulocytes/PMN-MDSCs. One possible implication of data in this thesis, in combination with patient data produced by Brouwer et al, is that monocytes/M-MDSCs may not have as significant a role in driving immunosuppression as granulocytes/PMN-MDSCs given differences in frequency in the tumour locale and CD8 T-cell suppressive capacity (Brouwer et al., 2022). This data indicates that PMN-MDSCs play a significant role not only at late-stage PDAC, but more importantly throughout progression of high-grade lesions to invasive carcinoma. Upregulation of circulatory GM-CSF at late-stage PDAC and high-grade PanIN lesion time-points (9 – 12-months), also indicates the presence of MDSCs at these time-point considering GM-CSF has been shown to facilitate MDSC functionality (Barreda et al., 2004; Lechner et al., 2010; Bayne et al., 2012; Takeuchi et al., 2015). While Clark et al previously identified the suppressive capacity of splenic-derived MDSCs from KC mice containing PanIN lesions, MDSC association to specific time-points of PanIN lesion transition were not classified (Clark et al., 2007a). To our knowledge, the data presented in this thesis is the first to identify the specific time-point in which MDSC involvement is apparent. In addition, this data has distinguished between both PMN-MDSCs and M-MDSCs. The findings of this study suggest that an immune-suppressed microenvironment is being set up at 9-months, upon the transition from low to high-grade PanIN lesion. Although this experiment was conducted on splenocyte-derived cells due to cellular paucity in the pancreas, this experiment should be repeated on pancreatic-derived cells to determine whether PMN-MDSC and M-MDSCs are also able to infiltrate the surrounding PanIN lesions at these time-points to induce local suppression.

Macrophage populations, particularly M2 macrophages, were not significantly upregulated throughout PanIN lesion development to the same extent as macrophage infiltrate observed in the KPC GEMM tumour. While previously published data has found macrophage involvement at the initiator stage of disease and ADM development, this data

indicates that macrophage involvement is restricted to late-stage tumour rather than PanIN progression (Liou et al., 2015b; Schlesinger et al., 2020).

NK and CD8 T-cell infiltrate was significantly upregulated in the pancreas at 6-months but lost upon transition to high-grade PanIN lesion at 9-months. This would indicate that PanIN lesion control is lost between 6 and 9-months, during high-grade transition, with subsequent upregulation of PMN-MDSCs generating an immunosuppressive microenvironment without the ability to eradicate PanIN lesions via NK or CD8 T-cell activity. More importantly, this data indicates a suppressive microenvironment is established at 9-months, before invasive carcinoma is present.

B-cell contribution to the pathogenesis and later-stages of PDAC is controversial with opposing reports in the literature (Gunderson et al., 2016; Lee et al., 2016b; Pylayeva-Gupta et al., 2016; Brunner et al., 2020; Mirlekar et al., 2020; Delvecchio et al., 2022). No significant B-cell infiltration was found in the pancreata of KC mice throughout PanIN lesion development. Technical issues with IHC spatial investigation warrant future investigation with further optimisation of IF staining. However, a significant reduction in circulatory B-cells during early lesion development (3 – 6-months), was subsequently restored to WT control baseline upon transition to high-grade PanIN lesion (9 – 12-months). At the same time, circulatory IL-27 was also significantly reduced at early-time points and restored to WT baseline control at the transition to high-grade lesions. This significant finding opens a new line of questioning. Does the systemic loss of IL-27 have beneficial or detrimental implications for PanIN progression during early development? Data in this thesis found a significant upregulation of CD19+ B-cells in the spleens of KC GEMMS at 3-months, predominantly localised to the red pulp, although further investigation is required to better understand this spatiality. Given IL-27 has been shown to directly enhance germinal centre B-cell function, it was hypothesised that IL-27 loss may prevent IL-27-dependent B-cell development at this time-point (Larousserie et al., 2006; Vijayan et al., 2016). The data in this thesis has contributed towards a growing body

of literature regarding B-cell involvement during early PanIN lesion development. Further investigation is necessary to elucidate the role of B-cells regarding the clearance or promotion of PanIN lesions harbouring *Kras* mutations. This may allow therapeutic intervention to promote PanIN resolution, by enhancing or preventing B-cell action depending on their role in PanIN development.

Considering the association of pancreatitis and localised inflammation during ADM, early PanIN stages were hypothesised to be associated with a systemic inflammatory microenvironment (Guerra et al., 2007; Guerra et al., 2011b; Daniluk et al., 2012; Huang et al., 2014; Liou et al., 2015b). Yet, systemic inflammatory IFNγ, TNFα, GM-CSF and IL-23 was associated with the transition to high-grade lesions and tumorigenesis rather than early, low-grade PanIN lesions. This data would suggest that, at the systemic level, an anti-inflammatory microenvironment may promote PanIN progression during the early stages of disease, detailed in the loss of inflammatory IL-27.

The findings of this thesis may also contribute towards disease monitoring of at-risk patients, such as chronic pancreatitis or diabetes. Similar to chronic pancreatitis patients, circulatory B-cells were significantly reduced in KC GEMMs harbouring early PanIN lesions, but restored to WT control baseline upon high-grade PanIN lesion transition and loss of control (Wei et al., 2019). Monitoring prolonged B-cell reduction over time, and subsequent restoration of B-cell numbers in the blood, may indicate a transition to high-grade disease. This may stratify patients requiring additional disease screening and may allow earlier PDAC diagnosis. However, the use of this as a biomarker requires additional *in vivo* and clinical investigation in at-risk patient groups.

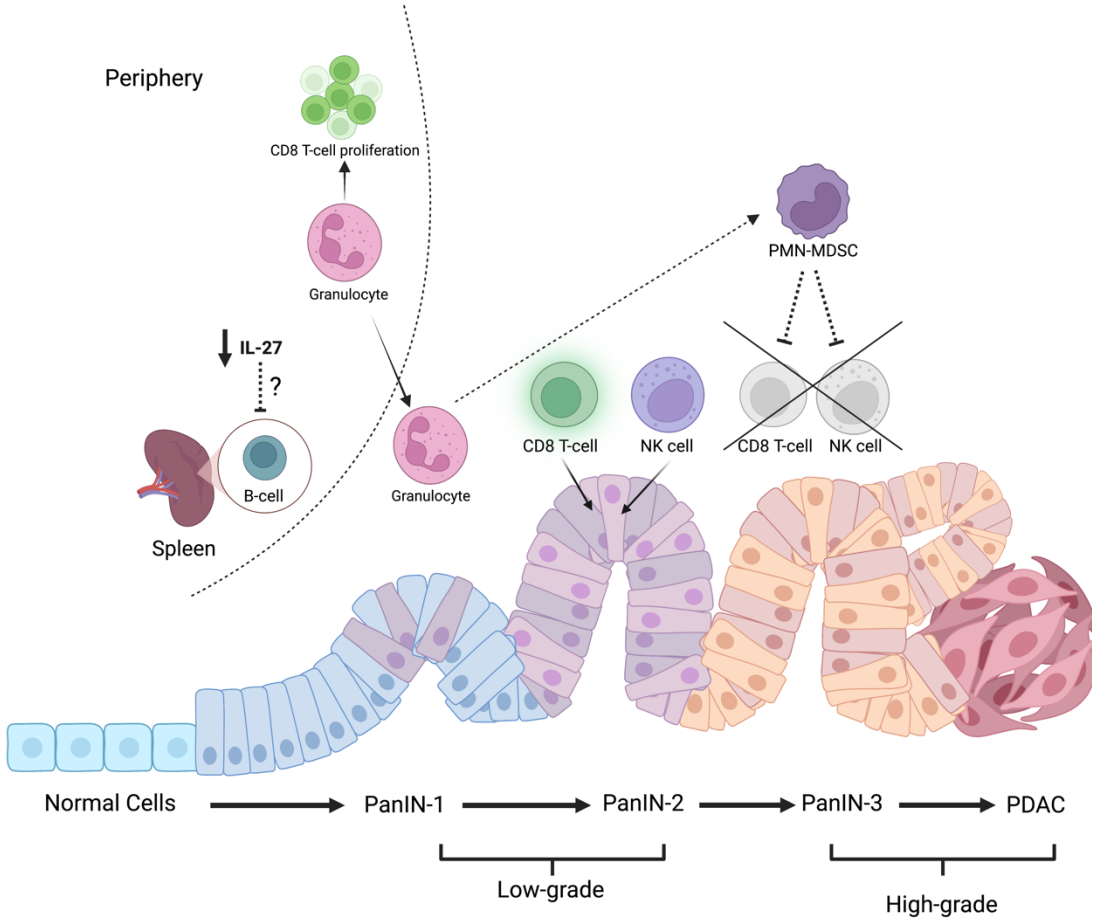


Figure 7.1: Proposed model of the immune microenvironment during PanIN lesion progression.
During low-grade PanIN lesion development (PanIN-1), B-cells are reduced in the blood and sequestered in the spleen. A systemic reduction of IL-27 is thought to elicit B-cell accumulation in the spleen and perturb function during early lesion development but requires additional investigation. Upregulation of granulocytes in the blood, during low-grade lesions, are thought to traffic in from the periphery to the local microenvironment where they are maintained throughout lesion progression to carcinoma. Splenic granulocytes taken from KC GEMMs harboring low-grade lesions are capable of instigating CD8 T-cell proliferation and may be involved in early PanIN lesion clearance. CD8 T and NK cells infiltrate PanIN-2 lesions at 6-months. However, their presence is lost upon high-grade transition. Around 6-months, upon transition from low to high-grade PanIN lesion, loss of control is thought to occur. During the transition to PanIN-3 and high-grade lesions at 9-months, splenic PMN-MDSCs are capable of T-cell suppression and thought to establish an immunosuppressive microenvironment. PMN-MDSCs may suppress CD8 T-cell and NK cell activity after the transition to high-grade lesion and allow loss of control.

7.1 Future work

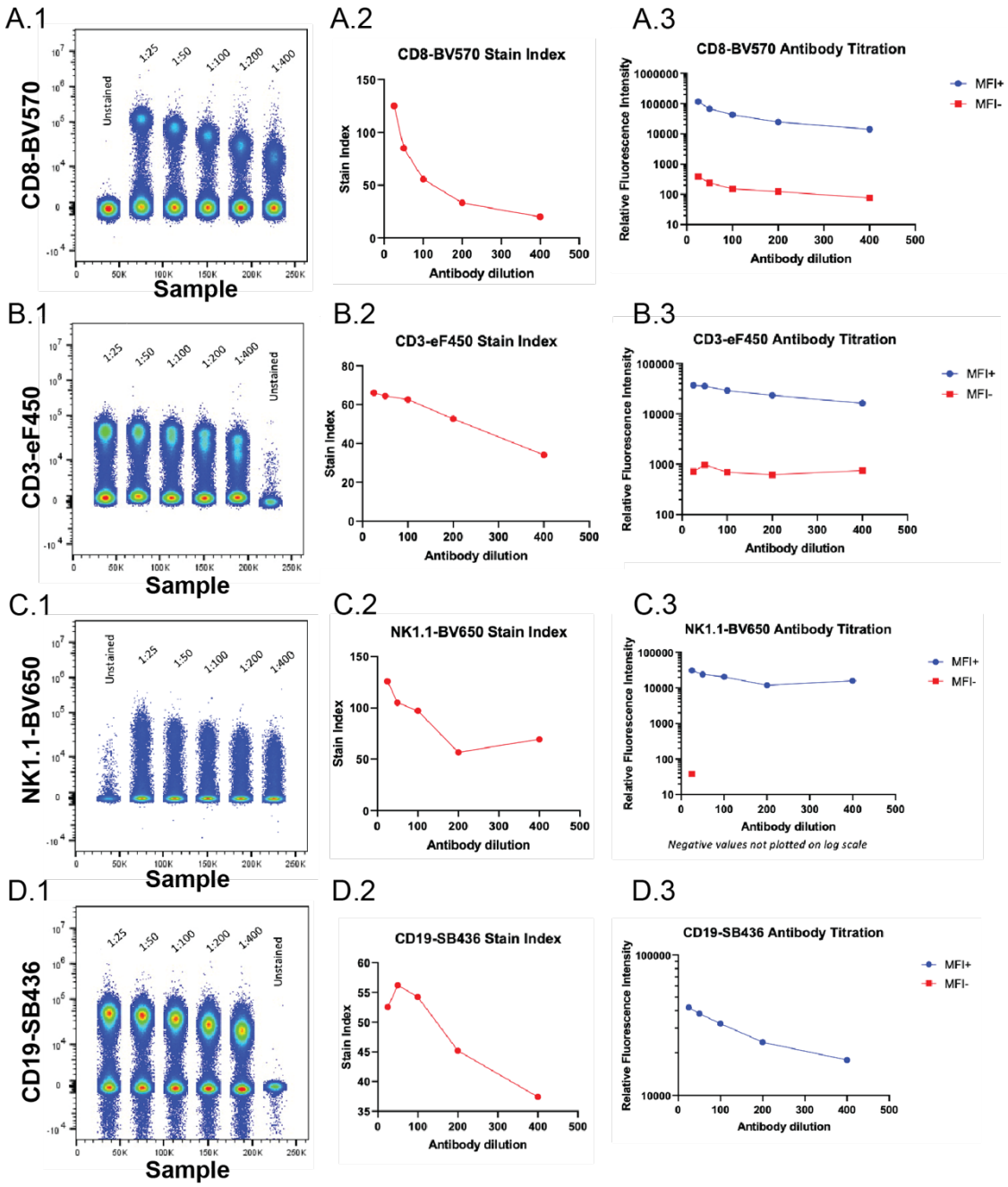
The status of splenic B-cells at 3-month KC GEMMs with low-grade lesions should be evaluated to determine whether B-cells may be clearing of exacerbating PanIN lesions. To do so, plasma cell differentiation status using CD138 staining, or B-regulatory cell status using $CD19^{+}CD5^{+}CD1d^{+}$ and IL-10 production, should be evaluated. The KC GEMM pancreatic infiltration status of B-cells should be optimised and repeated to gain further clarity as to B-cell involvement in early lesion development. To determine whether B-cells are capable of *Kras* mutant PanIN recognition, B-cell receptor genomic sequencing and mass spectrometry could be conducted (Díez et al., 2017). In addition, experimental data produced in this thesis should be conducted at time-points prior to 3-months to determine whether B-cells are involved in PanIN initiation.

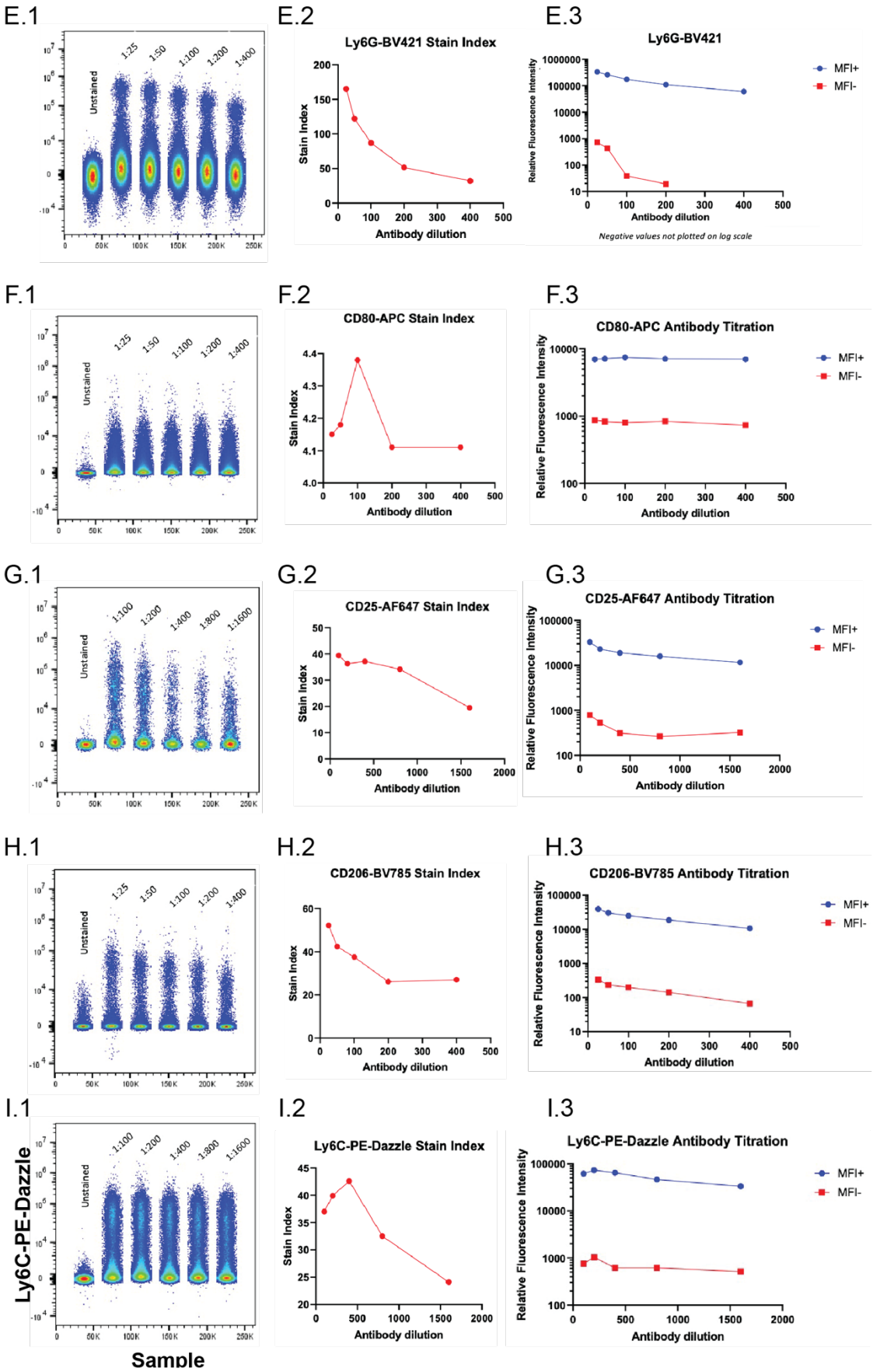
Further investigation surrounding the involvement of IL-27 during early lesion development should be conducted. Furthermore, enhancing the bioactivity of IL-27 with targeted gene delivery *in vivo* may reveal the role of IL-27 in PanIN progression (Figueiredo et al., 2020). Indeed, enhanced IL-27 activity may prevent or delay PanIN formation in KC mice. Additionally, this experiment may shed light on the role of IL-27 on B-cell activity if enhanced activity allows the rescue of B-cells in the blood and resolution of splenic accumulation. Future evaluation regarding the activation or exhaustion status of NK and CD8 T-cells, and their ability to clear PanIN lesions prior to the high-grade lesion transition, is necessary and may contribute towards our understanding of PanIN resolution and clearance. Adoptive transfer of granulocytes during early ADM/PanIN-1 lesion development may elucidate whether they play a role in early lesion clearance. The *ex vivo* T-cell suppression assay should be conducted in granulocytes isolated from the pancreata of KC GEMMs to evaluate whether infiltrating PMN-MDSC are establishing an immunosuppressive microenvironment locally at the high-grade transition (9-months).

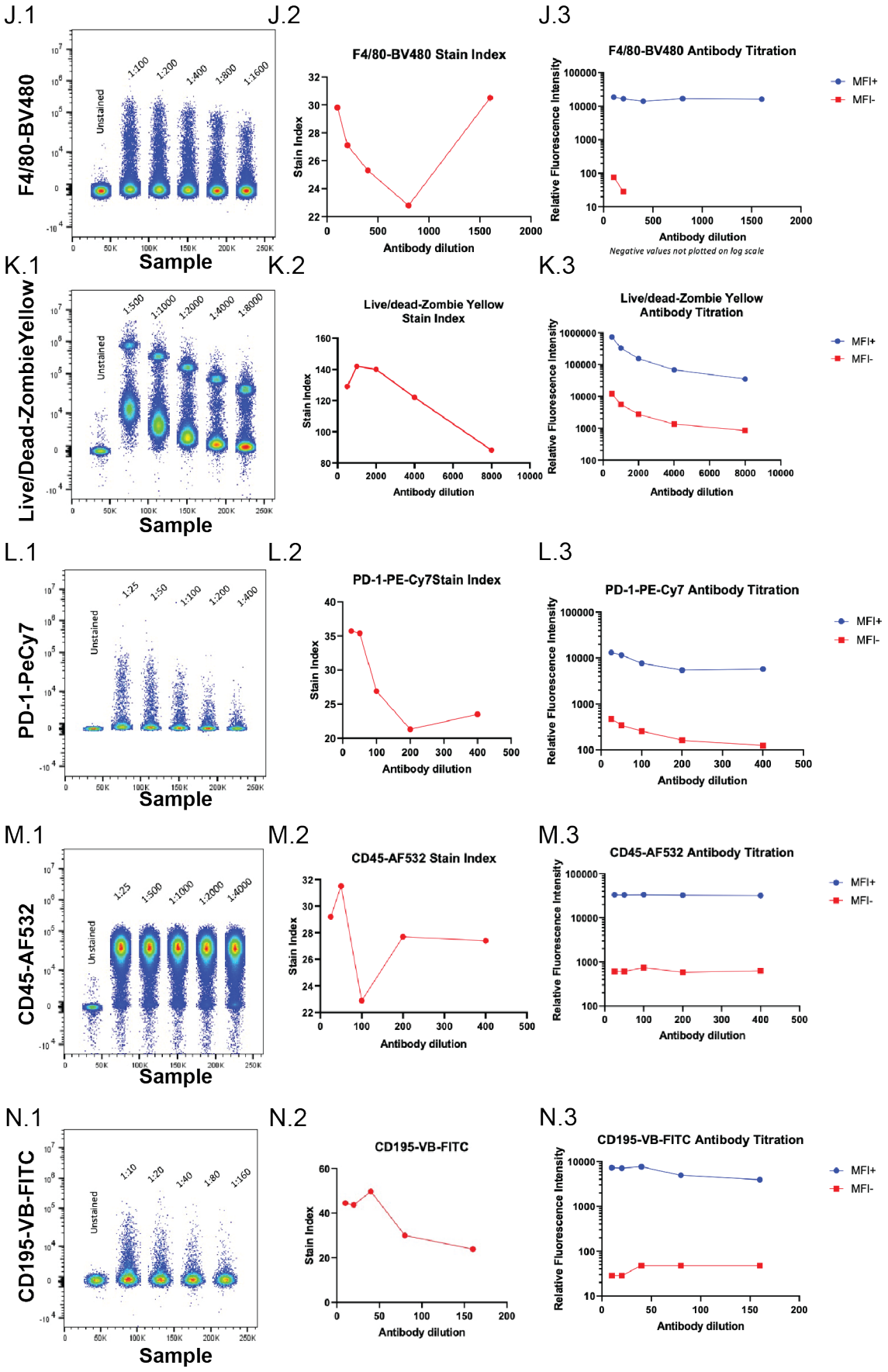
7.2 Conclusion

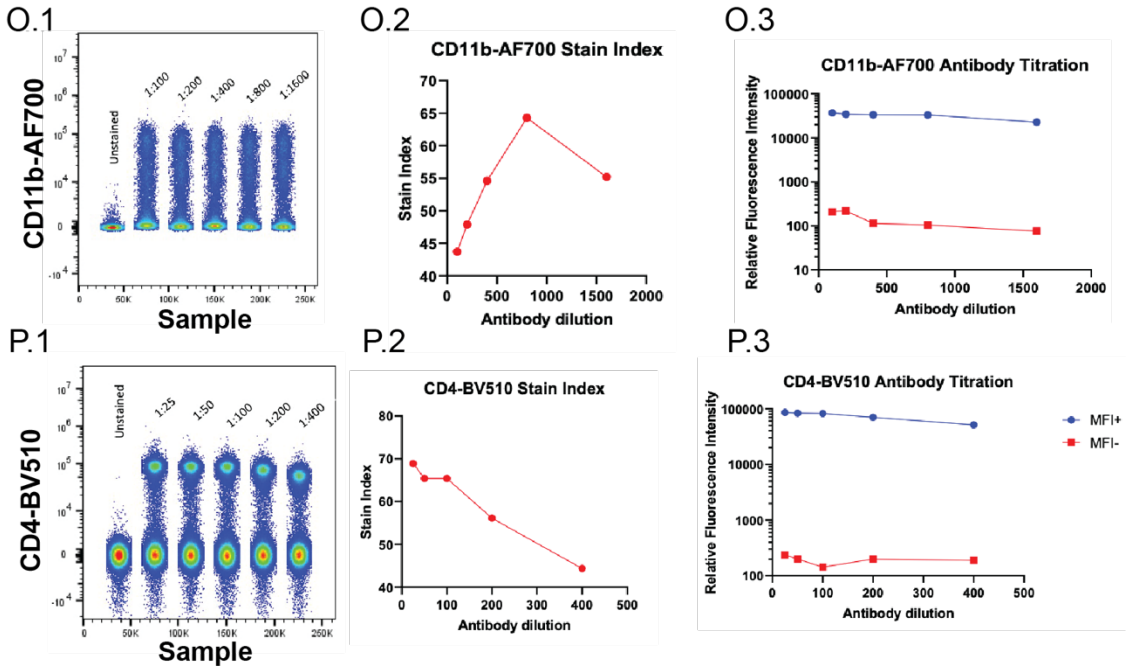
In conclusion, this work has broadly elucidated the immune microenvironment during sequential PanIN lesion development over time. To the best of our knowledge, this is the first longitudinal study carried out in KC GEMMs to determine immune status during 3-month intervals of progression. Taken together, the data in this thesis presents the local and systemic response to *Kras* oncogene expression, how this is perturbed and the point at which an immunosuppressive microenvironment is supported. In doing so, earlier therapeutic intervention of the immune subsets characterised may be possible in the future.

8. Supplementary

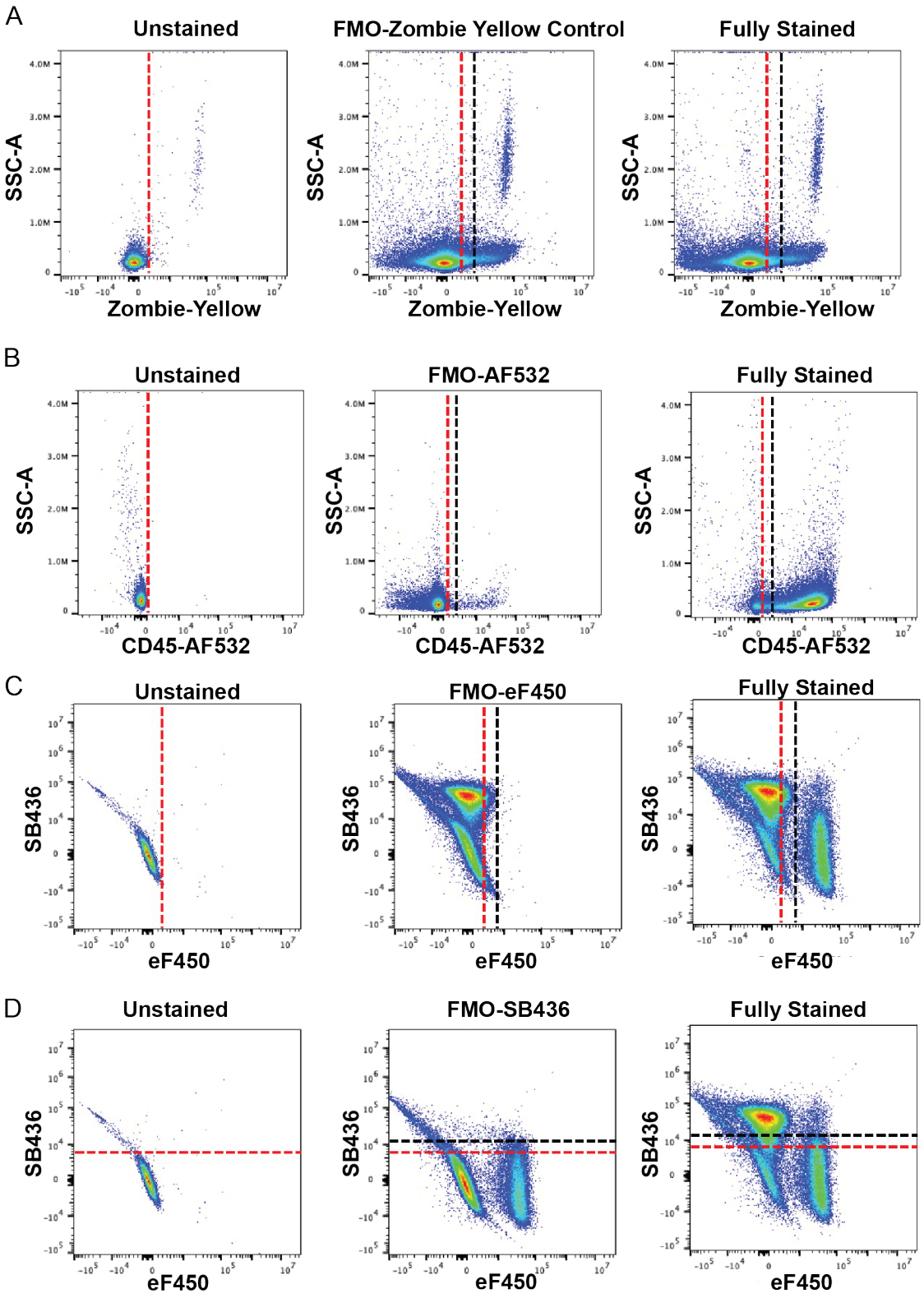


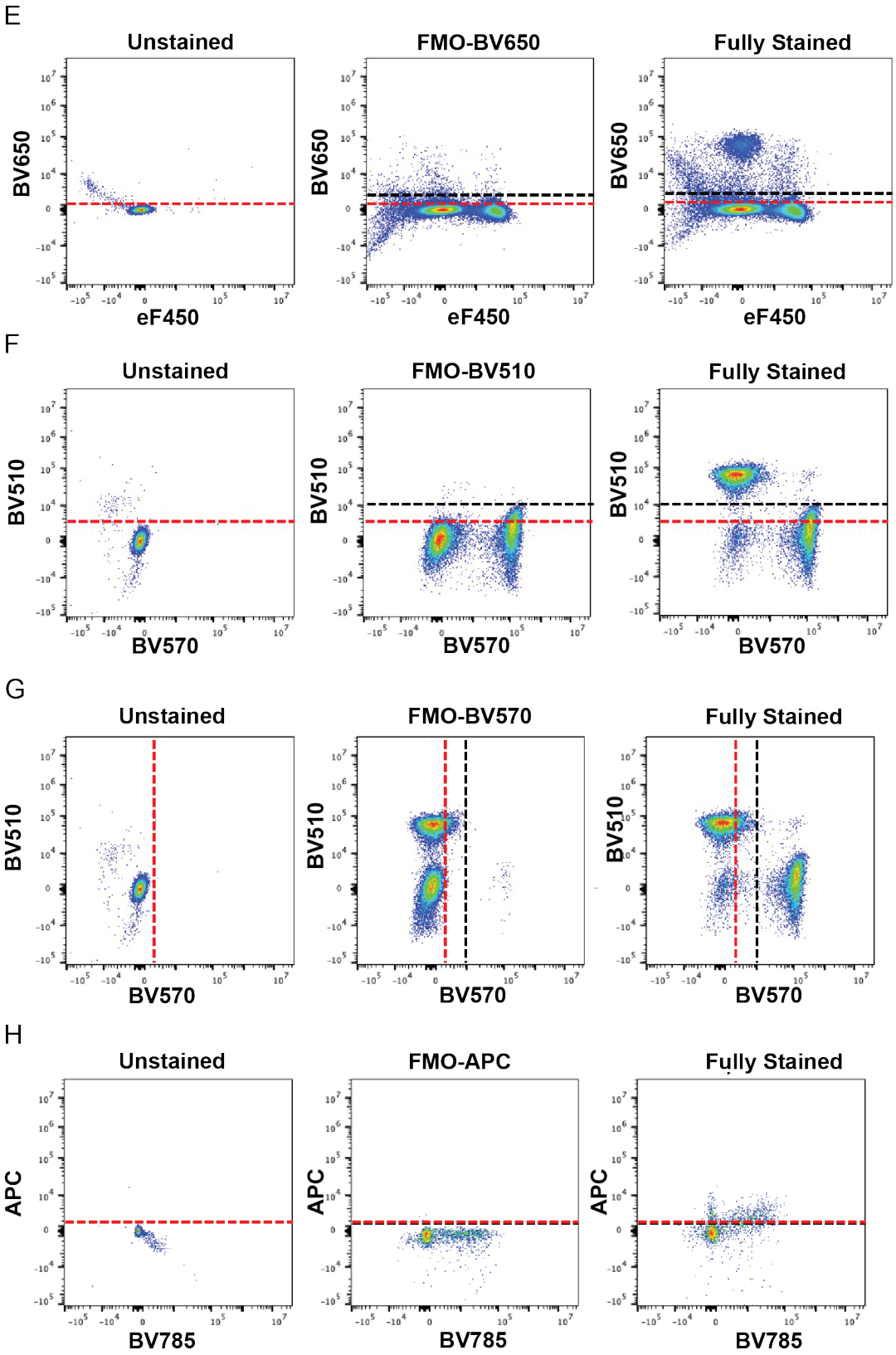

E.1
Unstained
1:25
1:50
1:100
1:200
1:400
E.2
Ly6G-BV421 Stain Index
Stain Index
Antibody dilution
E.3
Ly6G-BV421
Relative Fluorescence Intensity
MFI+
MFI-
Antibody dilution
Negative values not plotted on log scale
F.1
Unstained
1:25
1:50
1:100
1:200
1:400
F.2
CD80-APC Stain Index
Stain Index
Antibody dilution
F.3
CD80-APC Antibody Titration
Relative Fluorescence Intensity
MFI+
MFI-
Antibody dilution
G.1
Unstained
1:100
1:200
1:400
1:800
1:1600
G.2
CD25-AF647 Stain Index
Stain Index
Antibody dilution
G.3
CD25-AF647 Antibody Titration
Relative Fluorescence Intensity
MFI+
MFI-
Antibody dilution
H.1
Unstained
1:25
1:50
1:100
1:200
1:400
H.2
CD206-BV785 Stain Index
Stain Index
Antibody dilution
H.3
CD206-BV785 Antibody Titration
Relative Fluorescence Intensity
MFI+
MFI-
Antibody dilution
I.1
Ly6C-PE-Dazzle
Unstained
1:100
1:200
1:400
1:800
1:1600
Sample
I.2
Ly6C-PE-Dazzle Stain Index
Stain Index
Antibody dilution
I.3
Ly6C-PE-Dazzle Antibody Titration
Relative Fluorescence Intensity
MFI+
MFI-
Antibody dilution

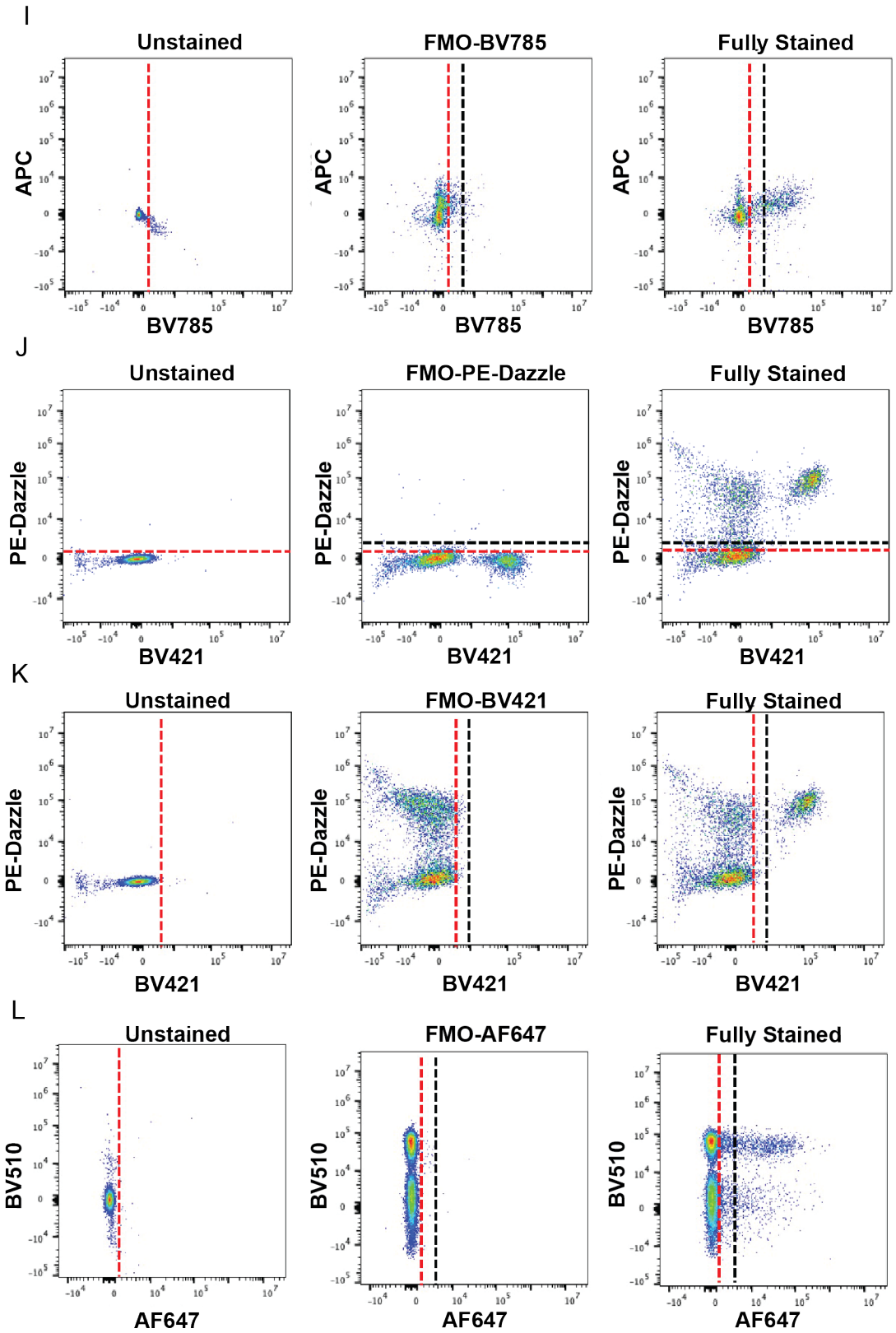

J.1
F4/80-BV480
Unstained
1:100
1:200
1:400
1:800
1:1600
Sample
J.2
F4/80-BV480 Stain Index
Stain Index
Antibody dilution
J.3
F4/80-BV480 Antibody Titration
Relative Fluorescence Intensity
Antibody dilution
Negative values not plotted on log scale
MFI+
MFI-
K.1
Live/Dead-ZombieYellow
Unstained
1:500
1:1000
1:2000
1:4000
1:8000
Sample
K.2
Live/dead-Zombie Yellow
Stain Index
Stain Index
Antibody dilution
K.3
Live/dead-Zombie Yellow
Antibody Titration
Relative Fluorescence Intensity
Antibody dilution
MFI+
MFI-
L.1
PD-1-PeCy7
Unstained
1:25
1:50
1:100
1:200
1:400
Sample
L.2
PD-1-PE-Cy7Stain Index
Stain Index
Antibody dilution
L.3
PD-1-PE-Cy7 Antibody Titration
Relative Fluorescence Intensity
Antibody dilution
MFI+
MFI-
M.1
CD45-AF532
Unstained
1:25
1:500
1:1000
1:2000
1:4000
Sample
M.2
CD45-AF532 Stain Index
Stain Index
Antibody dilution
M.3
CD45-AF532 Antibody Titration
Relative Fluorescence Intensity
Antibody dilution
MFI+
MFI-
N.1
CD195-VB-FITC
Unstained
1:10
1:20
1:40
1:80
1:160
Sample
N.2
CD195-VB-FITC
Stain Index
Antibody dilution
N.3
CD195-VB-FITC Antibody Titration
Relative Fluorescence Intensity
Antibody dilution
MFI+
MFI-

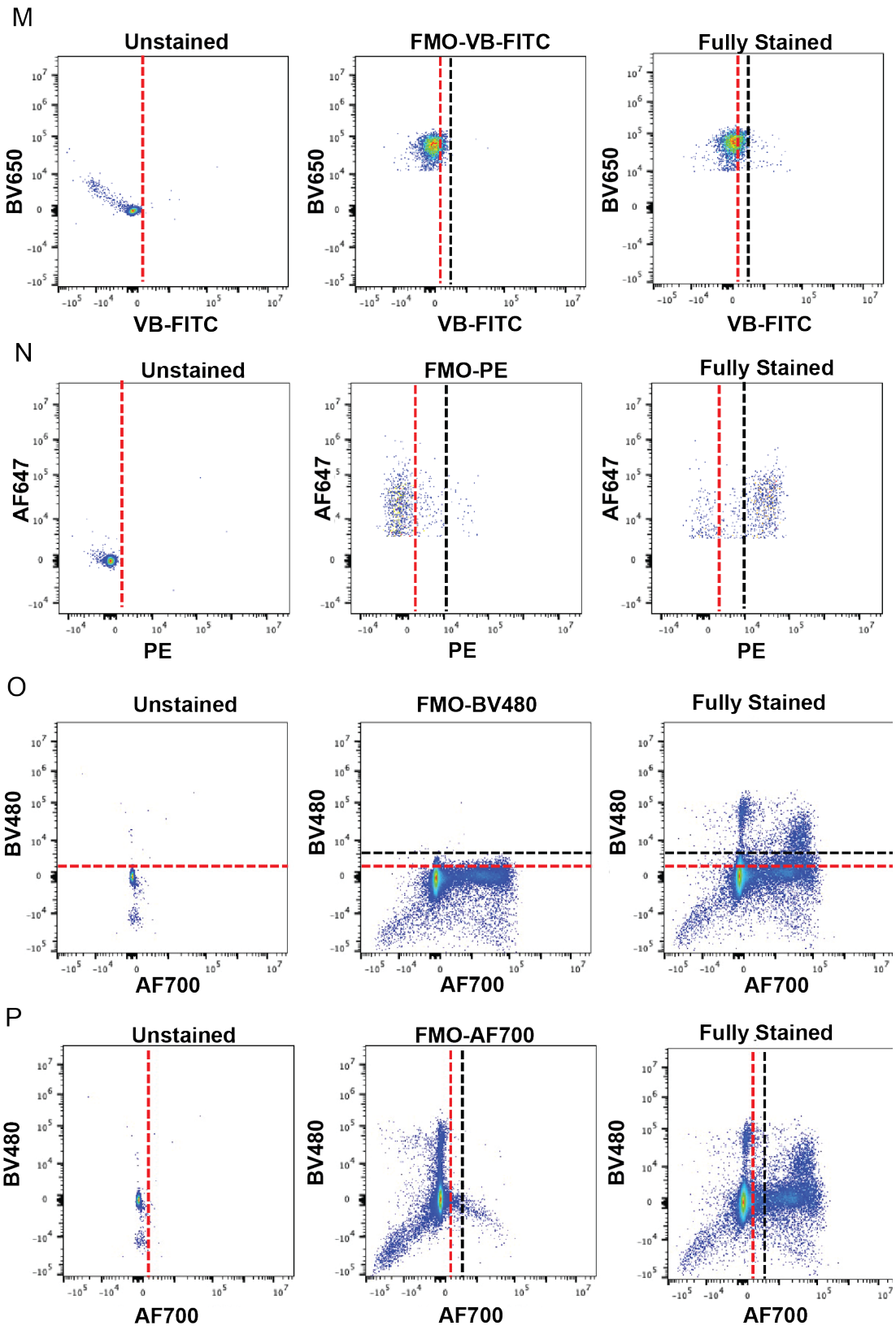


Supplementary 8.1: Antibody titrations.
All titrations used splenocytes isolated from C57BL/6 mouse. All counterstains were determined from previous titrations. All titrations were 1:2 over a 5-point dilution (concentrations shown on dot plot for each figure). (A.1) CD8-BV570 titration visualised on dot plot, counterstained with CD3-eF450 (1:50). (A.2) Positive and negative MFI for each titration. (A.3) CD8-BV570 SI. (B.1) CD3-eF450 titration visualised on dot plot. (B.2) Positive and negative MFI for each titration. (B.3) CD3-eF450 SI. (C.1) NK1.1-BV650 titration visualised on dot plot. (C.2) Positive and negative MFI for each titration. (C.3) NK1.1-BV560 SI. (D.1) CD19-SB436 titration visualised on dot plot. (D.2) Positive and negative MFI for each titration. (D.3) CD19-SB436 SI. (E.1) Ly6G-BV421 titration visualised on dot plot, counterstained with CD11b-AF700 (1:100). (E.2) Positive and negative MFI for each titration. (E.3) Ly6G-BV421 SI. (F.1) CD80-APC titration visualised on dot plot, counterstained with F4/80-BV480 (1:100). (F.2) Positive and negative MFI for each titration. (F.3) CD80-APC SI. (G.1) CD25-AF647 titration visualised on dot plot, counterstained with CD4-BV510 (1:100). (G.2) Positive and negative MFI for each titration. (G.3) CD25-AF647 SI. (H.1) CD206-BV785 titration visualised on dot plot, counterstained with F4/80-BV480 (1:100). (H.2) Positive and negative MFI for each titration. (H.3) CD206-BV785 SI. (I.1) Ly6C-PE-Dazzle titration visualised on dot plot, counterstained with CD11b-AF700 (1:100). (I.2) Positive and negative MFI for each titration. (I.3) Ly6C-PE-Dazzle SI. (J.1) F4/80-BV480 titration visualised on dot plot. (J.2) Positive and negative MFI for each titration. (J.3) F4/80-BV480 SI. (K.1) Live/dead-Zombie Yellow titration visualised on dot plot. (K.2) Positive and negative MFI for each titration. (K.3) Live/dead-Zombie Yellow SI. (L.1) PD-1-PeCy7 titration visualised on dot plot, counterstained with CD8-BV570 (1:25). (L.2) Positive and negative MFI for each titration. (L.3) PD-1-PeCy7 SI. (M.1) CD45-AF532 titration visualised on dot plot. (M.2) Positive and negative MFI for each titration. (M.3) CD45-AF532 SI. (N.1) CD195-VB-FITC titration visualised on dot plot, counterstained with CD8-BV570 (1:25). (N.2) Positive and negative MFI for each titration. (N.3) CD195-VB-FITC SI. (O.1) CD11b-AF700 titration visualised on dot plot. (O.2) Positive and negative MFI for each titration. (O.3) CD11b-AF700 SI. (P.1) CD4-BV510 titration visualised on dot plot, counterstained with CD3-eF450 (1:50). (P.2) Positive and negative MFI for each titration. (P.3) CD4-BV510 SI.

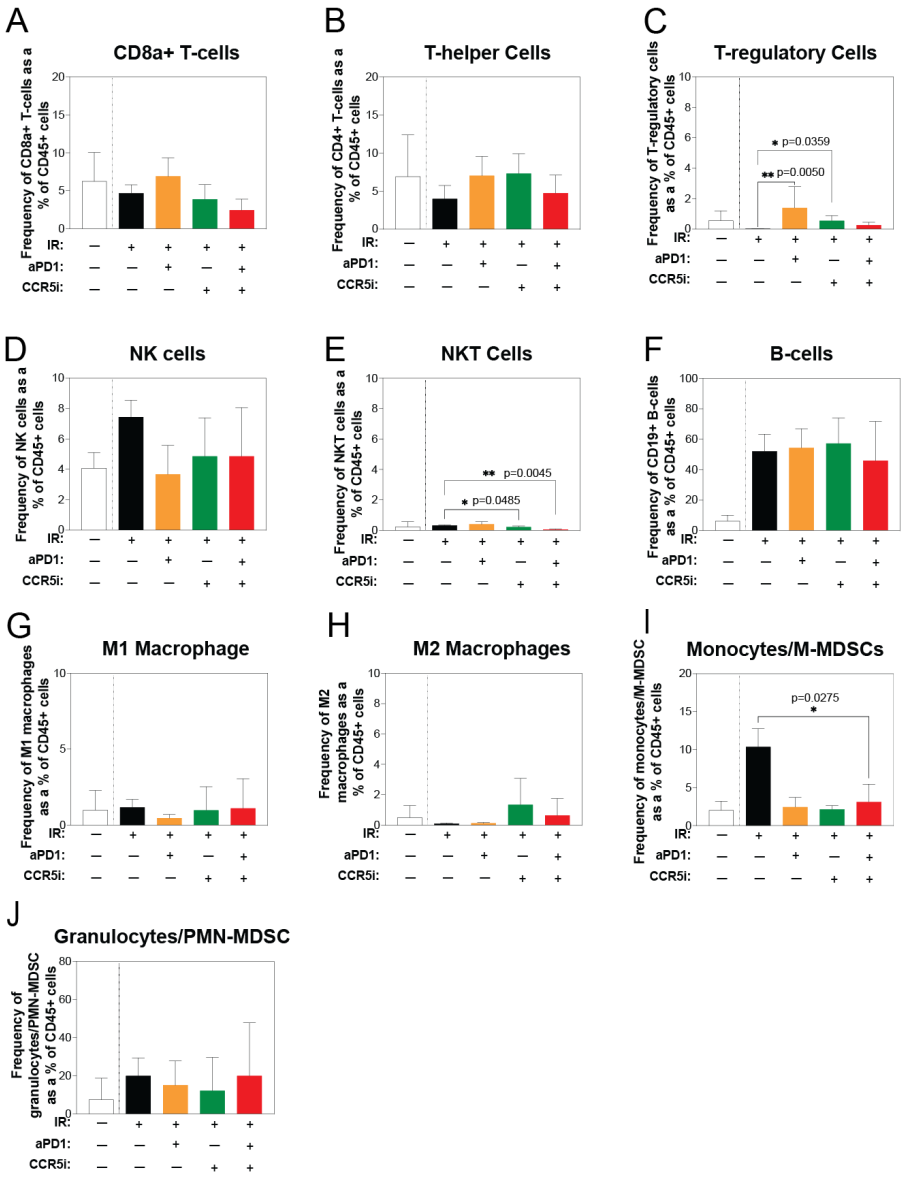

A
Unstained
FMO-Zombie Yellow Control
Fully Stained
SSC-A
Zombie-Yellow
B
Unstained
FMO-AF532
Fully Stained
SSC-A
CD45-AF532
C
Unstained
FMO-eF450
Fully Stained
SB436
eF450
D
Unstained
FMO-SB436
Fully Stained
SB436
eF450


E
Unstained
FMO-BV650
Fully Stained
BV650
eF450
F
Unstained
FMO-BV510
Fully Stained
BV510
BV570
G
Unstained
FMO-BV570
Fully Stained
BV510
BV570
H
Unstained
FMO-APC
Fully Stained
APC
BV785


I
Unstained
FMO-BV785
Fully Stained
APC
BV785
J
Unstained
FMO-PE-Dazzle
Fully Stained
PE-Dazzle
BV421
K
Unstained
FMO-BV421
Fully Stained
PE-Dazzle
BV421
L
Unstained
FMO-AF647
Fully Stained
BV510
AF647

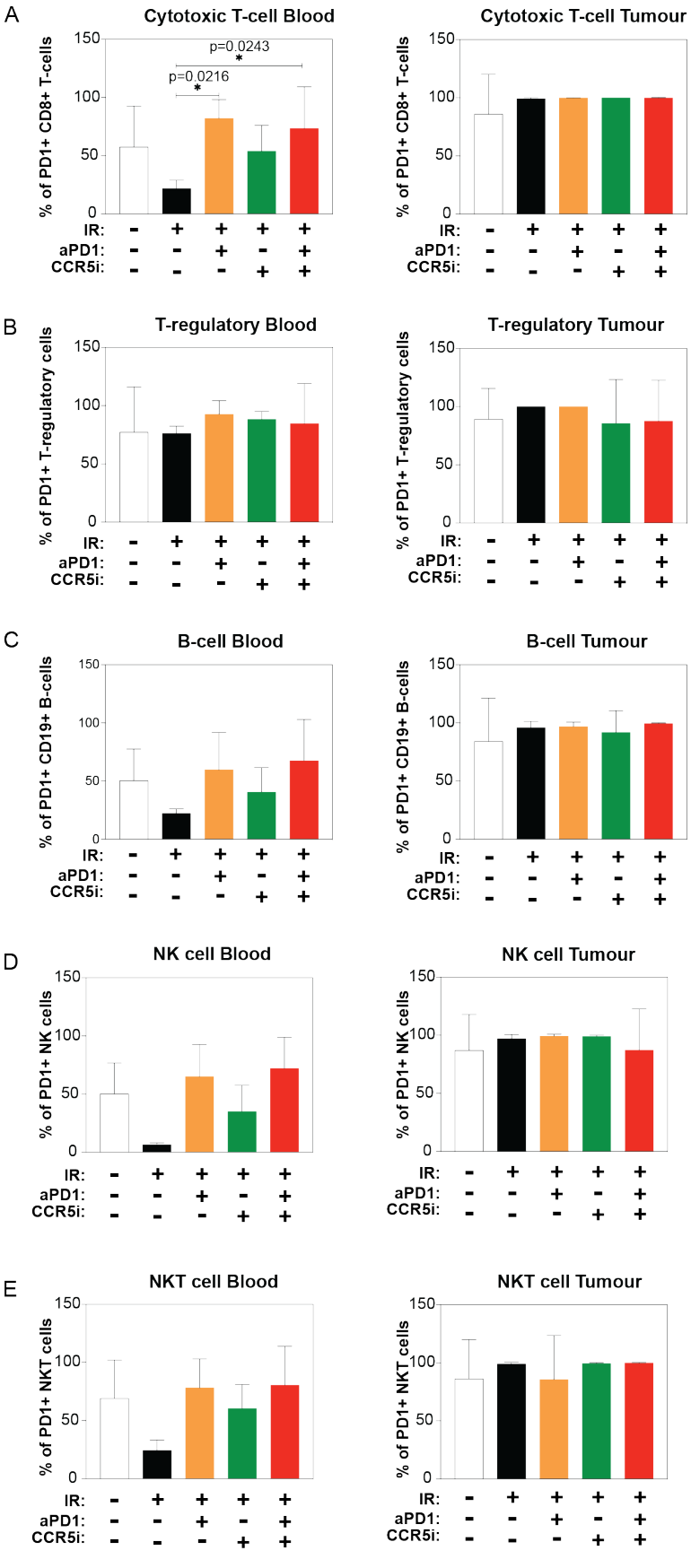

M
Unstained
FMO-VB-FITC
Fully Stained
BV650
VB-FITC
N
Unstained
FMO-PE
Fully Stained
AF647
PE
O
Unstained
FMO-BV480
Fully Stained
BV480
AF700
P
Unstained
FMO-AF700
Fully Stained
BV480
AF700

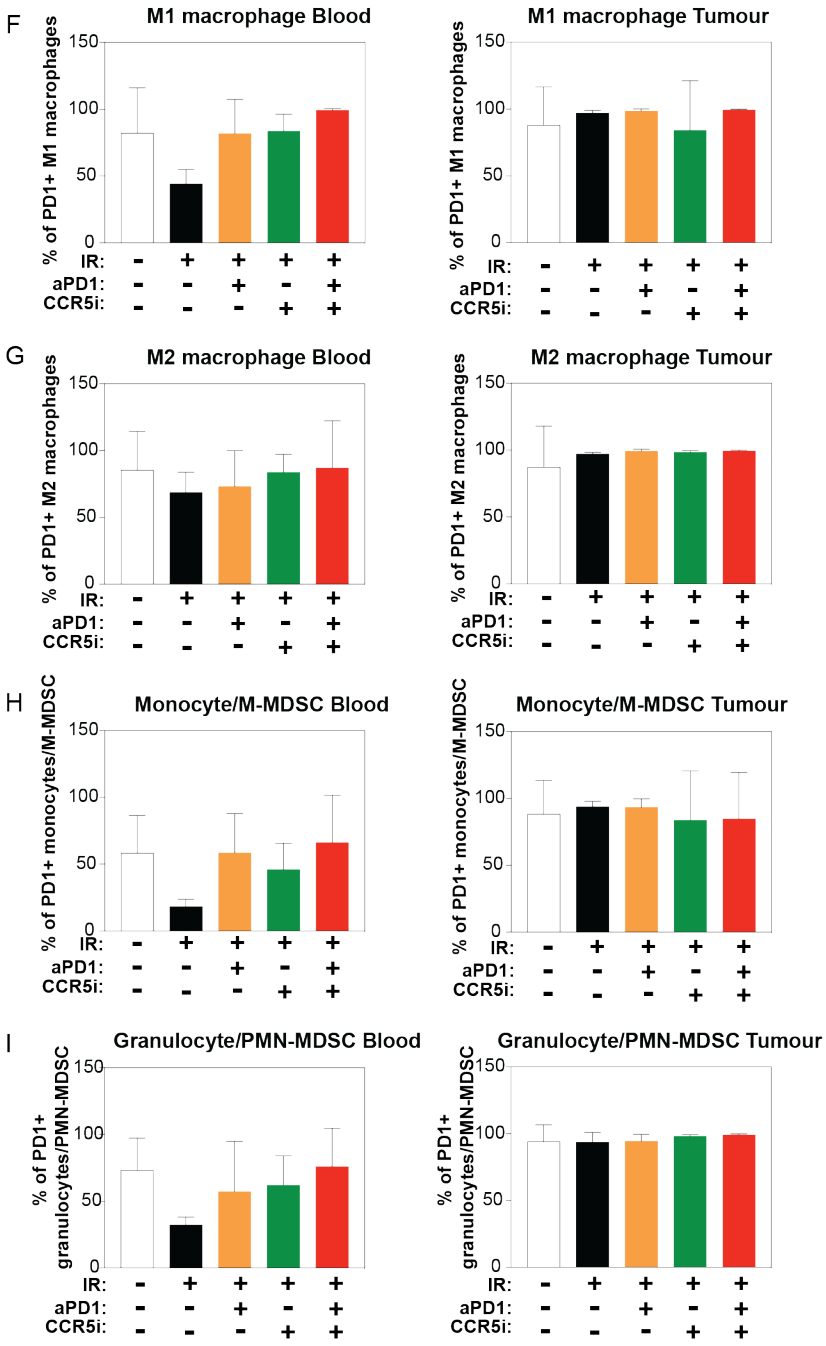
Supplementary 8.2: FMO controls to determine fluorescence spread.
Dot plots of multicolour flow cytometry showing fluorescence spread into each channel compared to unstained control. Black dotted line represents FMO gating boundary compared to unstained boundary in red. (A) Live/dead-Zombie Yellow FMO control. (B) CD45-AF532 FMO control. (C) CD3-eF450 FMO control. (D) CD19-SB436 FMO control. (E) NK1.1-BV650 FMO control. (F) CD4-BV510 FMO control. (G) CD8a-BV570 FMO control. (H) CD80-APC FMO control. (I) CD206-BV785 FMO control (J) Ly6C-PE-Dazzle FMO control. (K) Ly6G-BV421 FMO control. (L) CD25-AF647 FMO control. (M) CD195-VB-FITC FMO control. (N) FOXP3-PE FMO control. (O) F4/80-BV421 FMO control. (P) CD11b-AF700 FMO control.



Supplementary 8.3: Modulation of systemic immune populations following fractionated low-dose radiotherapy and combination immunotherapies in an orthotopic mouse.

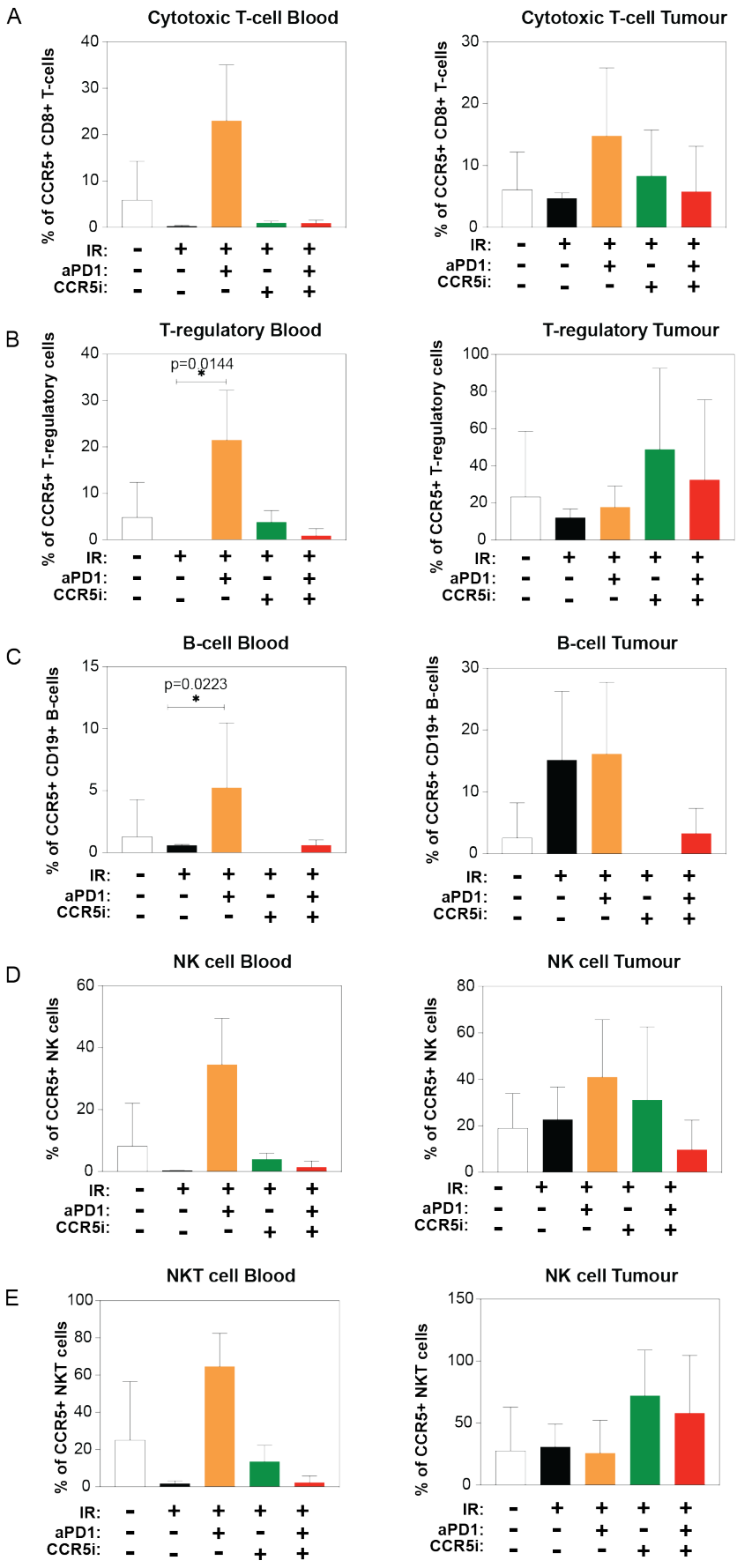
Graphs showing percentage of immune cells relative to CD45+ cells within an orthotopic PDAC peripheral blood following treatment. Mock untreated (white), IR (black), aPD1+IR (yellow), CCR5i+IR (green), aPD1+CCR5i+IR (red). Immune cells characterised include (A) CD8+ T-cells, (B) CD4+ T-helper cells, (C) T-regulatory cells, (D) NK cells, (E) NKT cells, (F) B-cells, (G) M1 macrophages, (H) M2 macrophages, (I) Monocytes/M-MDSCs and (J) Granulocytes/PMN-MDSCs. Data represented as mean percentage positive cells ± SD. Statistical significance denoted by * ($p<0.01$), ** ($p<0.001$) and *** ($p<0.0001$) and performed using a *Welch* and Brown-Forsythe *ANOVA* for parametric data or Kruskal-Wallis test for non-parametric data. Mock (n=6), IR (n=3), aPD1 (n=8), aPD1+IR (n=8), CCR5i (n=3), CCR5i+IR (n=8), aPD1+CCR5i (n=5), aPD1+CCR5i+IR (n=8).

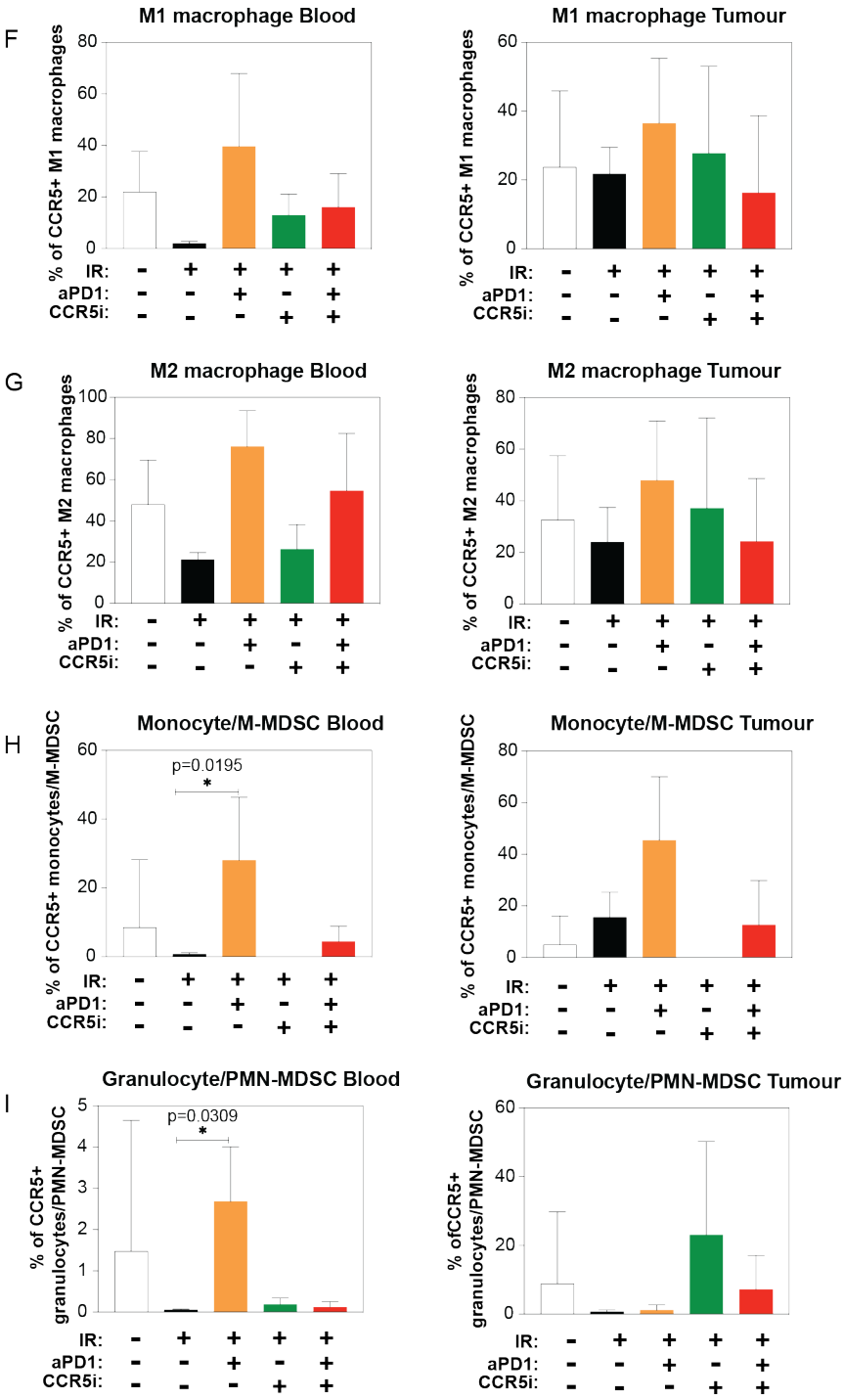

A
Cytotoxic T-cell Blood
% of PD1+ CD8+ T-cells
p=0.0243
p=0.0216
Cytotoxic T-cell Tumour
B
T-regulatory Blood
% of PD1+ T-regulatory cells
T-regulatory Tumour
C
B-cell Blood
% of PD1+ CD19+ B-cells
B-cell Tumour
D
NK cell Blood
% of PD1+ NK cells
NK cell Tumour
E
NKT cell Blood
% of PD1+ NKT cells
NKT cell Tumour
IR:
aPD1:
CCR5i:



Supplementary 8.4: PD1 expression of immune populations following fractionated low-dose radiotherapy and combination immunotherapies in an orthotopic mouse.

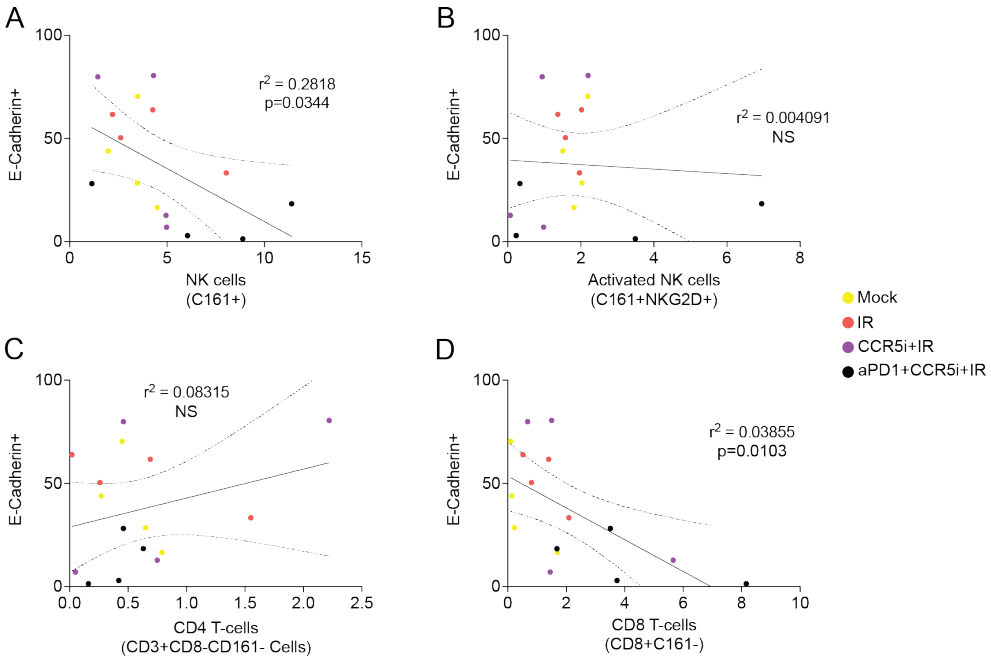
Graphs showing percentage of PD1 expression relative to immune cell within orthotopic PDAC peripheral blood and local tumour following treatment. Mock untreated (white), IR (black), aPD1+IR (yellow), CCR5i+IR (green), aPD1+CCR5i+IR (red). Immune cells characterised include (A) CD8+ T-cells, (B) T-regulatory cells, (C) B-cells, (D) NK cells, (E) NKT cells, (F) M1 macrophages (G) M2 macrophages, (H) Monocytes/M-MDSCs and (I) Granulocytes/PMN-MDSCs. Data represented as mean percentage positive cells ± SD. Statistical significance denoted by * ($p<0.01$), ** ($p<0.001$) and *** ($p<0.0001$) and performed using a *Welch* and Brown-Forsythe *ANOVA* for parametric data or Kruskal-Wallis test for non-parametric data. Mock (n=6), IR (n=3), aPD1 (n=8), aPD1+IR (n=8), CCR5i (n=3), CCR5i+IR (n=8), aPD1+CCR5i (n=5), aPD1+CCR5i+IR (n=8).


A
Cytotoxic T-cell Blood
% of CCR5+ CD8+ T-cells
Cytotoxic T-cell Tumour
% of CCR5+ CD8+ T-cells
B
T-regulatory Blood
% of CCR5+ T-regulatory cells
p=0.0144
*
T-regulatory Tumour
% of CCR5+ T-regulatory cells
C
B-cell Blood
% of CCR5+ CD19+ B-cells
p=0.0223
*
B-cell Tumour
% of CCR5+ CD19+ B-cells
D
NK cell Blood
% of CCR5+ NK cells
NK cell Tumour
% of CCR5+ NK cells
E
NKT cell Blood
% of CCR5+ NKT cells
NK cell Tumour
% of CCR5+ NKT cells
IR:
aPD1:
CCR5i:



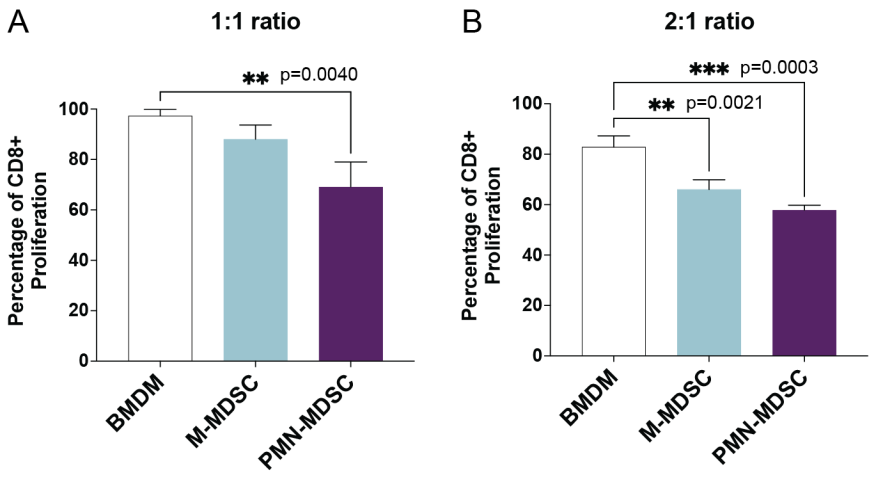
Supplementary 8.5: CCR5 expression of immune populations following fractionated low-dose radiotherapy and combination immunotherapies in an orthotopic mouse.

Graphs showing percentage of CCR5 expression relative to immune cell within orthotopic PDAC peripheral blood and local tumour following treatment. Mock untreated (white), IR (black), aPD1+IR (yellow), CCR5i+IR (green), aPD1+CCR5i+IR (red). Immune cells characterised include (A) CD8+ T-cells, (B) T-regulatory cells, (C) B-cells, (D) NK cells, (E) NKT cells, (F) M1 macrophages (G) M2 macrophages, (H) Monocytes/M-MDSCs and (I) Granulocytes/PMN-MDSCs. Data represented as mean percentage positive cells ± SD. Statistical significance denoted by * ($p<0.01$), ** ($p<0.001$) and *** ($p<0.0001$) and performed using a *Welch* and Brown-Forsythe *ANOVA* for parametric data or Kruskal-Wallis test for non-parametric data. Mock (n=6), IR (n=3), aPD1 (n=8), aPD1+IR (n=8), CCR5i (n=3), CCR5i+IR (n=8), aPD1+CCR5i (n=5), aPD1+CCR5i+IR (n=8).

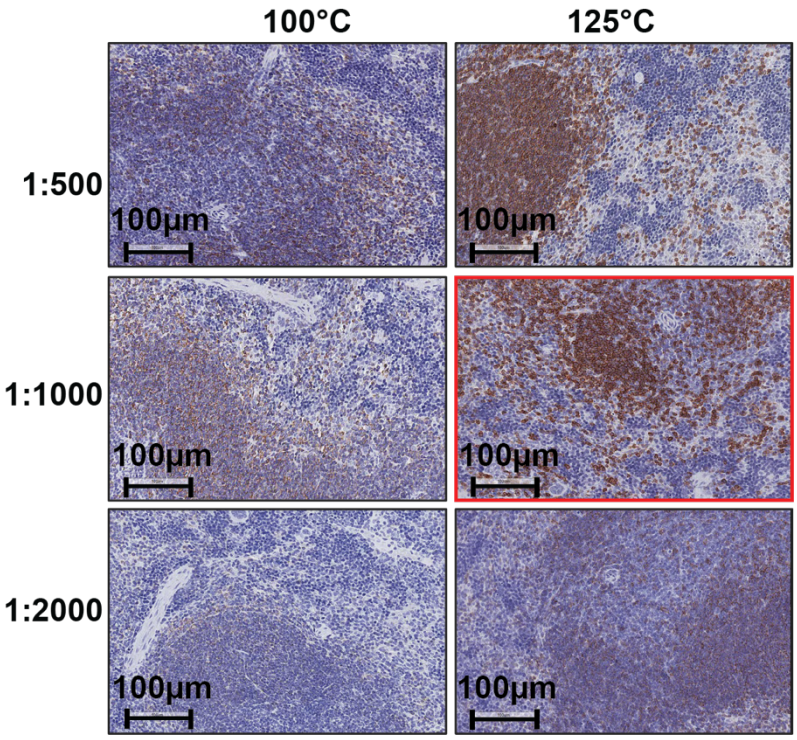


Supplementary 8.6: Association between E-cadherin and NK, activated NK, CD4 and CD8 T-cells.

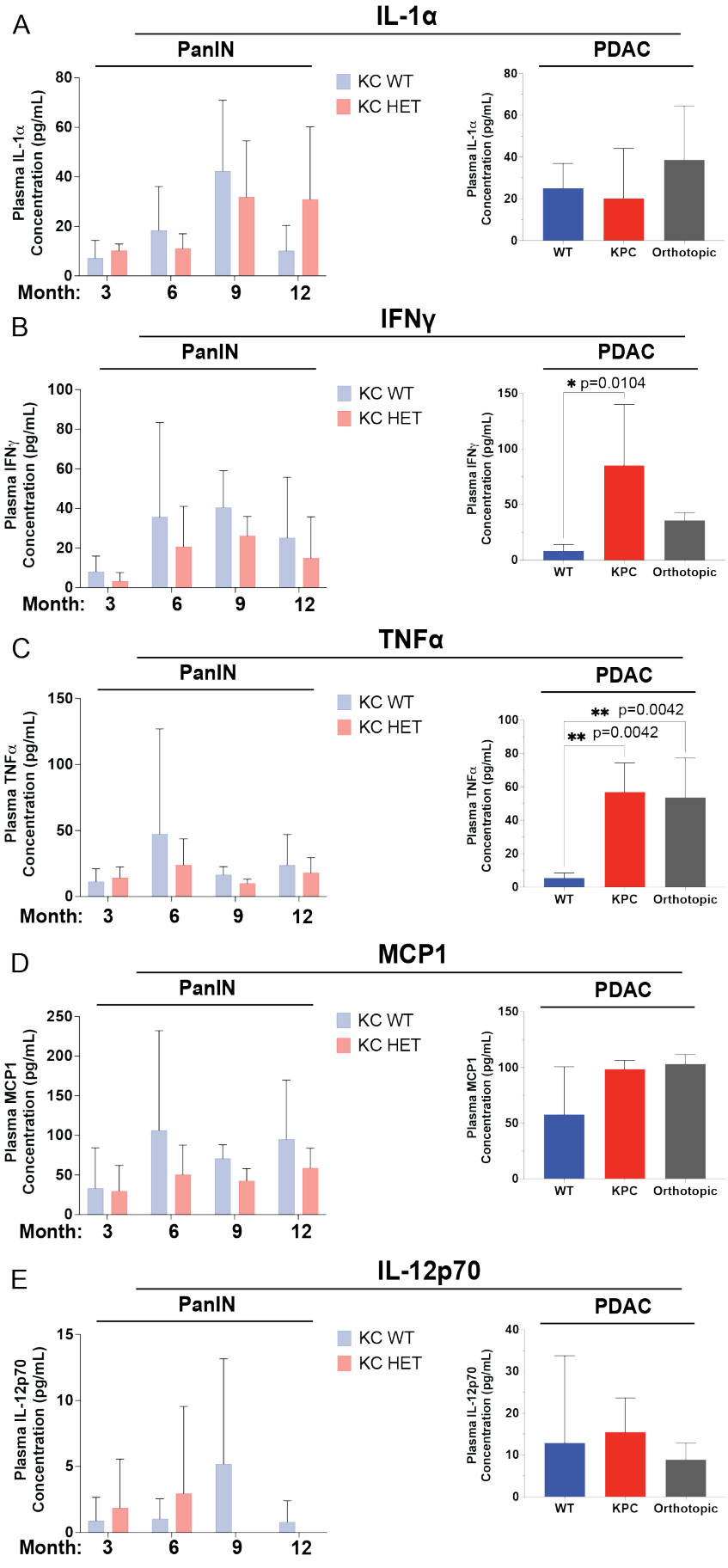
Graphs showing correlation between E-cadherin and (A) total NK cells (CD161+), (B) activated NL cells (CD161+NKG2D+), (C) CD4 T-cells (CD3+CD8-CD161-) and (D) CD8 T-cells. Data points represent biological replicates from Mock (yellow), IR (red), CCR5i+IR (purple), and aPD1+CCR5i+IR (black), treatment groups. Sold line displays simple linear regression with 95% confidence intervals (dotted black lines). Mock (n=4), IR (n=3), CCR5i+IR (n=4), aPD1+CCR5i+IR (n=4). Analysis was conducted by Simei Go and Professor Eric O'Neill.

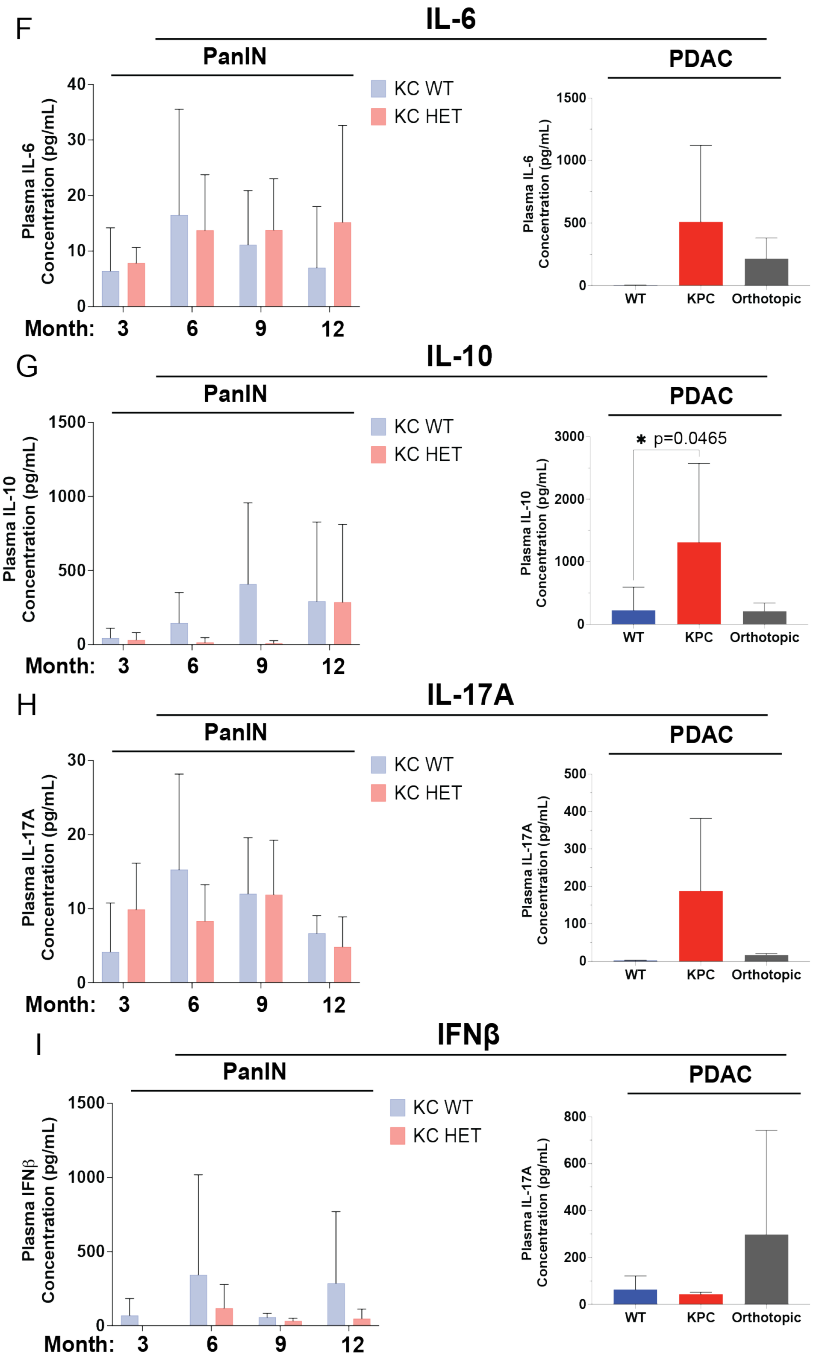


Supplementary 8.7: Optimisation of ex vivo T-cell suppression.
Co-culture of bone marrow derived macrophages, M-MDSCs or PMN-MDSC with CD8+ T-cells isolated from C57BL/6 spleens. M-MDSCs and PMN-MDSCs were differentiated from C57BL/6 bone marrow with IL-6 and GM-CSF prior to co-culture. Quantification of BMDM, M-MDSC and PMN-MDSC T-cell suppression in a (A)1:1 (myeloid cell: T-cell) or (B) 2:1 (myeloid cell: T-cell) ratio. All quantifications were relative to CD8+ T-cell only controls, represented as mean ± SD. Statistical significance denoted by * ($p<0.01$), ** ($p<0.001$) and *** ($p<0.0001$) and performed using a one-way ANOVA. Data points are representative of n=3 technical replicates. BMDM; bone marrow derived macrophages. M-MDSC; monocytic myeloid derived suppressor cells. PMN-MDSC; polymorphonuclear myeloid derived suppressor cells.



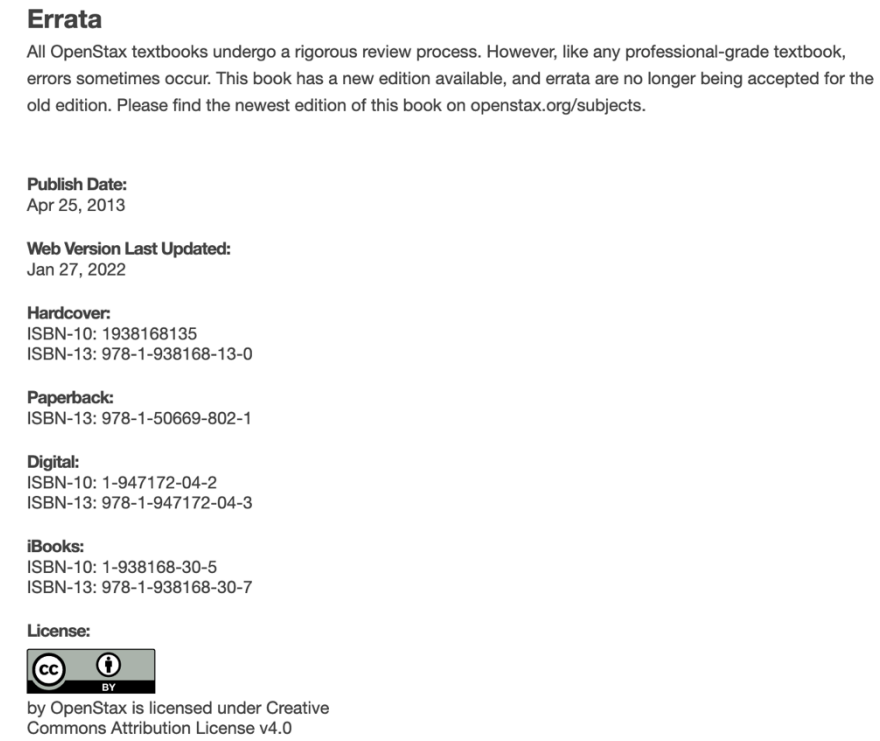
Supplementary 8.8: CD19 antibody IHC optimisation.
Representative IHC images of CD19 antibody optimisation in a spleen from a wild-type C57BL/6 mouse over a 2-fold 3-point dilution at the indicated concentrations and temperatures for antigen retrieval. Red box indicates the chosen concentration and antigen retrieval condition based on visual inspection including low background staining, n=3. Magnification; 20X. Scale bar = 100 µM.


A
IL-1α
PanIN
PDAC
KC WT
KC HET
Plasma IL-1α Concentration (pg/mL)
Month: 3 6 9 12
WT KPC Orthotopic
B
IFNγ
PanIN
PDAC
KC WT
KC HET
Plasma IFNγ Concentration (pg/mL)
* p=0.0104
Month: 3 6 9 12
WT KPC Orthotopic
C
TNFα
PanIN
PDAC
KC WT
KC HET
Plasma TNFα Concentration (pg/mL)
** p=0.0042
** p=0.0042
Month: 3 6 9 12
WT KPC Orthotopic
D
MCP1
PanIN
PDAC
KC WT
KC HET
Plasma MCP1 Concentration (pg/mL)
Month: 3 6 9 12
WT KPC Orthotopic
E
IL-12p70
PanIN
PDAC
KC WT
KC HET
Plasma IL-12p70 Concentration (pg/mL)
Month: 3 6 9 12
WT KPC Orthotopic



Supplementary 8.9: Systemic cytokine response during PanIN lesion progression.
13-plex inflammatory cytokine array on plasma of *Kras*$^{LSL.G12D/+}$*;Pdx-1-Cre* (KC HET), *Kras*$^{LSL.G12D+/+}$*;Pdx-1-Cre* (KC WT), C57BL/6 (WT), *LSL-Kras*$^{G12D/+}$; *LSL-Trp53*$^{R172H/+}$(KPC) and orthotopic PDAC mice. Quantification of (A) IL-1α, (B) IFNγ, (C) TNFα, (D) MCP1, (E) IL-12p70, (F) IL-6, (G) IL-10, (H) IL-17A and (I) IFNβ. All quantifications were a concentration of each cytokine in pg/mL represented as a mean ± SD. Statistical significance denoted by * (p<0.01), ** (p<0.001) and *** (p<0.0001) and performed using an unpaired T-test for parametric data or Mann-Whitney test for non-parametric data (PanIN analysis) or one-way ANOVA for parametric data or Kruskal-Wallis test for non-parametric data (PDAC analysis). 3-month KC HET and KC WT (n=4), 6-month KC HET and KC WT (n=5), 9-month KC HET and KC WT (n=3), 12-month KC HET and KC WT (n=4). C57BL/6 WT (n=4), KPC (n=4), Orthotopic (n=4). Data points representative of technical duplicates were averaged for each biological replicate

Appendix



Errata

All OpenStax textbooks undergo a rigorous review process. However, like any professional-grade textbook, errors sometimes occur. This book has a new edition available, and errata are no longer being accepted for the old edition. Please find the newest edition of this book on openstax.org/subjects.

Publish Date:
Apr 25, 2013

Web Version Last Updated:
Jan 27, 2022

Hardcover:
ISBN-10: 1938168135
ISBN-13: 978-1-938168-13-0

Paperback:
ISBN-13: 978-1-50669-802-1

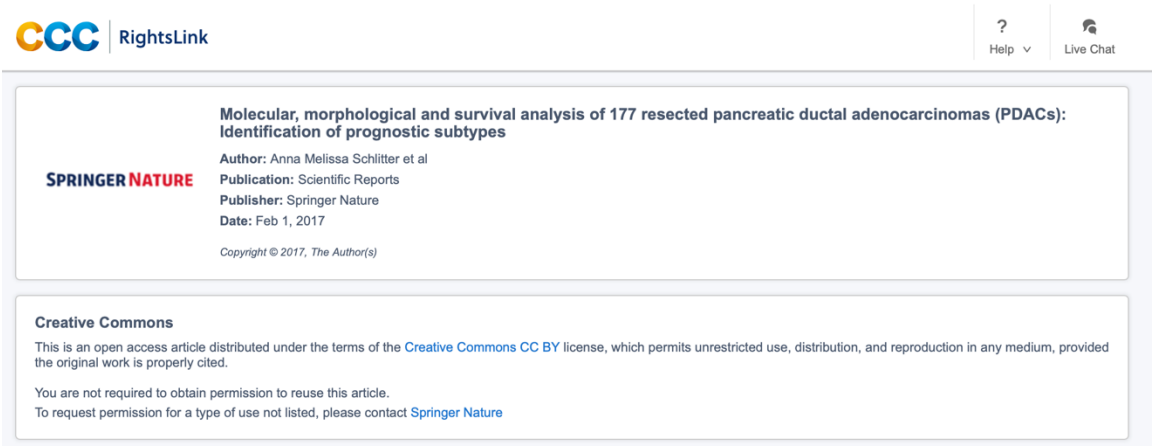
Digital:
ISBN-10: 1-947172-04-2
ISBN-13: 978-1-947172-04-3

iBooks:
ISBN-10: 1-938168-30-5
ISBN-13: 978-1-938168-30-7

License:

by OpenStax is licensed under Creative Commons Attribution License v4.0

Figure A.1: Copyright notice: Anatomy and Physiology by Open Stax



CCC RightsLink

Help Live Chat

SPRINGER NATURE

Molecular, morphological and survival analysis of 177 resected pancreatic ductal adenocarcinomas (PDACs): Identification of prognostic subtypes

Author: Anna Melissa Schlitter et al
Publication: Scientific Reports
Publisher: Springer Nature
Date: Feb 1, 2017

Copyright © 2017, The Author(s)

Creative Commons

This is an open access article distributed under the terms of the Creative Commons CC BY license, which permits unrestricted use, distribution, and reproduction in any medium, provided the original work is properly cited.

You are not required to obtain permission to reuse this article.
To request permission for a type of use not listed, please contact Springer Nature

Figure A.2: Copyright notice: Schlitter et al. Molecular, morphological and survival analysis of 177 resected pancreatic ductal adenocarcinomas (PDACs): Identification of prognostic subtypes. By Springer Nature.

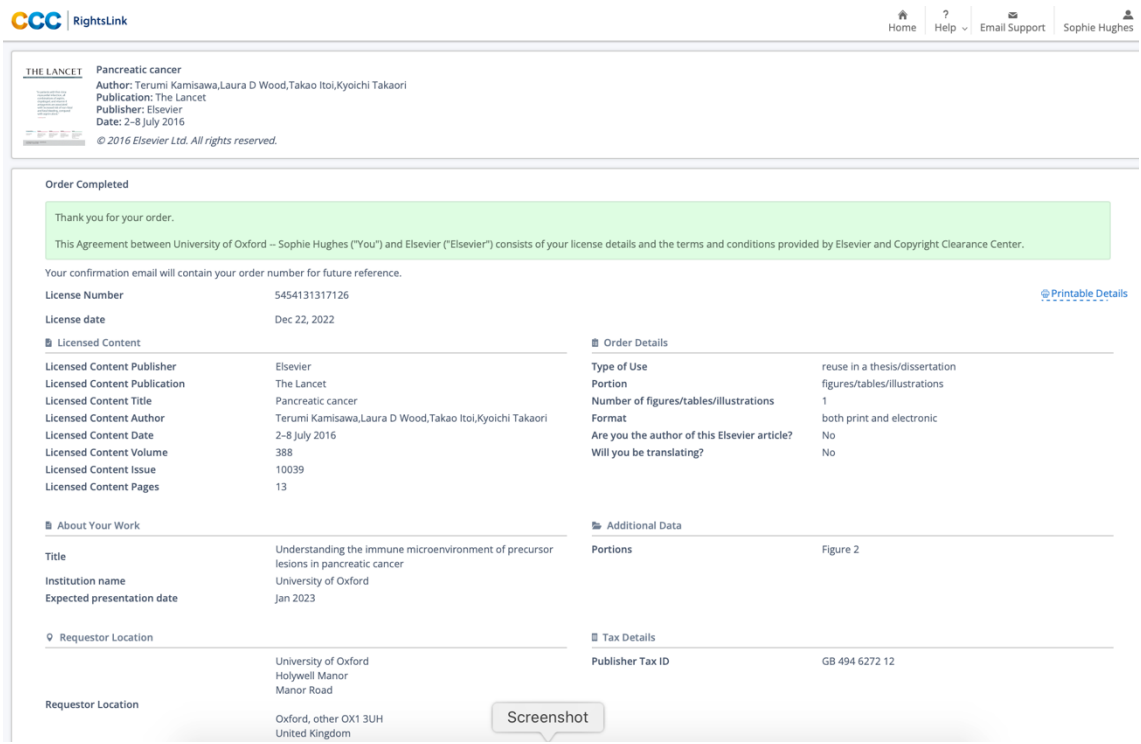
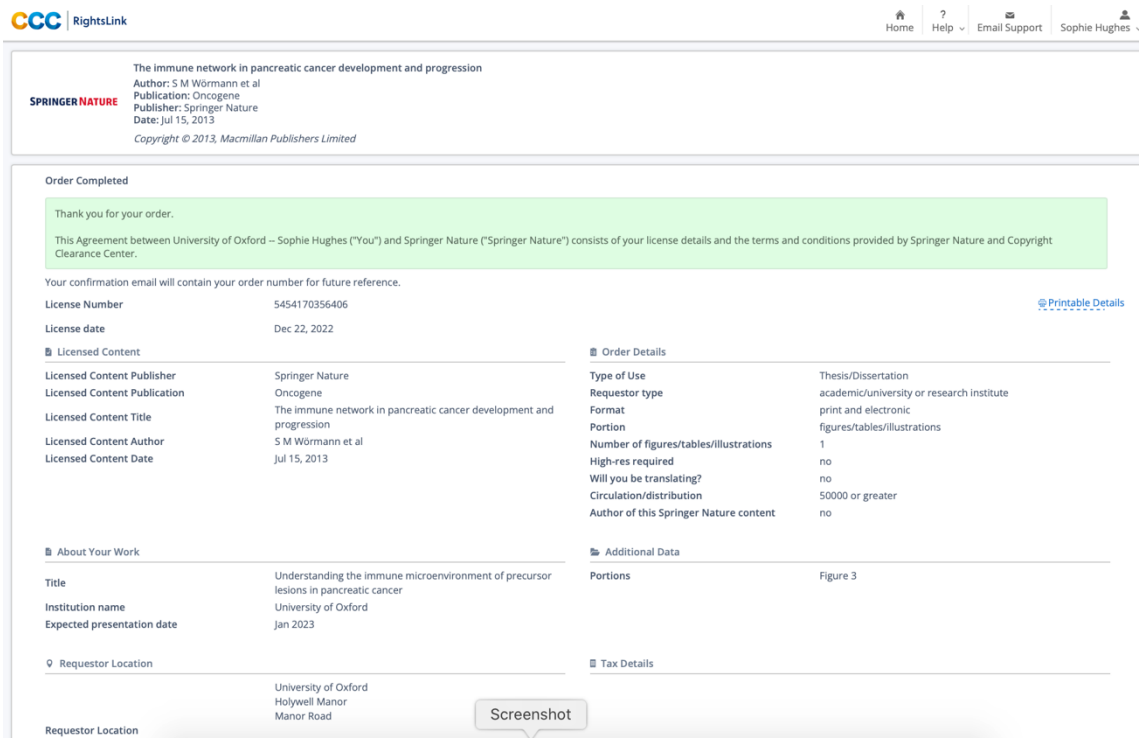


Figure A.3: Copyright notice: Kamisawa, Wood, Itoi and Takaori, 2016. Pancreatic Cancer. By Elsevier. License Number: 5454131317126



Figure A.4: Copyright notice: Morris et al. KRAS, Hedgehog, Wnt and the twisted developmental biology of pancreatic ductal adenocarcinoma. By Springer Nature. License Number: 5452490900634



CCC RightsLink

Home | Help | Email Support | Sophie Hughes

SPRINGER NATURE

The immune network in pancreatic cancer development and progression
Author: S M Wörmann et al
Publication: Oncogene
Publisher: Springer Nature
Date: Jul 15, 2013
Copyright © 2013, Macmillan Publishers Limited

Order Completed

Thank you for your order.

This Agreement between University of Oxford -- Sophie Hughes ("You") and Springer Nature ("Springer Nature") consists of your license details and the terms and conditions provided by Springer Nature and Copyright Clearance Center.

Your confirmation email will contain your order number for future reference.

Printable Details

License Number	5454170356406
License date	Dec 22, 2022

Licensed Content

Licensed Content Publisher	Springer Nature
Licensed Content Publication	Oncogene
Licensed Content Title	The immune network in pancreatic cancer development and progression
Licensed Content Author	S M Wörmann et al
Licensed Content Date	Jul 15, 2013

Order Details

Type of Use	Thesis/Dissertation
Requestor type	academic/university or research institute
Format	print and electronic
Portion	figures/tables/illustrations
Number of figures/tables/illustrations	1
High-res required	no
Will you be translating?	no
Circulation/distribution	50000 or greater
Author of this Springer Nature content	no

About Your Work

Title	Understanding the immune microenvironment of precursor lesions in pancreatic cancer
Institution name	University of Oxford
Expected presentation date	Jan 2023

Additional Data

Portions	Figure 3

Requestor Location

Requestor Location	University of Oxford Holywell Manor Manor Road

Tax Details

Screenshot

Figure A.5: Copyright notice: Wörmann et al. The immune network in pancreatic cancer development and progression. By Springer Nature. License Number: 5454170356406

Bibliography

Abdel-Fatah TM, Powe DG, Hodi Z, Lee AH, Reis-Filho JS, Ellis IO. 2007. High frequency of coexistence of columnar cell lesions, lobular neoplasia, and low grade ductal carcinoma in situ with invasive tubular carcinoma and invasive lobular carcinoma. Am J Surg Pathol 31:417-26.

Abdel-Fatah TM, Powe DG, Hodi Z, Reis-Filho JS, Lee AH, Ellis IO. 2008. Morphologic and molecular evolutionary pathways of low nuclear grade invasive breast cancers and their putative precursor lesions: further evidence to support the concept of low nuclear grade breast neoplasia family. Am J Surg Pathol 32:513-23.

Abraham SC, Wu TT, Klimstra DS, Finn LS, Lee JH, Yeo CJ, Cameron JL, Hruban RH. 2001. Distinctive molecular genetic alterations in sporadic and familial adenomatous polyposis-associated pancreatoblastomas : frequent alterations in the APC/beta-catenin pathway and chromosome 11p. Am J Pathol 159:1619-27.

Adamska A, Domenichini A, Falasca M. 2017. Pancreatic Ductal Adenocarcinoma: Current and Evolving Therapies. Int J Mol Sci 18.

Affara NI, Ruffell B, Medler TR, Gunderson AJ, Johansson M, Bornstein S, Bergsland E, Steinhoff M, Li Y, Gong Q, Ma Y, Wiesen JF, Wong MH, Kulesz-Martin M, Irving B, Coussens LM. 2014. B cells regulate macrophage phenotype and response to chemotherapy in squamous carcinomas. Cancer Cell 25:809-821.

Agarwal B, Abu-Hamda E, Molke KL, Correa AM, Ho L. 2004. Endoscopic ultrasound-guided fine needle aspiration and multidetector spiral CT in the diagnosis of pancreatic cancer. Am J Gastroenterol 99:844-50.

Aggarwal S, Ghilardi N, Xie MH, de Sauvage FJ, Gurney AL. 2003. Interleukin-23 promotes a distinct CD4 T cell activation state characterized by the production of interleukin-17. J Biol Chem 278:1910-4.

Aichler M, Seiler C, Tost M, Siveke J, Mazur PK, Da Silva-Buttkus P, Bartsch DK, Langer P, Chiblak S, Durr A, Hofler H, Kloppel G, Muller-Decker K, Brielmeier M, Esposito I. 2012. Origin of pancreatic ductal adenocarcinoma from atypical flat lesions: a comparative study in transgenic mice and human tissues. J Pathol 226:723-34.

Al-Hawary MM, Francis IR, Chari ST, Fishman EK, Hough DM, Lu DS, Macari M, Megibow AJ, Miller FH, Mortele KJ, Merchant NB, Minter RM, Tamm EP, Sahani DV, Simeone DM. 2014. Pancreatic ductal adenocarcinoma radiology reporting template: consensus statement of the Society of Abdominal Radiology and the American Pancreatic Association. Radiology 270:248-60.

Aldinucci D, Borghese C, Casagrande N. 2020. The CCL5/CCR5 Axis in Cancer Progression. Cancers (Basel) 12.

Allred DC, Mohsin SK, Fuqua SA. 2001. Histological and biological evolution of human premalignant breast disease. Endocr Relat Cancer 8:47-61.

Almeida AS, Fein MR, Egeblad M. 2021. Multi-color Flow Cytometry for Comprehensive Analysis of the Tumor Immune Infiltrate in a Murine Model of Breast Cancer. Bio Protoc 11:e4012.

Ambe P, Kautz C, Shadouh S, Heggemann S, Köhler L. 2011. Primary sarcoma of the pancreas, a rare histopathological entity. A case report with review of literature. World J Surg Oncol 9:85.

Ancrile BB, O'Hayer KM, Counter CM. 2008. Oncogenic ras-induced expression of cytokines: a new target of anti-cancer therapeutics. Mol Interv 8:22-7.

Andea A, Sarkar F, Adsay VN. 2003. Clinicopathological correlates of pancreatic intraepithelial neoplasia: a comparative analysis of 82 cases with and 152 cases without pancreatic ductal adenocarcinoma. Mod Pathol 16:996-1006.

Ando K, Oki E, Saeki H, Yan Z, Tsuda Y, Hidaka G, Kasagi Y, Otsu H, Kawano H, Kitao H, Morita M, Maehara Y. 2015. Discrimination of p53 immunohistochemistry-positive tumors by its staining pattern in gastric cancer. Cancer Med 4:75-83.

Andreu P, Johansson M, Affara NI, Pucci F, Tan T, Junankar S, Korets L, Lam J, Tawfik D, DeNardo DG, Naldini L, de Visser KE, De Palma M, Coussens LM. 2010. FcRgamma activation regulates inflammation-associated squamous carcinogenesis. Cancer Cell 17:121-34.

Anlauf M, Garbrecht N, Bauersfeld J, Schmitt A, Henopp T, Komminoth P, Heitz PU, Perren A, Klöppel G. 2007. Hereditary neuroendocrine tumors of the gastroenteropancreatic system. Virchows Arch 451 Suppl 1:S29-38.

Ansari D, Gustafsson A, Andersson R. 2015. Update on the management of pancreatic cancer: surgery is not enough. World J Gastroenterol 21:3157-65.

Apte RN, Dotan S, Elkabets M, White MR, Reich E, Carmi Y, Song X, Dvozkin T, Krelin Y, Voronov E. 2006. The involvement of IL-1 in tumorigenesis, tumor invasiveness, metastasis and tumor-host interactions. Cancer and Metastasis Reviews 25:387-408.

Arnoletti JP, Reza J, Rosales A, Monreal A, Fanaian N, Whisner S, Srivastava M, Rivera-Otero J, Yu G, Phanstiel Iv O, Altomare DA, Tran Q, Litherland SA. 2022. Pancreatic Ductal Adenocarcinoma (PDAC) circulating tumor cells influence myeloid cell differentiation to support their survival and immunoresistance in portal vein circulation. PLoS One 17:e0265725.

Arslan AA, Helzlsouer KJ, Kooperberg C, Shu XO, Steplowski E, Bueno-de-Mesquita HB, Fuchs CS, Gross MD, Jacobs EJ, Lacroix AZ, Petersen GM, Stolzenberg-Solomon RZ, Zheng W, Albanes D, Amundadottir L, Bamlet WR, Barricarte A, Bingham SA, Boeing H, Boutron-Ruault MC, Buring JE, Chanock SJ, Clipp S, Gaziano JM, Giovannucci EL, Hankinson SE, Hartge P, Hoover RN, Hunter DJ, Hutchinson A, Jacobs KB, Kraft P, Lynch SM, Manjer J, Manson JE, McTiernan A, McWilliams RR, Mendelsohn JB, Michaud DS, Palli D, Rohan TE, Slimani N, Thomas G, Tjønneland A, Tobias GS, Trichopoulos D, Virtamo J, Wolpin BM, Yu K, Zeleniuch-Jacquotte A, Patel AV. 2010. Anthropometric measures, body mass index, and pancreatic cancer: a pooled analysis from the Pancreatic Cancer Cohort Consortium (PanScan). Arch Intern Med 170:791-802.

Autengruber A, Gereke M, Hansen G, Hennig C, Bruder D. 2012. Impact of enzymatic tissue disintegration on the level of surface molecule expression and immune cell function. Eur J Microbiol Immunol (Bp) 2:112-20.

Azad A, Yin Lim S, D'Costa Z, Jones K, Diana A, Sansom OJ, Kruger P, Liu S, McKenna WG, Dushek O, Muschel RJ, Fokas E. 2017. PD-L1 blockade enhances response of pancreatic ductal adenocarcinoma to radiotherapy. EMBO Mol Med 9:167-180.

Bailey P, Chang DK, Nones K, Johns AL, Patch AM, Gingras MC, Miller DK, Christ AN, Bruxner TJ, Quinn MC, Nourse C, Murtaugh LC, Harliwong I, Idrisoglu S, Manning S, Nourbakhsh E, Wani S, Fink L, Holmes O, Chin V, Anderson MJ, Kazakoff S, Leonard C, Newell F, Waddell N, Wood S, Xu Q, Wilson PJ, Cloonan N, Kassahn KS, Taylor D, Quek K, Robertson A, Pantano L, Mincarelli L, Sanchez LN, Evers L, Wu J, Pinese M, Cowley MJ, Jones MD, Colvin EK, Nagrial AM, Humphrey ES, Chantrill LA, Mawson A, Humphris J, Chou A, Pajic M, Scarlett CJ, Pinho AV, Giry-Laterriere M, Rooman I, Samra JS, Kench JG, Lovell JA, Merrett ND, Toon CW, Epari K, Nguyen NQ, Barbour A, Zeps N, Moran-Jones K, Jamieson NB, Graham JS, Duthie F, Oien K, Hair J, Grützmann R, Maitra A, Iacobuzio-Donahue CA, Wolfgang CL, Morgan RA, Lawlor RT, Corbo V, Bassi C, Rusev B, Capelli P, Salvia R, Tortora G, Mukhopadhyay D, Petersen GM, Munzy DM, Fisher WE, Karim SA, Eshleman JR, Hruban RH, Pilarsky C, Morton JP, Sansom OJ, Scarpa A, Musgrove EA, Bailey UM, Hofmann O, Sutherland RL, Wheeler DA, Gill AJ, Gibbs RA, Pearson JV, Waddell N, et al. 2016. Genomic analyses identify molecular subtypes of pancreatic cancer. Nature 531:47-52.

Baker SJ, Preisinger AC, Jessup JM, Paraskeva C, Markowitz S, Willson JK, Hamilton S, Vogelstein B. 1990. p53 gene mutations occur in combination with 17p allelic deletions as late events in colorectal tumorigenesis. Cancer Res 50:7717-22.

Ballehaninna UK, Chamberlain RS. 2012. The clinical utility of serum CA 19-9 in the diagnosis, prognosis and management of pancreatic adenocarcinoma: An evidence based appraisal. J Gastrointest Oncol 3:105-19.

Bamford S, Dawson E, Forbes S, Clements J, Pettett R, Dogan A, Flanagan A, Teague J, Futreal PA, Stratton MR, Wooster R. 2004. The COSMIC (Catalogue of Somatic Mutations in Cancer) database and website. Br J Cancer 91:355-8.

Ban D, Shimada K, Sekine S, Sakamoto Y, Kosuge T, Kanai Y, Hiraoka N. 2010. Pancreatic ducts as an important route of tumor extension for acinar cell carcinoma of the pancreas. Am J Surg Pathol 34:1025-36.

Bandura DR, Baranov VI, Ornatsky OI, Antonov A, Kinach R, Lou X, Pavlov S, Vorobiev S, Dick JE, Tanner SD. 2009. Mass cytometry: technique for real time single cell multitarget immunoassay based on inductively coupled plasma time-of-flight mass spectrometry. Anal Chem 81:6813-22.

Bang S, Kim HS, Choo YS, Park SW, Chung JB, Song SY. 2006. Differences in immune cells engaged in cell-mediated immunity after chemotherapy for far advanced pancreatic cancer. Pancreas 32:29-36.

Barreda DR, Hanington PC, Belosevic M. 2004. Regulation of myeloid development and function by colony stimulating factors. Dev Comp Immunol 28:509-54.

Basturk O, Hong SM, Wood LD, Adsay NV, Albores-Saavedra J, Biankin AV, Brosens LA, Fukushima N, Goggins M, Hruban RH, Kato Y, Klimstra DS, Kloppel G, Krasinskas A, Longnecker DS, Matthaei H, Offerhaus GJ, Shimizu M, Takaori K, Terris B, Yachida S, Esposito I, Furukawa T. 2015. A Revised Classification System and Recommendations From the Baltimore Consensus Meeting for Neoplastic Precursor Lesions in the Pancreas. Am J Surg Pathol 39:1730-41.

Basu S, Hodgson G, Zhang HH, Katz M, Quilici C, Dunn AR. 2000. "Emergency" granulopoiesis in G-CSF-deficient mice in response to Candida albicans infection. Blood 95:3725-33.

Bauer TM, El-Rayes BF, Li X, Hammad N, Philip PA, Shields AF, Zalupski MM, Bekaii-Saab T. 2013. Carbohydrate antigen 19-9 is a prognostic and predictive biomarker in patients with advanced pancreatic cancer who receive gemcitabine-containing chemotherapy: a pooled analysis of 6 prospective trials. Cancer 119:285-92.

Baylor SM, Berg JW. 1973. Cross-classification and survival characteristics of 5,000 cases of cancer of the pancreas. J Surg Oncol 5:335-58.

Bayne LJ, Beatty GL, Jhala N, Clark CE, Rhim AD, Stanger BZ, Vonderheide RH. 2012. Tumor-derived granulocyte-macrophage colony-stimulating factor regulates myeloid inflammation and T cell immunity in pancreatic cancer. Cancer Cell 21:822-35.

Bayry J, Tchilian EZ, Davies MN, Forbes EK, Draper SJ, Kaveri SV, Hill AV, Kazatchkine MD, Beverley PC, Flower DR, Tough DF. 2008. In silico identified CCR4 antagonists target regulatory T cells and exert adjuvant activity in vaccination. Proc Natl Acad Sci U S A 105:10221-6.

Beatty GL, Chiorean EG, Fishman MP, Saboury B, Teitelbaum UR, Sun W, Huhn RD, Song W, Li D, Sharp LL, Torigian DA, O'Dwyer PJ, Vonderheide RH. 2011. CD40 agonists alter tumor stroma and show efficacy against pancreatic carcinoma in mice and humans. Science 331:1612-6.

Beatty GL, Winograd R, Evans RA, Long KB, Luque SL, Lee JW, Clendenin C, Gladney WL, Knoblock DM, Guirnalda PD, Vonderheide RH. 2015. Exclusion of T Cells From Pancreatic Carcinomas in Mice Is Regulated by Ly6C(low) F4/80(+) Extratumoral Macrophages. Gastroenterology 149:201-10.

Beauvillain C, Delneste Y, Scotet M, Peres A, Gascan H, Guermonprez P, Barnaba V, Jeannin P. 2007. Neutrophils efficiently cross-prime naive T cells in vivo. Blood 110:2965-73.

Ben-Aharon I, Elkabets M, Pelossof R, Yu KH, Iacubuzio-Donahue CA, Leach SD, Lowery MA, Goodman KA, O'Reilly EM. 2019. Genomic Landscape of Pancreatic Adenocarcinoma in Younger versus Older Patients: Does Age Matter? Clin Cancer Res 25:2185-2193.

Ben-David U, Ha G, Tseng YY, Greenwald NF, Oh C, Shih J, McFarland JM, Wong B, Boehm JS, Beroukhim R, Golub TR. 2017. Patient-derived xenografts undergo mouse-specific tumor evolution. Nat Genet 49:1567-1575.

Bent R, Moll L, Grabbe S, Bros M. 2018. Interleukin-1 beta—a friend or foe in malignancies? International journal of molecular sciences 19:2155.

Bernard V, Semaan A, Huang J, San Lucas FA, Mulu FC, Stephens BM, Guerrero PA, Huang Y, Zhao J, Kamyabi N, Sen S, Scheet PA, Taniguchi CM, Kim MP, Tzeng CW, Katz MH, Singhi AD, Maitra A, Alvarez HA. 2019. Single-Cell Transcriptomics of Pancreatic Cancer Precursors Demonstrates Epithelial and Microenvironmental Heterogeneity as an Early Event in Neoplastic Progression. Clin Cancer Res 25:2194-2205.

Biankin AV, Waddell N, Kassahn KS, Gingras MC, Muthuswamy LB, Johns AL, Miller DK, Wilson PJ, Patch AM, Wu J, Chang DK, Cowley MJ, Gardiner BB, Song S, Harliwong I, Idrisoglu S, Nourse C, Nourbakhsh E, Manning S, Wani S, Gongora M, Pajic M, Scarlett CJ, Gill AJ, Pinho AV, Rooman I, Anderson M, Holmes O, Leonard C, Taylor D, Wood S, Xu Q, Nones K, Fink JL, Christ A, Bruxner T, Cloonan N, Kolle G, Newell F, Pinese M, Mead RS, Humphris JL, Kaplan W, Jones MD, Colvin EK, Nagrial AM, Humphrey ES, Chou A, Chin VT, Chantrill LA, Mawson A, Samra JS, Kench JG, Lovell JA, Daly RJ, Merrett ND, Toon C, Epari K, Nguyen NQ, Barbour A, Zeps N, Kakkar N, Zhao F, Wu YQ, Wang M, Muzny DM, Fisher WE, Brunicardi FC, Hodges SE, Reid JG, Drummond J, Chang K, Han Y, Lewis LR, Dinh H, Buhay CJ, Beck T, Timms L, Sam M, Begley K, Brown A, Pai D, Panchal A, Buchner N, De Borja R, Denroche RE, Yung CK, Serra S, Onetto N, Mukhopadhyay D, Tsao MS, Shaw PA, Petersen GM, Gallinger S, Hruban RH, Maitra A, Iacobuzio-Donahue CA, Schulick RD, Wolfgang CL, Morgan RA, et al. 2012. Pancreatic cancer genomes reveal aberrations in axon guidance pathway genes. Nature 491:399-405.

Bingisser RM, Tilbrook PA, Holt PG, Kees UR. 1998. Macrophage-derived nitric oxide regulates T cell activation via reversible disruption of the Jak3/STAT5 signaling pathway. J Immunol 160:5729-34.

Blackstone MO, Riddell RH, Rogers BH, Levin B. 1981. Dysplasia-associated lesion or mass (DALM) detected by colonoscopy in long-standing ulcerative colitis: an indication for colectomy. Gastroenterology 80:366-74.

Blair PA, Noreña LY, Flores-Borja F, Rawlings DJ, Isenberg DA, Ehrenstein MR, Mauri C. 2010. CD19(+)CD24(hi)CD38(hi) B cells exhibit regulatory capacity in healthy individuals but are functionally impaired in systemic Lupus Erythematosus patients. Immunity 32:129-40.

Bosetti C, Rosato V, Li D, Silverman D, Petersen GM, Bracci PM, Neale RE, Muscat J, Anderson K, Gallinger S, Olson SH, Miller AB, Bas Bueno-de-Mesquita H, Scelo G, Janout V, Holcatova I, Lagiou P, Serraino D, Lucenteforte E, Fabianova E, Baghurst PA, Zatonski W, Foretova L, Fontham E, Bamlet WR, Holly EA, Negri E, Hassan M, Prizment A, Cotterchio M, Cleary S, Kurtz RC, Maisonneuve P, Trichopoulos D, Polesel J, Duell EJ, Boffetta P, La Vecchia C, Ghadirian P. 2014. Diabetes, antidiabetic medications, and pancreatic cancer risk: an analysis from the International Pancreatic Cancer Case-Control Consortium. Ann Oncol 25:2065-2072.

Böttcher JP, Reis e Sousa C. 2018. The Role of Type 1 Conventional Dendritic Cells in Cancer Immunity. Trends Cancer 4:784-792.

Bournet B, Muscari F, Buscail C, Assenat E, Barthet M, Hammel P, Selves J, Guimbaud R, Cordelier P, Buscail L. 2016. KRAS G12D Mutation Subtype Is A Prognostic Factor for Advanced Pancreatic Adenocarcinoma. Clin Transl Gastroenterol 7:e157.

Bracci PM. 2012. Obesity and pancreatic cancer: overview of epidemiologic evidence and biologic mechanisms. Mol Carcinog 51:53-63.

Brat DJ, Lillemoe KD, Yeo CJ, Warfield PB, Hruban RH. 1998. Progression of pancreatic intraductal neoplasias to infiltrating adenocarcinoma of the pancreas. Am J Surg Pathol 22:163-9.

Brenner H, Hoffmeister M, Stegmaier C, Brenner G, Altenhofen L, Haug U. 2007. Risk of progression of advanced adenomas to colorectal cancer by age and sex: estimates based on 840,149 screening colonoscopies. Gut 56:1585-9.

Brockie E, Anand A, Albores-Saavedra J. 1998. Progression of atypical ductal hyperplasia/carcinoma in situ of the pancreas to invasive adenocarcinoma. Ann Diagn Pathol 2:286-92.

Broderick L, Brooks SP, Takita H, Baer AN, Bernstein JM, Bankert RB. 2006. IL-12 reverses anergy to T cell receptor triggering in human lung tumor-associated memory T cells. Clin Immunol 118:159-69.

Bronte V, Brandau S, Chen SH, Colombo MP, Frey AB, Greten TF, Mandruzzato S, Murray PJ, Ochoa A, Ostrand-Rosenberg S, Rodriguez PC, Sica A, Umansky V, Vonderheide RH, Gabrilovich DI. 2016. Recommendations for myeloid-derived suppressor cell nomenclature and characterization standards. Nat Commun 7:12150.

Brose MS, Rebbeck TR, Calzone KA, Stopfer JE, Nathanson KL, Weber BL. 2002. Cancer risk estimates for BRCA1 mutation carriers identified in a risk evaluation program. J Natl Cancer Inst 94:1365-72.

Brouwer TP, de Vries NL, Abdelaal T, Krog RT, Li Z, Ruano D, Fariña A, Lelieveldt BPF, Morreau H, Bonsing BA, Vahrmeijer AL, Koning F, de Miranda N. 2022. Local and systemic immune profiles of human pancreatic ductal adenocarcinoma revealed by single-cell mass cytometry. J Immunother Cancer 10.

Brune K, Abe T, Canto M, O'Malley L, Klein AP, Maitra A, Volkan Adsay N, Fishman EK, Cameron JL, Yeo CJ, Kern SE, Goggins M, Hruban RH. 2006. Multifocal neoplastic precursor lesions associated with lobular atrophy of the pancreas in patients having a strong family history of pancreatic cancer. Am J Surg Pathol 30:1067-76.

Brunner M, Maier K, Rümmele P, Jacobsen A, Merkel S, Benard A, Krautz C, Kersting S, Grützmann R, Weber GF. 2020. Upregulation of CD20 Positive B-Cells and B-Cell Aggregates in the Tumor Infiltration Zone is Associated with Better Survival of Patients with Pancreatic Ductal Adenocarcinoma. Int J Mol Sci 21.

Burris HA, 3rd, Moore MJ, Andersen J, Green MR, Rothenberg ML, Modiano MR, Cripps MC, Portenoy RK, Storniolo AM, Tarassoff P, Nelson R, Dorr FA, Stephens CD, Von Hoff DD. 1997. Improvements in survival and clinical benefit with gemcitabine as first-line therapy for patients with advanced pancreas cancer: a randomized trial. J Clin Oncol 15:2403-13.

Candido JB, Morton JP, Bailey P, Campbell AD, Karim SA, Jamieson T, Lapienyte L, Gopinathan A, Clark W, McGhee EJ, Wang J, Escorcio-Correia M, Zollinger R, Roshani R, Drew L, Rishi L, Arkell R, Evans TRJ, Nixon C, Jodrell DI, Wilkinson RW, Biankin AV, Barry ST, Balkwill FR, Sansom OJ. 2018. CSF1R(+) Macrophages Sustain Pancreatic Tumor Growth through T Cell Suppression and Maintenance of Key Gene Programs that Define the Squamous Subtype. Cell Rep 23:1448-1460.

Carstens JL, Correa de Sampaio P, Yang D, Barua S, Wang H, Rao A, Allison JP, LeBleu VS, Kalluri R. 2017. Spatial computation of intratumoral T cells correlates with survival of patients with pancreatic cancer. Nat Commun 8:15095.

Carter JD, Dula SB, Corbin KL, Wu R, Nunemaker CS. 2009. A practical guide to rodent islet isolation and assessment. Biol Proced Online 11:3-31.

Carter NA, Vasconcellos R, Rosser EC, Tulone C, Muñoz-Suano A, Kamanaka M, Ehrenstein MR, Flavell RA, Mauri C. 2011. Mice lacking endogenous IL-10-producing regulatory B cells develop exacerbated disease and present with an increased frequency of Th1/Th17 but a decrease in regulatory T cells. J Immunol 186:5569-79.

Cassetta L, Baekkevold ES, Brandau S, Bujko A, Cassatella MA, Dorhoi A, Krieg C, Lin A, Loré K, Marini O, Pollard JW, Roussel M, Scapini P, Umansky V, Adema GJ. 2019. Deciphering myeloid-derived suppressor cells: isolation and markers in humans, mice and non-human primates. Cancer Immunol Immunother 68:687-697.

Castino GF, Cortese N, Capretti G, Serio S, Di Caro G, Mineri R, Magrini E, Grizzi F, Cappello P, Novelli F, Spaggiari P, Roncalli M, Ridolfi C, Gavazzi F, Zerbi A, Allavena P, Marchesi F. 2016. Spatial distribution of B cells predicts prognosis in human pancreatic adenocarcinoma. Oncoimmunology 5:e1085147.

Cetta F, Montalto G, Petracci M. 1997. Hepatoblastoma and APC gene mutation in familial adenomatous polyposis. Gut 41:417.

Chan A, Prassas I, Dimitromanolakis A, Brand RE, Serra S, Diamandis EP, Blasutig IM. 2014. Validation of biomarkers that complement CA19.9 in detecting early pancreatic cancer. Clin Cancer Res 20:5787-95.

Chauhan VP, Martin JD, Liu H, Lacorre DA, Jain SR, Kozin SV, Stylianopoulos T, Mousa AS, Han X, Adstamongkonkul P, Popović Z, Huang P, Bawendi MG, Boucher Y, Jain RK. 2013. Angiotensin inhibition enhances drug delivery and potentiates chemotherapy by decompressing tumour blood vessels. Nat Commun 4:2516.

Chávez-Galán L, Olleros ML, Vesin D, Garcia I. 2015. Much More than M1 and M2 Macrophages, There are also CD169(+) and TCR(+) Macrophages. Front Immunol 6:263.

Chen D, Li W, Liu S, Su Y, Han G, Xu C, Liu H, Zheng T, Zhou Y, Mao C. 2015. Interleukin-23 promotes the epithelial-mesenchymal transition of oesophageal carcinoma cells via the Wnt/β-catenin pathway. Sci Rep 5:8604.

Chen F, Childs EJ, Mocci E, Bracci P, Gallinger S, Li D, Neale RE, Olson SH, Scelo G, Bamlet WR, Blackford AL, Borges M, Brennan P, Chaffee KG, Duggal P, Hassan MJ, Holly EA, Hung RJ, Goggins MG, Kurtz RC, Oberg AL, Orlow I, Yu H, Petersen GM, Risch HA, Klein AP. 2019. Analysis of Heritability and Genetic Architecture of Pancreatic Cancer: A PanC4 Study. Cancer Epidemiol Biomarkers Prev 28:1238-1245.

Chen L, Huang CF, Li YC, Deng WW, Mao L, Wu L, Zhang WF, Zhang L, Sun ZJ. 2018. Blockage of the NLRP3 inflammasome by MCC950 improves anti-tumor immune responses in head and neck squamous cell carcinoma. Cell Mol Life Sci 75:2045-2058.

Chow LQM, Haddad R, Gupta S, Mahipal A, Mehra R, Tahara M, Berger R, Eder JP, Burtness B, Lee SH, Keam B, Kang H, Muro K, Weiss J, Geva R, Lin CC, Chung HC, Meister A, Dolled-Filhart M, Pathiraja K, Cheng JD, Seiwert TY. 2016. Antitumor Activity of Pembrolizumab in Biomarker-Unselected Patients With Recurrent and/or Metastatic Head and Neck Squamous Cell Carcinoma: Results From the Phase Ib KEYNOTE-012 Expansion Cohort. J Clin Oncol 34:3838-3845.

Christmas BJ, Rafie CI, Hopkins AC, Scott BA, Ma HS, Cruz KA, Woolman S, Armstrong TD, Connolly RM, Azad NA, Jaffee EM, Roussos Torres ET. 2018. Entinostat Converts Immune-Resistant Breast and Pancreatic Cancers into Checkpoint-Responsive Tumors by Reprogramming Tumor-Infiltrating MDSCs. Cancer Immunol Res 6:1561-1577.

Chuah S, Chew V. 2020. High-dimensional immune-profiling in cancer: implications for immunotherapy. J Immunother Cancer 8.

Clark CE, Hingorani SR, Mick R, Combs C, Tuveson DA, Vonderheide RH. 2007a. Dynamics of the immune reaction to pancreatic cancer from inception to invasion. Cancer Res 67:9518-27.

Clark EJ, Connor S, Taylor MA, Madhavan KK, Garden OJ, Parks RW. 2007b. Preoperative lymphocyte count as a prognostic factor in resected pancreatic ductal adenocarcinoma. HPB (Oxford) 9:456-60.

Clarke RB, Howell A, Potten CS, Anderson E. 1997. Dissociation between steroid receptor expression and cell proliferation in the human breast. Cancer Res 57:4987-91.

Collison LW, Chaturvedi V, Henderson AL, Giacomin PR, Guy C, Bankoti J, Finkelstein D, Forbes K, Workman CJ, Brown SA, Rehg JE, Jones ML, Ni HT, Artis D, Turk MJ, Vignali DA. 2010. IL-35-mediated induction of a potent regulatory T cell population. Nat Immunol 11:1093-101.

Collison LW, Delgoffe GM, Guy CS, Vignali KM, Chaturvedi V, Fairweather D, Satoskar AR, Garcia KC, Hunter CA, Drake CG, Murray PJ, Vignali DA. 2012. The composition and signaling of the IL-35 receptor are unconventional. Nat Immunol 13:290-9.

Collisson EA, Sadanandam A, Olson P, Gibb WJ, Truitt M, Gu S, Cooc J, Weinkle J, Kim GE, Jakkula L, Feiler HS, Ko AH, Olshen AB, Danenberg KL, Tempero MA, Spellman PT, Hanahan D, Gray JW. 2011. Subtypes of pancreatic ductal adenocarcinoma and their differing responses to therapy. Nat Med 17:500-3.

Conroy T, Desseigne F, Ychou M, Bouché O, Guimbaud R, Bécouarn Y, Adenis A, Raoul JL, Gourgou-Bourgade S, de la Fouchardière C, Bennouna J, Bachet JB, Khemissa-Akouz F, Péré-Vergé D, Delbaldo C, Assenat E, Chauffert B, Michel P, Montoto-Grillot C, Ducreux M. 2011. FOLFIRINOX versus gemcitabine for metastatic pancreatic cancer. N Engl J Med 364:1817-25.

Conroy T, Hammel P, Hebbar M, Ben Abdelghani M, Wei AC, Raoul JL, Choné L, Francois E, Artru P, Biagi JJ, Lecomte T, Assenat E, Faroux R, Ychou M, Volet J, Sauvanet A, Breysacher G, Di Fiore F, Cripps C, Kavan P, Texereau P, Bouhier-Leporrier K, Khemissa-Akouz F, Legoux JL, Juzyna B, Gourgou S, O'Callaghan CJ, Jouffroy-Zeller C, Rat P, Malka D, Castan F, Bachet JB. 2018. FOLFIRINOX or Gemcitabine as Adjuvant Therapy for Pancreatic Cancer. N Engl J Med 379:2395-2406.

Constanzo J, Faget J, Ursino C, Badie C, Pouget JP. 2021. Radiation-Induced Immunity and Toxicities: The Versatility of the cGAS-STING Pathway. Front Immunol 12:680503.

Cooks T, Pateras IS, Tarcic O, Solomon H, Schetter AJ, Wilder S, Lozano G, Pikarsky E, Forshew T, Rosenfeld N, Harpaz N, Itzkowitz S, Harris CC, Rotter V, Gorgoulis VG, Oren M. 2013. Mutant p53 prolongs NF-κB activation and promotes chronic inflammation and inflammation-associated colorectal cancer. Cancer Cell 23:634-46.

Coppé JP, Patil CK, Rodier F, Sun Y, Muñoz DP, Goldstein J, Nelson PS, Desprez PY, Campisi J. 2008. Senescence-associated secretory phenotypes reveal cell-nonautonomous functions of oncogenic RAS and the p53 tumor suppressor. PLoS Biol 6:2853-68.

Corcoran RB, Contino G, Deshpande V, Tzatsos A, Conrad C, Benes CH, Levy DE, Settleman J, Engelman JA, Bardeesy N. 2011. STAT3 plays a critical role in KRAS-induced pancreatic tumorigenesis. Cancer Res 71:5020-9.

Cortez-Retamozo V, Etzrodt M, Newton A, Rauch PJ, Chudnovskiy A, Berger C, Ryan RJ, Iwamoto Y, Marinelli B, Gorbatov R, Forghani R, Novobrantseva TI, Koteliansky V, Figueiredo JL, Chen JW, Anderson DG, Nahrendorf M, Swirski FK, Weissleder R, Pittet MJ. 2012. Origins of tumor-associated macrophages and neutrophils. Proc Natl Acad Sci U S A 109:2491-6.

Cossarizza A, Chang HD, Radbruch A, Acs A, Adam D, Adam-Klages S, Agace WW, Aghaeepour N, Akdis M, Allez M, Almeida LN, Alvisi G, Anderson G, Andrä I, Annunziato F, Anselmo A, Bacher P, Baldari CT, Bari S, Barnaba V, Barros-Martins J, Battistini L, Bauer W, Baumgart S, Baumgarth N, Baumjohann D, Baying B, Bebawy M, Becher B, Beisker W, Benes V, Beyaert R, Blanco A, Boardman DA, Bogdan C, Borger JG, Borsellino G, Boulais PE, Bradford JA, Brenner D, Brinkman RR, Brooks AES, Busch DH, Büscher M, Bushnell TP, Calzetti F, Cameron G, Cammarata I, Cao X, Cardell SL, Casola S, Cassatella MA, Cavani A, Celada A, Chatenoud L, Chattopadhyay PK, Chow S, Christakou E, Čičin-Šain L, Clerici M, Colombo FS, Cook L, Cooke A, Cooper AM, Corbett AJ, Cosma A, Cosmi L, Coulie PG, Cumano A, Cvetkovic L, Dang VD, Dang-Heine C, Davey MS, Davies D, De Biasi S, Del Zotto G, Dela Cruz GV, Delacher M, Della Bella S, Dellabona P, Deniz G, Dessing M, Di Santo JP, Diefenbach A, Dieli F, Dolf A, Dörner T, Dress RJ, Dudziak D, Dustin M, Dutertre CA, Ebner F, Eckle SBG, Edinger M, Eede P, Ehrhardt GRA, Eich M, Engel P, Engelhardt B, Erdei A, et al. 2019. Guidelines for the use of flow cytometry and cell sorting in immunological studies (second edition). Eur J Immunol 49:1457-1973.

Cossarizza A, Chang HD, Radbruch A, Akdis M, Andrä I, Annunziato F, Bacher P, Barnaba V, Battistini L, Bauer WM, Baumgart S, Becher B, Beisker W, Berek C, Blanco A, Borsellino G, Boulais PE, Brinkman RR, Büscher M, Busch DH, Bushnell TP, Cao X, Cavani A, Chattopadhyay PK, Cheng Q, Chow S, Clerici M, Cooke A, Cosma A, Cosmi L, Cumano A, Dang VD, Davies D, De Biasi S, Del Zotto G, Della Bella S, Dellabona P, Deniz G, Dessing M, Diefenbach A, Di Santo J, Dieli F, Dolf A, Donnenberg VS, Dörner T, Ehrhardt GRA, Endl E, Engel P, Engelhardt B, Esser C, Everts B, Dreher A, Falk CS, Fehniger TA, Filby A, Fillatreau S, Follo M, Förster I, Foster J, Foulds GA, Frenette PS, Galbraith D, Garbi N, García-Godoy MD, Geginat J, Ghoreschi K, Gibellini L, Goettlinger C, Goodyear CS, Gori A, Grogan J, Gross M, Grützkau A, Grummitt D, Hahn J, Hammer Q, Hauser AE, Haviland DL, Hedley D, Herrera G, Herrmann M, Hiepe F, Holland T, Hombrink P, Houston JP, Hoyer BF, Huang B, Hunter CA, Iannone A, Jäck HM, Jávega B, Jonjic S, Juelke K, Jung S, Kaiser T, Kalina T, Keller B, Khan S, Kienhöfer D, Kroneis T, et al. 2017. Guidelines for the use of flow cytometry and cell sorting in immunological studies. Eur J Immunol 47:1584-1797.

Couch FJ, Johnson MR, Rabe KG, Brune K, de Andrade M, Goggins M, Rothenmund H, Gallinger S, Klein A, Petersen GM, Hruban RH. 2007. The prevalence of BRCA2 mutations in familial pancreatic cancer. Cancer Epidemiol Biomarkers Prev 16:342-6.

Crippa S, Fernández-Del Castillo C, Salvia R, Finkelstein D, Bassi C, Domínguez I, Muzikansky A, Thayer SP, Falconi M, Mino-Kenudson M, Capelli P, Lauwers GY, Partelli S, Pederzoli P, Warshaw AL. 2010. Mucin-producing neoplasms of the pancreas: an analysis of distinguishing clinical and epidemiologic characteristics. Clin Gastroenterol Hepatol 8:213-9.

Cubilla AL, Fitzgerald PJ. 1976. Morphological lesions associated with human primary invasive nonendocrine pancreas cancer. Cancer Res 36:2690-8.

Daley D, Mani VR, Mohan N, Akkad N, Ochi A, Heindel DW, Lee KB, Zambirinis CP, Pandian GSB, Savadkar S, Torres-Hernandez A, Nayak S, Wang D, Hundeyin M, Diskin B, Aykut B, Werba G, Barilla RM, Rodriguez R, Chang S, Gardner L, Mahal LK, Ueberheide B, Miller G. 2017. Dectin 1 activation on macrophages by galectin 9 promotes pancreatic carcinoma and peritumoral immune tolerance. Nat Med 23:556-567.

Daniluk J, Liu Y, Deng D, Chu J, Huang H, Gaiser S, Cruz-Monserrate Z, Wang H, Ji B, Logsdon CD. 2012. An NF-κB pathway-mediated positive feedback loop amplifies Ras activity to pathological levels in mice. J Clin Invest 122:1519-28.

Darvishian F, Sullivan J, Teichberg S, Basham K. 2002. Carcinosarcoma of the pancreas: a case report and review of the literature. Arch Pathol Lab Med 126:1114-7.

Das S, Shapiro B, Vucic EA, Vogt S, Bar-Sagi D. 2020. Tumor Cell-Derived IL1β Promotes Desmoplasia and Immune Suppression in Pancreatic Cancer. Cancer Res 80:1088-1101.

Davies H, Bignell GR, Cox C, Stephens P, Edkins S, Clegg S, Teague J, Woffendin H, Garnett MJ, Bottomley W, Davis N, Dicks E, Ewing R, Floyd Y, Gray K, Hall S, Hawes R, Hughes J, Kosmidou V, Menzies A, Mould C, Parker A, Stevens C, Watt S, Hooper S, Wilson R, Jayatilake H, Gusterson BA, Cooper C, Shipley J, Hargrave D, Pritchard-Jones K, Maitland N, Chenevix-Trench G, Riggins GJ, Bigner DD, Palmieri G, Cossu A, Flanagan A, Nicholson A, Ho JW, Leung SY, Yuen ST, Weber BL, Seigler HF, Darrow TL, Paterson H, Marais R, Marshall CJ, Wooster R, Stratton MR, Futreal PA. 2002. Mutations of the BRAF gene in human cancer. Nature 417:949-54.

De La OJ, Emerson LL, Goodman JL, Froebe SC, Illum BE, Curtis AB, Murtaugh LC. 2008. Notch and Kras reprogram pancreatic acinar cells to ductal intraepithelial neoplasia. Proc Natl Acad Sci U S A 105:18907-12.

De Monte L, Wörmann S, Brunetto E, Heltai S, Magliacane G, Reni M, Paganoni AM, Recalde H, Mondino A, Falconi M, Aleotti F, Balzano G, Algül H, Doglioni C, Protti MP. 2016. Basophil Recruitment into Tumor-Draining Lymph Nodes Correlates with Th2 Inflammation and Reduced Survival in Pancreatic Cancer Patients. Cancer Res 76:1792-803.

Delvecchio FR, Goulart MR, Fincham REA, Bombadieri M, Kocher HM. 2022. B cells in pancreatic cancer stroma. World J Gastroenterol 28:1088-1101.

Devaud C, Westwood JA, John LB, Flynn JK, Paquet-Fifield S, Duong CP, Yong CS, Pegram HJ, Stacker SA, Achen MG, Stewart TJ, Snyder LA, Teng MW, Smyth MJ, Darcy PK, Kershaw MH. 2014. Tissues in different anatomical sites can sculpt and vary the tumor microenvironment to affect responses to therapy. Mol Ther 22:18-27.

Dibra D, Cutrera J, Xia X, Kallakury B, Mishra L, Li S. 2012. Interleukin-30: a novel antiinflammatory cytokine candidate for prevention and treatment of inflammatory cytokine-induced liver injury. Hepatology 55:1204-14.

Dibra D, Mitra A, Newman M, Xia X, Cutrera JJ, Gagea M, Kleinerman ES, Lozano G, Li S. 2016. Lack of Immunomodulatory Interleukin-27 Enhances Oncogenic Properties of Mutant p53 In Vivo. Clin Cancer Res 22:3876-83.

Diehl SJ, Lehmann KJ, Sadick M, Lachmann R, Georgi M. 1998. Pancreatic cancer: value of dual-phase helical CT in assessing resectability. Radiology 206:373-8.

Dieu-Nosjean MC, Giraldo NA, Kaplon H, Germain C, Fridman WH, Sautès-Fridman C. 2016. Tertiary lymphoid structures, drivers of the anti-tumor responses in human cancers. Immunol Rev 271:260-75.

Díez P, Ibarrola N, Dégano RM, Lécrevisse Q, Rodriguez-Caballero A, Criado I, Nieto WG, Góngora R, González M, Almeida J, Orfao A, Fuentes M. 2017. A systematic approach for peptide characterization of B-cell receptor in chronic lymphocytic leukemia cells. Oncotarget 8:42836-42846.

Dinarello CA. 2018. Overview of the IL-1 family in innate inflammation and acquired immunity. Immunol Rev 281:8-27.

Distler M, Kersting S, Niedergethmann M, Aust DE, Franz M, Rückert F, Ehehalt F, Pilarsky C, Post S, Saeger HD, Grützmann R. 2013. Pathohistological subtype predicts survival in patients with intraductal papillary mucinous neoplasm (IPMN) of the pancreas. Ann Surg 258:324-30.

Dolcetti L, Peranzoni E, Ugel S, Marigo I, Fernandez Gomez A, Mesa C, Geilich M, Winkels G, Traggiai E, Casati A, Grassi F, Bronte V. 2010. Hierarchy of immunosuppressive strength among myeloid-derived suppressor cell subsets is determined by GM-CSF. Eur J Immunol 40:22-35.

Dominguez CX, Müller S, Keerthivasan S, Koeppen H, Hung J, Gierke S, Breart B, Foreman O, Bainbridge TW, Castiglioni A, Senbabaoglu Y, Modrusan Z, Liang Y, Junttila MR, Klijn C, Bourgon R, Turley SJ. 2020. Single-Cell RNA Sequencing Reveals Stromal Evolution into LRRC15(+) Myofibroblasts as a Determinant of Patient Response to Cancer Immunotherapy. Cancer Discov 10:232-253.

Donepudi M, Jovasevic VM, Raychaudhuri P, Mokyr MB. 2003. Melphalan-induced up-regulation of B7-1 surface expression on normal splenic B cells. Cancer Immunol Immunother 52:162-70.

Ducreux M, Cuhna AS, Caramella C, Hollebecque A, Burtin P, Goéré D, Seufferlein T, Haustermans K, Van Laethem JL, Conroy T, Arnold D. 2015. Cancer of the pancreas: ESMO Clinical Practice Guidelines for diagnosis, treatment and follow-up. Ann Oncol 26 Suppl 5:v56-68.

Dunn GP, Bruce AT, Ikeda H, Old LJ, Schreiber RD. 2002. Cancer immunoediting: from immunosurveillance to tumor escape. Nat Immunol 3:991-8.
Dunn GP, Old LJ, Schreiber RD. 2004. The immunobiology of cancer immunosurveillance and immunoediting. Immunity 21:137-48.

Eblen ST. 2018. Extracellular-Regulated Kinases: Signaling From Ras to ERK Substrates to Control Biological Outcomes. Adv Cancer Res 138:99-142.
Egawa T, Kawabata K, Kawamoto H, Amada K, Okamoto R, Fujii N, Kishimoto T, Katsura Y, Nagasawa T. 2001. The earliest stages of B cell development require a chemokine stromal cell-derived factor/pre-B cell growth-stimulating factor. Immunity 15:323-34.

Elbanna KY, Jang HJ, Kim TK. 2020. Imaging diagnosis and staging of pancreatic ductal adenocarcinoma: a comprehensive review. Insights Imaging 11:58.

Ene-Obong A, Clear AJ, Watt J, Wang J, Fatah R, Riches JC, Marshall JF, Chin-Aleong J, Chelala C, Gribben JG, Ramsay AG, Kocher HM. 2013. Activated pancreatic stellate cells sequester CD8+ T cells to reduce their infiltration of the juxtatumoral compartment of pancreatic ductal adenocarcinoma. Gastroenterology 145:1121-32.

Eriksson E, Milenova I, Wenthe J, Moreno R, Alemany R, Loskog A. 2019. IL-6 Signaling Blockade during CD40-Mediated Immune Activation Favors Antitumor Factors by Reducing TGF-β, Collagen Type I, and PD-L1/PD-1. J Immunol 202:787-798.

Erkan M, Michalski CW, Rieder S, Reiser-Erkan C, Abiatari I, Kolb A, Giese NA, Esposito I, Friess H, Kleeff J. 2008. The activated stroma index is a novel and independent prognostic marker in pancreatic ductal adenocarcinoma. Clin Gastroenterol Hepatol 6:1155-61.

Esni F, Ghosh B, Biankin AV, Lin JW, Albert MA, Yu X, MacDonald RJ, Civin CI, Real FX, Pack MA, Ball DW, Leach SD. 2004. Notch inhibits Ptf1 function and acinar cell differentiation in developing mouse and zebrafish pancreas. Development 131:4213-24.
Everhart J, Wright D. 1995. Diabetes mellitus as a risk factor for pancreatic cancer. A meta-analysis. Jama 273:1605-9.

Falconi M, Eriksson B, Kaltsas G, Bartsch DK, Capdevila J, Caplin M, Kos-Kudla B, Kwekkeboom D, Rindi G, Klöppel G, Reed N, Kianmanesh R, Jensen RT. 2016. ENETS Consensus Guidelines Update for the Management of Patients with Functional Pancreatic Neuroendocrine Tumors and Non-Functional Pancreatic Neuroendocrine Tumors. Neuroendocrinology 103:153-71.

Fearon ER, Vogelstein B. 1990. A genetic model for colorectal tumorigenesis. Cell 61:759-67.

Feig C, Jones JO, Kraman M, Wells RJ, Deonarine A, Chan DS, Connell CM, Roberts EW, Zhao Q, Caballero OL, Teichmann SA, Janowitz T, Jodrell DI, Tuveson DA, Fearon DT. 2013. Targeting CXCL12 from FAP-expressing carcinoma-associated fibroblasts synergizes with anti-PD-L1 immunotherapy in pancreatic cancer. Proc Natl Acad Sci U S A 110:20212-7.

Felix K, Gaida MM. 2016. Neutrophil-Derived Proteases in the Microenvironment of Pancreatic Cancer -Active Players in Tumor Progression. Int J Biol Sci 12:302-13.
Feng XM, Chen XL, Liu N, Chen Z, Zhou YL, Han ZB, Zhang L, Han ZC. 2007. Interleukin-27 upregulates major histocompatibility complex class II expression in primary human endothelial cells through induction of major histocompatibility complex class II transactivator. Hum Immunol 68:965-72.

Feng XM, Liu N, Yang SG, Hu LY, Chen XL, Fang ZH, Ren Q, Lu SH, Liu B, Han ZC. 2008. Regulation of the class II and class I MHC pathways in human THP-1 monocytic cells by interleukin-27. Biochem Biophys Res Commun 367:553-9.

Ferrer-Font L, Mayer JU, Old S, Hermans IF, Irish J, Price KM. 2020a. High-Dimensional Data Analysis Algorithms Yield Comparable Results for Mass Cytometry and Spectral Flow Cytometry Data. Cytometry A 97:824-831.

Ferrer-Font L, Pellefigues C, Mayer JU, Small SJ, Jaimes MC, Price KM. 2020b. Panel Design and Optimization for High-Dimensional Immunophenotyping Assays Using Spectral Flow Cytometry. Curr Protoc Cytom 92:e70.

Figueiredo ML, Figueiredo Neto M, Salameh JW, Decker RE, Letteri R, Chan-Seng D, Emrick T. 2020. Ligand-Mediated Targeting of Cytokine Interleukin-27 Enhances Its Bioactivity In Vivo. Mol Ther Methods Clin Dev 17:739-751.

Fink G, Yang J, Carter G, Norman J. 1997. Acute pancreatitis-induced enzyme release and necrosis are attenuated by IL-1 antagonism through an indirect mechanism. J Surg Res 67:94-7.

Finotello F, Trajanoski Z. 2018. Quantifying tumor-infiltrating immune cells from transcriptomics data. Cancer Immunol Immunother 67:1031-1040.

Fleming M, Ravula S, Tatishchev SF, Wang HL. 2012. Colorectal carcinoma: Pathologic aspects. J Gastrointest Oncol 3:153-73.

Fontenot JD, Gavin MA, Rudensky AY. 2003. Foxp3 programs the development and function of CD4+CD25+ regulatory T cells. Nat Immunol 4:330-6.

Fujita H, Ohuchida K, Mizumoto K, Nakata K, Yu J, Kayashima T, Cui L, Manabe T, Ohtsuka T, Tanaka M. 2010a. alpha-Smooth Muscle Actin Expressing Stroma Promotes an Aggressive Tumor Biology in Pancreatic Ductal Adenocarcinoma. Pancreas 39:1254-1262.

Fujita T, Nakagohri T, Gotohda N, Takahashi S, Konishi M, Kojima M, Kinoshita T. 2010b. Evaluation of the prognostic factors and significance of lymph node status in invasive ductal carcinoma of the body or tail of the pancreas. Pancreas 39:e48-54.

Fujiwara K, Saung MT, Jing H, Herbst B, Zarecki M, Muth S, Wu A, Bigelow E, Chen L, Li K, Jurcak N, Blair AB, Ding D, Wichroski M, Blum J, Cheadle N, Koenitzer J, Zheng L. 2020. Interrogating the immune-modulating roles of radiation therapy for a rational combination with immune-checkpoint inhibitors in treating pancreatic cancer. J Immunother Cancer 8.

Fukuda A, Wang SC, Morris JPt, Folias AE, Liou A, Kim GE, Akira S, Boucher KM, Firpo MA, Mulvihill SJ, Hebrok M. 2011. Stat3 and MMP7 contribute to pancreatic ductal adenocarcinoma initiation and progression. Cancer Cell 19:441-55.

Fukunaga A, Miyamoto M, Cho Y, Murakami S, Kawarada Y, Oshikiri T, Kato K, Kurokawa T, Suzuoki M, Nakakubo Y, Hiraoka K, Itoh T, Morikawa T, Okushiba S, Kondo S, Katoh H. 2004. CD8+ tumor-infiltrating lymphocytes together with CD4+ tumor-infiltrating lymphocytes and dendritic cells improve the prognosis of patients with pancreatic adenocarcinoma. Pancreas 28:e26-31.

Fung AS, Lee C, Yu M, Tannock IF. 2015. The effect of chemotherapeutic agents on tumor vasculature in subcutaneous and orthotopic human tumor xenografts. BMC Cancer 15:112.

Furukawa T, Chiba R, Kobari M, Matsuno S, Nagura H, Takahashi T. 1994. Varying grades of epithelial atypia in the pancreatic ducts of humans. Classification based on morphometry and multivariate analysis and correlated with positive reactions of carcinoembryonic antigen. Arch Pathol Lab Med 118:227-34.

Gabitass RF, Annels NE, Stocken DD, Pandha HA, Middleton GW. 2011. Elevated myeloid-derived suppressor cells in pancreatic, esophageal and gastric cancer are an independent prognostic factor and are associated with significant elevation of the Th2 cytokine interleukin-13. Cancer Immunol Immunother 60:1419-30.

Gabrilovich DI, Ostrand-Rosenberg S, Bronte V. 2012. Coordinated regulation of myeloid cells by tumours. Nat Rev Immunol 12:253-68.

Gadalla R, Noamani B, MacLeod BL, Dickson RJ, Guo M, Xu W, Lukhele S, Elsaesser HJ, Razak ARA, Hirano N, McGaha TL, Wang B, Butler M, Guidos CJ, Ohashi PS, Siu LL, Brooks DG. 2019. Validation of CyTOF Against Flow Cytometry for Immunological Studies and Monitoring of Human Cancer Clinical Trials. Front Oncol 9:415.

Gajiwala S, Torgeson A, Garrido-Laguna I, Kinsey C, Lloyd S. 2018. Combination immunotherapy and radiation therapy strategies for pancreatic cancer-targeting multiple steps in the cancer immunity cycle. J Gastrointest Oncol 9:1014-1026.

Gandhi L, Rodríguez-Abreu D, Gadgeel S, Esteban E, Felip E, De Angelis F, Domine M, Clingan P, Hochmair MJ, Powell SF, Cheng SY, Bischoff HG, Peled N, Grossi F, Jennens RR, Reck M, Hui R, Garon EB, Boyer M, Rubio-Viqueira B, Novello S, Kurata T, Gray JE, Vida J, Wei Z, Yang J, Raftopoulos H, Pietanza MC, Garassino MC. 2018. Pembrolizumab plus Chemotherapy in Metastatic Non-Small-Cell Lung Cancer. N Engl J Med 378:2078-2092.

Gao Y, Souza-Fonseca-Guimaraes F, Bald T, Ng SS, Young A, Ngiow SF, Rautela J, Straube J, Waddell N, Blake SJ, Yan J, Bartholin L, Lee JS, Vivier E, Takeda K, Messaoudene M, Zitvogel L, Teng MWL, Belz GT, Engwerda CR, Huntington ND, Nakamura K, Hölzel M, Smyth MJ. 2017. Tumor immunoevasion by the conversion of effector NK cells into type 1 innate lymphoid cells. Nat Immunol 18:1004-1015.

Garcia PL, Council LN, Christein JD, Arnoletti JP, Heslin MJ, Gamblin TL, Richardson JH, Bjornsti MA, Yoon KJ. 2013. Development and histopathological characterization of tumorgraft models of pancreatic ductal adenocarcinoma. PLoS One 8:e78183.

Garud SS, Willingham FF. 2012. Molecular analysis of cyst fluid aspiration in the diagnosis and risk assessment of cystic lesions of the pancreas. Clin Transl Sci 5:102-7.

Gemenetzis G, McKay S, Pathak S, Moir J, Laing R, Jamieson NB, Young AL, Chatzizacharias NA, Giovinazzo F, Roberts KJ. 2021. Surgical Management of Non-Metastatic Pancreatic Cancer in the United Kingdom: Results of a Nationwide Survey on Current Practice. Front Oncol 11:791946.

Ghiringhelli F, Puig PE, Roux S, Parcellier A, Schmitt E, Solary E, Kroemer G, Martin F, Chauffert B, Zitvogel L. 2005. Tumor cells convert immature myeloid dendritic cells into TGF-beta-secreting cells inducing CD4+CD25+ regulatory T cell proliferation. J Exp Med 202:919-29.

Giardiello FM, Petersen GM, Brensinger JD, Luce MC, Cayouette MC, Bacon J, Booker SV, Hamilton SR. 1996. Hepatoblastoma and APC gene mutation in familial adenomatous polyposis. Gut 39:867-9.

Giardiello FM, Welsh SB, Hamilton SR, Offerhaus GJ, Gittelsohn AM, Booker SV, Krush AJ, Yardley JH, Luk GD. 1987. Increased risk of cancer in the Peutz-Jeghers syndrome. N Engl J Med 316:1511-4.

Giorda R, Weisberg EP, Ip TK, Trucco M. 1992. Genomic structure and strain-specific expression of the natural killer cell receptor NKR-P1. J Immunol 149:1957-63.

Gjertsen MK, Saeterdal I, Saebøe-Larssen S, Gaudernack G. 2003. HLA-A3 restricted mutant ras specific cytotoxic T-lymphocytes induced by vaccination with T-helper epitopes. J Mol Med (Berl) 81:43-50.

Glodek AM, Honczarenko M, Le Y, Campbell JJ, Silberstein LE. 2003. Sustained activation of cell adhesion is a differentially regulated process in B lymphopoiesis. J Exp Med 197:461-73.

Gnerlich JL, Mitchem JB, Weir JS, Sankpal NV, Kashiwagi H, Belt BA, Porembka MR, Herndon JM, Eberlein TJ, Goedegebuure P, Linehan DC. 2010. Induction of Th17 cells in the tumor microenvironment improves survival in a murine model of pancreatic cancer. J Immunol 185:4063-71.

Golan T, Hammel P, Reni M, Van Cutsem E, Macarulla T, Hall MJ, Park JO, Hochhauser D, Arnold D, Oh DY, Reinacher-Schick A, Tortora G, Algül H, O'Reilly EM, McGuinness D, Cui KY, Schlienger K, Locker GY, Kindler HL. 2019. Maintenance Olaparib for Germline BRCA-Mutated Metastatic Pancreatic Cancer. N Engl J Med 381:317-327.

Goldberg MV, Drake CG. 2011. LAG-3 in Cancer Immunotherapy. Curr Top Microbiol Immunol 344:269-78.

Golden EB, Chhabra A, Chachoua A, Adams S, Donach M, Fenton-Kerimian M, Friedman K, Ponzo F, Babb JS, Goldberg J, Demaria S, Formenti SC. 2015. Local radiotherapy and granulocyte-macrophage colony-stimulating factor to generate abscopal responses in patients with metastatic solid tumours: a proof-of-principle trial. Lancet Oncol 16:795-803.

Golden EB, Frances D, Pellicciotta I, Demaria S, Helen Barcellos-Hoff M, Formenti SC. 2014. Radiation fosters dose-dependent and chemotherapy-induced immunogenic cell death. Oncoimmunology 3:e28518.

Goldstein AM, Fraser MC, Struewing JP, Hussussian CJ, Ranade K, Zametkin DP, Fontaine LS, Organic SM, Dracopoli NC, Clark WH, Jr., et al. 1995. Increased risk of pancreatic cancer in melanoma-prone kindreds with p16INK4 mutations. N Engl J Med 333:970-4.

Gosselin EJ, Wardwell K, Rigby WF, Guyre PM. 1993. Induction of MHC class II on human polymorphonuclear neutrophils by granulocyte/macrophage colony-stimulating factor, IFN-gamma, and IL-3. J Immunol 151:1482-90.

Gough NM, Gough J, Metcalf D, Kelso A, Grail D, Nicola NA, Burgess AW, Dunn AR. 1984. Molecular cloning of cDNA encoding a murine haematopoietic growth regulator, granulocyte-macrophage colony stimulating factor. Nature 309:763-7.

Grange C, Létourneau J, Forget MA, Godin-Ethier J, Martin J, Liberman M, Latour M, Widmer H, Lattouf JB, Piccirillo CA, Cailhier JF, Lapointe R. 2011. Phenotypic characterization and functional analysis of human tumor immune infiltration after mechanical and enzymatic disaggregation. J Immunol Methods 372:119-26.

Greenberg AK, Yee H, Rom WN. 2002. Preneoplastic lesions of the lung. Respir Res 3:20.

Greten TF, Manns MP, Korangy F. 2011. Myeloid derived suppressor cells in human diseases. Int Immunopharmacol 11:802-7.

Guerra C, Collado M, Navas C, Schuhmacher AJ, Hernandez-Porras I, Canamero M, Rodriguez-Justo M, Serrano M, Barbacid M. 2011a. Pancreatitis-induced inflammation contributes to pancreatic cancer by inhibiting oncogene-induced senescence. Cancer Cell 19:728-39.

Guerra C, Collado M, Navas C, Schuhmacher AJ, Hernández-Porras I, Cañamero M, Rodriguez-Justo M, Serrano M, Barbacid M. 2011b. Pancreatitis-induced inflammation contributes to pancreatic cancer by inhibiting oncogene-induced senescence. Cancer Cell 19:728-39.

Guerra C, Schuhmacher AJ, Canamero M, Grippo PJ, Verdaguer L, Perez-Gallego L, Dubus P, Sandgren EP, Barbacid M. 2007. Chronic pancreatitis is essential for induction of pancreatic ductal adenocarcinoma by K-Ras oncogenes in adult mice. Cancer Cell 11:291-302.

Gunderson AJ, Kaneda MM, Tsujikawa T, Nguyen AV, Affara NI, Ruffell B, Gorjestani S, Liudahl SM, Truitt M, Olson P, Kim G, Hanahan D, Tempero MA, Sheppard B, Irving B, Chang BY, Varner JA, Coussens LM. 2016. Bruton Tyrosine Kinase-Dependent Immune Cell Cross-talk Drives Pancreas Cancer. Cancer Discov 6:270-85.

Gunderson AJ, Rajamanickam V, Bui C, Bernard B, Pucilowska J, Ballesteros-Merino C, Schmidt M, McCarty K, Philips M, Piening B, Dubay C, Medler T, Newell P, Hansen P, Tran E, Tang E, Bifulco C, Crittenden M, Gough M, Young KH. 2021. Germinal center reactions in tertiary lymphoid structures associate with neoantigen burden, humoral immunity and long-term survivorship in pancreatic cancer. Oncoimmunology 10:1900635.

Guo X, Zheng L, Jiang J, Zhao Y, Wang X, Shen M, Zhu F, Tian R, Shi C, Xu M, Li X, Peng F, Zhang H, Feng Y, Xie Y, Xu X, Jia W, He R, Xie C, Hu J, Ye D, Wang M, Qin R. 2016. Blocking NF-κB Is Essential for the Immunotherapeutic Effect of Recombinant IL18 in Pancreatic Cancer. Clin Cancer Res 22:5939-5950.

Guzzo C, Ayer A, Basta S, Banfield BW, Gee K. 2012. IL-27 enhances LPS-induced proinflammatory cytokine production via upregulation of TLR4 expression and signaling in human monocytes. J Immunol 188:864-73.

Hahn SA, Schutte M, Hoque AT, Moskaluk CA, da Costa LT, Rozenblum E, Weinstein CL, Fischer A, Yeo CJ, Hruban RH, Kern SE. 1996. DPC4, a candidate tumor suppressor gene at human chromosome 18q21.1. Science 271:350-3.

Hall A, Marshall CJ, Spurr NK, Weiss RA. 1983. Identification of transforming gene in two human sarcoma cell lines as a new member of the ras gene family located on chromosome 1. Nature 303:396-400.

Hallet J, Law CH, Cukier M, Saskin R, Liu N, Singh S. 2015. Exploring the rising incidence of neuroendocrine tumors: a population-based analysis of epidemiology, metastatic presentation, and outcomes. Cancer 121:589-97.

Hamid O, Robert C, Daud A, Hodi FS, Hwu WJ, Kefford R, Wolchok JD, Hersey P, Joseph RW, Weber JS, Dronca R, Gangadhar TC, Patnaik A, Zarour H, Joshua AM, Gergich K, Elassaiss-Schaap J, Algazi A, Mateus C, Boasberg P, Tumeh PC, Chmielowski B, Ebbinghaus SW, Li XN, Kang SP, Ribas A. 2013. Safety and tumor responses with lambrolizumab (anti-PD-1) in melanoma. N Engl J Med 369:134-44.

Hammel P, Huguet F, van Laethem JL, Goldstein D, Glimelius B, Artru P, Borbath I, Bouché O, Shannon J, André T, Mineur L, Chibaudel B, Bonnetain F, Louvet C. 2016. Effect of Chemoradiotherapy vs Chemotherapy on Survival in Patients With Locally Advanced Pancreatic Cancer Controlled After 4 Months of Gemcitabine With or Without Erlotinib: The LAP07 Randomized Clinical Trial. Jama 315:1844-53.

Hammel PR, Vilgrain V, Terris B, Penfornis A, Sauvanet A, Correas JM, Chauveau D, Balian A, Beigelman C, O'Toole D, Bernades P, Ruszniewski P, Richard S. 2000. Pancreatic involvement in von Hippel-Lindau disease. The Groupe Francophone d'Etude de la Maladie de von Hippel-Lindau. Gastroenterology 119:1087-95.

Hanahan D, Weinberg RA. 2011. Hallmarks of cancer: the next generation. Cell 144:646-74.

Haqq J, Howells LM, Garcea G, Metcalfe MS, Steward WP, Dennison AR. 2014. Pancreatic stellate cells and pancreas cancer: current perspectives and future strategies. Eur J Cancer 50:2570-82.

Harari O, Liao JK. 2004. Inhibition of MHC II gene transcription by nitric oxide and antioxidants. Curr Pharm Des 10:893-8.

Harvey JJ. 1964. AN UNIDENTIFIED VIRUS WHICH CAUSES THE RAPID PRODUCTION OF TUMOURS IN MICE. Nature 204:1104-5.

He M, Henderson M, Muth S, Murphy A, Zheng L. 2020. Preclinical mouse models for immunotherapeutic and non-immunotherapeutic drug development for pancreatic ductal adenocarcinoma. Ann Pancreat Cancer 3.

He S, Fei M, Wu Y, Zheng D, Wan D, Wang L, Li D. 2011. Distribution and clinical significance of Th17 cells in the tumor microenvironment and peripheral blood of pancreatic cancer patients. Int J Mol Sci 12:7424-37.

Hegde S, Krisnawan VE, Herzog BH, Zuo C, Breden MA, Knolhoff BL, Hogg GD, Tang JP, Baer JM, Mpoy C, Lee KB, Alexander KA, Rogers BE, Murphy KM, Hawkins WG, Fields RC, DeSelm CJ, Schwarz JK, DeNardo DG. 2020. Dendritic Cell Paucity Leads to Dysfunctional Immune Surveillance in Pancreatic Cancer. Cancer Cell 37:289-307.e9.

Helm O, Held-Feindt J, Grage-Griebenow E, Reiling N, Ungefroren H, Vogel I, Krüger U, Becker T, Ebsen M, Röcken C, Kabelitz D, Schäfer H, Sebens S. 2014. Tumor-associated macrophages exhibit pro- and anti-inflammatory properties by which they impact on pancreatic tumorigenesis. Int J Cancer 135:843-61.

Henderson JR, Daniel PM, Fraser PA. 1981. The pancreas as a single organ: the influence of the endocrine upon the exocrine part of the gland. Gut 22:158-67.

Hendry S, Salgado R, Gevaert T, Russell PA, John T, Thapa B, Christie M, van de Vijver K, Estrada MV, Gonzalez-Ericsson PI, Sanders M, Solomon B, Solinas C, Van den Eynden G, Allory Y, Preusser M, Hainfellner J, Pruneri G, Vingiani A, Demaria S, Symmans F, Nuciforo P, Comerma L, Thompson EA, Lakhani S, Kim SR, Schnitt S, Colpaert C, Sotiriou C, Scherer SJ, Ignatiadis M, Badve S, Pierce RH, Viale G, Sirtaine N, Penault-Llorca F, Sugie T, Fineberg S, Paik S, Srinivasan A, Richardson A, Wang Y, Chmielik E, Brock J, Johnson DB, Balko J, Wienert S, Bossuyt V, Michiels S, Ternes N, Burchardi N, Luen SJ, Savas P, Klauschen F, Watson PH, Nelson BH, Criscitiello C, O'Toole S, Larsimont D, de Wind R, Curigliano G, André F, Lacroix-Triki M, van de Vijver M, Rojo F, Floris G, Bedri S, Sparano J, Rimm D, Nielsen T, Kos Z, Hewitt S, Singh B, Farshid G, Loibl S, Allison KH, Tung N, Adams S, Willard-Gallo K, Horlings HM, Gandhi L, Moreira A, Hirsch F, Dieci MV, Urbanowicz M, Brcic I, Korski K, Gaire F, Koeppen H, Lo A, Giltnane J, Rebelatto MC, Steele KE, Zha J, Emancipator K, Juco JW, Denkert C, Reis-Filho J, Loi S, Fox SB. 2017. Assessing Tumor-infiltrating Lymphocytes in Solid Tumors: A Practical Review for Pathologists and Proposal for a Standardized Method From the International Immunooncology Biomarkers Working Group: Part 1: Assessing the Host Immune Response, TILs in Invasive Breast Carcinoma and Ductal Carcinoma In Situ, Metastatic Tumor Deposits and Areas for Further Research. Adv Anat Pathol 24:235-251.

Herman JM, Swartz MJ, Hsu CC, Winter J, Pawlik TM, Sugar E, Robinson R, Laheru DA, Jaffee E, Hruban RH, Campbell KA, Wolfgang CL, Asrari F, Donehower R, Hidalgo M, Diaz LA, Jr., Yeo C, Cameron JL, Schulick RD, Abrams R. 2008. Analysis of fluorouracil-based adjuvant chemotherapy and radiation after pancreaticoduodenectomy for ductal adenocarcinoma of the pancreas: results of a large, prospectively collected database at the Johns Hopkins Hospital. J Clin Oncol 26:3503-10.

Hingorani SR, Petricoin EF, Maitra A, Rajapakse V, King C, Jacobetz MA, Ross S, Conrads TP, Veenstra TD, Hitt BA, Kawaguchi Y, Johann D, Liotta LA, Crawford HC, Putt ME, Jacks T, Wright CV, Hruban RH, Lowy AM, Tuveson DA. 2003. Preinvasive and invasive ductal pancreatic cancer and its early detection in the mouse. Cancer Cell 4:437-50.

Hingorani SR, Wang L, Multani AS, Combs C, Deramaudt TB, Hruban RH, Rustgi AK, Chang S, Tuveson DA. 2005. Trp53R172H and KrasG12D cooperate to promote chromosomal instability and widely metastatic pancreatic ductal adenocarcinoma in mice. Cancer Cell 7:469-83.

Hirai H, Zhang P, Dayaram T, Hetherington CJ, Mizuno S, Imanishi J, Akashi K, Tenen DG. 2006. C/EBPbeta is required for 'emergency' granulopoiesis. Nat Immunol 7:732-9. Hoechst B, Ormandy LA, Ballmaier M, Lehner F, Krüger C, Manns MP, Greten TF, Korangy F. 2008. A new population of myeloid-derived suppressor cells in hepatocellular carcinoma patients induces CD4(+)CD25(+)Foxp3(+) T cells. Gastroenterology 135:234-43.

Hong DS, Angelo LS, Kurzrock R. 2007. Interleukin-6 and its receptor in cancer: implications for translational therapeutics. Cancer 110:1911-28.

Hong DS, Kuo J, Sacher AG, Barlesi F, Besse B, Kuboki Y, Dy GK, Dembla V, Krauss JC, Burns TF. 2020. CodeBreak 100: Phase I study of AMG 510, a novel KRASG12C inhibitor, in patients (pts) with advanced solid tumors other than non-small cell lung cancer (NSCLC) and colorectal cancer (CRC)editor^editors: American Society of Clinical Oncology.

Hori S, Nomura T, Sakaguchi S. 2003. Control of regulatory T cell development by the transcription factor Foxp3. Science 299:1057-61.

Horie A, Yano Y, Kotoo Y, Miwa A. 1977. Morphogenesis of pancreatoblastoma, infantile carcinoma of the pancreas: report of two cases. Cancer 39:247-54.

Hosein AN, Huang H, Wang Z, Parmar K, Du W, Huang J, Maitra A, Olson E, Verma U, Brekken RA. 2019. Cellular heterogeneity during mouse pancreatic ductal adenocarcinoma progression at single-cell resolution. JCI Insight 5.

Hosseini SM, Gholijani N, Chenari N, Kalantar K. 2020. Decreased levels of interleukin 27 in the serum of vitiligo patients. An Bras Dermatol 95:570-574.

Hruban RH, Adsay NV, Albores-Saavedra J, Compton C, Garrett ES, Goodman SN, Kern SE, Klimstra DS, Klöppel G, Longnecker DS, Lüttges J, Offerhaus GJ. 2001. Pancreatic intraepithelial neoplasia: a new nomenclature and classification system for pancreatic duct lesions. Am J Surg Pathol 25:579-86.

Hruban RH, Maitra A, Goggins M. 2008. Update on pancreatic intraepithelial neoplasia. Int J Clin Exp Pathol 1:306-16.

Hruban RH, Maitra A, Kern SE, Goggins M. 2007. Precursors to pancreatic cancer. Gastroenterol Clin North Am 36:831-49, vi.

Hruban RH, Takaori K, Klimstra DS, Adsay NV, Albores-Saavedra J, Biankin AV, Biankin SA, Compton C, Fukushima N, Furukawa T, Goggins M, Kato Y, Kloppel G, Longnecker DS, Luttges J, Maitra A, Offerhaus GJ, Shimizu M, Yonezawa S. 2004. An illustrated consensus on the classification of pancreatic intraepithelial neoplasia and intraductal papillary mucinous neoplasms. Am J Surg Pathol 28:977-87.

Hu F, Guo F, Zhu Y, Zhou Q, Li T, Xiang H, Shang D. 2020. IL-17 in pancreatic disease: pathogenesis and pharmacotherapy. Am J Cancer Res 10:3551-3564.

Hu WH, Chen HH, Yen SL, Huang HY, Hsiao CC, Chuang JH. 2017a. Increased expression of interleukin-23 associated with progression of colorectal cancer. J Surg Oncol 115:208-212.

Hu ZI, McArthur HL, Ho AY. 2017b. The Abscopal Effect of Radiation Therapy: What Is It and How Can We Use It in Breast Cancer? Curr Breast Cancer Rep 9:45-51.

Huang H, Daniluk J, Liu Y, Chu J, Li Z, Ji B, Logsdon CD. 2014. Oncogenic K-Ras requires activation for enhanced activity. Oncogene 33:532-5.

Huang Q, Huang M, Meng F, Sun R. 2019. Activated pancreatic stellate cells inhibit NK cell function in the human pancreatic cancer microenvironment. Cell Mol Immunol 16:87-89.

Hulspas R. 2010. Titration of fluorochrome-conjugated antibodies for labeling cell surface markers on live cells. Curr Protoc Cytom Chapter 6:Unit 6.29.

Hundeyin M, Kurz E, Mishra A, Rossi JAK, Liudahl SM, Leis KR, Mehrotra H, Kim M, Torres LE, Ogunsakin A, Link J, Sears RC, Sivagnanam S, Goecks J, Islam KMS, Dolgalev I, Savadkar S, Wang W, Aykut B, Leinwand J, Diskin B, Adam S, Israr M, Gelas M, Lish J, Chin K, Farooq MS, Wadowski B, Wu J, Shah S, Adeegbe DO, Pushalkar S, Vasudevaraja V, Saxena D, Wong KK, Coussens LM, Miller G. 2019. Innate αβ T Cells Mediate Antitumor Immunity by Orchestrating Immunogenic Macrophage Programming. Cancer Discov 9:1288-1305.

Hunter CA, Kastelein R. 2012. Interleukin-27: balancing protective and pathological immunity. Immunity 37:960-9.

Hussain SM, Reed LF, Krasnick BA, Miranda-Carboni G, Fields RC, Bi Y, Elahi A, Ajidahun A, Dickson PV, Deneve JL, Hawkins WG, Shibata D, Glazer ES. 2018. IL23 and TGF-ß diminish macrophage associated metastasis in pancreatic carcinoma. Sci Rep 8:5808.

Hutcheson J, Balaji U, Porembka MR, Wachsmann MB, McCue PA, Knudsen ES, Witkiewicz AK. 2016. Immunologic and Metabolic Features of Pancreatic Ductal Adenocarcinoma Define Prognostic Subtypes of Disease. Clin Cancer Res 22:3606-17.

Hwang HK, Kim HI, Kim SH, Choi J, Kang CM, Kim KS, Lee WJ. 2016. Prognostic impact of the tumor-infiltrating regulatory T-cell (Foxp3(+))/activated cytotoxic T lymphocyte (granzyme B(+)) ratio on resected left-sided pancreatic cancer. Oncol Lett 12:4477-4484.

Iacobaeus E, Douagi I, Jitschin R, Marcusson-Ståhl M, Andrén AT, Gavin C, Lefsihane K, Davies LC, Mougiakakos D, Kadri N, Le Blanc K. 2018. Phenotypic and functional alterations of myeloid-derived suppressor cells during the disease course of multiple sclerosis. Immunol Cell Biol 96:820-830.

Ikemoto T, Yamaguchi T, Morine Y, Imura S, Soejima Y, Fujii M, Maekawa Y, Yasutomo K, Shimada M. 2006. Clinical roles of increased populations of Foxp3+CD4+ T cells in peripheral blood from advanced pancreatic cancer patients. Pancreas 33:386-90.

Ikenaga N, Ohuchida K, Mizumoto K, Cui L, Kayashima T, Morimatsu K, Moriyama T, Nakata K, Fujita H, Tanaka M. 2010. CD10+ pancreatic stellate cells enhance the progression of pancreatic cancer. Gastroenterology 139:1041-51, 1051.e1-8.

Imai K, Matsuyama S, Miyake S, Suga K, Nakachi K. 2000. Natural cytotoxic activity of peripheral-blood lymphocytes and cancer incidence: an 11-year follow-up study of a general population. Lancet 356:1795-9.

Ino Y, Yamazaki-Itoh R, Shimada K, Iwasaki M, Kosuge T, Kanai Y, Hiraoka N. 2013. Immune cell infiltration as an indicator of the immune microenvironment of pancreatic cancer. Br J Cancer 108:914-23.

Itoh T, Kishi K, Tojo M, Kitajima N, Kinoshita Y, Inatome T, Fukuzaki H, Nishiyama N, Tachibana H, Takahashi H, et al. 1992. Acinar cell carcinoma of the pancreas with elevated serum alpha-fetoprotein levels: a case report and a review of 28 cases reported in Japan. Gastroenterol Jpn 27:785-91.

Ivanov, II, McKenzie BS, Zhou L, Tadokoro CE, Lepelley A, Lafaille JJ, Cua DJ, Littman DR. 2006. The orphan nuclear receptor RORgammat directs the differentiation program of proinflammatory IL-17+ T helper cells. Cell 126:1121-33.

Iwai Y, Ishida M, Tanaka Y, Okazaki T, Honjo T, Minato N. 2002. Involvement of PD-L1 on tumor cells in the escape from host immune system and tumor immunotherapy by PD-L1 blockade. Proc Natl Acad Sci U S A 99:12293-7.

Jackson EL, Willis N, Mercer K, Bronson RT, Crowley D, Montoya R, Jacks T, Tuveson DA. 2001. Analysis of lung tumor initiation and progression using conditional expression of oncogenic K-ras. Genes Dev 15:3243-8.

Jacobetz MA, Chan DS, Neesse A, Bapiro TE, Cook N, Frese KK, Feig C, Nakagawa T, Caldwell ME, Zecchini HI, Lolkema MP, Jiang P, Kultti A, Thompson CB, Maneval DC, Jodrell DI, Frost GI, Shepard HM, Skepper JN, Tuveson DA. 2013. Hyaluronan impairs vascular function and drug delivery in a mouse model of pancreatic cancer. Gut 62:112-20.

Janakiram NB, Mohammed A, Bryant T, Ritchie R, Stratton N, Jackson L, Lightfoot S, Benbrook DM, Asch AS, Lang ML, Rao CV. 2017. Loss of natural killer T cells promotes pancreatic cancer in LSL-Kras(G12D/+) mice. Immunology 152:36-51.

Jiang H, Gebhardt C, Umansky L, Beckhove P, Schulze TJ, Utikal J, Umansky V. 2015. Elevated chronic inflammatory factors and myeloid-derived suppressor cells indicate poor prognosis in advanced melanoma patients. Int J Cancer 136:2352-60.

Jiao Z, Hua S, Wang W, Wang H, Gao J, Wang X. 2013. Increased circulating myeloid-derived suppressor cells correlated negatively with Th17 cells in patients with rheumatoid arthritis. Scand J Rheumatol 42:85-90.

Jin L, Xu X, Ye B, Pan M, Shi Z, Hu Y. 2015. Elevated serum interleukin-35 levels correlate with poor prognosis in patients with clear cell renal cell carcinoma. Int J Clin Exp Med 8:18861-6.

Jin P, Ren H, Sun W, Xin W, Zhang H, Hao J. 2014. Circulating IL-35 in pancreatic ductal adenocarcinoma patients. Hum Immunol 75:29-33.

Johnson AM, Bullock BL, Neuwelt AJ, Poczobutt JM, Kaspar RE, Li HY, Kwak JW, Hopp K, Weiser-Evans MCM, Heasley LE, Schenk EL, Clambey ET, Nemenoff RA. 2020. Cancer Cell-Intrinsic Expression of MHC Class II Regulates the Immune Microenvironment and Response to Anti-PD-1 Therapy in Lung Adenocarcinoma. J Immunol 204:2295-2307.

Jones S, Zhang X, Parsons DW, Lin JC, Leary RJ, Angenendt P, Mankoo P, Carter H, Kamiyama H, Jimeno A, Hong SM, Fu B, Lin MT, Calhoun ES, Kamiyama M, Walter K, Nikolskaya T, Nikolsky Y, Hartigan J, Smith DR, Hidalgo M, Leach SD, Klein AP, Jaffee EM, Goggins M, Maitra A, Iacobuzio-Donahue C, Eshleman JR, Kern SE, Hruban RH, Karchin R, Papadopoulos N, Parmigiani G, Vogelstein B, Velculescu VE, Kinzler KW. 2008. Core signaling pathways in human pancreatic cancers revealed by global genomic analyses. Science 321:1801-6.

Jordan KR, Kapoor P, Spongberg E, Tobin RP, Gao D, Borges VF, McCarter MD. 2017. Immunosuppressive myeloid-derived suppressor cells are increased in splenocytes from cancer patients. Cancer Immunol Immunother 66:503-513.

Kabacaoglu D, Ciecielski KJ, Ruess DA, Algul H. 2018. Immune Checkpoint Inhibition for Pancreatic Ductal Adenocarcinoma: Current Limitations and Future Options. Front Immunol 9:1878.

Kadaba R, Birke H, Wang J, Hooper S, Andl CD, Di Maggio F, Soylu E, Ghallab M, Bor D, Froeling FE, Bhattacharya S, Rustgi AK, Sahai E, Chelala C, Sasieni P, Kocher HM. 2013. Imbalance of desmoplastic stromal cell numbers drives aggressive cancer processes. J Pathol 230:107-17.

Kalser MH, Ellenberg SS. 1985. Pancreatic cancer. Adjuvant combined radiation and chemotherapy following curative resection. Arch Surg 120:899-903.

Kamisawa T, Wood LD, Itoi T, Takaori K. 2016. Pancreatic cancer. Lancet 388:73-85.

Karakhanova S, Link J, Heinrich M, Shevchenko I, Yang Y, Hassenpflug M, Bunge H, von Ahn K, Brecht R, Mathes A, Maier C, Umansky V, Werner J, Bazhin AV. 2015. Characterization of myeloid leukocytes and soluble mediators in pancreatic cancer: importance of myeloid-derived suppressor cells. Oncoimmunology 4:e998519.

Karoumpalis I, Christodoulou DK. 2016. Cystic lesions of the pancreas. Ann Gastroenterol 29:155-61.

Karpińska M, Czauderna M. 2022. Pancreas-Its Functions, Disorders, and Physiological Impact on the Mammals' Organism. Front Physiol 13:807632.

Kasi A, Allen J, Mehta K, Dandawate P, Saha S, Bossmann S, Anant S, Sun W. 2021. Association of losartan with outcomes in metastatic pancreatic cancer patients treated with chemotherapy. J Clin Transl Res 7:257-262.

Kastelein RA, Hunter CA, Cua DJ. 2007. Discovery and biology of IL-23 and IL-27: related but functionally distinct regulators of inflammation. Annu Rev Immunol 25:221-42.

Kastrinos F, Mukherjee B, Tayob N, Wang F, Sparr J, Raymond VM, Bandipalliam P, Stoffel EM, Gruber SB, Syngal S. 2009. Risk of pancreatic cancer in families with Lynch syndrome. Jama 302:1790-5.

Kato S, Iida S, Higuchi T, Ishikawa T, Takagi Y, Yasuno M, Enomoto M, Uetake H, Sugihara K. 2007. PIK3CA mutation is predictive of poor survival in patients with colorectal cancer. Int J Cancer 121:1771-8.

Kaur K, Chang HH, Topchyan P, Cook JM, Barkhordarian A, Eibl G, Jewett A. 2018. Deficiencies in Natural Killer Cell Numbers, Expansion, and Function at the Pre-Neoplastic Stage of Pancreatic Cancer by KRAS Mutation in the Pancreas of Obese Mice. Front Immunol 9:1229.

Kawaguchi Y, Cooper B, Gannon M, Ray M, MacDonald RJ, Wright CV. 2002. The role of the transcriptional regulator Ptf1a in converting intestinal to pancreatic progenitors. Nat Genet 32:128-34.

Keane MG, Horsfall L, Rait G, Pereira SP. 2014. A case-control study comparing the incidence of early symptoms in pancreatic and biliary tract cancer. BMJ Open 4:e005720.

Kelly A, Gunaltay S, McEntee CP, Shuttleworth EE, Smedley C, Houston SA, Fenton TM, Levison S, Mann ER, Travis MA. 2018. Human monocytes and macrophages regulate immune tolerance via integrin αvβ8-mediated TGFβ activation. J Exp Med 215:2725-2736.

Kenkel JA, Tseng WW, Davidson MG, Tolentino LL, Choi O, Bhattacharya N, Seeley ES, Winer DA, Reticker-Flynn NE, Engleman EG. 2017. An Immunosuppressive Dendritic Cell Subset Accumulates at Secondary Sites and Promotes Metastasis in Pancreatic Cancer. Cancer Res 77:4158-4170.

Kerr KM. 2001. Pulmonary preinvasive neoplasia. J Clin Pathol 54:257-71.

Kersemans V, Beech JS, Gilchrist S, Kinchesh P, Allen PD, Thompson J, Gomes AL, D'Costa Z, Bird L, Tullis IDC, Newman RG, Corroyer-Dulmont A, Falzone N, Azad A, Vallis KA, Sansom OJ, Muschel RJ, Vojnovic B, Hill MA, Fokas E, Smart SC. 2017. An efficient and robust MRI-guided radiotherapy planning approach for targeting abdominal organs and tumours in the mouse. PLoS One 12:e0176693.

Khaled YS, Ammori BJ, Elkord E. 2014. Increased levels of granulocytic myeloid-derived suppressor cells in peripheral blood and tumour tissue of pancreatic cancer patients. J Immunol Res 2014:879897.

Kilinc MO, Aulakh KS, Nair RE, Jones SA, Alard P, Kosiewicz MM, Egilmez NK. 2006. Reversing tumor immune suppression with intratumoral IL-12: activation of tumor-associated T effector/memory cells, induction of T suppressor apoptosis, and infiltration of CD8+ T effectors. J Immunol 177:6962-73.

Kim MP, Gallick GE. 2008. Gemcitabine resistance in pancreatic cancer: picking the key players. Clin Cancer Res 14:1284-5.

Kim MS, Lee SY, Cho WH, Song WS, Koh JS, Lee JA, Yoo JY, Jeon DG. 2008. Tumor necrosis rate adjusted by tumor volume change is a better predictor of survival of localized osteosarcoma patients. Ann Surg Oncol 15:906-14.

Kimura N, Komuro K, Uchino S, Yagihashi S, Ishidate T, Ishizaka M. 2010. Multiple endocrine neoplasia type 1-associated cystic pancreatic endocrine neoplasia and multifocal cholesterol granulomas. Pathol Int 60:321-5.

Kinchesh P, Allen PD, Gilchrist S, Kersemans V, Lanfredini S, Thapa A, O'Neill E, Smart SC. 2019. Reduced respiratory motion artefact in constant TR multi-slice MRI of the mouse. Magn Reson Imaging 60:1-6.

Kirsten WH, Mayer LA. 1967. Morphologic responses to a murine erythroblastosis virus. J Natl Cancer Inst 39:311-35.

Kiryu S, Ito Z, Suka M, Bito T, Kan S, Uchiyama K, Saruta M, Hata T, Takano Y, Fujioka S, Misawa T, Yamauchi T, Yanagisawa H, Sato N, Ohkusa T, Sugiyama H, Koido S. 2021. Prognostic value of immune factors in the tumor microenvironment of patients with pancreatic ductal adenocarcinoma. BMC Cancer 21:1197.

Kleeff J, Beckhove P, Esposito I, Herzig S, Huber PE, Lohr JM, Friess H. 2007. Pancreatic cancer microenvironment. Int J Cancer 121:699-705.

Klein G, Sjogren HO, Klein E, Hellstrom KE. 1960. Demonstration of resistance against methylcholanthrene-induced sarcomas in the primary autochthonous host. Cancer Res 20:1561-72.

Klimstra DS. 2007. Nonductal neoplasms of the pancreas. Mod Pathol 20 Suppl 1:S94-112.

Klimstra DS, Heffess CS, Oertel JE, Rosai J. 1992. Acinar cell carcinoma of the pancreas. A clinicopathologic study of 28 cases. Am J Surg Pathol 16:815-37.
Klimstra DS, Longnecker DS. 1994. K-ras mutations in pancreatic ductal proliferative lesions. Am J Pathol 145:1547-50.

Knudsen ES, Vail P, Balaji U, Ngo H, Botros IW, Makarov V, Riaz N, Balachandran V, Leach S, Thompson DM, Chan TA, Witkiewicz AK. 2017. Stratification of Pancreatic Ductal Adenocarcinoma: Combinatorial Genetic, Stromal, and Immunologic Markers. Clin Cancer Res 23:4429-4440.

Koh TH, Cooper JE, Newman CL, Walker TM, Kiely EM, Hoffmann EB. 1986. Pancreatoblastoma in a neonate with Wiedemann-Beckwith syndrome. Eur J Pediatr 145:435-8.

Kohda E, Iseki M, Ikawa H, Endoh M, Yokoyama J, Mukai M, Hata J, Yamazaki H, Miyauchi J, Saeki M. 2000. Pancreatoblastoma. Three original cases and review of the literature. Acta Radiol 41:334-7.

Koizumi M, Hiasa Y, Kumagi T, Yamanishi H, Azemoto N, Kobata T, Matsuura B, Abe M, Onji M. 2013. Increased B cell-activating factor promotes tumor invasion and metastasis in human pancreatic cancer. PLoS One 8:e71367.

Komura T, Sakai Y, Harada K, Kawaguchi K, Takabatake H, Kitagawa H, Wada T, Honda M, Ohta T, Nakanuma Y, Kaneko S. 2015. Inflammatory features of pancreatic cancer highlighted by monocytes/macrophages and CD4+ T cells with clinical impact. Cancer Sci 106:672-86.

Koorstra JB, Feldmann G, Habbe N, Maitra A. 2008. Morphogenesis of pancreatic cancer: role of pancreatic intraepithelial neoplasia (PanINs). Langenbecks Arch Surg 393:561-70.

Kosmahl M, Pauser U, Peters K, Sipos B, Lüttges J, Kremer B, Klöppel G. 2004. Cystic neoplasms of the pancreas and tumor-like lesions with cystic features: a review of 418 cases and a classification proposal. Virchows Arch 445:168-78.

Kourko O, Seaver K, Odoardi N, Basta S, Gee K. 2019. IL-27, IL-30, and IL-35: A Cytokine Triumvirate in Cancer. Front Oncol 9:969.

Kovacs SB, Oh C, Aachoui Y, Miao EA. 2021. Evaluating cytokine production by flow cytometry using brefeldin A in mice. STAR Protoc 2:100244.

Kozuka S, Sassa R, Taki T, Masamoto K, Nagasawa S, Saga S, Hasegawa K, Takeuchi M. 1979. Relation of pancreatic duct hyperplasia to carcinoma. Cancer 43:1418-28.

Kranenburg O, Gebbink MF, Voest EE. 2004. Stimulation of angiogenesis by Ras proteins. Biochim Biophys Acta 1654:23-37.

Kroeger DR, Milne K, Nelson BH. 2016. Tumor-Infiltrating Plasma Cells Are Associated with Tertiary Lymphoid Structures, Cytolytic T-Cell Responses, and Superior Prognosis in Ovarian Cancer. Clin Cancer Res 22:3005-15.

Kubuschok B, Neumann F, Breit R, Sester M, Schormann C, Wagner C, Sester U, Hartmann F, Wagner M, Remberger K, Schilling M, Pfreundschuh M. 2006. Naturally occurring T-cell response against mutated p21 ras oncoprotein in pancreatic cancer. Clin Cancer Res 12:1365-72.

Kurahara H, Shinchi H, Mataki Y, Maemura K, Noma H, Kubo F, Sakoda M, Ueno S, Natsugoe S, Takao S. 2011. Significance of M2-polarized tumor-associated macrophage in pancreatic cancer. J Surg Res 167:e211-9.

Landau E, Kalnicki S. 2018. The Evolving Role of Radiation in Pancreatic Cancer. Surg Clin North Am 98:113-125.

Lane DP. 1992. Cancer. p53, guardian of the genome. Nature 358:15-6.
Lanfranca MP, Lazarus J, Shao X, Nathan H, Di Magliano MP, Zou W, Piert M, Frankel TL. 2018. Tracking Macrophage Infiltration in a Mouse Model of Pancreatic Cancer with the Positron Emission Tomography Tracer [11C]PBR28. J Surg Res 232:570-577.

Larkin J, Chiarion-Sileni V, Gonzalez R, Grob JJ, Rutkowski P, Lao CD, Cowey CL, Schadendorf D, Wagstaff J, Dummer R, Ferrucci PF, Smylie M, Hogg D, Hill A, Márquez-Rodas I, Haanen J, Guidoboni M, Maio M, Schöffski P, Carlino MS, Lebbé C, McArthur G, Ascierto PA, Daniels GA, Long GV, Bastholt L, Rizzo JI, Balogh A, Moshyk A, Hodi FS, Wolchok JD. 2019. Five-Year Survival with Combined Nivolumab and Ipilimumab in Advanced Melanoma. N Engl J Med 381:1535-1546.

Larousserie F, Charlot P, Bardel E, Froger J, Kastelein RA, Devergne O. 2006. Differential effects of IL-27 on human B cell subsets. J Immunol 176:5890-7.

Lasek W, Zagożdżon R, Jakobisiak M. 2014. Interleukin 12: still a promising candidate for tumor immunotherapy? Cancer Immunol Immunother 63:419-35.

Laskowski TJ, Hazen AL, Collazo RS, Haviland D. 2020. Rigor and Reproducibility of Cytometry Practices for Immuno-Oncology: A multifaceted challenge. Cytometry A 97:116-125.

Lawrence WG, Varadi G, Entine G, Podniesinski E, Wallace PK. 2008. Enhanced red and near infrared detection in flow cytometry using avalanche photodiodes. Cytometry A 73:767-76.

Lechner MG, Liebertz DJ, Epstein AL. 2010. Characterization of cytokine-induced myeloid-derived suppressor cells from normal human peripheral blood mononuclear cells. J Immunol 185:2273-84.

Lee CC, Lin JC, Hwang WL, Kuo YJ, Chen HK, Tai SK, Lin CC, Yang MH. 2018a. Macrophage-secreted interleukin-35 regulates cancer cell plasticity to facilitate metastatic colonization. Nat Commun 9:3763.

Lee CR, Lee W, Cho SK, Park SG. 2018b. Characterization of Multiple Cytokine Combinations and TGF-β on Differentiation and Functions of Myeloid-Derived Suppressor Cells. Int J Mol Sci 19.

Lee JW, Komar CA, Bengsch F, Graham K, Beatty GL. 2016a. Genetically Engineered Mouse Models of Pancreatic Cancer: The KPC Model (LSL-Kras(G12D/+) ;LSL-Trp53(R172H/+) ;Pdx-1-Cre), Its Variants, and Their Application in Immuno-oncology Drug Discovery. Curr Protoc Pharmacol 73:14.39.1-14.39.20.

Lee KE, Spata M, Bayne LJ, Buza EL, Durham AC, Allman D, Vonderheide RH, Simon MC. 2016b. Hif1a Deletion Reveals Pro-Neoplastic Function of B Cells in Pancreatic Neoplasia. Cancer Discov 6:256-69.

Lesina M, Kurkowski MU, Ludes K, Rose-John S, Treiber M, Kloppel G, Yoshimura A, Reindl W, Sipos B, Akira S, Schmid RM, Algul H. 2011. Stat3/Socs3 activation by IL-6 transsignaling promotes progression of pancreatic intraepithelial neoplasia and development of pancreatic cancer. Cancer Cell 19:456-69.

Lesokhin AM, Ansell SM, Armand P, Scott EC, Halwani A, Gutierrez M, Millenson MM, Cohen AD, Schuster SJ, Lebovic D, Dhodapkar M, Avigan D, Chapuy B, Ligon AH, Freeman GJ, Rodig SJ, Cattry D, Zhu L, Grosso JF, Bradley Garelik MB, Shipp MA, Borrello I, Timmerman J. 2016. Nivolumab in Patients With Relapsed or Refractory Hematologic Malignancy: Preliminary Results of a Phase Ib Study. J Clin Oncol 34:2698-704.

Leuschner F, Rauch PJ, Ueno T, Gorbatov R, Marinelli B, Lee WW, Dutta P, Wei Y, Robbins C, Iwamoto Y, Sena B, Chudnovskiy A, Panizzi P, Keliher E, Higgins JM, Libby P, Moskowitz MA, Pittet MJ, Swirski FK, Weissleder R, Nahrendorf M. 2012. Rapid monocyte kinetics in acute myocardial infarction are sustained by extramedullary monocytopoiesis. J Exp Med 209:123-37.

Li H, Shaham U, Stanton KP, Yao Y, Montgomery RR, Kluger Y. 2017. Gating mass cytometry data by deep learning. Bioinformatics 33:3423-3430.

Lim SA, Kim J, Jeon S, Shin MH, Kwon J, Kim TJ, Im K, Han Y, Kwon W, Kim SW, Yee C, Kim SJ, Jang JY, Lee KM. 2019. Defective Localization With Impaired Tumor Cytotoxicity Contributes to the Immune Escape of NK Cells in Pancreatic Cancer Patients. Front Immunol 10:496.

Lim SH, Sun JM, Lee SH, Ahn JS, Park K, Ahn MJ. 2016. Pembrolizumab for the treatment of non-small cell lung cancer. Expert Opin Biol Ther 16:397-406.
Lin JC, Liu TP, Yang PM. 2020a. CDKN2A-Inactivated Pancreatic Ductal Adenocarcinoma Exhibits Therapeutic Sensitivity to Paclitaxel: A Bioinformatics Study. J Clin Med 9.

Lin JH, Huffman AP, Wattenberg MM, Walter DM, Carpenter EL, Feldser DM, Beatty GL, Furth EE, Vonderheide RH. 2020b. Type 1 conventional dendritic cells are systemically dysregulated early in pancreatic carcinogenesis. J Exp Med 217.
Linard B, Bézieau S, Benlalam H, Labarrière N, Guilloux Y, Diez E, Jotereau F. 2002. A ras-mutated peptide targeted by CTL infiltrating a human melanoma lesion. J Immunol 168:4802-8.

Lines JL, Pantazi E, Mak J, Sempere LF, Wang L, O'Connell S, Ceeraz S, Suriawinata AA, Yan S, Ernstoff MS, Noelle R. 2014. VISTA is an immune checkpoint molecule for human T cells. Cancer Res 74:1924-32.

Liou GY, Bastea L, Fleming A, Doppler H, Edenfield BH, Dawson DW, Zhang L, Bardeesy N, Storz P. 2017a. The Presence of Interleukin-13 at Pancreatic ADM/PanIN Lesions Alters Macrophage Populations and Mediates Pancreatic Tumorigenesis. Cell Rep 19:1322-1333.

Liou GY, Bastea L, Fleming A, Döppler H, Edenfield BH, Dawson DW, Zhang L, Bardeesy N, Storz P. 2017b. The Presence of Interleukin-13 at Pancreatic ADM/PanIN Lesions Alters Macrophage Populations and Mediates Pancreatic Tumorigenesis. Cell Rep 19:1322-1333.

Liou GY, Döppler H, Braun UB, Panayiotou R, Scotti Buzhardt M, Radisky DC, Crawford HC, Fields AP, Murray NR, Wang QJ, Leitges M, Storz P. 2015a. Protein kinase D1 drives pancreatic acinar cell reprogramming and progression to intraepithelial neoplasia. Nat Commun 6:6200.

Liou GY, Döppler H, Necela B, Edenfield B, Zhang L, Dawson DW, Storz P. 2015b. Mutant KRAS-induced expression of ICAM-1 in pancreatic acinar cells causes attraction of macrophages to expedite the formation of precancerous lesions. Cancer Discov 5:52-63.

Liou GY, Döppler H, Necela B, Krishna M, Crawford HC, Raimondo M, Storz P. 2013. Macrophage-secreted cytokines drive pancreatic acinar-to-ductal metaplasia through NF-κB and MMPs. J Cell Biol 202:563-77.

Liou GY, Storz P. 2015. Inflammatory macrophages in pancreatic acinar cell metaplasia and initiation of pancreatic cancer. Oncoscience 2:247-51.

Liu P, Wang Y, Li X. 2019. Targeting the untargetable KRAS in cancer therapy. Acta Pharm Sin B 9:871-879.

Liu Z, Liu JQ, Talebian F, Wu LC, Li S, Bai XF. 2013. IL-27 enhances the survival of tumor antigen-specific CD8+ T cells and programs them into IL-10-producing, memory precursor-like effector cells. Eur J Immunol 43:468-79.

Livak KJ, Schmittgen TD. 2001. Analysis of relative gene expression data using real-time quantitative PCR and the 2(-Delta Delta C(T)) Method. Methods 25:402-8.

Lo A, Wang LS, Scholler J, Monslow J, Avery D, Newick K, O'Brien S, Evans RA, Bajor DJ, Clendenin C, Durham AC, Buza EL, Vonderheide RH, June CH, Albelda SM, Puré E. 2015. Tumor-Promoting Desmoplasia Is Disrupted by Depleting FAP-Expressing Stromal Cells. Cancer Res 75:2800-2810.

Loder F, Mutschler B, Ray RJ, Paige CJ, Sideras P, Torres R, Lamers MC, Carsetti R. 1999. B cell development in the spleen takes place in discrete steps and is determined by the quality of B cell receptor-derived signals. J Exp Med 190:75-89.

Löhr M, Klöppel G, Maisonneuve P, Lowenfels AB, Lüttges J. 2005. Frequency of K-ras mutations in pancreatic intraductal neoplasias associated with pancreatic ductal adenocarcinoma and chronic pancreatitis: a meta-analysis. Neoplasia 7:17-23.

Lonardo E, Frias-Aldeguer J, Hermann PC, Heeschen C. 2012. Pancreatic stellate cells form a niche for cancer stem cells and promote their self-renewal and invasiveness. Cell Cycle 11:1282-90.

Loncle C, Bonjoch L, Folch-Puy E, Lopez-Millan MB, Lac S, Molejon MI, Chuluyan E, Cordelier P, Dubus P, Lomberk G, Urrutia R, Closa D, Iovanna JL. 2015. IL17 Functions through the Novel REG3β-JAK2-STAT3 Inflammatory Pathway to Promote the Transition from Chronic Pancreatitis to Pancreatic Cancer. Cancer Res 75:4852-62.

Lowenfels AB, Maisonneuve P, Cavallini G, Ammann RW, Lankisch PG, Andersen JR, Dimagno EP, Andrén-Sandberg A, Domellöf L. 1993. Pancreatitis and the risk of pancreatic cancer. International Pancreatitis Study Group. N Engl J Med 328:1433-7.

Lowenfels AB, Maisonneuve P, DiMagno EP, Elitsur Y, Gates LK, Jr., Perrault J, Whitcomb DC. 1997. Hereditary pancreatitis and the risk of pancreatic cancer. International Hereditary Pancreatitis Study Group. J Natl Cancer Inst 89:442-6.

Lucenteforte E, La Vecchia C, Silverman D, Petersen GM, Bracci PM, Ji BT, Bosetti C, Li D, Gallinger S, Miller AB, Bueno-de-Mesquita HB, Talamini R, Polesel J, Ghadirian P, Baghurst PA, Zatonski W, Fontham E, Bamlet WR, Holly EA, Gao YT, Negri E, Hassan M, Cotterchio M, Su J, Maisonneuve P, Boffetta P, Duell EJ. 2012. Alcohol consumption and pancreatic cancer: a pooled analysis in the International Pancreatic Cancer Case-Control Consortium (PanC4). Ann Oncol 23:374-82.

Lüttges J, Feyerabend B, Buchelt T, Pacena M, Klöppel G. 2002. The mucin profile of noninvasive and invasive mucinous cystic neoplasms of the pancreas. Am J Surg Pathol 26:466-71.

Lüttges J, Galehdari H, Bröcker V, Schwarte-Waldhoff I, Henne-Bruns D, Klöppel G, Schmiegel W, Hahn SA. 2001. Allelic loss is often the first hit in the biallelic inactivation of the p53 and DPC4 genes during pancreatic carcinogenesis. Am J Pathol 158:1677-83.

Lynch SM, Vrieling A, Lubin JH, Kraft P, Mendelsohn JB, Hartge P, Canzian F, Steplowski E, Arslan AA, Gross M, Helzlsouer K, Jacobs EJ, LaCroix A, Petersen G, Zheng W, Albanes D, Amundadottir L, Bingham SA, Boffetta P, Boutron-Ruault MC, Chanock SJ, Clipp S, Hoover RN, Jacobs K, Johnson KC, Kooperberg C, Luo J, Messina C, Palli D, Patel AV, Riboli E, Shu XO, Rodriguez Suarez L, Thomas G, Tjønneland A, Tobias GS, Tong E, Trichopoulos D, Virtamo J, Ye W, Yu K, Zeleniuch-Jacquette A, Bueno-de-Mesquita HB, Stolzenberg-Solomon RZ. 2009. Cigarette smoking and pancreatic cancer: a pooled analysis from the pancreatic cancer cohort consortium. Am J Epidemiol 170:403-13.

Magnuson MA, Osipovich AB. 2013. Pancreas-specific Cre driver lines and considerations for their prudent use. Cell Metab 18:9-20.

Mahajan UM, Langhoff E, Goni E, Costello E, Greenhalf W, Halloran C, Ormanns S, Kruger S, Boeck S, Ribback S, Beyer G, Dombroswki F, Weiss FU, Neoptolemos JP, Werner J, D'Haese JG, Bazhin A, Peterhansl J, Pichlmeier S, Büchler MW, Kleeff J, Ganeh P, Sendler M, Palmer DH, Kohlmann T, Rad R, Regel I, Lerch MM, Mayerle J. 2018. Immune Cell and Stromal Signature Associated With Progression-Free Survival of Patients With Resected Pancreatic Ductal Adenocarcinoma. Gastroenterology 155:1625-1639.e2.

Mahnke YD, Roederer M. 2007. Optimizing a multicolor immunophenotyping assay. Clin Lab Med 27:469-85, v.

Maisonneuve P, Amar S, Lowenfels AB. 2017. Periodontal disease, edentulism, and pancreatic cancer: a meta-analysis. Ann Oncol 28:985-995.

Maisonneuve P, Marshall BC, Lowenfels AB. 2007. Risk of pancreatic cancer in patients with cystic fibrosis. Gut 56:1327-8.

Maitra A, Adsay NV, Argani P, Iacobuzio-Donahue C, De Marzo A, Cameron JL, Yeo CJ, Hruban RH. 2003. Multicomponent analysis of the pancreatic adenocarcinoma progression model using a pancreatic intraepithelial neoplasia tissue microarray. Mod Pathol 16:902-12.

Majumder K, Arora N, Modi S, Chugh R, Nomura A, Giri B, Dawra R, Ramakrishnan S, Banerjee S, Saluja A, Dudeja V. 2016. A Novel Immunocompetent Mouse Model of Pancreatic Cancer with Robust Stroma: a Valuable Tool for Preclinical Evaluation of New Therapies. J Gastrointest Surg 20:53-65; discussion 65.

Maker AV, Katabi N, Qin LX, Klimstra DS, Schattner M, Brennan MF, Jarnagin WR, Allen PJ. 2011. Cyst fluid interleukin-1beta (IL1beta) levels predict the risk of carcinoma in intraductal papillary mucinous neoplasms of the pancreas. Clin Cancer Res 17:1502-8.

Malka D, Hammel P, Maire F, Rufat P, Madeira I, Pessione F, Lévy P, Ruszniewski P. 2002. Risk of pancreatic adenocarcinoma in chronic pancreatitis. Gut 51:849-52.

Mallya K, Haridas D, Seshacharyulu P, Pothuraju R, Junker WM, Krishn SR, Muniyan S, Vengoji R, Batra SK, Rachagani S. 2020. Acinar transformed ductal cells exhibit differential mucin expression in a tamoxifen-induced pancreatic ductal adenocarcinoma mouse model. Biol Open 9.

Marcon F, Zuo J, Pearce H, Nicol S, Margielewska-Davies S, Farhat M, Mahon B, Middleton G, Brown R, Roberts KJ, Moss P. 2020. NK cells in pancreatic cancer demonstrate impaired cytotoxicity and a regulatory IL-10 phenotype. Oncoimmunology 9:1845424.

Marigo I, Bosio E, Solito S, Mesa C, Fernandez A, Dolcetti L, Ugel S, Sonda N, Bicciato S, Falisi E, Calabrese F, Basso G, Zanovello P, Cozzi E, Mandruzzato S, Bronte V. 2010. Tumor-induced tolerance and immune suppression depend on the C/EBPbeta transcription factor. Immunity 32:790-802.

Marthey L, Sa-Cunha A, Blanc JF, Gauthier M, Cueff A, Francois E, Trouilloud I, Malka D, Bachet JB, Coriat R, Terrebonne E, De La Fouchardière C, Manfredi S, Solub D, Lécaille C, Thirot Bidault A, Carbonnel F, Taieb J. 2015. FOLFIRINOX for locally advanced pancreatic adenocarcinoma: results of an AGEO multicenter prospective observational cohort. Ann Surg Oncol 22:295-301.

Masia R, Mino-Kenudson M, Warshaw AL, Pitman MB, Misdraji J. 2011. Pancreatic mucinous cystic neoplasm of the main pancreatic duct. Arch Pathol Lab Med 135:264-7.

Matsuda Y, Furukawa T, Yachida S, Nishimura M, Seki A, Nonaka K, Aida J, Takubo K, Ishiwata T, Kimura W, Arai T, Mino-Kenudson M. 2017. The Prevalence and Clinicopathological Characteristics of High-Grade Pancreatic Intraepithelial Neoplasia: Autopsy Study Evaluating the Entire Pancreatic Parenchyma. Pancreas 46:658-664.

Matsuda Y, Ishiwata T, Izumiyama-Shimomura N, Hamayasu H, Fujiwara M, Tomita K, Hiraishi N, Nakamura K, Ishikawa N, Aida J, Takubo K, Arai T. 2015. Gradual telomere shortening and increasing chromosomal instability among PanIN grades and normal ductal epithelia with and without cancer in the pancreas. PLoS One 10:e0117575.

Matsuo Y, Ochi N, Sawai H, Yasuda A, Takahashi H, Funahashi H, Takeyama H, Tong Z, Guha S. 2009. CXCL8/IL-8 and CXCL12/SDF-1alpha co-operatively promote invasiveness and angiogenesis in pancreatic cancer. Int J Cancer 124:853-61.

Matsushita H, Vesely MD, Koboldt DC, Rickert CG, Uppaluri R, Magrini VJ, Arthur CD, White JM, Chen YS, Shea LK, Hundal J, Wendl MC, Demeter R, Wylie T, Allison JP, Smyth MJ, Old LJ, Mardis ER, Schreiber RD. 2012. Cancer exome analysis reveals a T-cell-dependent mechanism of cancer immunoediting. Nature 482:400-4.

Mayer J, Rau B, Gansauge F, Beger HG. 2000. Inflammatory mediators in human acute pancreatitis: clinical and pathophysiological implications. Gut 47:546-52.

McAllister F, Bailey JM, Alsina J, Nirschl CJ, Sharma R, Fan H, Rattigan Y, Roeser JC, Lankapalli RH, Zhang H, Jaffee EM, Drake CG, Housseau F, Maitra A, Kolls JK, Sears CL, Pardoll DM, Leach SD. 2014. Oncogenic Kras activates a hematopoietic-to-epithelial IL-17 signaling axis in preinvasive pancreatic neoplasia. Cancer Cell 25:621-37.

McGowan PF, Hyter SD, Cui W, Plummer RM, Godwin AK, Zhang D. 2022. Comparison of flow cytometry and next-generation sequencing in minimal residual disease monitoring of acute myeloid leukemia: One institute's practical clinical experience. Int J Lab Hematol 44:118-126.

McKelvey KJ, Hudson AL, Prasanna Kumar R, Wilmott JS, Attrill GH, Long GV, Scolyer RA, Clarke SJ, Wheeler HR, Diakos CI, Howell VM. 2020. Temporal and spatial modulation of the tumor and systemic immune response in the murine Gl261 glioma model. PLOS ONE 15:e0226444.

McWilliams RR, Petersen GM, Rabe KG, Holtegaard LM, Lynch PJ, Bishop MD, Highsmith WE, Jr. 2010. Cystic fibrosis transmembrane conductance regulator (CFTR) gene mutations and risk for pancreatic adenocarcinoma. Cancer 116:203-9.

Menees KB, Earls RH, Chung J, Jernigan J, Filipov NM, Carpenter JM, Lee JK. 2021. Sex- and age-dependent alterations of splenic immune cell profile and NK cell phenotypes and function in C57BL/6J mice. Immun Ageing 18:3.

Meng Q, Liu Z, Rangelova E, Poiret T, Ambati A, Rane L, Xie S, Verbeke C, Dodoo E, Del Chiaro M, Löhr M, Segersvärd R, Maeurer MJ. 2016. Expansion of Tumor-reactive T Cells From Patients With Pancreatic Cancer. J Immunother 39:81-9.

Meyers JH, Sabatos CA, Chakravarti S, Kuchroo VK. 2005. The TIM gene family regulates autoimmune and allergic diseases. Trends Mol Med 11:362-9.

Millikan KW, Deziel DJ, Silverstein JC, Kanjo TM, Christein JD, Doolas A, Prinz RA. 1999. Prognostic factors associated with resectable adenocarcinoma of the head of the pancreas. Am Surg 65:618-23; discussion 623-4.

Minici C, Rigamonti E, Lanzillotta M, Monno A, Rovati L, Maehara T, Kaneko N, Deshpande V, Protti MP, De Monte L, Scielzo C, Crippa S, Arcidiacono PG, Dugnani E, Piemonti L, Falconi M, Pillai S, Manfredi AA, Della-Torre E. 2020. B lymphocytes contribute to stromal reaction in pancreatic ductal adenocarcinoma. Oncoimmunology 9:1794359.

Mirlekar B, Michaud D, Lee SJ, Kren NP, Harris C, Greene K, Goldman EC, Gupta GP, Fields RC, Hawkins WG, DeNardo DG, Rashid NU, Yeh JJ, McRee AJ, Vincent BG, Vignali DAA, Pylayeva-Gupta Y. 2020. B cell-Derived IL35 Drives STAT3-Dependent CD8(+) T-cell Exclusion in Pancreatic Cancer. Cancer Immunol Res 8:292-308.

Mirlekar B, Michaud D, Searcy R, Greene K, Pylayeva-Gupta Y. 2018. IL35 Hinders Endogenous Antitumor T-cell Immunity and Responsiveness to Immunotherapy in Pancreatic Cancer. Cancer Immunol Res 6:1014-1024.

Mirlekar B, Wang Y, Li S, Zhou M, Entwistle S, De Buysscher T, Morrison A, Herrera G, Harris C, Vincent BG, Ting JP, Rashid N, Kim WY, Yeh JJ, Pylayeva-Gupta Y. 2022. Balance between immunoregulatory B cells and plasma cells drives pancreatic tumor immunity. Cell Rep Med 3:100744.

Mitra A, Satelli A, Yan J, Xueqing X, Gagea M, Hunter CA, Mishra L, Li S. 2014. IL-30 (IL27p28) attenuates liver fibrosis through inducing NKG2D-rae1 interaction between NKT and activated hepatic stellate cells in mice. Hepatology 60:2027-39.

Mitsunaga S, Ikeda M, Shimizu S, Ohno I, Furuse J, Inagaki M, Higashi S, Kato H, Terao K, Ochiai A. 2013. Serum levels of IL-6 and IL-1β can predict the efficacy of gemcitabine in patients with advanced pancreatic cancer. Br J Cancer 108:2063-9. Mizrahi JD, Surana R, Valle JW, Shroff RT. 2020. Pancreatic cancer. Lancet 395:2008-2020.

Moffitt RA, Marayati R, Flate EL, Volmar KE, Loeza SG, Hoadley KA, Rashid NU, Williams LA, Eaton SC, Chung AH, Smyla JK, Anderson JM, Kim HJ, Bentrem DJ, Talamonti MS, Iacobuzio-Donahue CA, Hollingsworth MA, Yeh JJ. 2015. Virtual microdissection identifies distinct tumor- and stroma-specific subtypes of pancreatic ductal adenocarcinoma. Nat Genet 47:1168-78.

Mole RH. 1953. Whole body irradiation; radiobiology or medicine? Br J Radiol 26:234-41.

Moo-Young TA, Larson JW, Belt BA, Tan MC, Hawkins WG, Eberlein TJ, Goedegebuure PS, Linehan DC. 2009. Tumor-derived TGF-beta mediates conversion of CD4+Foxp3+ regulatory T cells in a murine model of pancreas cancer. J Immunother 32:12-21.

Moodie SA, Willumsen BM, Weber MJ, Wolfman A. 1993. Complexes of Ras.GTP with Raf-1 and mitogen-activated protein kinase kinase. Science 260:1658-61.

Morales JK, Kmieciak M, Knutson KL, Bear HD, Manjili MH. 2010. GM-CSF is one of the main breast tumor-derived soluble factors involved in the differentiation of CD11b-Gr1- bone marrow progenitor cells into myeloid-derived suppressor cells. Breast Cancer Res Treat 123:39-49.

Mori M, Rao SK, Popper HH, Cagle PT, Fraire AE. 2001. Atypical adenomatous hyperplasia of the lung: a probable forerunner in the development of adenocarcinoma of the lung. Mod Pathol 14:72-84.

Morris JPt, Wang SC, Hebrok M. 2010. KRAS, Hedgehog, Wnt and the twisted developmental biology of pancreatic ductal adenocarcinoma. Nat Rev Cancer 10:683-95.

Moskaluk CA, Hruban RH, Kern SE. 1997. p16 and K-ras gene mutations in the intraductal precursors of human pancreatic adenocarcinoma. Cancer Res 57:2140-3.

Movahedi K, Guilliams M, Van den Bossche J, Van den Bergh R, Gysemans C, Beschin A, De Baetselier P, Van Ginderachter JA. 2008. Identification of discrete tumor-induced myeloid-derived suppressor cell subpopulations with distinct T cell-suppressive activity. Blood 111:4233-44.

Mullan MH, Gauger PG, Thompson NW. 2001. Endocrine tumours of the pancreas: review and recent advances. ANZ J Surg 71:475-82.

Mundy-Bosse BL, Young GS, Bauer T, Binkley E, Bloomston M, Bill MA, Bekaii-Saab T, Carson WE, 3rd, Lesinski GB. 2011. Distinct myeloid suppressor cell subsets correlate with plasma IL-6 and IL-10 and reduced interferon-alpha signaling in $CD4^+$ T cells from patients with GI malignancy. Cancer Immunol Immunother 60:1269-79.

Munigala S, Singh A, Gelrud A, Agarwal B. 2015. Predictors for Pancreatic Cancer Diagnosis Following New-Onset Diabetes Mellitus. Clin Transl Gastroenterol 6:e118.
Murakami M, Kamimura D, Hirano T. 2019. Pleiotropy and Specificity: Insights from the Interleukin 6 Family of Cytokines. Immunity 50:812-831.

Murphy KM, Brune KA, Griffin C, Sollenberger JE, Petersen GM, Bansal R, Hruban RH, Kern SE. 2002. Evaluation of candidate genes MAP2K4, MADH4, ACVR1B, and BRCA2 in familial pancreatic cancer: deleterious BRCA2 mutations in 17%. Cancer Res 62:3789-93.

Murray PJ, Allen JE, Biswas SK, Fisher EA, Gilroy DW, Goerdt S, Gordon S, Hamilton JA, Ivashkiv LB, Lawrence T, Locati M, Mantovani A, Martinez FO, Mege JL, Mosser DM, Natoli G, Saeij JP, Schultze JL, Shirey KA, Sica A, Suttles J, Udalova I, van Ginderachter JA, Vogel SN, Wynn TA. 2014. Macrophage activation and polarization: nomenclature and experimental guidelines. Immunity 41:14-20.

Nathan CF, Murray HW, Wiebe ME, Rubin BY. 1983. Identification of interferon-gamma as the lymphokine that activates human macrophage oxidative metabolism and antimicrobial activity. J Exp Med 158:670-89.

Neesse A, Algül H, Tuveson DA, Gress TM. 2015. Stromal biology and therapy in pancreatic cancer: a changing paradigm. Gut 64:1476-84.

Neoptolemos JP, Palmer DH, Ghaneh P, Psarelli EE, Valle JW, Halloran CM, Faluyi O, O'Reilly DA, Cunningham D, Wadsley J, Darby S, Meyer T, Gillmore R, Anthoney A, Lind P, Glimelius B, Falk S, Izbicki JR, Middleton GW, Cummins S, Ross PJ, Wasan H, McDonald A, Crosby T, Ma YT, Patel K, Sherriff D, Soomal R, Borg D, Sothi S, Hammel P, Hackert T, Jackson R, Büchler MW. 2017. Comparison of adjuvant gemcitabine and capecitabine with gemcitabine monotherapy in patients with resected pancreatic cancer (ESPAC-4): a multicentre, open-label, randomised, phase 3 trial. Lancet 389:1011-1024.

Neoptolemos JP, Stocken DD, Bassi C, Ghaneh P, Cunningham D, Goldstein D, Padbury R, Moore MJ, Gallinger S, Mariette C, Wente MN, Izbicki JR, Friess H, Lerch MM, Dervenis C, Oláh A, Butturini G, Doi R, Lind PA, Smith D, Valle JW, Palmer DH, Buckels JA, Thompson J, McKay CJ, Rawcliffe CL, Büchler MW. 2010. Adjuvant chemotherapy with fluorouracil plus folinic acid vs gemcitabine following pancreatic cancer resection: a randomized controlled trial. Jama 304:1073-81.

Neoptolemos JP, Stocken DD, Friess H, Bassi C, Dunn JA, Hickey H, Beger H, Fernandez-Cruz L, Dervenis C, Lacaine F, Falconi M, Pederzoli P, Pap A, Spooner D, Kerr DJ, Büchler MW. 2004. A randomized trial of chemoradiotherapy and chemotherapy after resection of pancreatic cancer. N Engl J Med 350:1200-10.

Nguyen R, Perfetto S, Mahnke YD, Chattopadhyay P, Roederer M. 2013. Quantifying spillover spreading for comparing instrument performance and aiding in multicolor panel design. Cytometry A 83:306-15.

Nicholl MB, Ledgewood CL, Chen X, Bai Q, Qin C, Cook KM, Herrick EJ, Diaz-Arias A, Moore BJ, Fang Y. 2014. IL-35 promotes pancreas cancer growth through enhancement of proliferation and inhibition of apoptosis: evidence for a role as an autocrine growth factor. Cytokine 70:126-33.

Nielsen SR, Strøbech JE, Horton ER, Jackstadt R, Laitala A, Bravo MC, Maltese G, Jensen ARD, Reuten R, Rafaeva M, Karim SA, Hwang CI, Arnes L, Tuveson DA, Sansom OJ, Morton JP, Erler JT. 2021. Suppression of tumor-associated neutrophils by lorlatinib attenuates pancreatic cancer growth and improves treatment with immune checkpoint blockade. Nat Commun 12:3414.

Niewold P, Ashhurst TM, Smith AL, King NJC. 2020. Evaluating spectral cytometry for immune profiling in viral disease. Cytometry A 97:1165-1179.

Nojima T, Kojima T, Kato H, Sato T, Koito K, Nagashima K. 1992. Alpha-fetoprotein-producing acinar cell carcinoma of the pancreas. Hum Pathol 23:828-30.

Nolan JP, Condello D. 2013. Spectral flow cytometry. Curr Protoc Cytom Chapter 1:Unit1.27.

Nouël A, Pochard P, Simon Q, Ségalen I, Le Meur Y, Pers JO, Hillion S. 2015. B-Cells induce regulatory T cells through TGF-β/IDO production in A CTLA-4 dependent manner. J Autoimmun 59:53-60.

O'Malley FP. 2010. Lobular neoplasia: morphology, biological potential and management in core biopsies. Mod Pathol 23 Suppl 2:S14-25.

O'Malley FP, Mohsin SK, Badve S, Bose S, Collins LC, Ennis M, Kleer CG, Pinder SE, Schnitt SJ. 2006. Interobserver reproducibility in the diagnosis of flat epithelial atypia of the breast. Mod Pathol 19:172-9.

O'Reilly EM, Oh DY, Dhani N, Renouf DJ, Lee MA, Sun W, Fisher G, Hezel A, Chang SC, Vlahovic G, Takahashi O, Yang Y, Fitts D, Philip PA. 2019. Durvalumab With or Without Tremelimumab for Patients With Metastatic Pancreatic Ductal Adenocarcinoma: A Phase 2 Randomized Clinical Trial. JAMA Oncol 5:1431-1438.

Oettle H, Neuhaus P, Hochhaus A, Hartmann JT, Gellert K, Ridwelski K, Niedergethmann M, Zülke C, Fahlke J, Arning MB, Sinn M, Hinke A, Riess H. 2013. Adjuvant chemotherapy with gemcitabine and long-term outcomes among patients with resected pancreatic cancer: the CONKO-001 randomized trial. Jama 310:1473-81.

Oettle H, Post S, Neuhaus P, Gellert K, Langrehr J, Ridwelski K, Schramm H, Fahlke J, Zuelke C, Burkart C, Gutberlet K, Kettner E, Schmalenberg H, Weigang-Koehler K, Bechstein WO, Niedergethmann M, Schmidt-Wolf I, Roll L, Doerken B, Riess H. 2007. Adjuvant chemotherapy with gemcitabine vs observation in patients undergoing curative-intent resection of pancreatic cancer: a randomized controlled trial. Jama 297:267-77.

Ogino S, Goel A. 2008. Molecular classification and correlates in colorectal cancer. J Mol Diagn 10:13-27.

Olive KP, Tuveson DA, Ruhe ZC, Yin B, Willis NA, Bronson RT, Crowley D, Jacks T. 2004. Mutant p53 gain of function in two mouse models of Li-Fraumeni syndrome. Cell 119:847-60.

Olivier M, Eeles R, Hollstein M, Khan MA, Harris CC, Hainaut P. 2002. The IARC TP53 database: new online mutation analysis and recommendations to users. Hum Mutat 19:607-14.

Page DL, Dupont WD, Rogers LW, Landenberger M. 1982. Intraductal carcinoma of the breast: follow-up after biopsy only. Cancer 49:751-8.

Park W, Chawla A, O'Reilly EM. 2021. Pancreatic Cancer: A Review. Jama 326:851-862.

Peng PJ, Li Y, Sun S. 2017. On the significance of Tim-3 expression in pancreatic cancer. Saudi J Biol Sci 24:1754-1757.

Peng YP, Xi CH, Zhu Y, Yin LD, Wei JS, Zhang JJ, Liu XC, Guo S, Fu Y, Miao Y. 2016. Altered expression of CD226 and CD96 on natural killer cells in patients with pancreatic cancer. Oncotarget 7:66586-66594.

Peters MLB, Eckel A, Mueller PP, Tramontano AC, Weaver DT, Lietz A, Hur C, Kong CY, Pandharipande PV. 2018. Progression to pancreatic ductal adenocarcinoma from pancreatic intraepithelial neoplasia: Results of a simulation model. Pancreatology 18:928-934.

Petes C, Mintsopoulos V, Finnen RL, Banfield BW, Gee K. 2018. The effects of CD14 and IL-27 on induction of endotoxin tolerance in human monocytes and macrophages. J Biol Chem 293:17631-17645.

Petes C, Wynick C, Guzzo C, Mehta D, Logan S, Banfield BW, Basta S, Cooper A, Gee K. 2017. IL-27 enhances LPS-induced IL-1β in human monocytes and murine macrophages. J Leukoc Biol 102:83-94.

Philip PA, Lacy J, Portales F, Sobrero A, Pazo-Cid R, Manzano Mozo JL, Kim EJ, Dowden S, Zakari A, Borg C, Terrebonne E, Rivera F, Sastre J, Bathini V, López-Trabada D, Asselah J, Saif MW, Shiansong Li J, Ong TJ, Nydam T, Hammel P. 2020. Nab-paclitaxel plus gemcitabine in patients with locally advanced pancreatic cancer (LAPACT): a multicentre, open-label phase 2 study. Lancet Gastroenterol Hepatol 5:285-294.

Pinchuk LM, Filipov NM. 2008. Differential effects of age on circulating and splenic leukocyte populations in C57BL/6 and BALB/c male mice. Immun Ageing 5:1.

Pinder SE, Ellis IO. 2003. The diagnosis and management of pre-invasive breast disease: ductal carcinoma in situ (DCIS) and atypical ductal hyperplasia (ADH)--current definitions and classification. Breast Cancer Res 5:254-7.

Plesca I, Benešová I, Beer C, Sommer U, Müller L, Wehner R, Heiduk M, Aust D, Baretton G, Bachmann MP, Feldmann A, Weitz J, Seifert L, Seifert AM, Schmitz M. 2022. Clinical Significance of Tumor-Infiltrating Conventional and Plasmacytoid Dendritic Cells in Pancreatic Ductal Adenocarcinoma. Cancers (Basel) 14.

Porembka MR, Mitchem JB, Belt BA, Hsieh CS, Lee HM, Herndon J, Gillanders WE, Linehan DC, Goedegebuure P. 2012. Pancreatic adenocarcinoma induces bone marrow mobilization of myeloid-derived suppressor cells which promote primary tumor growth. Cancer Immunol Immunother 61:1373-85.

Potter NS, Harding CV. 2001. Neutrophils process exogenous bacteria via an alternate class I MHC processing pathway for presentation of peptides to T lymphocytes. J Immunol 167:2538-46.

Pouget JP, Georgakilas AG, Ravanat JL. 2018. Targeted and Off-Target (Bystander and Abscopal) Effects of Radiation Therapy: Redox Mechanisms and Risk/Benefit Analysis. Antioxid Redox Signal 29:1447-1487.

Pourshams A, Sepanlou SG, Ikuta KS, Bisignano C, Saeid Safiri GR, Mehdi Sharif, Morteza Khatibian, Christina Fitzmaurice, Molly R Nixon, Nooshin Abbasi, Mohsen Afarideh, Elham Ahmadian, Tomi Akinyemiju, Fares Alahdab, Tahiya Alam, Vahid Alipour, Christine A Allen, Nahla Hamed Anber, Alireza Ansari-Moghaddam, Jalal Arabloo, Alaa Badawi, Mojtaba Bagherzadeh, Yaschilal Muche Belayneh, Belete Biadgo, Ali Bijani, Antonio Biondi, Tone Bjørge, Antonio M Borzì, Cristina Bosetti, Andrey Nikolaevich Briko, Nikolay Ivanovich Briko, Giulia Carreras, Félix Carvalho, Jee-Young J Choi, Dinh-Toi Chu, Anh Kim Dang, Ahmad Daryani, Dragos Virgil Davitoiu, Gebre Teklemariam Demoz, Rupak Desai, Subhojit Dey, Hoa Thi Do, Huyen Phuc Do, Aziz Eftekhari, Alireza Esteghamati, Farshad Farzadfar, Eduarda Fernandes, Irina Filip, Florian Fischer, Masoud Foroutan, Mohamed M Gad, Silvano Gallus, Birhanu Geta, Giuseppe Gorini, Nima Hafezi-Nejad, James D Harvey, Milad Hasankhani, Amir Hasanzadeh, Soheil Hassanipour, Simon I Hay, Hagos D Hidru, Chi Linh Hoang, Sorin Hostiuc, Mowafa Househ, Olayinka Stephen Ilesanmi, Milena D Ilic, Seyed Sina Naghibi Irvani, Nader Jafari Balalami, Spencer L James, Farahnaz Joukar, Amir Kasaeian, Tesfaye Dessale Kassa, Andre Pascal Kengne, Rovshan Khalilov, Ejaz Ahmad Khan, Amir Khater, Fatemeh Khosravi Shadmani, Jonathan M Kocarnik, Hamidreza Komaki, Ai Koyanagi, Vivek Kumar, Carlo La Vecchia, Platon D Lopukhov, Farzad Manafi, Navid Manafi, Ana-Laura Manda, Fariborz Mansour-Ghanaei, Dhruv Mehta, Varshil Mehta, Toni Meier, Hagazi Gebre Meles, Getnet Mengistu, Tomasz Miazgowski, Mehdi Mohamadnejad, Abdollah Mohammadian-Hafshejani, Milad Mohammadoo-Khorasani, Shafiu Mohammed, Farnam Mohebi, Ali H Mokdad, Lorenzo Monasta, Maryam Moossavi, Rahmatollah Moradzadeh, Gurudatta Naik, Ionut Negoi, Cuong Tat Nguyen, Long Hoang Nguyen, Trang Huyen Nguyen, Andrew T Olagunju, Tinuke O Olagunju, Alyssa Pennini, Mohammad Rabiee, Navid Rabiee, Amir Radfar, Mahdi Rahimi, Goura Kishor Rath, David Laith Rawaf, Salman Rawaf, Robert C Reiner Jr, Nima Rezaei, Aziz Rezapour, Anas M Saad, Seyedmohammad Saadatagah, Amirhossein Sahebkar, Hamideh Salimzadeh, Abdallah M Samy, Juan Sanabria, Arash Sarveazad, Monika Sawhney, Mario Sekerija, Pavel Shabalkin, Masood Ali Shaikh, Rajesh Sharma, Sara Sheikhbahaei, Reza Shirkoohi, Sudeep K Siddappa Malleshappa, Mekonnen Sisay,

Kjetil Soreide, Sergey Soshnikov, Rasoul Sotoudehmanesh, Vladimir I Starodubov, Michelle L Subart, Rafael Tabarés-Seisdedos, Degena Bahray Bahrey Tadesse, Eugenio Traini, Bach Xuan Tran, Khanh Bao Tran, Irfan Ullah, Marco Vacante, Amir Vahedian-Azimi, Elena Varavikova, Ronny Westerman, Dawit Dawit Zewdu Wondafrash, Rixing Xu, Naohiro Yonemoto, Vesna Zadnik, Zhi-Jiang Zhang, Reza Malekzadeh, Mohsen Naghavi. 2019. The global, regional, and national burden of pancreatic cancer and its attributable risk factors in 195 countries and territories, 1990-2017: a systematic analysis for the Global Burden of Disease Study 2017. Lancet Gastroenterol Hepatol 4:934-947.

Powell SM, Zilz N, Beazer-Barclay Y, Bryan TM, Hamilton SR, Thibodeau SN, Vogelstein B, Kinzler KW. 1992. APC mutations occur early during colorectal tumorigenesis. Nature 359:235-7.

Prehn RT, Main JM. 1957. Immunity to methylcholanthrene-induced sarcomas. J Natl Cancer Inst 18:769-78.

Principe DR, DeCant B, Mascariñas E, Wayne EA, Diaz AM, Akagi N, Hwang R, Pasche B, Dawson DW, Fang D, Bentrem DJ, Munshi HG, Jung B, Grippo PJ. 2016. TGFβ Signaling in the Pancreatic Tumor Microenvironment Promotes Fibrosis and Immune Evasion to Facilitate Tumorigenesis. Cancer Res 76:2525-39.

Prior IA, Lewis PD, Mattos C. 2012. A comprehensive survey of Ras mutations in cancer. Cancer Res 72:2457-67.

Protti MP, De Monte L. 2013. Immune infiltrates as predictive markers of survival in pancreatic cancer patients. Front Physiol 4:210.

Provenzano PP, Cuevas C, Chang AE, Goel VK, Von Hoff DD, Hingorani SR. 2012. Enzymatic targeting of the stroma ablates physical barriers to treatment of pancreatic ductal adenocarcinoma. Cancer Cell 21:418-29.

Pu N, Zhao G, Yin H, Li JA, Nuerxiati A, Wang D, Xu X, Kuang T, Jin D, Lou W, Wu W. 2018a. CD25 and TGF-beta blockade based on predictive integrated immune ratio inhibits tumor growth in pancreatic cancer. J Transl Med 16:294.

Pu N, Zhao G, Yin H, Li JA, Nuerxiati A, Wang D, Xu X, Kuang T, Jin D, Lou W, Wu W. 2018b. CD25 and TGF-β blockade based on predictive integrated immune ratio inhibits tumor growth in pancreatic cancer. J Transl Med 16:294.

Puleo F, Nicolle R, Blum Y, Cros J, Marisa L, Demetter P, Quertinmont E, Svrcek M, Elarouci N, Iovanna J, Franchimont D, Verset L, Galdon MG, Devière J, de Reyniès A, Laurent-Puig P, Van Laethem JL, Bachet JB, Maréchal R. 2018. Stratification of Pancreatic Ductal Adenocarcinomas Based on Tumor and Microenvironment Features. Gastroenterology 155:1999-2013.e3.

Pylaeva E, Korschunow G, Spyra I, Bordbari S, Siakaeva E, Ozel I, Domnich M, Squire A, Hasenberg A, Thangavelu K, Hussain T, Goetz M, Lang KS, Gunzer M, Hansen W, Buer J, Bankfalvi A, Lang S, Jablonska J. 2022. During early stages of cancer, neutrophils initiate anti-tumor immune responses in tumor-draining lymph nodes. Cell Rep 40:111171.

Pylayeva-Gupta Y, Das S, Handler JS, Hajdu CH, Coffre M, Koralov SB, Bar-Sagi D. 2016. IL35-Producing B Cells Promote the Development of Pancreatic Neoplasia. Cancer Discov 6:247-55.

Pylayeva-Gupta Y, Lee KE, Hajdu CH, Miller G, Bar-Sagi D. 2012. Oncogenic Kras-induced GM-CSF production promotes the development of pancreatic neoplasia. Cancer Cell 21:836-47.

Qi W, Huang X, Wang J. 2013. Correlation between Th17 cells and tumor microenvironment. Cell Immunol 285:18-22.

Qiu C, Yang L, Wang B, Cui L, Li C, Zhuo Y, Zhang L, Zhang S, Zhang Q, Wang X. 2019. The role of 2-arachidonoylglycerol in the regulation of the tumor-immune microenvironment in murine models of pancreatic cancer. Biomed Pharmacother 115:108952.

Qiu W, Su GH. 2013. Development of orthotopic pancreatic tumor mouse models. Methods Mol Biol 980:215-23.

Quante AS, Ming C, Rottmann M, Engel J, Boeck S, Heinemann V, Westphalen CB, Strauch K. 2016. Projections of cancer incidence and cancer-related deaths in Germany by 2020 and 2030. Cancer Med 5:2649-56.

Quatromoni JG, Singhal S, Bhojnagarwala P, Hancock WW, Albelda SM, Eruslanov E. 2015. An optimized disaggregation method for human lung tumors that preserves the phenotype and function of the immune cells. J Leukoc Biol 97:201-9.

Quelle DE, Zindy F, Ashmun RA, Sherr CJ. 1995. Alternative reading frames of the INK4a tumor suppressor gene encode two unrelated proteins capable of inducing cell cycle arrest. Cell 83:993-1000.

Rachagani S, Torres MP, Kumar S, Haridas D, Baine M, Macha MA, Kaur S, Ponnusamy MP, Dey P, Seshacharyulu P, Johansson SL, Jain M, Wagner KU, Batra SK. 2012. Mucin (Muc) expression during pancreatic cancer progression in spontaneous mouse model: potential implications for diagnosis and therapy. J Hematol Oncol 5:68.

Rahib L, Smith BD, Aizenberg R, Rosenzweig AB, Fleshman JM, Matrisian LM. 2014. Projecting cancer incidence and deaths to 2030: the unexpected burden of thyroid, liver, and pancreas cancers in the United States. Cancer Res 74:2913-21.

Rahn S, Krüger S, Mennrich R, Goebel L, Wesch D, Oberg HH, Vogel I, Ebsen M, Röcken C, Helm O, Sebens S. 2019. POLE Score: a comprehensive profiling of programmed death 1 ligand 1 expression in pancreatic ductal adenocarcinoma. Oncotarget 10:1572-1588.

Raval RR, Sharabi AB, Walker AJ, Drake CG, Sharma P. 2014. Tumor immunology and cancer immunotherapy: summary of the 2013 SITC primer. J Immunother Cancer 2:14. Reay J, Kim SH, Lockhart E, Kolls J, Robbins PD. 2009. Adenoviral-mediated, intratumor gene transfer of interleukin 23 induces a therapeutic antitumor response. Cancer Gene Ther 16:776-85.

Redston MS, Caldas C, Seymour AB, Hruban RH, da Costa L, Yeo CJ, Kern SE. 1994. p53 mutations in pancreatic carcinoma and evidence of common involvement of homocopolymer tracts in DNA microdeletions. Cancer Res 54:3025-33.

Regine WF, Winter KA, Abrams RA, Safran H, Hoffman JP, Konski A, Benson AB, Macdonald JS, Kudrimoti MR, Fromm ML, Haddock MG, Schaefer P, Willett CG, Rich TA. 2008. Fluorouracil vs gemcitabine chemotherapy before and after fluorouracil-based chemoradiation following resection of pancreatic adenocarcinoma: a randomized controlled trial. Jama 299:1019-26.

Reichard A, Asosingh K. 2019. Best Practices for Preparing a Single Cell Suspension from Solid Tissues for Flow Cytometry. Cytometry A 95:219-226.

Ren B, Liu X, Suriawinata AA. 2019. Pancreatic Ductal Adenocarcinoma and Its Precursor Lesions: Histopathology, Cytopathology, and Molecular Pathology. Am J Pathol 189:9-21.

Righi E, Kashiwagi S, Yuan J, Santosuosso M, Leblanc P, Ingraham R, Forbes B, Edelblute B, Collette B, Xing D, Kowalski M, Mingari MC, Vianello F, Birrer M, Orsulic S, Dranoff G, Poznansky MC. 2011. CXCL12/CXCR4 blockade induces multimodal antitumor effects that prolong survival in an immunocompetent mouse model of ovarian cancer. Cancer Res 71:5522-5534.

Rini BI, Plimack ER, Stus V, Gafanov R, Hawkins R, Nosov D, Pouliot F, Alekseev B, Soulières D, Melichar B, Vynnychenko I, Kryzhanivska A, Bondarenko I, Azevedo SJ, Borchiellini D, Szczylik C, Markus M, McDermott RS, Bedke J, Tartas S, Chang YH, Tamada S, Shou Q, Perini RF, Chen M, Atkins MB, Powles T. 2019. Pembrolizumab plus Axitinib versus Sunitinib for Advanced Renal-Cell Carcinoma. N Engl J Med 380:1116-1127.

Rivoltini L, Carrabba M, Huber V, Castelli C, Novellino L, Dalerba P, Mortarini R, Arancia G, Anichini A, Fais S, Parmiani G. 2002. Immunity to cancer: attack and escape in T lymphocyte-tumor cell interaction. Immunol Rev 188:97-113.

Robbins CS, Chudnovskiy A, Rauch PJ, Figueiredo JL, Iwamoto Y, Gorbatov R, Etzrodt M, Weber GF, Ueno T, van Rooijen N, Mulligan-Kehoe MJ, Libby P, Nahrendorf M, Pittet MJ, Weissleder R, Swirski FK. 2012. Extramedullary hematopoiesis generates Ly-6C(high) monocytes that infiltrate atherosclerotic lesions. Circulation 125:364-74.

Roberts NJ, Jiao Y, Yu J, Kopelovich L, Petersen GM, Bondy ML, Gallinger S, Schwartz AG, Syngal S, Cote ML, Axilbund J, Schulick R, Ali SZ, Eshleman JR, Velculescu VE, Goggins M, Vogelstein B, Papadopoulos N, Hruban RH, Kinzler KW, Klein AP. 2012. ATM mutations in patients with hereditary pancreatic cancer. Cancer Discov 2:41-6.
Rodriguez PC, Hernandez CP, Quiceno D, Dubinett SM, Zabaleta J, Ochoa JB, Gilbert J, Ochoa AC. 2005. Arginase I in myeloid suppressor cells is induced by COX-2 in lung carcinoma. J Exp Med 202:931-9.

Rodriguez PC, Quiceno DG, Ochoa AC. 2007. L-arginine availability regulates T-lymphocyte cell-cycle progression. Blood 109:1568-73.

Rooman I, Real FX. 2012. Pancreatic ductal adenocarcinoma and acinar cells: a matter of differentiation and development? Gut 61:449-58.

Rose-John S. 2018. Interleukin-6 Family Cytokines. Cold Spring Harb Perspect Biol 10.
Rosty C, Geradts J, Sato N, Wilentz RE, Roberts H, Sohn T, Cameron JL, Yeo CJ, Hruban RH, Goggins M. 2003. p16 Inactivation in pancreatic intraepithelial neoplasias (PanINs) arising in patients with chronic pancreatitis. Am J Surg Pathol 27:1495-501.

Rubio-Viqueira B, Jimeno A, Cusatis G, Zhang X, Iacobuzio-Donahue C, Karikari C, Shi C, Danenberg K, Danenberg PV, Kuramochi H, Tanaka K, Singh S, Salimi-Moosavi H, Bouraoud N, Amador ML, Altiok S, Kulesza P, Yeo C, Messersmith W, Eshleman J, Hruban RH, Maitra A, Hidalgo M. 2006. An in vivo platform for translational drug development in pancreatic cancer. Clin Cancer Res 12:4652-61.

Ruffolo LI, Jackson KM, Kuhlers PC, Dale BS, Figueroa Guilliani NM, Ullman NA, Burchard PR, Qin SS, Juviler PG, Keilson JM, Morrison AB, Georger M, Jewell R, Calvi LM, Nywening TM, O'Dell MR, Hezel AF, De Las Casas L, Lesinski GB, Yeh JJ, Hernandez-Alejandro R, Belt BA, Linehan DC. 2022. GM-CSF drives myelopoiesis, recruitment and polarisation of tumour-associated macrophages in cholangiocarcinoma and systemic blockade facilitates antitumour immunity. Gut 71:1386-1398.

Saka D, Gökalp M, Piyade B, Cevik NC, Arik Sever E, Unutmaz D, Ceyhan GO, Demir IE, Asimgil H. 2020. Mechanisms of T-Cell Exhaustion in Pancreatic Cancer. Cancers (Basel) 12.

Sakamoto H, Shimizu J, Horio Y, Ueda R, Takahashi T, Mitsudomi T, Yatabe Y. 2007. Disproportionate representation of KRAS gene mutation in atypical adenomatous hyperplasia, but even distribution of EGFR gene mutation from preinvasive to invasive adenocarcinomas. J Pathol 212:287-94.

Salcedo R, Stauffer JK, Lincoln E, Back TC, Hixon JA, Hahn C, Shafer-Weaver K, Malyguine A, Kastelein R, Wigginton JM. 2004. IL-27 mediates complete regression of orthotopic primary and metastatic murine neuroblastoma tumors: role for CD8+ T cells. J Immunol 173:7170-82.

Sandrasegaran K, Nutakki K, Tahir B, Dhanabal A, Tann M, Cote GA. 2013. Use of diffusion-weighted MRI to differentiate chronic pancreatitis from pancreatic cancer. AJR Am J Roentgenol 201:1002-8.

Sausen M, Phallen J, Adleff V, Jones S, Leary RJ, Barrett MT, Anagnostou V, Parpart-Li S, Murphy D, Kay Li Q, Hruban CA, Scharpf R, White JR, O'Dwyer PJ, Allen PJ, Eshleman JR, Thompson CB, Klimstra DS, Linehan DC, Maitra A, Hruban RH, Diaz LA, Jr., Von Hoff DD, Johansen JS, Drebin JA, Velculescu VE. 2015. Clinical implications of genomic alterations in the tumour and circulation of pancreatic cancer patients. Nat Commun 6:7686.

Scarpa A, Capelli P, Mukai K, Zamboni G, Oda T, Iacono C, Hirohashi S. 1993. Pancreatic adenocarcinomas frequently show p53 gene mutations. Am J Pathol 142:1534-43.

Schilbach K, Kreyenberg H, Geiselhart A, Niethammer D, Handgretinger R. 2004. Cloning of a human antibody directed against human neuroblastoma cells and specific for human translation elongation factor 1alpha. Tissue Antigens 63:122-31.

Schlecker E, Stojanovic A, Eisen C, Quack C, Falk CS, Umansky V, Cerwenka A. 2012. Tumor-infiltrating monocytic myeloid-derived suppressor cells mediate CCR5-dependent recruitment of regulatory T cells favoring tumor growth. J Immunol 189:5602-11.

Schlesinger Y, Yosefov-Levi O, Kolodkin-Gal D, Granit RZ, Peters L, Kalifa R, Xia L, Nasereddin A, Shiff I, Amran O, Nevo Y, Elgavish S, Atlan K, Zamir G, Parnas O. 2020. Single-cell transcriptomes of pancreatic preinvasive lesions and cancer reveal acinar metaplastic cells' heterogeneity. Nat Commun 11:4516.

Schlitter AM, Segler A, Steiger K, Michalski CW, Jäger C, Konukiewitz B, Pfarr N, Endris V, Bettstetter M, Kong B, Regel I, Kleeff J, Klöppel G, Esposito I. 2017. Molecular, morphological and survival analysis of 177 resected pancreatic ductal adenocarcinomas (PDACs): Identification of prognostic subtypes. Sci Rep 7:41064.

Schmid P, Cortes J, Pusztai L, McArthur H, Kümmel S, Bergh J, Denkert C, Park YH, Hui R, Harbeck N, Takahashi M, Foukakis T, Fasching PA, Cardoso F, Untch M, Jia L, Karantza V, Zhao J, Aktan G, Dent R, O'Shaughnessy J. 2020. Pembrolizumab for Early Triple-Negative Breast Cancer. N Engl J Med 382:810-821.

Schmielau J, Finn OJ. 2001. Activated granulocytes and granulocyte-derived hydrogen peroxide are the underlying mechanism of suppression of t-cell function in advanced cancer patients. Cancer Res 61:4756-60.

Schneider R, Yaneva T, Beauseigle D, El-Khoury L, Arbour N. 2011. IL-27 increases the proliferation and effector functions of human naïve CD8+ T lymphocytes and promotes their development into Tc1 cells. Eur J Immunol 41:47-59.

Schnitt SJ, Vincent-Salomon A. 2003. Columnar cell lesions of the breast. Adv Anat Pathol 10:113-24.

Schreiber RD, Old LJ, Smyth MJ. 2011. Cancer immunoediting: integrating immunity's roles in cancer suppression and promotion. Science 331:1565-70.

Schreiber RD, Pace JL, Russell SW, Altman A, Katz DH. 1983. Macrophage-activating factor produced by a T cell hybridoma: physiochemical and biosynthetic resemblance to gamma-interferon. J Immunol 131:826-32.

Schutte M, Hruban RH, Geradts J, Maynard R, Hilgers W, Rabindran SK, Moskaluk CA, Hahn SA, Schwarte-Waldhoff I, Schmiegel W, Baylin SB, Kern SE, Herman JG. 1997. Abrogation of the Rb/p16 tumor-suppressive pathway in virtually all pancreatic carcinomas. Cancer Res 57:3126-30.

Schwartz AM, Henson DE. 2007. Familial and sporadic pancreatic carcinoma, epidemiologic concordance. Am J Surg Pathol 31:645-6.

Schwitalla S, Ziegler PK, Horst D, Becker V, Kerle I, Begus-Nahrmann Y, Lechel A, Rudolph KL, Langer R, Slotta-Huspenina J, Bader FG, Prazeres da Costa O, Neurath MF, Meining A, Kirchner T, Greten FR. 2013. Loss of p53 in enterocytes generates an inflammatory microenvironment enabling invasion and lymph node metastasis of carcinogen-induced colorectal tumors. Cancer Cell 23:93-106.

Sedger LM, Hou S, Osvath SR, Glaccum MB, Peschon JJ, van Rooijen N, Hyland L. 2002. Bone marrow B cell apoptosis during in vivo influenza virus infection requires TNF-alpha and lymphotoxin-alpha. J Immunol 169:6193-201.

Seifert AM, List J, Heiduk M, Decker R, von Renesse J, Meinecke AC, Aust DE, Welsch T, Weitz J, Seifert L. 2020. Gamma-delta T cells stimulate IL-6 production by pancreatic stellate cells in pancreatic ductal adenocarcinoma. J Cancer Res Clin Oncol 146:3233-3240.

Selamat SA, Galler JS, Joshi AD, Fyfe MN, Campan M, Siegmund KD, Kerr KM, Laird-Offringa IA. 2011. DNA methylation changes in atypical adenomatous hyperplasia, adenocarcinoma in situ, and lung adenocarcinoma. PLoS One 6:e21443.

Serrano M, Hannon GJ, Beach D. 1993. A new regulatory motif in cell-cycle control causing specific inhibition of cyclin D/CDK4. Nature 366:704-7.

Shah S, Divekar AA, Hilchey SP, Cho HM, Newman CL, Shin SU, Nechustan H, Challita-Eid PM, Segal BM, Yi KH, Rosenblatt JD. 2005. Increased rejection of primary tumors in mice lacking B cells: inhibition of anti-tumor CTL and TH1 cytokine responses by B cells. Int J Cancer 117:574-86.

Shankaran V, Ikeda H, Bruce AT, White JM, Swanson PE, Old LJ, Schreiber RD. 2001. IFNgamma and lymphocytes prevent primary tumour development and shape tumour immunogenicity. Nature 410:1107-11.

Sharpe AH. 2017. Introduction to checkpoint inhibitors and cancer immunotherapy. Immunol Rev 276:5-8.

Shen P, Roch T, Lampropoulou V, O'Connor RA, Stervbo U, Hilgenberg E, Ries S, Dang VD, Jaimes Y, Daridon C, Li R, Jouneau L, Boudinot P, Wilantri S, Sakwa I, Miyazaki Y, Leech MD, McPherson RC, Wirtz S, Neurath M, Hoehlig K, Meinl E, Grützkau A, Grün JR, Horn K, Kühl AA, Dörner T, Bar-Or A, Kaufmann SHE, Anderton SM, Fillatreau S. 2014. IL-35-producing B cells are critical regulators of immunity during autoimmune and infectious diseases. Nature 507:366-370.

Shen-Orr SS, Gaujoux R. 2013. Computational deconvolution: extracting cell type-specific information from heterogeneous samples. Curr Opin Immunol 25:571-8.

Shi C, Hong SM, Lim P, Kamiyama H, Khan M, Anders RA, Goggins M, Hruban RH, Eshleman JR. 2009a. KRAS2 mutations in human pancreatic acinar-ductal metaplastic lesions are limited to those with PanIN: implications for the human pancreatic cancer cell of origin. Mol Cancer Res 7:230-6.

Shi C, Klein AP, Goggins M, Maitra A, Canto M, Ali S, Schulick R, Palmisano E, Hruban RH. 2009b. Increased Prevalence of Precursor Lesions in Familial Pancreatic Cancer Patients. Clin Cancer Res 15:7737-7743.

Sinn HP, Elsawaf Z, Helmchen B, Aulmann S. 2010. Early Breast Cancer Precursor Lesions: Lessons Learned from Molecular and Clinical Studies. Breast Care (Basel) 5:218-226.

Siret C, Collignon A, Silvy F, Robert S, Cheyrol T, André P, Rigot V, Iovanna J, van de Pavert S, Lombardo D, Mas E, Martirosyan A. 2019. Deciphering the Crosstalk Between Myeloid-Derived Suppressor Cells and Regulatory T Cells in Pancreatic Ductal Adenocarcinoma. Front Immunol 10:3070.

Siva S, MacManus MP, Martin RF, Martin OA. 2015. Abscopal effects of radiation therapy: a clinical review for the radiobiologist. Cancer Lett 356:82-90.

Smittenaar CR, Petersen KA, Stewart K, Moitt N. 2016. Cancer incidence and mortality projections in the UK until 2035. Br J Cancer 115:1147-1155.

Sohn TA, Yeo CJ, Cameron JL, Koniaris L, Kaushal S, Abrams RA, Sauter PK, Coleman J, Hruban RH, Lillemoe KD. 2000. Resected adenocarcinoma of the pancreas-616 patients: results, outcomes, and prognostic indicators. J Gastrointest Surg 4:567-79.
Sommers SC, Murphy SA, Warren S. 1954. Pancreatic duct hyperplasia and cancer. Gastroenterology 27:629-40.

Spear S, Candido JB, McDermott JR, Ghirelli C, Maniati E, Beers SA, Balkwill FR, Kocher HM, Capasso M. 2019. Discrepancies in the Tumor Microenvironment of Spontaneous and Orthotopic Murine Models of Pancreatic Cancer Uncover a New Immunostimulatory Phenotype for B Cells. Front Immunol 10:542.

Steele NG, Carpenter ES, Kemp SB, Sirihorachai VR, The S, Delrosario L, Lazarus J, Amir ED, Gunchick V, Espinoza C, Bell S, Harris L, Lima F, Irizarry-Negron V, Paglia D, Macchia J, Chu AKY, Schofield H, Wamsteker EJ, Kwon R, Schulman A, Prabhu A, Law R, Sondhi A, Yu J, Patel A, Donahue K, Nathan H, Cho C, Anderson MA, Sahai V, Lyssiotis CA, Zou W, Allen BL, Rao A, Crawford HC, Bednar F, Frankel TL, Pasca di Magliano M. 2020. Multimodal Mapping of the Tumor and Peripheral Blood Immune Landscape in Human Pancreatic Cancer. Nat Cancer 1:1097-1112.

Stott FJ, Bates S, James MC, McConnell BB, Starborg M, Brookes S, Palmero I, Ryan K, Hara E, Vousden KH, Peters G. 1998. The alternative product from the human CDKN2A locus, p14(ARF), participates in a regulatory feedback loop with p53 and MDM2. Embo j 17:5001-14.

Strauss VY, Shaw R, Virdee PS, Hurt CN, Ward E, Tranter B, Patel N, Bridgewater J, Parsons P, Radhakrishna G, O'Neill E, Sebag-Montefiore D, Hawkins M, Corrie PG, Maughan T, Mukherjee S. 2019. Study protocol: a multi-centre randomised study of induction chemotherapy followed by capecitabine ± nelfinavir with high- or standard-dose radiotherapy for locally advanced pancreatic cancer (SCALOP-2). BMC Cancer 19:121.

Stromnes IM, Brockenbrough JS, Izeradjene K, Carlson MA, Cuevas C, Simmons RM, Greenberg PD, Hingorani SR. 2014. Targeted depletion of an MDSC subset unmasks pancreatic ductal adenocarcinoma to adaptive immunity. Gut 63:1769-81.

Stromnes IM, Schmitt TM, Hulbert A, Brockenbrough JS, Nguyen H, Cuevas C, Dotson AM, Tan X, Hotes JL, Greenberg PD, Hingorani SR. 2015. T Cells Engineered against a Native Antigen Can Surmount Immunologic and Physical Barriers to Treat Pancreatic Ductal Adenocarcinoma. Cancer Cell 28:638-652.

Stylianou A, Gkretsi V, Stylianopoulos T. 2018. Transforming growth factor-β modulates pancreatic cancer associated fibroblasts cell shape, stiffness and invasion. Biochim Biophys Acta Gen Subj 1862:1537-1546.

Sun Z, Nyberg R, Wu Y, Bernard B, Redmond WL. 2021. Developing an enhanced 7-color multiplex IHC protocol to dissect immune infiltration in human cancers. PLoS One 16:e0247238.

Sung H, Ferlay J, Siegel RL, Laversanne M, Soerjomataram I, Jemal A, Bray F. 2021. Global Cancer Statistics 2020: GLOBOCAN Estimates of Incidence and Mortality Worldwide for 36 Cancers in 185 Countries. CA Cancer J Clin 71:209-249.

Tachibana K, Hirota S, Iizasa H, Yoshida H, Kawabata K, Kataoka Y, Kitamura Y, Matsushima K, Yoshida N, Nishikawa S, Kishimoto T, Nagasawa T. 1998. The chemokine receptor CXCR4 is essential for vascularization of the gastrointestinal tract. Nature 393:591-4.

Takagi Y, Kohmura H, Futamura M, Kida H, Tanemura H, Shimokawa K, Saji S. 1996. Somatic alterations of the DPC4 gene in human colorectal cancers in vivo. Gastroenterology 111:1369-72.

Takahashi R, Macchini M, Sunagawa M, Jiang Z, Tanaka T, Valenti G, Renz BW, White RA, Hayakawa Y, Westphalen CB, Tailor Y, Iuga AC, Gonda TA, Genkinger J, Olive KP, Wang TC. 2021. Interleukin-1β-induced pancreatitis promotes pancreatic ductal adenocarcinoma via B lymphocyte-mediated immune suppression. Gut 70:330-341.

Takeuchi S, Baghdadi M, Tsuchikawa T, Wada H, Nakamura T, Abe H, Nakanishi S, Usui Y, Higuchi K, Takahashi M, Inoko K, Sato S, Takano H, Shichinohe T, Seino K, Hirano S. 2015. Chemotherapy-Derived Inflammatory Responses Accelerate the Formation of Immunosuppressive Myeloid Cells in the Tissue Microenvironment of Human Pancreatic Cancer. Cancer Res 75:2629-40.

Tamborero D, Rubio-Perez C, Muiños F, Sabarinathan R, Piulats JM, Muntasell A, Dienstmann R, Lopez-Bigas N, Gonzalez-Perez A. 2018. A Pan-cancer Landscape of Interactions between Solid Tumors and Infiltrating Immune Cell Populations. Clin Cancer Res 24:3717-3728.

Tan MC, Goedegebuure PS, Belt BA, Flaherty B, Sankpal N, Gillanders WE, Eberlein TJ, Hsieh CS, Linehan DC. 2009. Disruption of CCR5-dependent homing of regulatory T cells inhibits tumor growth in a murine model of pancreatic cancer. J Immunol 182:1746-55.

Tan PH, Chuah KL, Chiang G, Wong CY, Dong F, Bay BH. 2002. Correlation of p53 and cerbB2 expression and hormonal receptor status with clinicopathologic parameters in ductal carcinoma in situ of the breast. Oncol Rep 9:1081-6.

Tan WCC, Nerurkar SN, Cai HY, Ng HHM, Wu D, Wee YTF, Lim JCT, Yeong J, Lim TKH. 2020. Overview of multiplex immunohistochemistry/immunofluorescence techniques in the era of cancer immunotherapy. Cancer Commun (Lond) 40:135-153.

Tanaka M, Fernández-del Castillo C, Adsay V, Chari S, Falconi M, Jang JY, Kimura W, Levy P, Pitman MB, Schmidt CM, Shimizu M, Wolfgang CL, Yamaguchi K, Yamao K. 2012. International consensus guidelines 2012 for the management of IPMN and MCN of the pancreas. Pancreatology 12:183-97.

Taniguchi K, Karin M. 2014. IL-6 and related cytokines as the critical lynchpins between inflammation and cancer. Semin Immunol 26:54-74.

Terashima T, English D, Hogg JC, van Eeden SF. 1998. Release of polymorphonuclear leukocytes from the bone marrow by interleukin-8. Blood 92:1062-9.

Terashima T, Wiggs B, English D, Hogg JC, van Eeden SF. 1996. Polymorphonuclear leukocyte transit times in bone marrow during streptococcal pneumonia. Am J Physiol 271:L587-92.

Terhune PG, Phifer DM, Tosteson TD, Longnecker DS. 1998. K-ras mutation in focal proliferative lesions of human pancreas. Cancer Epidemiol Biomarkers Prev 7:515-21.
Tewari N, Zaitoun AM, Arora A, Madhusudan S, Ilyas M, Lobo DN. 2013. The presence of tumour-associated lymphocytes confers a good prognosis in pancreatic ductal adenocarcinoma: an immunohistochemical study of tissue microarrays. BMC Cancer 13:436.

Thyagarajan A, Alshehri MSA, Miller KLR, Sherwin CM, Travers JB, Sahu RP. 2019. Myeloid-Derived Suppressor Cells and Pancreatic Cancer: Implications in Novel Therapeutic Approaches. Cancers (Basel) 11.

Tjomsland V, Niklasson L, Sandström P, Borch K, Druid H, Bratthäll C, Messmer D, Larsson M, Spångeus A. 2011. The desmoplastic stroma plays an essential role in the accumulation and modulation of infiltrated immune cells in pancreatic adenocarcinoma. Clin Dev Immunol 2011:212810.

Tokoyoda K, Egawa T, Sugiyama T, Choi BI, Nagasawa T. 2004. Cellular niches controlling B lymphocyte behavior within bone marrow during development. Immunity 20:707-18.

Topalian SL, Hodi FS, Brahmer JR, Gettinger SN, Smith DC, McDermott DF, Powderly JD, Carvajal RD, Sosman JA, Atkins MB, Leming PD, Spigel DR, Antonia SJ, Horn L, Drake CG, Pardoll DM, Chen L, Sharfman WH, Anders RA, Taube JM, McMiller TL, Xu H, Korman AJ, Jure-Kunkel M, Agrawal S, McDonald D, Kollia GD, Gupta A, Wigginton JM, Sznol M. 2012. Safety, activity, and immune correlates of anti-PD-1 antibody in cancer. N Engl J Med 366:2443-54.

Torres MP, Rachagani S, Souchek JJ, Mallya K, Johansson SL, Batra SK. 2013. Novel pancreatic cancer cell lines derived from genetically engineered mouse models of spontaneous pancreatic adenocarcinoma: applications in diagnosis and therapy. PLoS One 8:e80580.

Trikudanathan G, Philip A, Dasanu CA, Baker WL. 2011. Association between Helicobacter pylori infection and pancreatic cancer. A cumulative meta-analysis. Jop 12:26-31.

Trovato R, Fiore A, Sartori S, Cane S, Giugno R, Cascione L, Paiella S, Salvia R, De Sanctis F, Poffe O, Anselmi C, Hofer F, Sartoris S, Piro G, Carbone C, Corbo V, Lawlor R, Solito S, Pinton L, Mandruzzato S, Bassi C, Scarpa A, Bronte V, Ugel S. 2019. Immunosuppression by monocytic myeloid-derived suppressor cells in patients with pancreatic ductal carcinoma is orchestrated by STAT3. J Immunother Cancer 7:255.

Tseng WW, Winer D, Kenkel JA, Choi O, Shain AH, Pollack JR, French R, Lowy AM, Engleman EG. 2010. Development of an orthotopic model of invasive pancreatic cancer in an immunocompetent murine host. Clin Cancer Res 16:3684-95.

Tuveson DA, Shaw AT, Willis NA, Silver DP, Jackson EL, Chang S, Mercer KL, Grochow R, Hock H, Crowley D, Hingorani SR, Zaks T, King C, Jacobetz MA, Wang L, Bronson RT, Orkin SH, DePinho RA, Jacks T. 2004. Endogenous oncogenic K-ras(G12D) stimulates proliferation and widespread neoplastic and developmental defects. Cancer Cell 5:375-87.

Tzeng CW, Balachandran A, Ahmad M, Lee JE, Krishnan S, Wang H, Crane CH, Wolff RA, Varadhachary GR, Pisters PW, Aloia TA, Vauthey JN, Fleming JB, Katz MH. 2014. Serum carbohydrate antigen 19-9 represents a marker of response to neoadjuvant therapy in patients with borderline resectable pancreatic cancer. HPB (Oxford) 16:430-8.

Ueda Y, Kondo M, Kelsoe G. 2005. Inflammation and the reciprocal production of granulocytes and lymphocytes in bone marrow. J Exp Med 201:1771-80.

Uehara H, Nakaizumi A, Ishikawa O, Iishi H, Tatsumi K, Takakura R, Ishida T, Takano Y, Tanaka S, Takenaka A. 2008. Development of ductal carcinoma of the pancreas during follow-up of branch duct intraductal papillary mucinous neoplasm of the pancreas. Gut 57:1561-5.

Van den Broeck A, Sergeant G, Ectors N, Van Steenbergen W, Aerts R, Topal B. 2009. Patterns of recurrence after curative resection of pancreatic ductal adenocarcinoma. Eur J Surg Oncol 35:600-4.

Van Heek NT, Meeker AK, Kern SE, Yeo CJ, Lillemoe KD, Cameron JL, Offerhaus GJ, Hicks JL, Wilentz RE, Goggins MG, De Marzo AM, Hruban RH, Maitra A. 2002. Telomere shortening is nearly universal in pancreatic intraepithelial neoplasia. Am J Pathol 161:1541-7.

Van Laethem JL, Hammel P, Mornex F, Azria D, Van Tienhoven G, Vergauwe P, Peeters M, Polus M, Praet M, Mauer M, Collette L, Budach V, Lutz M, Van Cutsem E, Haustermans K. 2010. Adjuvant gemcitabine alone versus gemcitabine-based chemoradiotherapy after curative resection for pancreatic cancer: a randomized EORTC-40013-22012/FFCD-9203/GERCOR phase II study. J Clin Oncol 28:4450-6.

Velasco-Velázquez M, Xolalpa W, Pestell RG. 2014. The potential to target CCL5/CCR5 in breast cancer. Expert Opin Ther Targets 18:1265-75.

Versteijne E, Suker M, Groothuis K, Akkermans-Vogelaar JM, Besselink MG, Bonsing BA, Buijsen J, Busch OR, Creemers GM, van Dam RM, Eskens F, Festen S, de Groot JWB, Groot Koerkamp B, de Hingh IH, Homs MYV, van Hooft JE, Kerver ED, Luelmo SAC, Neelis KJ, Nuyttens J, Paardekooper G, Patijn GA, van der Sangen MJC, de Vos-Geelen J, Wilmink JW, Zwinderman AH, Punt CJ, van Eijck CH, van Tienhoven G. 2020. Preoperative Chemoradiotherapy Versus Immediate Surgery for Resectable and Borderline Resectable Pancreatic Cancer: Results of the Dutch Randomized Phase III PREOPANC Trial. J Clin Oncol 38:1763-1773.

Vijayan D, Mohd Redzwan N, Avery DT, Wirasinha RC, Brink R, Walters G, Adelstein S, Kobayashi M, Gray P, Elliott M, Wong M, King C, Vinuesa CG, Ghilardi N, Ma CS, Tangye SG, Batten M. 2016. IL-27 Directly Enhances Germinal Center B Cell Activity and Potentiates Lupus in Sanroque Mice. J Immunol 197:3008-3017.

Vincent A, Herman J, Schulick R, Hruban RH, Goggins M. 2011. Pancreatic cancer. Lancet 378:607-20.

Vogelstein B, Papadopoulos N, Velculescu VE, Zhou S, Diaz LA, Jr., Kinzler KW. 2013. Cancer genome landscapes. Science 339:1546-58.

Vojtek AB, Hollenberg SM, Cooper JA. 1993. Mammalian Ras interacts directly with the serine/threonine kinase Raf. Cell 74:205-14.

Von Hoff DD, Ervin T, Arena FP, Chiorean EG, Infante J, Moore M, Seay T, Tjulandin SA, Ma WW, Saleh MN, Harris M, Reni M, Dowden S, Laheru D, Bahary N, Ramanathan RK, Tabernero J, Hidalgo M, Goldstein D, Van Cutsem E, Wei X, Iglesias J, Renschler MF. 2013. Increased survival in pancreatic cancer with nab-paclitaxel plus gemcitabine. N Engl J Med 369:1691-703.

Vonderheide RH, Bayne LJ. 2013. Inflammatory networks and immune surveillance of pancreatic carcinoma. Curr Opin Immunol 25:200-5.

Vuk-Pavlović S, Bulur PA, Lin Y, Qin R, Szumlanski CL, Zhao X, Dietz AB. 2010. Immunosuppressive CD14+HLA-DRlow/- monocytes in prostate cancer. Prostate 70:443-55.

Waddell N, Pajic M, Patch AM, Chang DK, Kassahn KS, Bailey P, Johns AL, Miller D, Nones K, Quek K, Quinn MC, Robertson AJ, Fadlullah MZ, Bruxner TJ, Christ AN, Harliwong I, Idrisoglu S, Manning S, Nourse C, Nourbakhsh E, Wani S, Wilson PJ, Markham E, Cloonan N, Anderson MJ, Fink JL, Holmes O, Kazakoff SH, Leonard C, Newell F, Poudel B, Song S, Taylor D, Waddell N, Wood S, Xu Q, Wu J, Pinese M, Cowley MJ, Lee HC, Jones MD, Nagrial AM, Humphris J, Chantrill LA, Chin V, Steinmann AM, Mawson A, Humphrey ES, Colvin EK, Chou A, Scarlett CJ, Pinho AV, Giry-Laterriere M, Rooman I, Samra JS, Kench JG, Pettitt JA, Merrett ND, Toon C, Epari K, Nguyen NQ, Barbour A, Zeps N, Jamieson NB, Graham JS, Niclou SP, Bjerkvig R, Grützmann R, Aust D, Hruban RH, Maitra A, Iacobuzio-Donahue CA, Wolfgang CL, Morgan RA, Lawlor RT, Corbo V, Bassi C, Falconi M, Zamboni G, Tortora G, Tempero MA, Gill AJ, Eshleman JR, Pilarsky C, Scarpa A, Musgrove EA, Pearson JV, Biankin AV, Grimmond SM. 2015. Whole genomes redefine the mutational landscape of pancreatic cancer. Nature 518:495-501.

Wang J, Liu X, Ji J, Luo J, Zhao Y, Zhou X, Zheng J, Guo M, Liu Y. 2022a. Orthotopic and Heterotopic Murine Models of Pancreatic Cancer Exhibit Different Immunological Microenvironments and Different Responses to Immunotherapy. Front Immunol 13:863346.

Wang J, Saung MT, Li K, Fu J, Fujiwara K, Niu N, Muth S, Wang J, Xu Y, Rozich N, Zlomke H, Chen S, Espinoza B, Henderson M, Funes V, Herbst B, Ding D, Twyman-Saint Victor C, Zhao Q, Narang A, He J, Zheng L. 2022b. CCR2/CCR5 inhibitor permits the radiation-induced effector T cell infiltration in pancreatic adenocarcinoma. J Exp Med 219.

Wang L, Rubinstein R, Lines JL, Wasiuk A, Ahonen C, Guo Y, Lu LF, Gondek D, Wang Y, Fava RA, Fiser A, Almo S, Noelle RJ. 2011. VISTA, a novel mouse Ig superfamily ligand that negatively regulates T cell responses. J Exp Med 208:577-92.

Wang QJ, Yu Z, Griffith K, Hanada K, Restifo NP, Yang JC. 2016. Identification of T-cell Receptors Targeting KRAS-Mutated Human Tumors. Cancer Immunol Res 4:204-14.
Wang RX, Yu CR, Dambuza IM, Mahdi RM, Dolinska MB, Sergeev YV, Wingfield PT, Kim SH, Egwuagu CE. 2014. Interleukin-35 induces regulatory B cells that suppress autoimmune disease. Nat Med 20:633-41.

Wang X, Allen S, Blake JF, Bowcut V, Briere DM, Calinisan A, Dahlke JR, Fell JB, Fischer JP, Gunn RJ, Hallin J, Laguer J, Lawson JD, Medwid J, Newhouse B, Nguyen P, O'Leary JM, Olson P, Pajk S, Rahbaek L, Rodriguez M, Smith CR, Tang TP, Thomas NC, Vanderpool D, Vigers GP, Christensen JG, Marx MA. 2022c. Identification of MRTX1133, a Noncovalent, Potent, and Selective KRAS(G12D) Inhibitor. J Med Chem 65:3123-3133.

Wang X, Lang M, Zhao T, Feng X, Zheng C, Huang C, Hao J, Dong J, Luo L, Li X, Lan C, Yu W, Yu M, Yang S, Ren H. 2017. Cancer-FOXP3 directly activated CCL5 to recruit FOXP3(+)Treg cells in pancreatic ductal adenocarcinoma. Oncogene 36:3048-3058.
Wang X, Wang G, Wang Z, Liu B, Han N, Li J, Lu C, Liu X, Zhang Q, Yang Q, Wang G. 2019. PD-1-expressing B cells suppress CD4(+) and CD8(+) T cells via PD-1/PD-L1-dependent pathway. Mol Immunol 109:20-26.

Wang Y, Zhang Y, Yang J, Ni X, Liu S, Li Z, Hodges SE, Fisher WE, Brunicardi FC, Gibbs RA, Gingras MC, Li M. 2012. Genomic sequencing of key genes in mouse pancreatic cancer cells. Curr Mol Med 12:331-41.

Wang Z, Liu JQ, Liu Z, Shen R, Zhang G, Xu J, Basu S, Feng Y, Bai XF. 2013. Tumor-derived IL-35 promotes tumor growth by enhancing myeloid cell accumulation and angiogenesis. J Immunol 190:2415-23.

Wartenberg M, Cibin S, Zlobec I, Vassella E, Eppenberger-Castori S, Terracciano L, Eichmann MD, Worni M, Gloor B, Perren A, Karamitopoulou E. 2018. Integrated Genomic and Immunophenotypic Classification of Pancreatic Cancer Reveals Three Distinct Subtypes with Prognostic/Predictive Significance. Clin Cancer Res 24:4444-4454.

Waters AM, Der CJ. 2018. KRAS: The Critical Driver and Therapeutic Target for Pancreatic Cancer. Cold Spring Harb Perspect Med 8.

Weber JS, D'Angelo SP, Minor D, Hodi FS, Gutzmer R, Neyns B, Hoeller C, Khushalani NI, Miller WH, Jr., Lao CD, Linette GP, Thomas L, Lorigan P, Grossmann KF, Hassel JC, Maio M, Sznol M, Ascierto PA, Mohr P, Chmielowski B, Bryce A, Svane IM, Grob JJ, Krackhardt AM, Horak C, Lambert A, Yang AS, Larkin J. 2015. Nivolumab versus chemotherapy in patients with advanced melanoma who progressed after anti-CTLA-4 treatment (CheckMate 037): a randomised, controlled, open-label, phase 3 trial. Lancet Oncol 16:375-84.

Wehr AY, Furth EE, Sangar V, Blair IA, Yu KH. 2011. Analysis of the human pancreatic stellate cell secreted proteome. Pancreas 40:557-66.

Wei X, Yao W, Li H, Qian J, Xie Y, Zhang Z, Lu H, Shi L, Lin X. 2019. B and NK Cells Closely Correlate with the Condition of Patients with Acute Pancreatitis. Gastroenterol Res Pract 2019:7568410.

Weinstock M, McDermott D. 2015. Targeting PD-1/PD-L1 in the treatment of metastatic renal cell carcinoma. Ther Adv Urol 7:365-77.

Whatcott CJ, Diep CH, Jiang P, Watanabe A, LoBello J, Sima C, Hostetter G, Shepard HM, Von Hoff DD, Han H. 2015. Desmoplasia in Primary Tumors and Metastatic Lesions of Pancreatic Cancer. Clin Cancer Res 21:3561-8.

Willenbrock F, Cox CM, Parkes EE, Wilhelm-Benartzi CS, Abraham AG, Owens R, Sabbagh A, Jones CM, Hughes DLI, Maughan T, Hurt CN, O'Neill EE, Mukherjee S. 2021. Circulating biomarkers and outcomes from a randomised phase 2 trial of gemcitabine versus capecitabine-based chemoradiotherapy for pancreatic cancer. Br J Cancer 124:581-586.

Wistuba, II, Berry J, Behrens C, Maitra A, Shivapurkar N, Milchgrub S, Mackay B, Minna JD, Gazdar AF. 2000. Molecular changes in the bronchial epithelium of patients with small cell lung cancer. Clin Cancer Res 6:2604-10.

Witkiewicz AK, McMillan EA, Balaji U, Baek G, Lin WC, Mansour J, Mollaee M, Wagner KU, Koduru P, Yopp A, Choti MA, Yeo CJ, McCue P, White MA, Knudsen ES. 2015. Whole-exome sequencing of pancreatic cancer defines genetic diversity and therapeutic targets. Nat Commun 6:6744.

Wong D, Ko AH, Hwang J, Venook AP, Bergsland EK, Tempero MA. 2008. Serum CA19-9 decline compared to radiographic response as a surrogate for clinical outcomes in patients with metastatic pancreatic cancer receiving chemotherapy. Pancreas 37:269-74.

Wörmann SM, Diakopoulos KN, Lesina M, Algül H. 2014. The immune network in pancreatic cancer development and progression. Oncogene 33:2956-67.

Wörmann SM, Song L, Ai J, Diakopoulos KN, Kurkowski MU, Görgülü K, Ruess D, Campbell A, Doglioni C, Jodrell D, Neesse A, Demir IE, Karpathaki AP, Barenboim M, Hagemann T, Rose-John S, Sansom O, Schmid RM, Protti MP, Lesina M, Algül H. 2016. Loss of P53 Function Activates JAK2-STAT3 Signaling to Promote Pancreatic Tumor Growth, Stroma Modification, and Gemcitabine Resistance in Mice and Is Associated With Patient Survival. Gastroenterology 151:180-193.e12.

Wu H, Li P, Shao N, Ma J, Ji M, Sun X, Ma D, Ji C. 2012. Aberrant expression of Treg-associated cytokine IL-35 along with IL-10 and TGF-β in acute myeloid leukemia. Oncol Lett 3:1119-1123.

Wu L, Zhang XH. 2020. Tumor-Associated Neutrophils and Macrophages-Heterogenous but Not Chaotic. Front Immunol 11:553967.

Wu YS, Chung I, Wong WF, Masamune A, Sim MS, Looi CY. 2017. Paracrine IL-6 signaling mediates the effects of pancreatic stellate cells on epithelial-mesenchymal transition via Stat3/Nrf2 pathway in pancreatic cancer cells. Biochim Biophys Acta Gen Subj 1861:296-306.

Xie MZ, Tang YP, Hu BL, Li KZ, Li JL, Liang XQ. 2021. Percentage of Natural Killer (NK) Cells in Peripheral Blood Is Associated with Prognosis in Patients with Gastric Cancer: A Retrospective Study from a Single Center. Med Sci Monit 27:e927464.

Xing-Mao Z, Hong-Juan Z, Qing L, Qiang H. 2018. Pancreatic acinar cell carcinoma-case report and literature review. BMC Cancer 18:1083.

Yamamoto T, Yanagimoto H, Satoi S, Toyokawa H, Hirooka S, Yamaki S, Yui R, Yamao J, Kim S, Kwon AH. 2012. Circulating CD4+CD25+ regulatory T cells in patients with pancreatic cancer. Pancreas 41:409-15.

Yan K, Yang J, Qian Q, Xu D, Liu H, Wei L, Li M, Xu W. 2019. Pathogenic Role of an IL-23/γδT17/Neutrophil Axis in Coxsackievirus B3-Induced Pancreatitis. J Immunol 203:3301-3312.

Yanagimoto H, Takai S, Satoi S, Toyokawa H, Takahashi K, Terakawa N, Kwon AH, Kamiyama Y. 2005. Impaired function of circulating dendritic cells in patients with pancreatic cancer. Clin Immunol 114:52-60.

Yang J, Hu S, Shangguan J, Eresen A, Li Y, Pan L, Ma Q, Velichko Y, Wang J, Hu C, Yaghmai V, Zhang Z. 2019. Dendritic cell immunotherapy induces anti-tumor effect in a transgenic mouse model of pancreatic ductal adenocarcinoma. Am J Cancer Res 9:2456-2468.

Yang J, Zhang Q, Wang J, Lou Y, Hong Z, Wei S, Sun K, Wang J, Chen Y, Sheng J, Su W, Bai X, Liang T. 2022. Dynamic profiling of immune microenvironment during pancreatic cancer development suggests early intervention and combination strategy of immunotherapy. EBioMedicine 78:103958.

Yang P, Li QJ, Feng Y, Zhang Y, Markowitz GJ, Ning S, Deng Y, Zhao J, Jiang S, Yuan Y, Wang HY, Cheng SQ, Xie D, Wang XF. 2012. TGF-β-miR-34a-CCL22 signaling-induced Treg cell recruitment promotes venous metastases of HBV-positive hepatocellular carcinoma. Cancer Cell 22:291-303.

Yoshimoto T, Chiba Y, Furusawa J, Xu M, Tsunoda R, Higuchi K, Mizoguchi I. 2015. Potential clinical application of interleukin-27 as an antitumor agent. Cancer Sci 106:1103-10.

Youn JI, Kumar V, Collazo M, Nefedova Y, Condamine T, Cheng P, Villagra A, Antonia S, McCaffrey JC, Fishman M, Sarnaik A, Horna P, Sotomayor E, Gabrilovich DI. 2013. Epigenetic silencing of retinoblastoma gene regulates pathologic differentiation of myeloid cells in cancer. Nat Immunol 14:211-20.

Yu JW, Bhattacharya S, Yanamandra N, Kilian D, Shi H, Yadavilli S, Katlinskaya Y, Kaczynski H, Conner M, Benson W, Hahn A, Seestaller-Wehr L, Bi M, Vitali NJ, Tsvetkov L, Halsey W, Hughes A, Traini C, Zhou H, Jing J, Lee T, Figueroa DJ, Brett S, Hopson CB, Smothers JF, Hoos A, Srinivasan R. 2018. Tumor-immune profiling of murine syngeneic tumor models as a framework to guide mechanistic studies and predict therapy response in distinct tumor microenvironments. PLoS One 13:e0206223.

Yu X, Harden K, Gonzalez LC, Francesco M, Chiang E, Irving B, Tom I, Ivelja S, Refino CJ, Clark H, Eaton D, Grogan JL. 2009. The surface protein TIGIT suppresses T cell activation by promoting the generation of mature immunoregulatory dendritic cells. Nat Immunol 10:48-57.

Yushkevich PA, Piven J, Hazlett HC, Smith RG, Ho S, Gee JC, Gerig G. 2006. User-guided 3D active contour segmentation of anatomical structures: significantly improved efficiency and reliability. Neuroimage 31:1116-28.

Zamboni G, Hirabayashi K, Castelli P, Lennon AM. 2013. Precancerous lesions of the pancreas. Best Pract Res Clin Gastroenterol 27:299-322.

Zauber P, Marotta S, Sabbath-Solitare M. 2013. KRAS gene mutations are more common in colorectal villous adenomas and in situ carcinomas than in carcinomas. Int J Mol Epidemiol Genet 4:1-10.

Zeng JC, Zhang Z, Li TY, Liang YF, Wang HM, Bao JJ, Zhang JA, Wang WD, Xiang WY, Kong B, Wang ZY, Wu BH, Chen XD, He L, Zhang S, Wang CY, Xu JF. 2013. Assessing the role of IL-35 in colorectal cancer progression and prognosis. Int J Clin Exp Pathol 6:1806-16.

Zeng Z, Lan T, Wei Y, Wei X. 2022. CCL5/CCR5 axis in human diseases and related treatments. Genes Dis 9:12-27.

Zhan Y, Wang N, Vasanthakumar A, Zhang Y, Chopin M, Nutt SL, Kallies A, Lew AM. 2020. CCR2 enhances CD25 expression by FoxP3(+) regulatory T cells and regulates their abundance independently of chemotaxis and CCR2(+) myeloid cells. Cell Mol Immunol 17:123-132.

Zhang D, Li L, Jiang H, Li Q, Wang-Gillam A, Yu J, Head R, Liu J, Ruzinova MB, Lim KH. 2018a. Tumor-Stroma IL1β-IRAK4 Feedforward Circuitry Drives Tumor Fibrosis, Chemoresistance, and Poor Prognosis in Pancreatic Cancer. Cancer Res 78:1700-1712.

Zhang H, Chen J. 2018. Current status and future directions of cancer immunotherapy. J Cancer 9:1773-1781.

Zhang H, Jensen MH, Farnell MB, Smyrk TC, Zhang L. 2010. Primary leiomyosarcoma of the pancreas: study of 9 cases and review of literature. Am J Surg Pathol 34:1849-56.

Zhang S, Liang R, Luo W, Liu C, Wu X, Gao Y, Hao J, Cao G, Chen X, Wei J, Xia S, Li Z, Wen T, Wu Y, Zhou X, Wang P, Zhao L, Wu Z, Xiong S, Gao X, Gao X, Chen Y, Ge Q, Tian Z, Yin Z. 2013a. High susceptibility to liver injury in IL-27 p28 conditional knockout mice involves intrinsic interferon-γ dysregulation of CD4+ T cells. Hepatology 57:1620-31.

Zhang T, Nie J, Liu X, Han Z, Ding N, Gai K, Liu Y, Chen L, Guo C. 2021. Correlation Analysis Among the Level of IL-35, Microvessel Density, Lymphatic Vessel Density, and Prognosis in Non-Small Cell Lung Cancer. Clin Transl Sci 14:389-394.

Zhang Y, Houchen CW, Li M. 2022. Attenuating DNA damage response and immunosuppression radiosensitizes pancreatic cancer. EBioMedicine 76:103822.

Zhang Y, Yan W, Collins MA, Bednar F, Rakshit S, Zetter BR, Stanger BZ, Chung I, Rhim AD, di Magliano MP. 2013b. Interleukin-6 is required for pancreatic cancer progression by promoting MAPK signaling activation and oxidative stress resistance. Cancer Res 73:6359-74.

Zhang Y, Zoltan M, Riquelme E, Xu H, Sahin I, Castro-Pando S, Montiel MF, Chang K, Jiang Z, Ling J, Gupta S, Horne W, Pruski M, Wang H, Sun SC, Lozano G, Chiao P, Maitra A, Leach SD, Kolls JK, Vilar E, Wang TC, Bailey JM, McAllister F. 2018b. Immune Cell Production of Interleukin 17 Induces Stem Cell Features of Pancreatic Intraepithelial Neoplasia Cells. Gastroenterology 155:210-223.e3.

Zhao X, Li L, Starr TK, Subramanian S. 2017. Tumor location impacts immune response in mouse models of colon cancer. Oncotarget 8:54775-54787.

Zhao Y, Shen M, Feng Y, He R, Xu X, Xie Y, Shi X, Zhou M, Pan S, Wang M, Guo X, Qin R. 2018. Regulatory B cells induced by pancreatic cancer cell-derived interleukin-18 promote immune tolerance via the PD-1/PD-L1 pathway. Oncotarget 9:14803-14814.

Zhou B, Zhang P, Tang T, Liao H, Zhang K, Pu Y, Chen P, Song Y, Zhang L. 2015. Polymorphisms and plasma levels of IL-27: impact on genetic susceptibility and clinical outcome of bladder cancer. BMC Cancer 15:433.

Zhou Q, Law AC, Rajagopal J, Anderson WJ, Gray PA, Melton DA. 2007. A multipotent progenitor domain guides pancreatic organogenesis. Dev Cell 13:103-14.

Zhu J, Wang Y, Li D, Zhang H, Guo Z, Yang X. 2020. Interleukin-35 promotes progression of prostate cancer and inhibits anti-tumour immunity. Cancer Cell Int 20:487.

Zhu Y, Herndon JM, Sojka DK, Kim KW, Knolhoff BL, Zuo C, Cullinan DR, Luo J, Bearden AR, Lavine KJ, Yokoyama WM, Hawkins WG, Fields RC, Randolph GJ, DeNardo DG. 2017. Tissue-Resident Macrophages in Pancreatic Ductal Adenocarcinoma Originate from Embryonic Hematopoiesis and Promote Tumor Progression. Immunity 47:597.

Zou JM, Qin J, Li YC, Wang Y, Li D, Shu Y, Luo C, Wang SS, Chi G, Guo F, Zhang GM, Feng ZH. 2017. IL-35 induces N2 phenotype of neutrophils to promote tumor growth. Oncotarget 8:33501-33514.